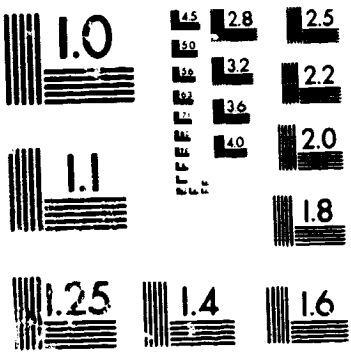

NASA CR-167934

COAXIAL PRIME FOCUS FEEDS FOR PARABOLOIDAL REFLECTORS

by

R.E. COLLIN, H. SCHILLING, and L. HEBERT

ELECTRICAL ENGINEERING & APPLIED PHYSICS DEPARTMENT
Case Institute of Technology
Case Western Reserve University
Cleveland, Ohio 44106

Prepared for

NATIONAL AERONAUTICS AND SPACE ADMINISTRATION
NASA Lewis Research Center
Contract NAS3-22342

1. Report No.	2. Government Accession No.	3. Recipient's Catalog No.
NASA CR 167934		

4. Title and Subtitle	5. Report Date
Coaxial Prime Focus Feeds for Paraboloidal Reflectors	July, 1982
	6. Performing Organization Code

7. Author(s)	8. Performing Organization Report No.
R. E. Collin, H. Schilling and L. Hebert	
	10. Work Unit No.

9. Performing Organization Name and Address	11. Contract or Grant No.
Case Western Reserve University Cleveland, OH 44106	NAS 3-22342
	13. Type of Report and Period Covered
12. Sponsoring Agency Name and Address	Contractor Report
National Aeronautics and Space Administration Washington, DC 20546	14. Sponsoring Agency Code

15. Supplementary Notes

Technical Manager, Jerry Smetana, Space Communications Division, NASA, Lewis Research Center, Cleveland, OH 44135

16. Abstract

A TE_{11} - TM_{11} dual mode coaxial feed for use in prime focus paraboloidal antenna systems is investigated. The scattering matrix parameters of the internal bifurcation junction was determined by the residue calculus technique. The scattering parameters and radiation fields of the aperture were found from the Weinstein solution. The optimum modeing ratio for minimum cross-polarization was determined along with the corresponding optimum feed dimensions. A peak cross-polarization level of -58 dB is predicted. The frequency characteristics were also investigated and a bandwidth of 5% is predicted over which the cross-polarization remains below -30 dB, the input VSWR is below 1.15, and the phase error is less than 10°. Theoretical radiation patterns and efficiency curves for a paraboloidal reflector illuminated by this feed were computed. The predicted sidelobe level is below -30 dB and aperture efficiencies greater than 70% are possible. Experimental results are also presented that substantiates the theoretical results. In addition, experimental results for a "short-cup" coaxial feed are given.

The report includes extensive design data for the dual-mode feed along with performance curves showing cross-polarization as a function of feed parameters. The feed is useful for low-cost ground based receiving antennas for use in direct television satellite broadcasting service.

17. Key Words (Suggested by Author(s))	18. Distribution Statement
	Unclassified - Unlimited

19. Security Classif. (of this report)	20. Security Classif. (of this page)	21. No. of Pages	22. Price*
Unclassified	Unclassified		

* For sale by the National Technical Information Service, Springfield, Virginia 22161

FORWARD

The reported work on the dual-mode coaxial feed is a follow up to earlier work done on NASA Contract NAS3-21365 (Technical Report NASA CR-159703). The analytical and computer numerical work was carried out by H. Schilling and was supported by the National Science Foundation under Grant ECS-7910269. The detailed theoretical analysis is presented in the Ph. D. dissertation submitted by H. Schilling.

TABLE OF CONTENTS

CHAPTER 1

PRIME FOCUS FEEDS - A REVIEW

1.1 INTRODUCTION

Receiving station atennas for use in the 12-14 ghz. band direct television satellite broadcast service are envisoned to use small paraboloidal reflectors illuminated by a simple prime focus feed for economical reasons. Although simplicity and cost are dominating factors the required prime focus feed paraboloidal antenna system is required to have a relatively high level of performance as regards low sidelobe levels, low cross-polarization, and high aperture illumination efficiency. Typical performance features are first and second sidelobes below -30 dB. with the remaining sidelobes below -40 dB., aperture illumination efficiency of 65% to 70%, cross-polarization below -30 dB. for frequency re-use applications, a bandwidth of 5% and an input VSWR of 1.5 or less. The last requirement, an input VSWR of less than 1.5, can be readily met by using well known matching techniques since the bandwidth of operation is only 5%. The requirement of low sidelobes can be met by using a sufficiently large amount of edge taper in the aperture illumination but at the expense of reduced aperture illumination efficiency. In theory sidelobes below -30 dB. and an aperture efficiency as high as 80% is realizable but not necessarily by any presently known simple feed structure. For example, with an aperture illumination function $1/7 + 6/7\ (1-r^2)^2$ where r is the normalized aperture radius the aperture efficiency is 71% and the largest sidelobe is -33.22 dB. below the main lobe peak (Kouznetsov, 1978). If a particular feed is chosen it will have its own characteristic radiation

pattern and when a paraboloid with the correct f/D (focal length/ diameter) is chosen so as to meet the sidelobe specification there is no control over the aperture efficiency that can be obtained.

Low cross-polarization is obtained from feeds that have rotationally symmetric radiation patterns, which implies equal E- and H-plane patterns. Feeds with rotationally symmetric patterns yield higher aperture efficiencies since the amount of taper in the illumination that is required for a given sidelobe level is the same in all pl es. A feed with an unsymmetric pattern generally leads to more tapering than desired in one plane in order to achieve the required sidelobe level in the plane with the least amount of taper. Feeds that will result in secondary patterns with sidelobes below -30 dB. usually produce an illumination edge taper of -15 dB. to -20 dB. and as a result exhibit very little spill over loss. A feed that produces very little cross-polarized radiation also leads to increased efficiency since there is less unwanted radiation in the polarization not used.

1.2 PRIME FOCUS FEEDS

Two basic approaches have been used to design feeds with rotationally symmetric radiation patterns. One approach is based on exciting the correct mixture of TE_{1m} and TM_{1m} modes in a circular waveguide, conical horn, or coaxial waveguide structure while the other is based on the use of a corrugated waveguide or horn that will support a dominant HE_{11} hybrid mode that radiates a rotationally symmetric pattern. Feeds based on both design principles have been considered by various authors and a reasonably complete review is given in a recent paper (Clarricoats and Poulton, 1977).

Figure 1.1 illustrates several feed configurations that can yield a cross-polarization of order -30 dB. or less. The corrugated horn, first introduced by Kay (Kay, 1964), in Fig. 1.1a normally produces a beam that is too directive for a paraboloid with an angular aperture greater than 130°. Wood reports that R. W. Ashton found a cross-polarization ranging from -30 dB. to -50 dB. for a 2.5° corrugated horn as the aperture diameter was varied from 1.5 to 10 wavelengths (Wood, 1980). For the 90° corrugated horn shown in Fig. 1.1c Hockham found that the peak cross-polarization level was around -26 dB. (Hockham, 1976). The measured on axis cross-polarization was -32 dB. The 90° corrugated horn has also been examined by James (James, 1977). It was found that using only a flange of radius 1.7 cm. on a circular guide of radius 1.34 cm. a cross-polarized radiation level of -26 to -29 dB. over the band 7.5 to 11.5 ghz. could be achieved. With the addition of 1 slot the cross-polarization was -25 to -26 dB. and with 3 slots it was -26 dB. to -28 dB. over the same band. The advantage of corrugated structures is the relatively large bandwidth but the cost is a rather heavy feed that is difficult to construct. The dual mode horn of Potter (Potter, 1963) shown in Fig. 1.1d and its variation shown in Fig. 1.1e and due to Satoh (Satoh, 1972) can produce very low cross-polarization over a bandwidth of a few percent when the step at the throat or the dielectric insert is properly adjusted to produce the optimum ratio (moding ratio) of the TE_{11} and TM_{11} modes in the aperture. The horn is excited by the TE_{11} mode in the input waveguide while the TM_{11} mode is excited parasitically by the discontinuity.

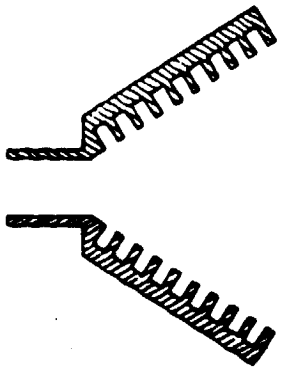

(a) Corrugated horn

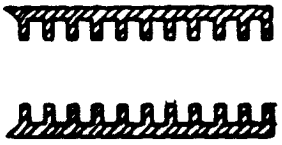

(b) Corrugated waveguide

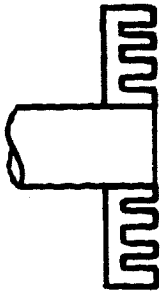

(c) Corrugated 90° horn

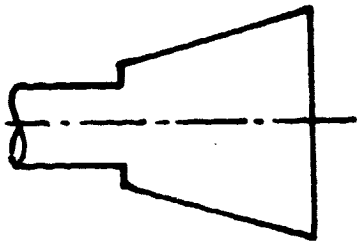

(d) Dual mode horn of Potter

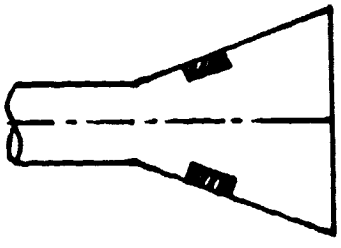

(e) Dual mode horn of Satoh.

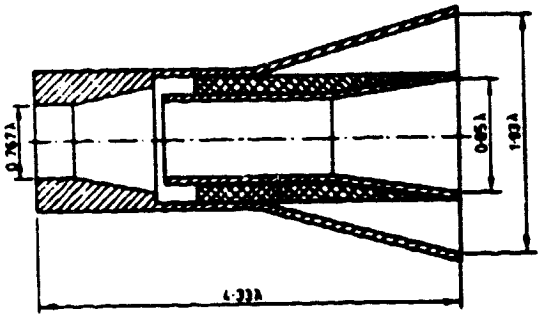

(f) Coaxial feed due to Koch.

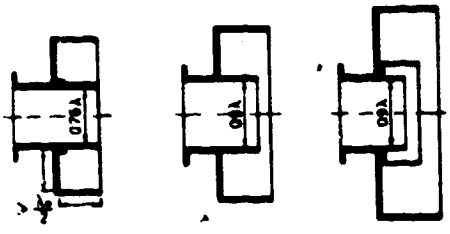

(g) Coaxial feeds studied by Scheffer.

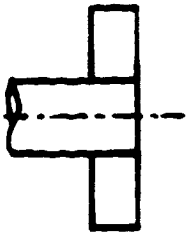

(h) Coaxial feed studied by Kumar.

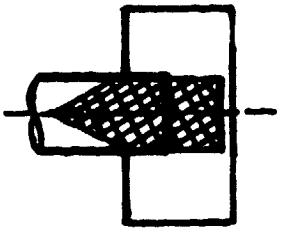

(i) Alternative feed due to Kumar.

Figure 1.1 - Low cross-polarization feeds.

For paraboloids with large angular apertures the horns are too directive and the coaxial waveguide feeds shown in Fig's. 1.1f- are more suitable. The feed in Fig. 1.1f is relatively complex and is described by Koch (Koch, 1973) and can yield a high aperture efficiency as well as low cross-polarization (-35 dB. or better). The feeds in Fig's. 1.1g and 1.1h have been studied by Scheffer and also by Kumar (Scheffer, 1975; Kumar, 1978). In an experimentally optimized two coaxial waveguide feed kumar reported a cross-polarization of -30 dB. to -31 dB. over a band from 8 to 9 ghz. This feed has the configuration shown in Fig. 1.1h and would be a multi-mode feed because of the excitation of many modes in the aperture. The feed shown in Fig. 1.1h is also due to Kumar and has a comparable performance (Kumar, 1976).

It is worth mentioning that a circular waveguide operated with the TE_{11} mode close to cutoff (diameter equal to 0.7 λ_o) has a low cross-polarization. Wood states that cross-polarization of -48 dB. is predicted using the approximate E and H aperture field method to compute the radiation pattern (Wood, 1980, p. 110). The cross-polarization level was computed for a TE_{11} mode in a circular waveguide with a radius of 0.36 λ_o and found to have a cross-polarization peak of -40 dB. at $\theta = 45°$ and a second peak of -32 dB. at $\theta = 90°$ (see Figure C3). The computation was based on the E-H aperture field method. Although approximate methods for calculating the co-polarized patterns may be quite accurate these methods usually fail to give good results for the cross-polarized pattern which depends on the difference in the E- and H-plane patterns and hence show large errors for small errors in the principle plane patterns.

When the exact solutions for the radiation from the TE_{11} circular waveguide mode, (as given by Weinstein) is used the predicted peak cross-polarization level varies from -22.5 dB. to-30 dB. as the diameter varies from $0.64\lambda_o$ to $1.1\lambda_o$ according to James and Greene (James and Greene, 1978). For a dipole excited circular waveguide it has been found that the cross-polarization was dependent on the length of the guide also (Hansen and Shafai, 1977). With a waveguide $2\lambda_o$ long and a $0.7\ \lambda_o$ diameter the cross-polarization was computed numerically to have one peak of -37 dB. and a second peak of -33 dB. at $\theta = 90°$. With a $3\lambda_o$ long guide the cross-polarization was about 3 dB. higher. It was also noted that the cross-polarization was dependent on the wall thickness. It is thus apparent that a number of factors enter in that can result in the cross-polarization for an actual feed to differ from that computed theoretically for an idealized model.

Although the circular waveguide excited by the TE_{11} mode can yield low cross-polarization the radiation pattern is very broad so this feed is useful only for paraboloids with a large angular aperture approaching 180°.

1.3 OVERVIEW

The reported experimental results for the coaxial waveguide feeds were deemed to be sufficiently attractive to warrant carrying out a complete analytical study to fully assess the merits of such feeds and to obtain design information. The feed chosen for detailed analysis is the "long-cup" coaxial dual-mode feed shown in Fig. 1.2a. The parameters were restricted such that in the input guide and coaxial section only the TE_{11} mode propagated while in the output guide both the TE_{11} and TM_{11} mode could propagate. An exact analytical solution for this

feed was obtained and from this optimum design data and performance was derived. A spot frequency cross-polarization as low as -58 dB. was predicted along with a bandwidth of around 5% for cross-polarization below -30 dB. Experimental results are also reported that shows that a feed of this type when used with a suitable paraboloidal reflector will have sidelobes below -30 dB. and a secondary radiation pattern with a cross-polarization below -30 dB., including the effects of scatter from the support rods, aperture blocking, etc.

Some experimental work was also done on the "short-cup" coaxial feed in Fig. 1.2b and the results obtained are in accord with those reported by Kumar. It would be desirable to carry out a complete analytical study of the short-cup feed also since it was found to have a greater bandwidth of operation (from 10% to 15%).

It was found that a cross-polarization level of -30 dB. or somewhat better could be measured for the feeds studied without any unusual precautions being taken. However, the experimental set-up was not adequate to verify that the cross-polarization could be as low as -50 dB. In a practical feed and measurement set up a number of factors enter in, such as finite feed length, finite wall thickness, less than perfect circular symmetry, scatter from the feed support, etc. that limits the minimum cross-polarization level that can be achieved and measured. Nevertheless the results obtained verify that simple coaxial feeds can be built to give cross-polarization below -30 dB. without any difficulty.

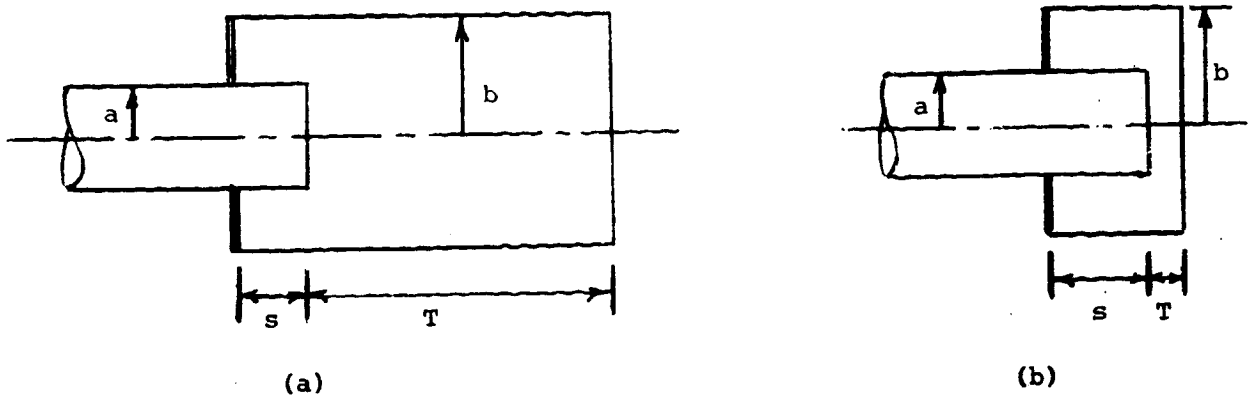

Figure 1.2 (a) Long-cup or dual-mode coaxial feed,

(b) Short-cup or multi-mode coaxial feed.

1.4 RADIATION FROM PARABOLOIDAL REFLECTOR

In this section the formulas that are used later on to evaluate the radiation pattern and the cross-polarization properties of a paraboloidal reflector are presented.

One procedure for calculating the far zone radiation field from a reflector antenna such as a paraboloid is based on the use of geometrical ray optics to obtain an approximation to the aperture field produced by the reflection of the field from the feed by the reflector.

Another approach is based on calculating the radiation field in terms of the currents induced on the reflector surface (Silver, 1949). In this method the reflector is treated as an infinite flat plate at each point so that locally the induced current is given by $\vec{J}_s = 2\vec{n}\times\vec{H}_{inc}$ where $\vec{n}$ is a unit normal to the reflector surface and $\vec{H}_{inc}$ is the incident

magnetic field from the feed as in Fig. 1.3. When the reflector is in the far zone of the feed $\vec{H}_{inc} = Y_o \vec{s}_i \times \vec{E}_{inc}$ where $\vec{s}_i$ is a unit vector along the incident ray.

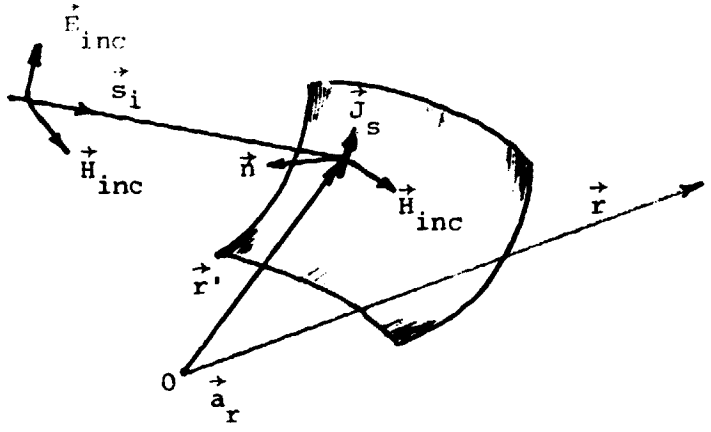

Figure 1.3 - Induced current on reflector surface

Hence we can write

$$\vec{J}_s(\vec{r}') = 2\vec{n} \times (Y_o \vec{s}_i \times \vec{E}_{inc}) = 2Y_o[(\vec{n} \cdot \vec{E}_{inc})\vec{s}_i - (\vec{n} \cdot \vec{s}_i)\vec{E}_{inc}] \quad (1.1)$$

The radiation field may be found from the general expression given below

$$\vec{E}(\vec{r}) = -jk_o Z_o \frac{e^{-jk_o r}}{4\pi r} \int_s [\vec{J}_s(\vec{r}') - \vec{a}_r \cdot \vec{J}_s(\vec{r}')\vec{a}_r] e^{jk_o \vec{a}_r \cdot \vec{r}'} \, ds' \quad (1.2)$$

where the integration is over the surface of the reflector and $\vec{J}_s$ is given by (1.1). It is generally felt that the induced current method is more accurate than the aperture field method since it involves one less geometrical optics approximation, i.e., the ray tracing of the field from the reflector surface to the aperture surface. In many instances, such as for large paraboloids, the

induced current method agrees closely with the fields calculated using the aperture field method.

Cross-Polarization In Paraboloidal Antenna

With regard to cross polarization there are several definitions of cross polarized radiation that can be adopted. Three definitions are discussed by Ludwig (Ludwig, 1973). For paraboloidal antennas the most useful definition is Ludwig's definition No. 3. This definition is based on the following measurement method. A linearly polarized horn antenna is used for receiving and oriented for maximum reception on the bore sight axis of the paraboloid antenna whose pattern is being measured. It is assumed that the paraboloid antenna radiates a linearly polarized field on axis. Let the field radiated by the paraboloid antenna be $\vec{E}(\theta,\phi)$ where θ,ϕ are defined as in Figure 1.4. The measured reference polarization pattern is then given by

$$R(\theta,\phi) = \vec{E}(\theta,\phi) \cdot [\sin\beta\ \vec{a}_\theta + \cos\beta\ \vec{a}_\phi] \tag{1.3}$$

where β is the polarization angle of the receiving horn. To measure the cross polarized pattern for the same pattern cut (same value of ϕ) the horn is rotated by 90°, i.e., β is increased by 90°. The measured cross polarization pattern is then given by

$$C(\theta,\phi) = \vec{E}(\theta,\phi) \cdot [\cos\beta\ \vec{a}_\theta - \sin\beta\ \vec{a}_\phi] \tag{1.4}$$

If the transmitted field is along the y axis in the bore sight direction then for a pattern cut at angle ϕ the values of β is ϕ for the reference polarization and $\phi \pm \pi/2$ for the cross polarization pattern since rotation of the paraboloid about its axis by an angle ϕ will require a similar rotation of the receiving horn and such a rotation is necessary to obtain a pattern cut at the angle ϕ.

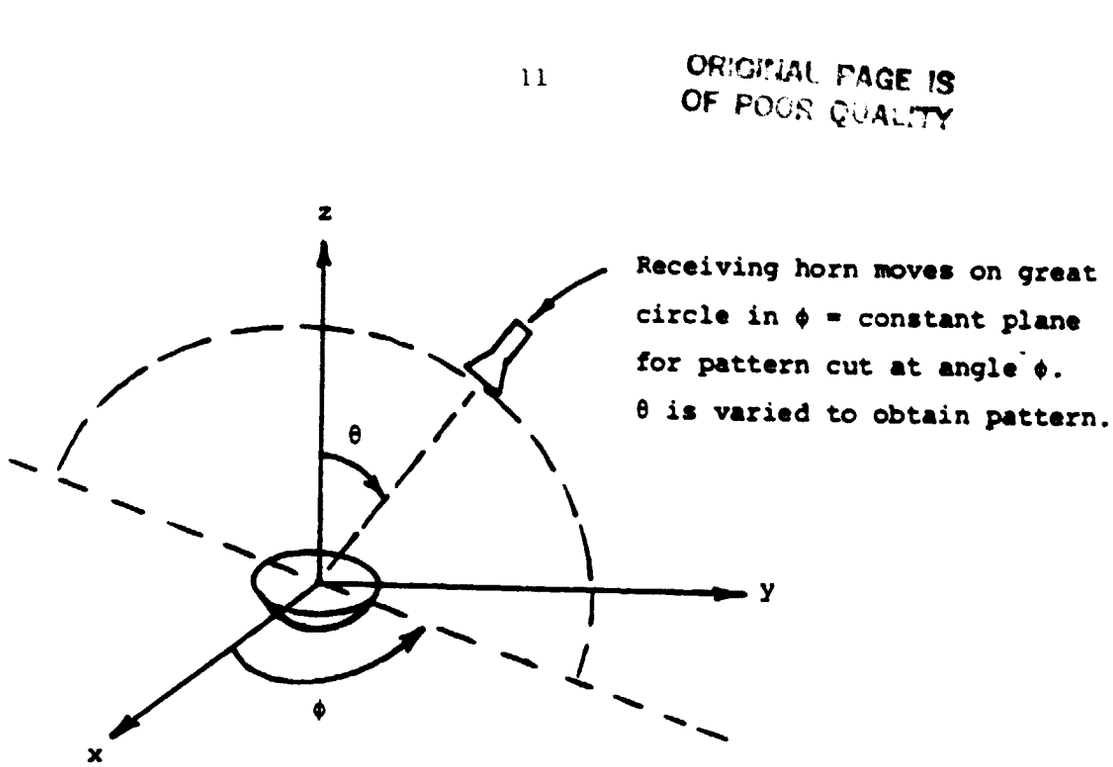

Figure 1.4 - Illustration of pattern measurement procedure. In practice, receiving horn is fixed and paraboloid antenna is rotated.

For a linearly polarized paraboloid antenna with a field along the y axis for $\theta = 0$, $\phi = 0$, we have $\beta = \phi$ or $\phi \pm \pi/2$, so that

$$R(\theta,\phi) = \vec{E}(\theta,\phi) \cdot [\sin\phi\ \vec{a}_\theta + \cos\phi\ \vec{a}_\phi] \tag{1.5a}$$

$$C(\theta,\phi) = \vec{E}(\theta,\phi) \cdot [\cos\phi\ \vec{a}_\theta - \sin\phi\ \vec{a}_\phi] \tag{1.5b}$$

These relations show that if $\vec{E}$ has the form

$$E_\theta \cos\phi = E_\phi \sin\phi \tag{1.6}$$

then

$$C(\theta,\phi) = E_\theta \cos\phi - E_\phi \sin\phi = 0$$

and there is zero cross polarization.

A feed with equal E and H plane amplitude and phase patterns and satisfying the relation (1.6) has zero cross polarization. Such a feed when used to illuminate a paraboloid results in an antenna with very small cross polarization as will be shown below.

Coaxial feeds excited by a mixture of TE_{1m} and TM_{1m} modes produce a feed primary pattern of the form

$$\vec{E}_f(\theta',\phi',r') = \frac{e^{-jk_o r'}}{r'} [e_{\theta'}(\theta')\sin\phi' \vec{a}_{\theta'} + e_{\phi'}(\theta')\cos\phi' \vec{a}_{\phi'}] \quad (1.7)$$

where $e_{\theta'}(\theta')$ and $e_{\phi'}(\theta')$ depend on the particular feed and excitation used.

In rectangular coordinates this field is given by

$$\vec{E}_f = \frac{e^{-jk_o r}}{r} [\vec{a}_x (e_\theta \cos\theta \cos\phi \sin\phi - e_\phi \sin\phi \cos\phi) + \vec{a}_y (e_\theta \cos\theta \sin^2\phi + e_\phi \cos^2\phi) - \vec{a}_z e_\theta \sin\theta \sin\phi] \quad (1.8)$$

Now assume that at $\theta = 0$ the field is polarized along y, then $e_\theta = e_\phi$ at $\theta = 0$. In the $\phi = 0$ plane or H-plane the feed pattern is proportional to $\vec{a}_y e_\phi = e_\phi \vec{a}_\phi$ while in the $\phi = \pi/2$ or E-plane the pattern is proportional to $\vec{a}_y e_\theta \cos\theta - \vec{a}_z e_\theta \sin\theta = e_\theta \vec{a}_\theta$. The E and H-plane patterns will be equal if $e_\theta(\theta) = e_\phi(\theta)$ for all values of θ. The cross polarized pattern as given by (1.8) will then also be zero for all values of θ and ϕ .

With reference to Figure 1.5 the unit normal $\vec{n}$ to the paraboloid is given by $\vec{n} = -\vec{a}_\rho \cos\frac{\theta'}{2} + \vec{a}_{\theta'} \sin\frac{\theta'}{2}$.

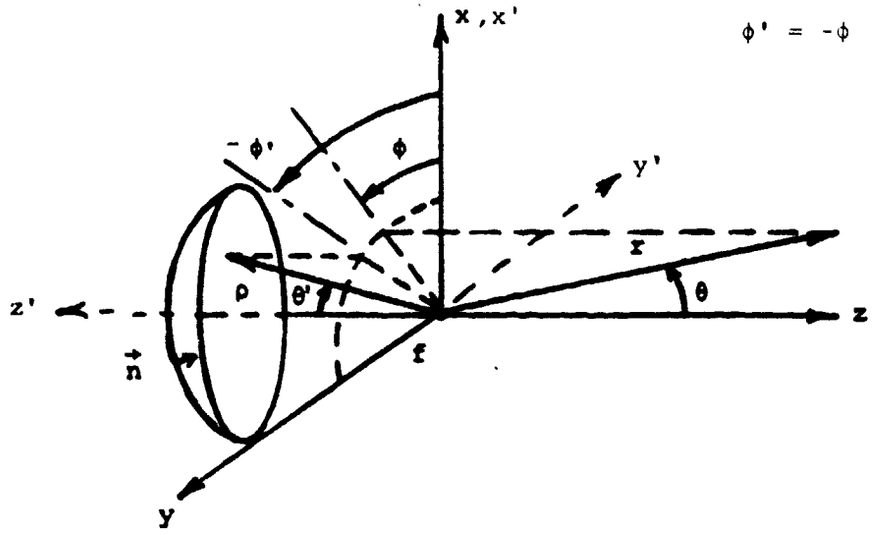

Figure 1.5 Coordinates used to describe fields associated with a paraboloid antenna.

The incident magnetic field on the paraboloid is $\vec{H}_f = Y_o \vec{a}_\rho \times \vec{E}_f$ where $\vec{E}_f$ is given by (1.7) but in terms of the variables θ', ϕ', ρ, i.e.

$$\vec{E}_f = \frac{e^{-jk_o\rho}}{\rho} [e_{\theta'}(\theta') \sin\phi' \vec{a}_{\theta'} + e_{\phi'}(\theta') \cos\phi' \vec{a}_{\phi'}]$$

On the paraboloid surface $\rho = 2f/(1 + \cos\theta') = f \sec^2\frac{\theta'}{2}$. If each portion of the paraboloid is treated as a flat reflecting surface then the surface currents produced on the paraboloid are given by

$$\vec{J}_s = 2\vec{n} \times \vec{H}_f = 2Y_o \vec{n} \times (\vec{a}_\rho \times \vec{E}_f)$$

$$= \frac{2e^{-jk_o\rho}}{Z_o\rho} [\cos\frac{\theta'}{2} (e_{\theta'} \sin\phi' \vec{a}_{\theta'} + e_{\phi'} \cos\phi' \vec{a}_{\phi'}) + \sin\frac{\theta'}{2} e_{\theta'} \sin\phi' \vec{a}_\rho]$$

(1.9)

In terms of these currents the radiated electric field is given by

$$\vec{E}(\vec{r}) = \frac{-jk_o Z_o}{4\pi r} e^{-jk_o r} \int_S [\vec{J}(\vec{r}') - \vec{a}_r \cdot \vec{J}(\vec{r}')\vec{a}_r] e^{jk_o \vec{a}_r \cdot \vec{r}'} dS$$

where $\vec{r}'$ is the position vector to a point on the paraboloid. By using (1.9) in (1.10) and carrying out the integration over ϕ we obtain

$$\vec{E}(\vec{r}) = \frac{jk_o f\, e^{-jk_o r}}{r} \int_0^{\theta_o} [(e_{\theta'} + e_{\phi'})J_o(v_1)(\vec{a}_\theta \cos\theta \sin\phi + \vec{a}_\phi \cos\phi)$$

$$-(e_{\theta'} - e_{\phi'})J_2(v_1)(\vec{a}_\theta \cos\theta \sin\phi - \vec{a}_\phi \cos\phi) - 2jJ_1(v_1)e_{\theta'} \sin\theta \sin\phi \tan\frac{\theta'}{2} \vec{a}_\theta]$$

$$[e^{-jv_2 \tan\frac{\theta'}{2}}] \, d\theta' \qquad (1.11)$$

where $v_1 = 2k_o f \sin\theta \tan\frac{\theta'}{2}$

$$v_2 = 2k_o f \frac{1+\cos\theta\cos\theta'}{1+\cos\theta'}$$

J_n = Bessel function of order n

and $2\theta_o$ is the angular aperture of the paraboloid with focal length f.

In the aperture field method the reflected field at the aperture surface is first found from the relation

$$\vec{E}_r = -\vec{E}_f + 2\vec{n} \cdot \vec{E}_f \vec{n} \qquad (1.12)$$

This field then is assumed to propagate as a plane wave to the aperture surface which will be taken as the z = 0 plane. The total path length

is 2f and hence we find that the x and y components of the aperture field are

$$\vec{E}_a = \frac{e^{-j2k_o f}}{\rho} [\vec{a}_x(e_{\phi'}, -e_{\theta'})\sin\phi' \cos\phi' + \vec{a}_y e_{\phi'} \cos^2\phi' + \vec{a}_y e_{\theta'} \sin^2\phi'] \quad (1.13)$$

In terms of the aperture electric field alone, the radiated electric field is given by

$$\vec{E}(\vec{r}') = \frac{jk_o f\, e^{-jk_o r - 2jk_o f}}{r} \int_0^{\theta_o} [(e_{\theta'}, +e_{\phi'})J_o(v_1)\ (\vec{a}_\theta \sin\phi + \vec{a}_\phi \cos\theta \cos\phi)$$

$$-(e_{\theta'}, -e_{\phi'})J_2(v_1)\ (\vec{a}_\theta \sin\phi - \vec{a}_\phi \cos\theta \cos\phi)] \tan\frac{\theta'}{2}\, d\theta' \quad (1.14)$$

If the radiated field is determined in terms of the tangential magnetic field alone on the aperture surface then it is found that

$$\vec{E}(\vec{r}) = \frac{jk_o f\, e^{-jk_o r - 2jk_o f}}{r} \int_0^{\theta_o} [(e_{\theta'}, +e_{\phi'})J_o(v_1)(\vec{a}_\theta \cos\theta \sin\phi$$

$$+\vec{a}_\phi \cos\phi) - (e_{\theta'}, -e_{\phi'})J_2(v_1)(\vec{a}_\theta \cos\theta \sin\phi - \vec{a}_\phi \cos\phi) \tan\frac{\theta'}{2}\, d\theta' \quad (1.15)$$

If a formulation in terms of both electric and magnetic fields on the aperture surface is used the result is the average of (1.14) and (1.15). This latter formulation is commonly used.

In the region close to the axis i.e., θ small, the use of the approximation $\cos\theta = 1$ makes v_2 in (1.11) equal to $2k_o f$. With this approximation (1.11) and (1.15) will agree with the exception of the small term involving $J_1(v_1)$ in (1.11). This latter term vanishes at $\theta = 0$ and remains small since it is multiplied by $\sin\theta$. It is due to the z component of current on the paraboloid.

The difference in the phase function in the surface current formulation and that in the aperture field method is due to the difference in path lengths as shown in Figure 1.6. In the aperture field method propagation from the paraboloid surface to the aperture surface is along a path parallel to the z axis in accordance with the geometrical optics theory that is used to determine the aperture field. The difference in phase between the two methods is $2k_o f - v_2 = 2k_o f \frac{(1-\cos\theta)\cos\theta'}{1+\cos\theta'}$. For a paraboloid with $f = 18\lambda_o$ and $\theta = 10°$ this phase difference varies from 0.547π at $\theta' = 0°$ to 0.365π at $\theta' = 60°$ or a total variation of 0.18π (32.4°) over the aperture. This amount of phase variation would not be expected to produce a significant change in the radiated pattern in the region $\theta \leq 10°$.

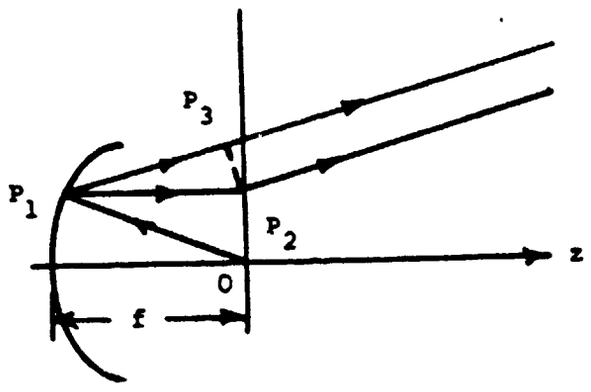

Figure 1.6- Path lengths OP_1P_2 for aperture field method and OP_1P_3 for surface current method of computing radiation from a paraboloid.

All of the above formulas show that low cross polarization is achieved by making $e_{\theta'} = e_{\phi'}$. As long as $\cos\theta$ can be approximated by unity the radiated electric field will then satisfy the relationship given by (1.6) provided the small term involving $J_1(v_1)$ in the expression for E_θ in (1.11) is neglected. This approximation will be good for values of θ up to at least 10° where $\cos\theta = 0.985$ and hence the cross polarization will be small over the region of interest for paraboloids with diameters exceeding 50 wavelengths. It is thus concluded that the desirable feed pattern should be of the form given by (1.7). This type of feed pattern also leads to small polarization loss in a paraboloid antenna (Ludwig, 1965). The objective in coaxial waveguide feed design is to excite the proper combination of TE_{11}, TM_{11} and TE_{12} modes in the aperture of the feed so as to obtain a pattern of the desired form as given by (1.7). The paraboloid sidelobe level is determined by the amplitude taper over the paraboloid and this is directly related to the directivity of the feed pattern.

With reference to (1.11) it is seen that the dominant part of the radiated field comes from the terms multiplied by $J_o(v_1)$. The radiated field can be resolved as components along the unit vectors $\vec{a}_1 = (\vec{a}_\theta \sin\phi + \vec{a}_\phi \cos\phi)$ and $\vec{a}_2 = (\vec{a}_\theta \cos\phi - \vec{a}_\phi \sin\phi)$ which define the co-polarized and cross-polarized fields. It is then found that the co-polarized pattern in the $\phi = \pi/4$ plane is given by

$$E_{co} = \frac{jk_o f}{r} e^{-jk_o r} \int_0^{\theta_o} [e_{\theta'} + e_{\phi'}) J_o \left(\frac{\cos\theta + 1}{2} \right) - (e_{\theta'} - e_{\phi'}) J_2 \left(\frac{\cos\theta - 1}{2} \right)$$

$$- j J_1 e_{\theta'} \sin\theta \tan\frac{\theta'}{2}] [e^{-jv_2 \tan\frac{\theta'}{2}}] d\theta' \qquad (1.16)$$

The term multiplied by J_o is the contribution from the co-polarized feed pattern, the term multiplied by J_2 comes from the feed cross-polarized pattern, and the last term multiplied by $J_1 \sin\theta$ comes from the z component of the induced current on the reflector.

The cross-polarized pattern is given by

$$E_{cross} = \frac{jk_o f}{r} e^{-jk_o r} \int_0^{\theta_o} [(e_{\theta'} + e_{\phi'}) J_o(\cos\theta - 1) \sin\phi\cos\phi$$

$$-(e_{\theta'} - e_{\phi'}) J_2(\cos\theta + 1)\sin\phi\cos\phi - 2jJ_1 e_{\theta'} \sin\theta\sin\phi\cos\phi\tan\frac{\theta'}{2} \left[e^{-jv_2 \tan\frac{\theta'}{2}}\right] d\theta' \tag{1.17}$$

The three terms contributing to the cross-polarized field consist of a contribution from the feed co-polarized pattern (term with J_o factor) caused by reflector depolarization, a contribution from the feed cross-polarized pattern, and a contribution from the z component of the induced current. Usually the amount of depolarization caused by the reflector is small. Note that the cross-polarized field is zero in the principal planes and is a maximum in the 45° planes.

Significant cross-polarization will occur only when $e_{\theta'} \neq e_{\phi'}$. For example consider the x-directed dipole field shown in Figure 1.6a. Apart from irrelevant constants the feed pattern is given by

$$\vec{E}_f = \frac{e^{-jk_0 r}}{r} [\vec{a}_\theta \cos\theta \cos\phi - \vec{a}_\phi \sin\phi]$$

$$= \frac{e^{-jk_o r}}{r} [(\cos\theta\cos^2\phi + \sin^2\phi)\ (\vec{a}_\theta\cos\phi - \vec{a}_\phi\sin\phi)]$$

$$+ \frac{e^{-jk_o r}}{r} [\frac{1}{2}\sin 2\phi(\cos\theta - 1)\ (\vec{a}_\theta\sin\phi + \vec{a}_\phi\cos\phi)]$$

The second factor is the cross-polarized field and since θ can be as large as the half-angular width of the dish the dish illumination has a significant cross-polarized component over the outer regions. At θ = 45° the cross-polarized field is only 15 dB. below the co-polarized component. Thus a dipole feed does not give a low-cross polarization when used to illuminate a paraboloid.

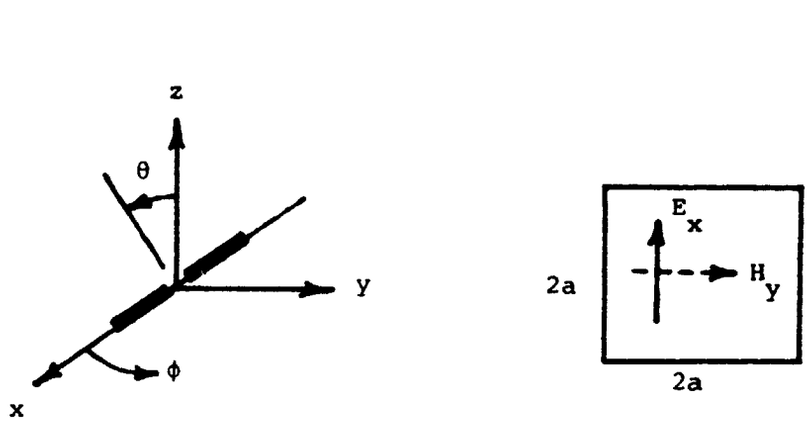

Figure 1.7 Elementary Feeds, (a) dipole, (b) Huygen's source,

A Huygen's source is a small patch of a plane electromagnetic wave as shown in Figure 1.7. If the radiation from this patch is calculated using both the electric and magnetic fields it is found that

$$\vec{E}_f = \frac{e^{-jk_0 r}}{r} (1+\cos\theta) f_x [\vec{a}_\theta \cos\phi - \vec{a}_\phi \sin\phi]$$

where f_x is the pattern function $\frac{\sin k_x a}{k_x a} \quad \frac{\sin k_y a}{k_y a}$ with

$k_x = k_0 \sin\theta \cos\phi$, $k_y = k_0 \sin\theta \sin\phi$. This feed pattern has no cross polarization.

If the radiation from the Huygen's source is calculated using only the electric field or only the magnetic field then it is found that the feed pattern is proportional to $\vec{a}_\theta \cos\phi - \vec{a}_\phi \cos\theta \sin\phi$ and $\vec{a}_\theta \cos\theta \cos\phi - \vec{a}_\phi \sin\phi$ respectively. These patterns have the same level of cross-polarization as the dipole feed does so depending on the point of view the Huygen's source can be considered to either have no cross-polarization or to have the same cross-polarization as a dipole.

Aperture Efficiency

By using (1.11) the radiated field on the z axis is readily found by setting $\theta = 0$, thus

$$\vec{E}(\vec{r}) = \vec{a}_y \frac{jk_o f}{r} e^{-jk_o r - j2k_o f} \int_0^{\theta_o} [e_{\theta'}(\theta') + e_{\phi'}(\theta')] \tan\frac{\theta'}{2} d\theta'$$

The radiated power per unit solid angle is $1/2\ Y_o r^2 |\vec{E}|^2$.

Let P_a be the total power radiated from the aperture. If the aperture illumination was uniform the aperture electric field would be

$$E_a = (2Z_o P_a/\pi a^2)^{1/2}$$

where a is the aperture radius. With uniform illumination the radiated power per unit solid angle on the z axis would be

$$\frac{1}{2} Y_o r^2 \left(\frac{k_o}{2\pi r} \pi a^2 E_a\right)^2 = \frac{k_o^2 \pi a^2}{4\pi^2} P_a$$

The aperture efficiency η_A is given by

$$\eta_A = \frac{\frac{1}{2} Y_o r^2 |\vec{E}|^2}{k_o^2 \pi a^2 P_a/4\pi^2} = \frac{\lambda_o^2 Y_o r^2 |\vec{E}|^2}{2 \pi a^2 P_a}$$

The total power radiated from the aperture equals the incident power from the feed that is intercepted by the aperture, thus

$$P_a = \frac{1}{2} Y_o \int_0^{2\pi} \int_0^{\theta_o} [|e_{\theta'}|^2 \sin^2\phi' + |e_{\phi'}|^2 \cos^2\phi'] \sin\theta' \, d\theta' \, d\phi'$$

$$= \frac{\pi Y_o}{2} \int_0^{\theta_o} [|e_{\theta'}|^2 + |e_{\phi'}|^2] \sin\theta' \, d\theta'$$

Hence

$$\eta_A = \frac{4 f^2}{a^2} \frac{\left| \int_0^{\theta_o} (e_{\theta'} + e_{\phi'}) \tan\frac{\theta'}{2} d\theta' \right|^2}{\int_0^{\theta_o} [|e_{\theta'}|^2 + |e_{\phi'}|^2] \sin\theta' \, d\theta'} \qquad (1.18)$$

For a feed with a very low cross-polarization $e_{\theta'} \approx e_{\phi'}$ and then

$$\eta_A = \frac{8\pi f^2}{\pi a^2} \frac{\left| \int_0^{\theta_o} e_{\theta'} \tan\frac{\theta'}{2} d\theta' \right|^2}{\int_0^{\theta_o} |e_{\theta'}|^2 \sin\theta' d\theta'} \qquad (1.19)$$

The definition used here for the aperture efficiency includes cross-polarization loss, phase error loss, and cross-polarization, i.e., η_A can be factored into the product η_p, η_i, and η_x as defined by Thomas (Thomas, 1971).

The gain of the antenna can be expressed as

$$G = \frac{4\pi}{\lambda_o^2} \eta_A \eta_s \eta_f \pi a^2 \qquad (1.20)$$

where η_s is the spillover efficiency and η_f is the feed efficiency that accounts for feed losses. For a large edge taper of order -20 dB. the spillover efficiency is close to unity.

CHAPTER 2

THE LONG-CUP DUAL-MODE COAXIAL FEED

In this chapter the results of the analytical and experimental investigation of the dual-mode coaxial feed are presented. Section 2.1 outlines the analytical procedure followed, Sec. 2.2 presents numerical results for the scattering matrix parameters. The following sections give results for the optimum feed parameters, typical feed radiation patterns, and the frequency sensitivity of the cross-polarization, phase error, and input reflection coefficient. The experimentally measured patterns for a typical feed are given in Sec. 2.7 while Sec. 2.8 gives measured patterns for a 1.22m paraboloid with f/D = 0.33 when illuminated with this feed.

2.1 OUTLINE OF ANALYTICAL PROCEDURE

The long-cup dual-mode coaxial feed is shown in Fig. 2.1. The waveguide dimensions a and b were chosen so that only the TE_{11} mode would propagate in regions 1 and 3 and only the TE_{11} and TM_{11} modes would propagate in region 2. The length T is chosen long enough so that the only modes incident at the aperture are the TE_{11} and TM_{11} modes - hence this is a dual-mode feed. The parameter S is adjusted to obtain the optimum moding ratio and T is adjusted to obtain the correct phase relationship between the TE_{11} and TM_{11} modes at the aperture. The two parameters are inter-related. The steps followed in analyzing this feed and optimizing its parameters were as follows:

(1) The scattering matrix parameters for the inner junction, which is that of a bifurcated circular waveguide, were found using the residue calculus method.

(2) The TE_{11} and TM_{11} mode reflection coefficients and the TE_{11} to TM_{11} mode coupling coefficient at the aperture was determined using Weinstein's solution for radiation from a circular waveguide.

(3) The TE_{11} and TM_{11} mode radiation patterns were computed using the solution given by Weinstein. The ratio of the incident TM_{11} mode to TE_{11} mode amplitudes was varied until the minimum cross-polarization in the combined radiation pattern was obtained. This provided the optimum moding ratio as a function of the waveguide radius b.

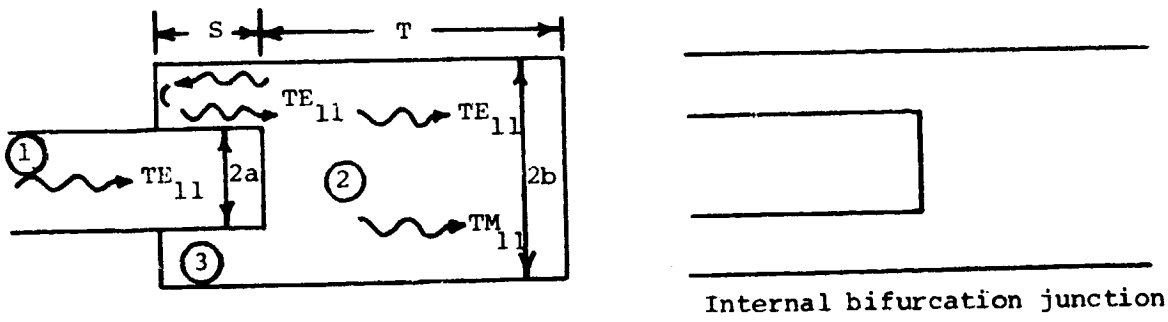

Figure 2.1 Dual-mode coaxial feed.

(4) By using the scattering matrices for the internal junction and the aperture the ratio of the TE_{11} to TM_{11} incident mode amplitudes at the aperture was computed with a unit amplitude TE_{11} mode incident in the input waveguide. A computer optimization procedure was then used to find the values of S and T for given radii a and b so as to obtain the optimum moding ratio found in Step 3.

2.2 SCATTERING MATRIX FOR INTERNAL BIFURCATION

The scattering matrix parameters S_{ij} have been determined for the internal bifurcation junction shown in Fig. 2.1 by the residue calculus method. The analytical solution is outlined in Appendix A. The only propagating modes are the TE_{11} modes in regions 1 and 3 and the TE_{11} and TM_{11} modes in region 2 so the junction is a four-port network. The subscripts refer to the modes in the various regions according to the following scheme:

S_{ij} , i = 1,2,3,4; j = 1,2,3,4

Subscript 1 corresponds to TE_{11} mode in region 1

Subscript 2 corresponds to TE_{11} mode in region 2

Subscript 3 corresponds to TE_{11} mode in region 3

Subscript 4 corresponds to TM_{11} mode in region 4

The numerical values of the S_{ij} are shown in Fig.'s 2.2a through 2.2j as contours in the complex plane with a and b, the waveguide radii, as parameters. The numerical values are for a frequency of 12 ghz. and with a and b in cm. The values for the S_{ij} are, of course, valid at any frequency for the same a/λ_o and b/λ_o values.

When region 3 is terminated in a short circuit at a distance S to the left of the bifurcation (see Fig. 2.1) the junction may be viewed as a 3-port with scattering matrix parameters S'_{ij} given by

$$S'_{ij} = S_{ij} - \frac{S_{i3}\, S_{j3}}{S_{33} + e^{j\theta}} \qquad (2.1)$$

where i,j = 1,2,4, and $\theta = 2\,\beta_{31}\,S$ is the total phase shift through the short-circuited coaxial waveguide section.

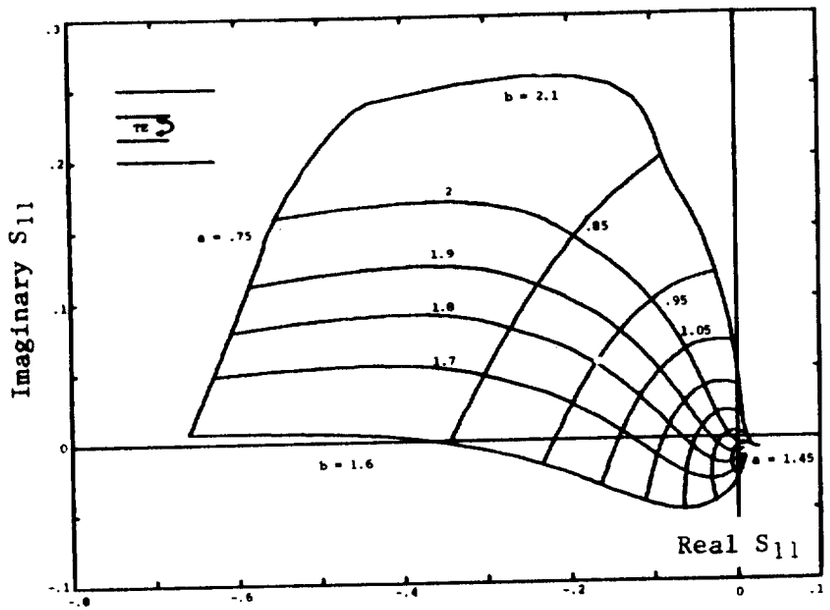

Figure 2.2a, Scattering matrix parameter S_{11}

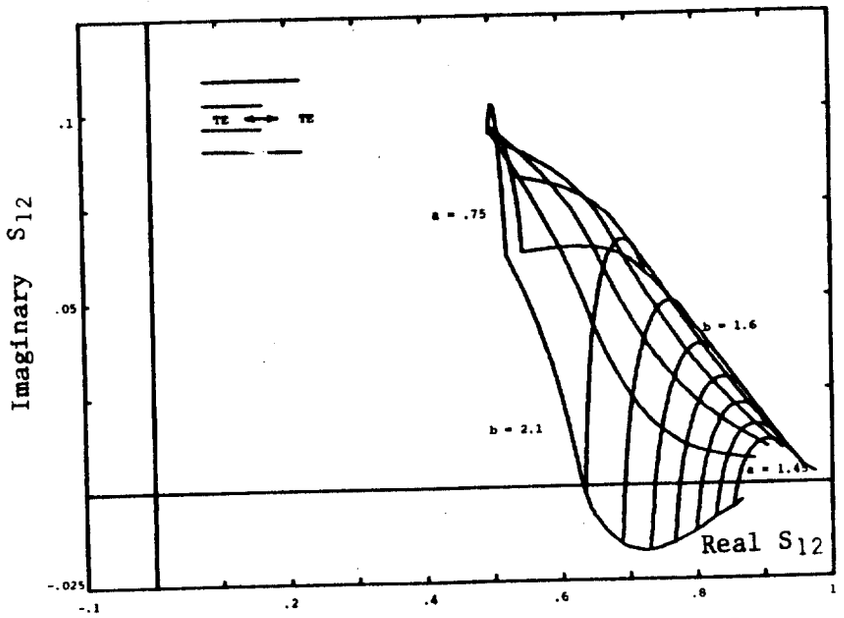

Figure 2.2b, Scattering matrix parameter S_{12}

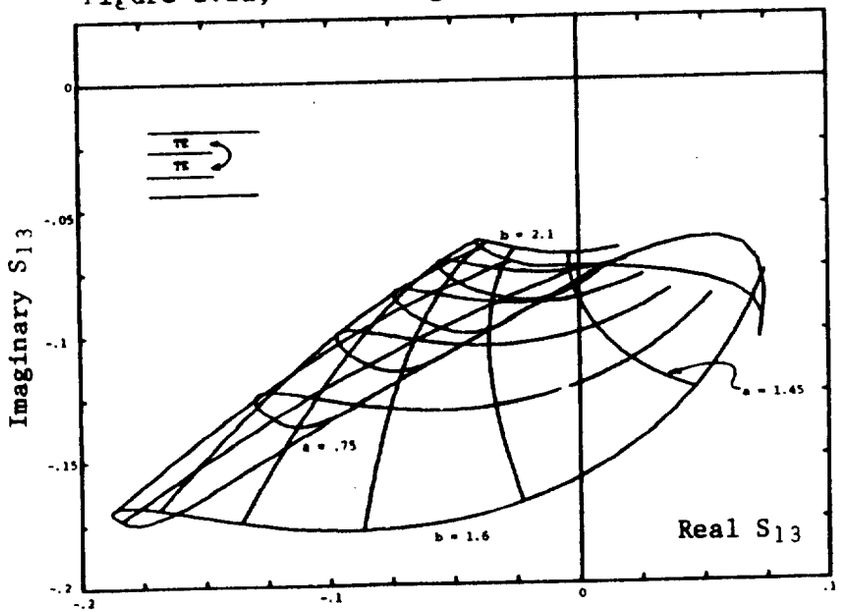

Figure 2.2c, Scattering matrix parameter S_{13}

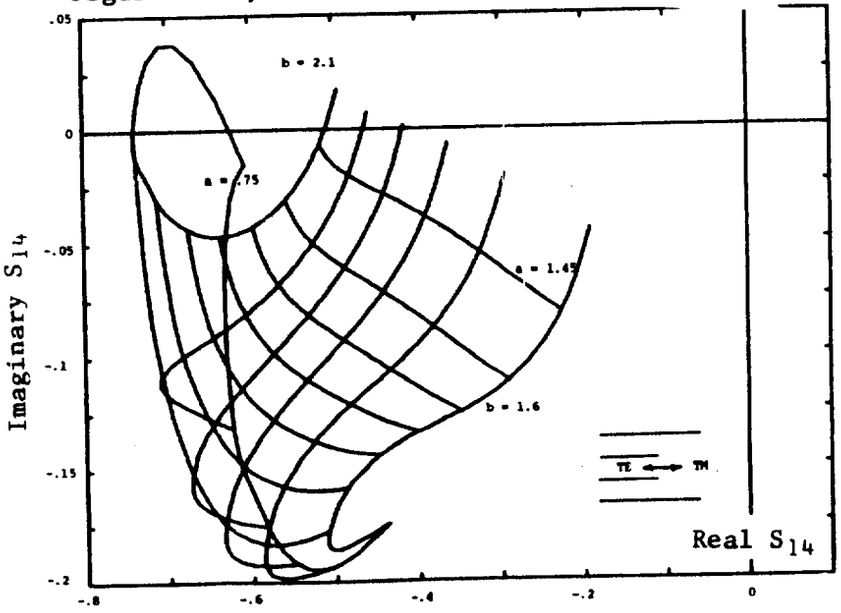

Figure 2.2d, Scattering matrix parameter S_{14}

Figure 2.2, Scattering matrix parameters for internal bifurcation junction.

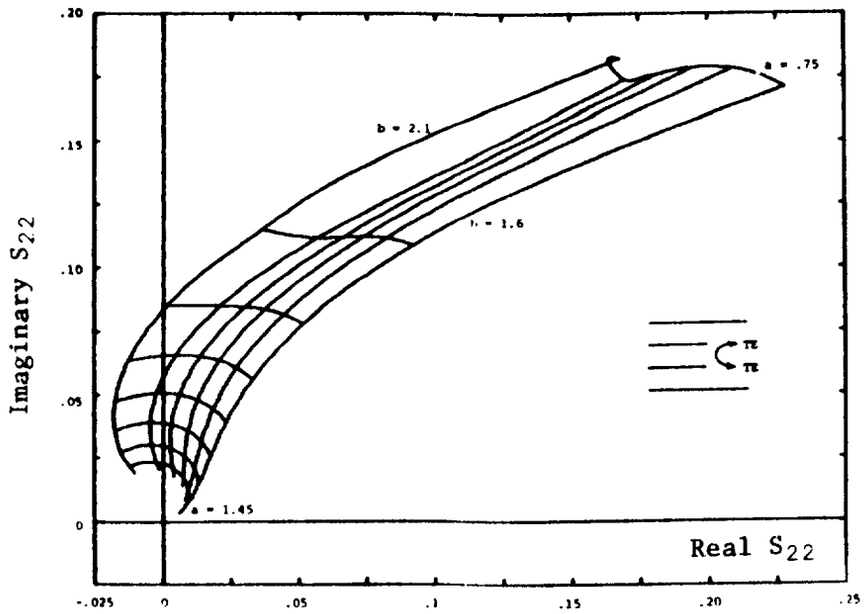

Figure 2.2e, Scattering matrix parameter S_{22}

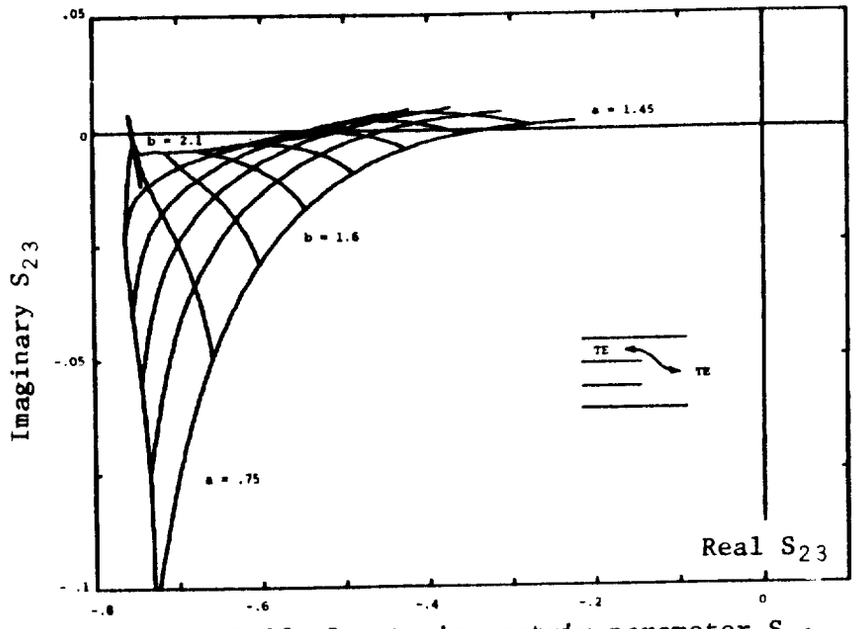

Figure 2.2f, Scattering matrix parameter S_{23}

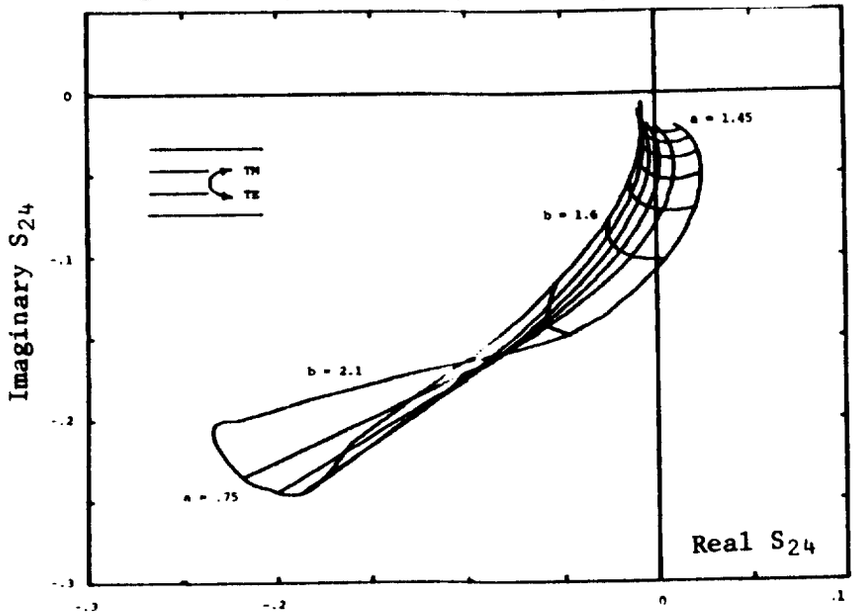

Figure 2.2g, Scattering matrix parameter S_{24}

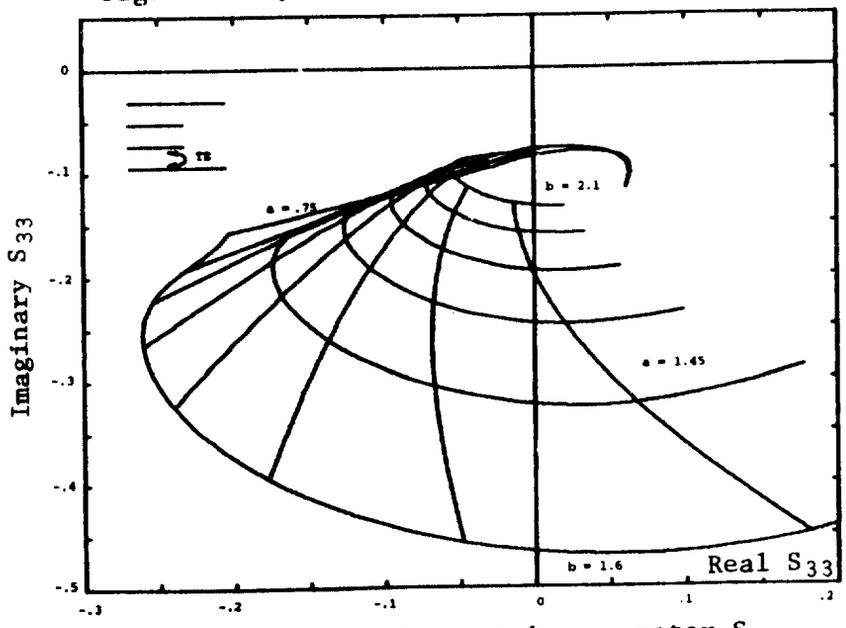

Figure 2.2h, Scattering matrix parameter S_{33}

Figure 2.2,(cont.) Scattering matrix parameters for internal bifurcation junction.

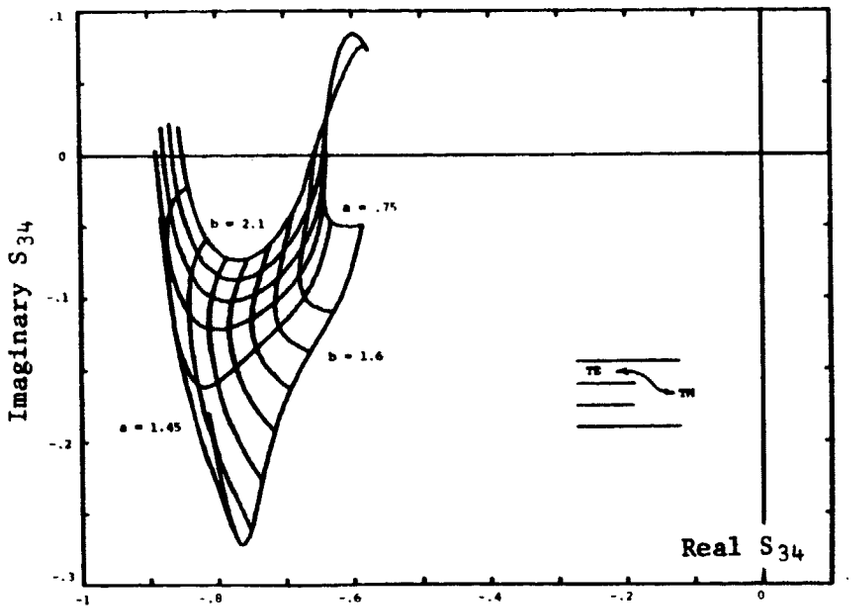

Figure 2.2i, Scattering matrix parameter S_{34}

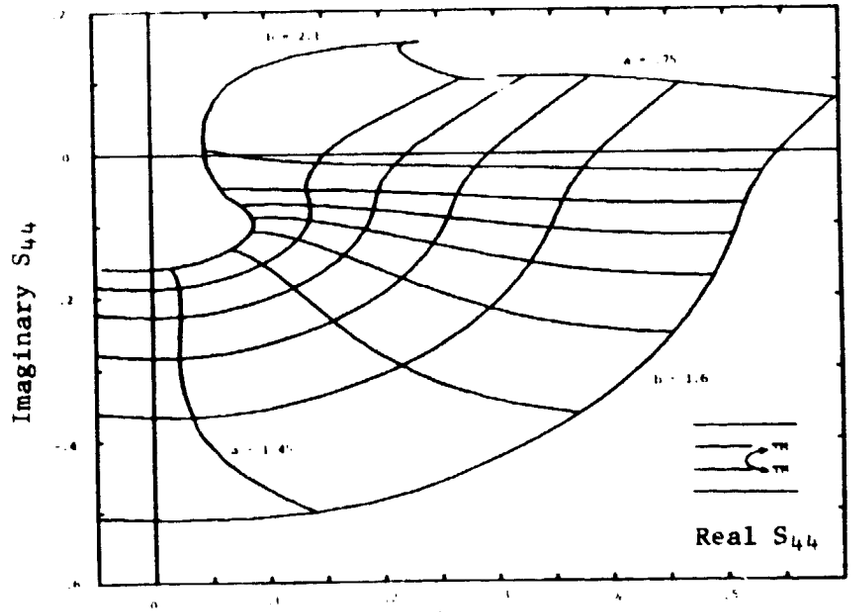

Figure 2.2j, Scattering matrix parameter S_{44}

Figure 2.2, (cont.) Scattering matrix parameters for internal bifurcation junction.

2.3 APERTURE SCATTERING MATRIX

When a unit amplitude TE_{11} mode from the waveguide is incident on the aperture with radius b in Fig. 2.1 a reflected TE_{11} mode with reflection coefficient Γ_{11} and a scattered TM_{11} mode of amplitude Γ_{12} is produced. Similarly an incident TM_{11} mode of unit amplitude produces a reflected TM_{11} mode with amplitude Γ_{22} and a scattered TE_{11} mode with amplitude Γ_{12}. The aperture internal scattering matrix parameters were found from the solution given by Weinstein (Weinstein, 1969). They may also be obtained from the scattering parameters given by Johnson and Moffatt[†] (Johnson and Moffatt, 1980). The aperture internal scattering matrix parameters are shown in Fig.'s 2.3a-c as a function of b in cm. for f = 12 ghz. Note that in particular the TM_{11} mode reflection coefficient can be quite large for values of b close to the cutoff value for the TM_{11} mode e.g. for b = 1.6, $|\Gamma_{22}| = 0.45$. Also the TE_{11} to TM_{11} mode coupling at the aperture is not negligible. It is thus apparent that there will be significant interaction between the internal bifurcation junction and the aperture and this interaction must be taken into account in optimizing the feed parameters.

2.4 DUAL-MODE FEED RADIATION PATTERNS AND CROSS-POLARIZATION

The Weinstein solutions were used to compute the E- and H-plane patterns as well as the co-polarized and cross-polarized radiation patterns for pure TE_{11} and pure TM_{11} mode excitation as well as for

---

[†] In Appendix B of this report Eq. (B-18) should have a minus sign and the denominator of Eq. (B-26) should have an additional factor j_{nm}.

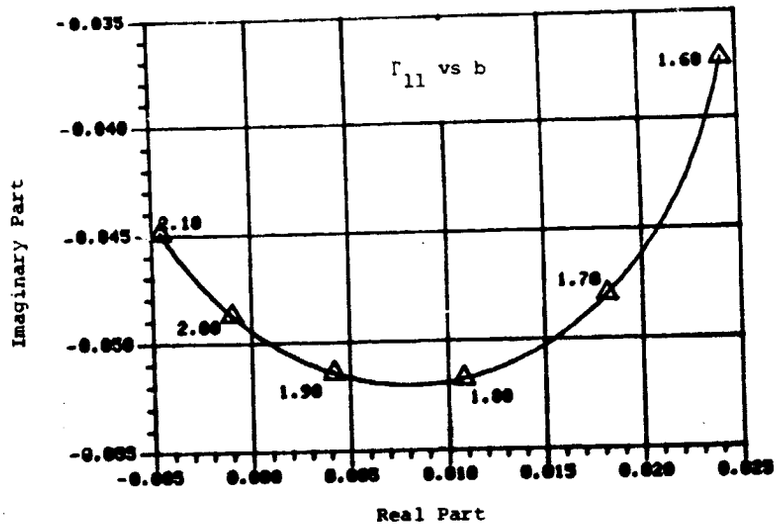

Fig. 2.3a TE_{11} mode aperture reflection coefficient.

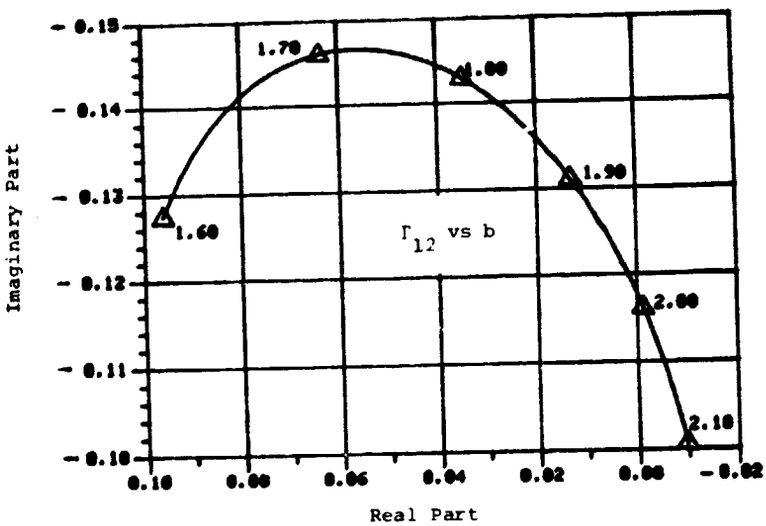

Fig. 2.3b TE_{11} to TM_{11} mode coupling coefficient.

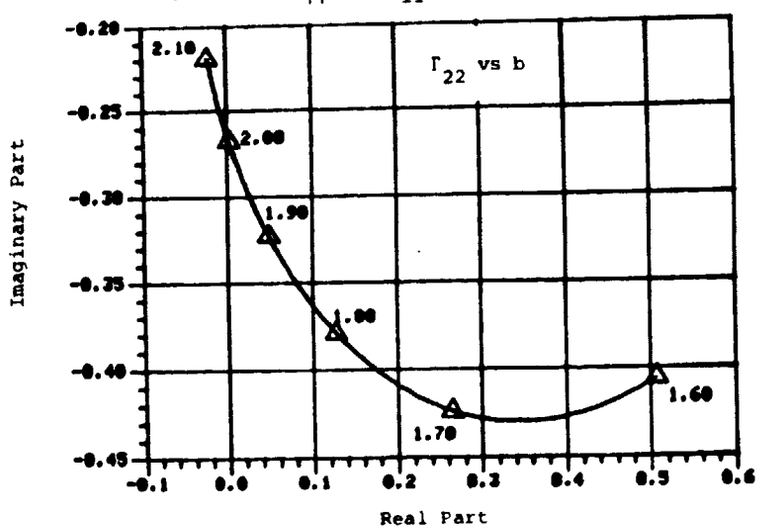

Fig. 2.3c TM_{11} mode aperture reflection coefficient.

Figure 2.3, TE_{11} and TM_{11} mode aperture reflection and coupling coefficients.

various relative amplitude values of combined incident TE_{11} and TM_{11} modes. The moding ratio giving the smallest maximum cross-polarization was found through a computer evaluation of the cross-polarization as a function of the moding ratio. The Weinstein solution is summarized in Appendix B.

The pure mode E- and H-plane patterns are shown in Fig.'s 2.4a-o. For comparison the patterns were also computed with the aperture field approximate method using the aperture electric field alone or using both the aperture electric and magnetic fields and taking the mode reflection coefficients into account (see Silver, 1949). The formulas used in the latter computation are summarized in Appendix C. Although the approximate methods give reasonably accurate patterns the accuracy is not sufficient to predict the cross-polarization with good accuracy.

The optimum moding ratio (ratio of incident TE_{11} mode amplitude to incident TM_{11} mode amplitude) for minimum cross-polarization is shown in Fig. 2.5. The moding ratio depends on the waveguide radius b and becomes smaller (a larger amount of the TM_{11} mode is required) as b becomes larger. The amplitude ratio is complex with a small positive imaginary component.[†]

The total radiated field in the $\phi = 0$ plane (E-plane) and the phase deviation from that of a spherical wave are shown in Fig.'s 2.6a-f. Note that for polar angles such that the field is above the -20 dB. level that the phase error is small - less than 10°. This is the useful range of the pattern for illuminating a paraboloid.

[†]The optimization of the feed was based on the criterion of minimum cross-polarization over range $0 < \theta \leq 78°$. If the range of θ is up to 90° the minimum achievable cross-polarization is approximately 2 dB. higher.

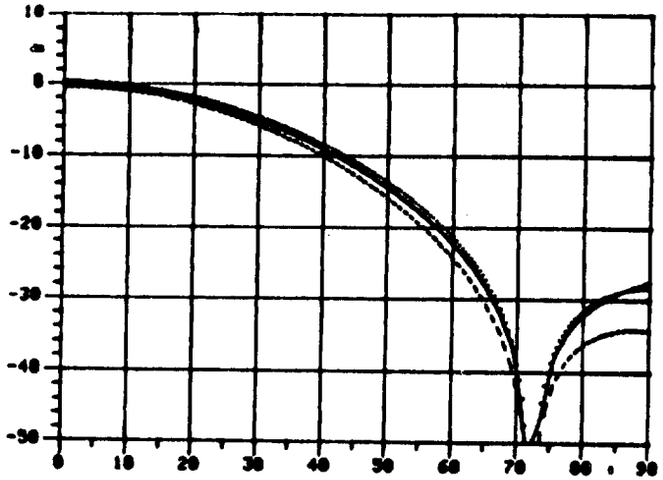

Fig. 2.4a TE_{11} mode E-plane radiation pattern, b = 1.6 cm.,
_____ exact, ... E-field only, ------ E-H field.

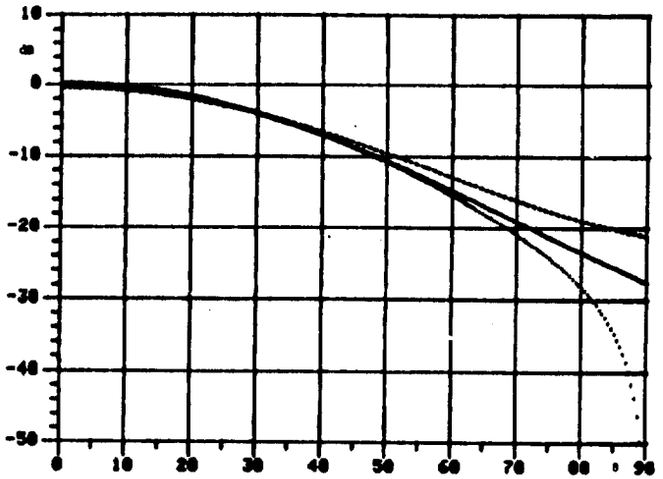

Fig. 2.4b TE_{11} mode H-plane pattern, b = 1.6 cm.,
_____ exact, ... E-field only, ------ E-H field.

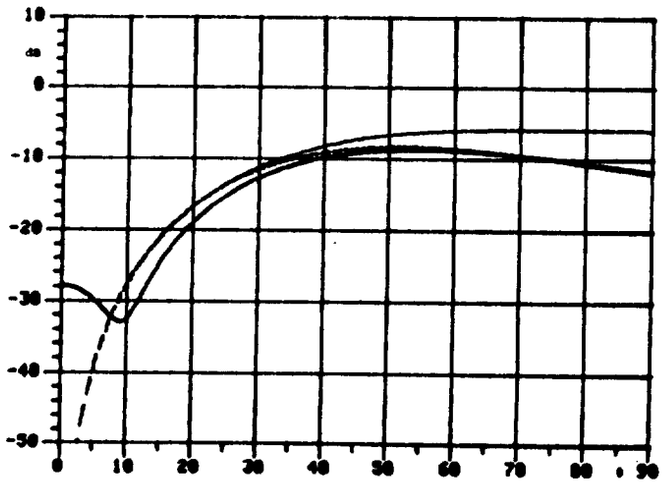

Fig. 2.4c TM_{11} mode E-plane radiation pattern, b = 1.6 cm.,
_____ exact, ... E-field only, ------ E-H field.

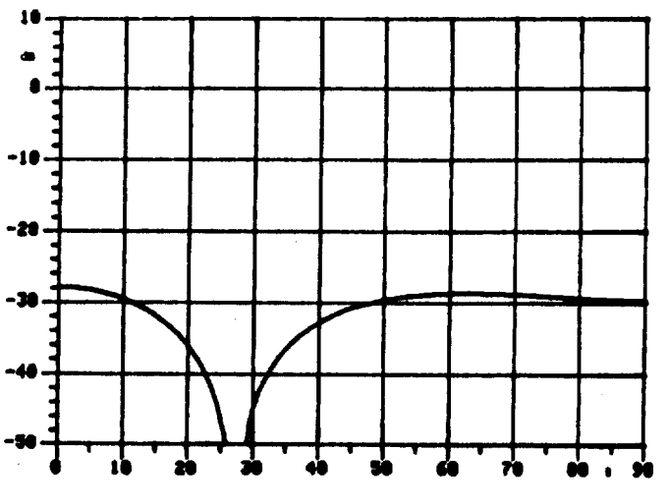

Fig. 2.4d TM_{11} mode H-plane radiation pattern, b = 1.6 cm.,
_____ eact, aperture field method gives zero.

Figure 2.4, Circular waveguide radiation patterns.

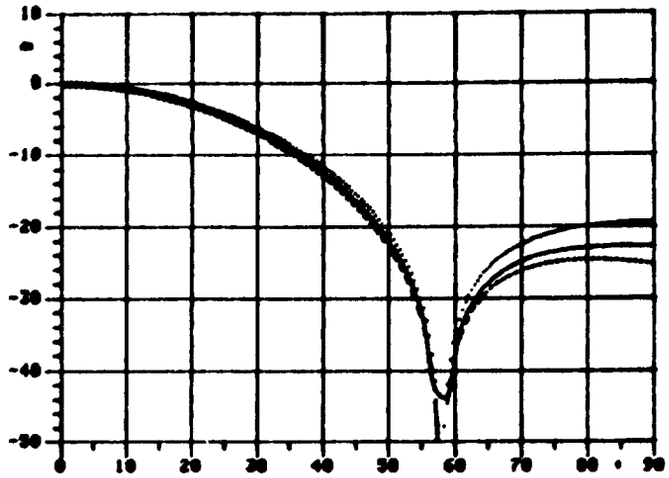

Fig. 2.4e TE_{11} mode E-plane radiation pattern, b = 1.8 cm.,
_____ exact, ... E-field only, ------ E-H field.

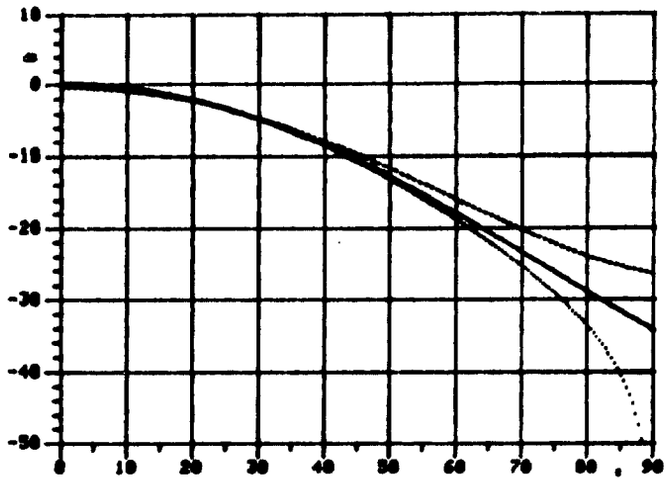

Fig. 2.4f TE_{11} mode H-plane radiation pattern b = 1.8 cm.,
_____ exact, ... E-field only, ------ E-H field.

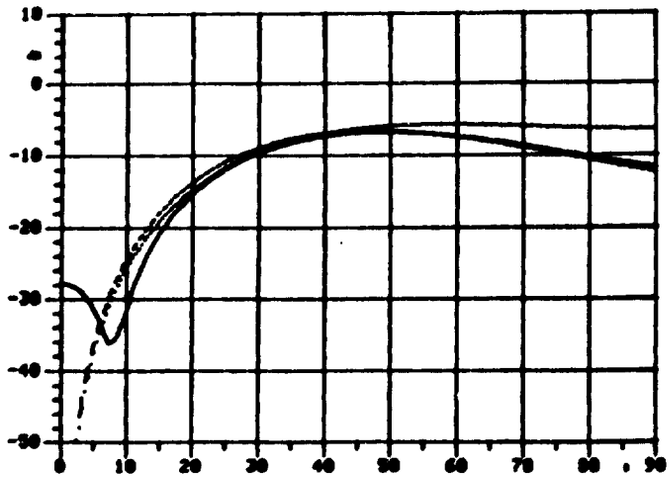

Fig. 2.4g TM_{11} mode E-plane radiation pattern, b = 1.8 cm.,
_____ exact, ... E-field only, ------ E-H field.

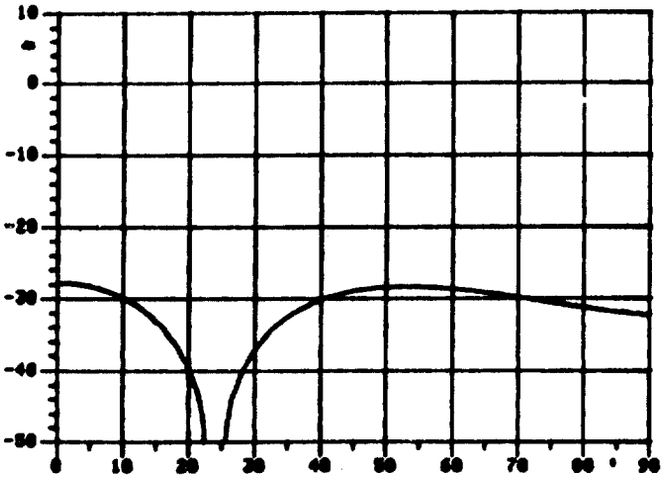

Fig. 2.4h TM_{11} mode H-plane radiation pattern, b = 1.8 cm.,
_____ exact, aperture field method give zero.

Figure 2.4, (cont.) Circular waveguide radiation patterns.

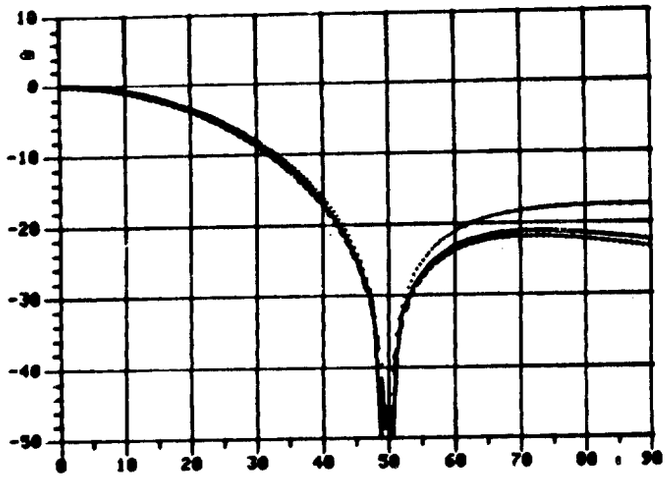

Fig. 2.4i TE_{11} mode E-plane radiation pattern, b = 2 cm.,

_____ exact, ... E-field only, ------ E-H field.

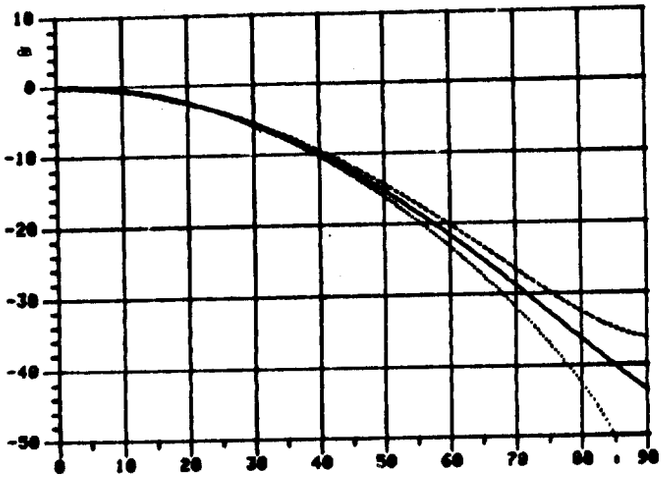

Fig. 2.4j TE_{11} mode H-plane radiation pattern, b = 2 cm.,

_____ exact, ... E-field only, ------ E-H field.

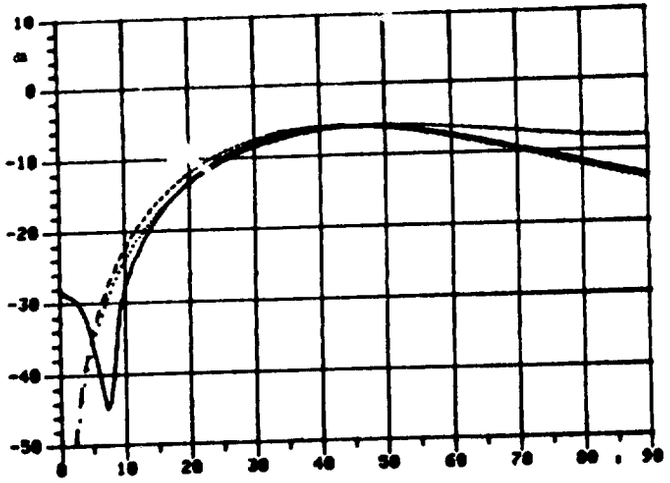

Fig. 2.4k TM_{11} mode E-plane radiation pattern, b = 2 cm.,

_____ exact, ... E-field only, ------ E-H field.

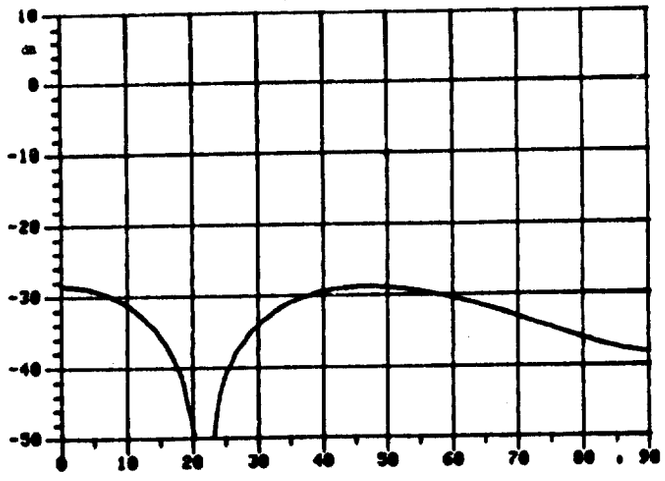

Fig. 2.4l TM_{11} mode H-plane radiation pattern, b = 2 cm.,

_____ exact, aperture field method gives zero.

Figure 2.4, (cont.) Circular waveguide radiation patterns.

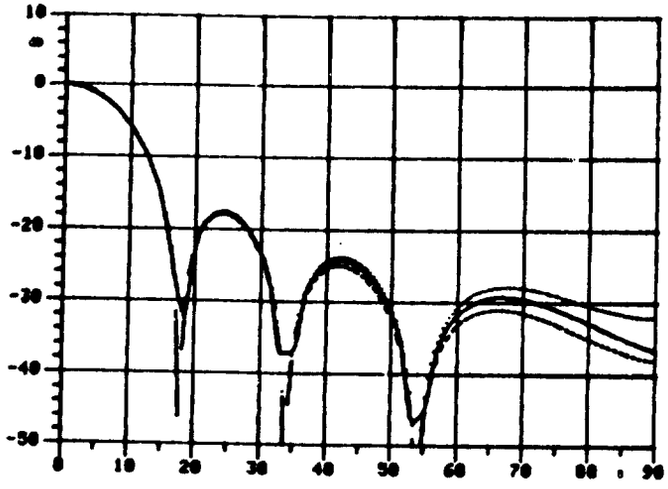

Fig. 2.4m TE_{11} mode E-plane radiation pattern, b = 5 cm.,

_____ exact, ... E-plane only, ------ E-H field.

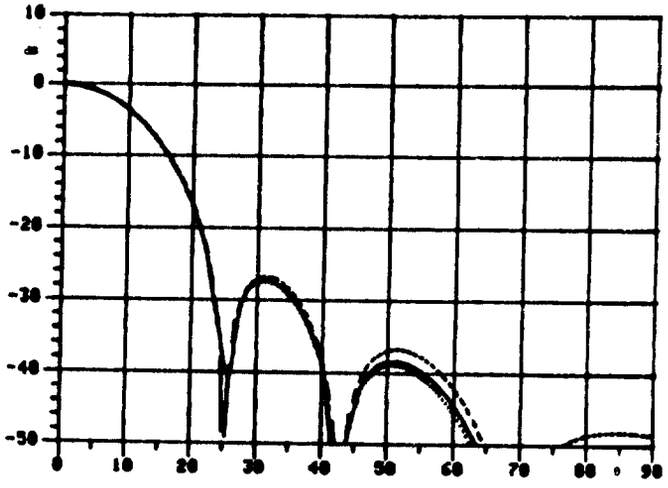

Fig. 2.4n TE_{11} mode H-plane radiation pattern, b = 5 cm.,

_____ exact, ... E-field only, ------ E-H field.

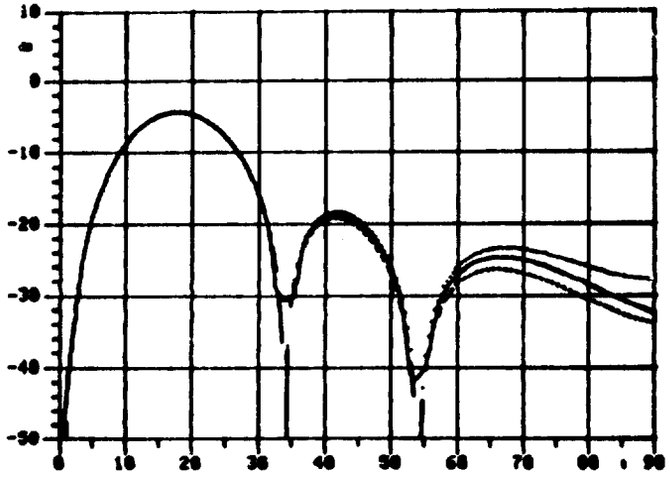

Fig. 2.4o TM_{11} mode E-plane radiation pattern, b = 5 cm.,

_____ exact, ... E-field only, ------ E-H field.

H-plane pattern is below - 50 dB.

Figure 2.4, (cont.) Circular waveguide radiation patterns.

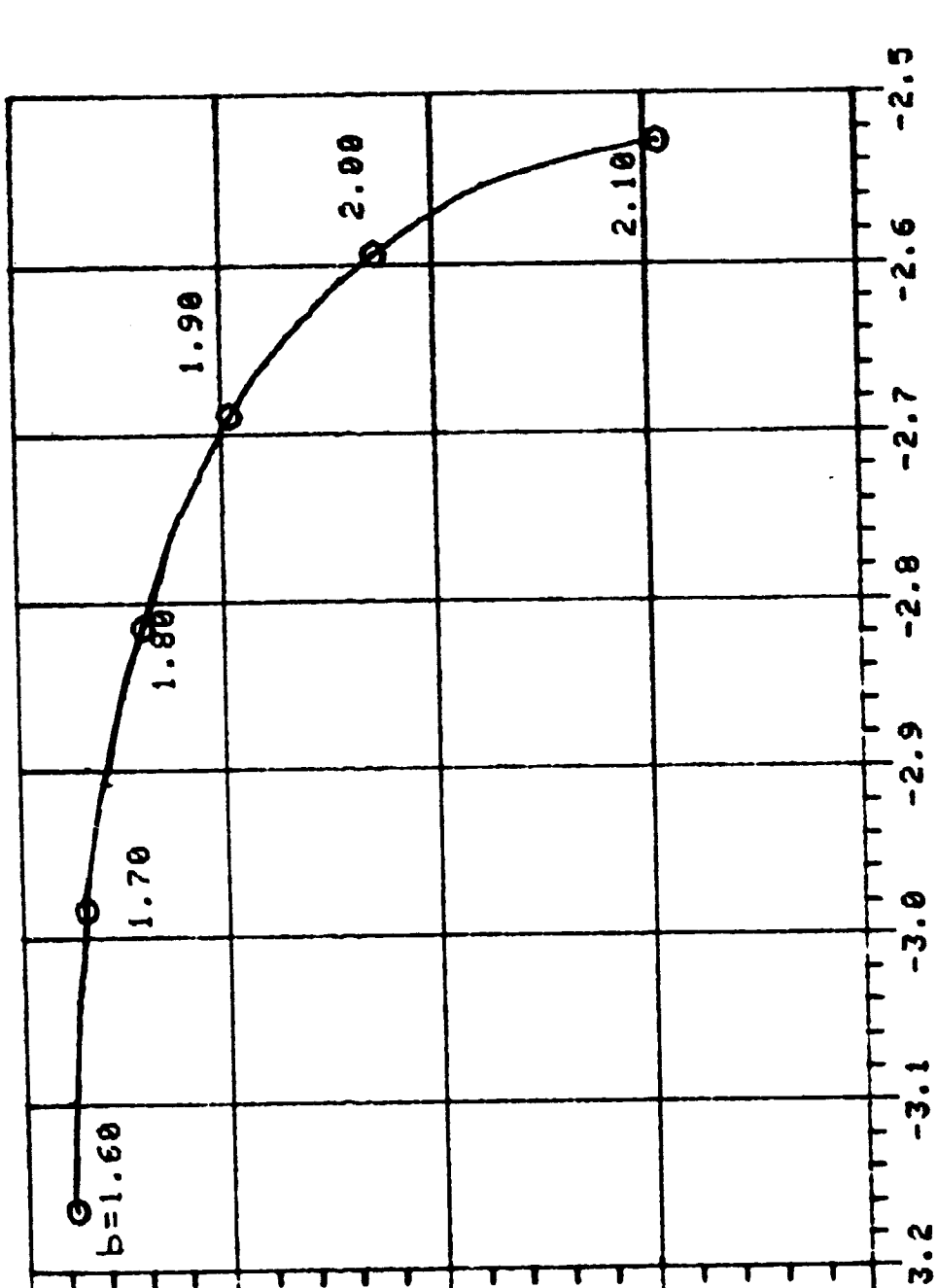

Figure 2.5 Optimum TE_{11}/TM_{11} incident mode ratio at aperture for minimum cross polarization as a function of b in cm.

The co- and cross-polarized patterns in the $\phi = 45°$ plane for the dual-mode feed with the optimum moding ratio is shown in Fig's. 2.7a-f. The maximum cross-polarization is very small being close to-58 dB. With the optimum moding ratio the dual-mode feed has excellent cross-polarization discrimination. Dual mode horns of the type studied by Potter and with small flare angles and apertures should have comparable performance.

For comparison purposes the radiation patterns and cross-polarization properties of the dual-mode feed was also evaluated using the aperture field method to evaluate the radiated field and neglecting reflection and mode conversion at the aperture. The results of this evaluation is summarized in Appendix C. It was found that the optimum moding ratio when using the combined aperture electric and magnetic fields was -2.5 and the predicted cross-polarization was higher than that given by the exact theory. The conclusion arrived at is that approximate methods of computing the radiation from small aperture feeds will not, in general, give good results for the cross-polarized field.

2.5 OPTIMUM FEED DIMENSIONS

By using the bifurcation junction scattering matrix and the aperture scattering matrix parameters the resultant TE_{11} and TM_{11} incident mode amplitudes at the aperture can be found using conventional transmission line theory. The moding ratio can then be computed as a function of the parameters S and T for a given set of waveguide radii a and b. In addition the cross-polarization level can be readily found for any given set of parameters as well as the optimum values of S and T that gives the smallest cross-polarization.

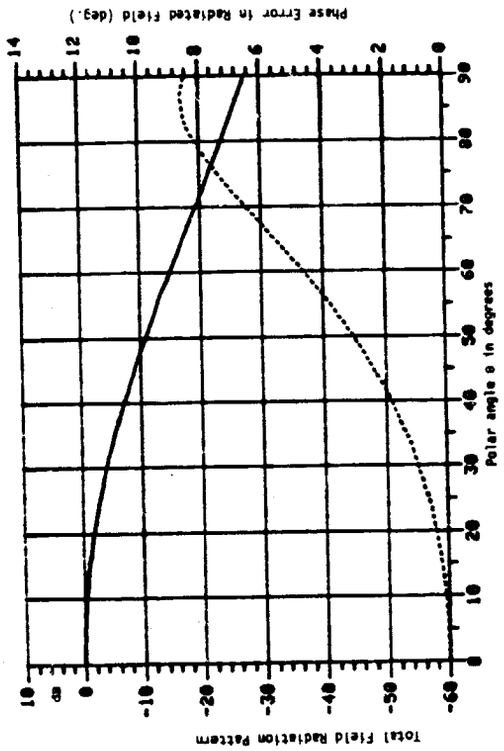

Fig. 2.6a b = 1.6 cm., ϕ = 0°

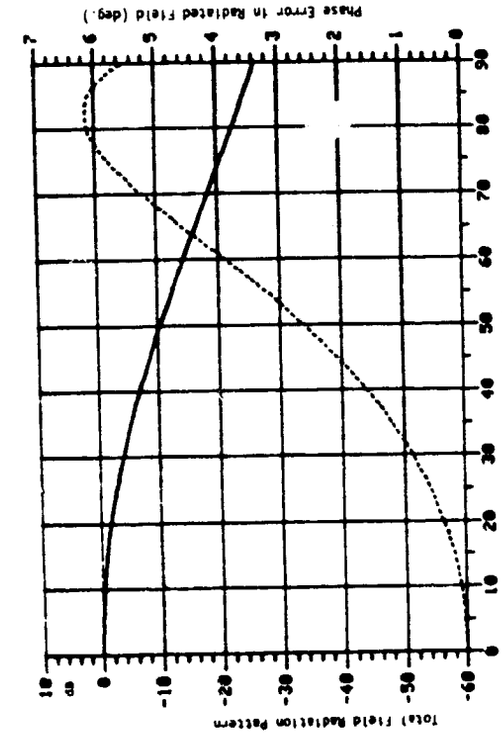

Fig. 2.6b b = 1.65 cm., ϕ = 0°

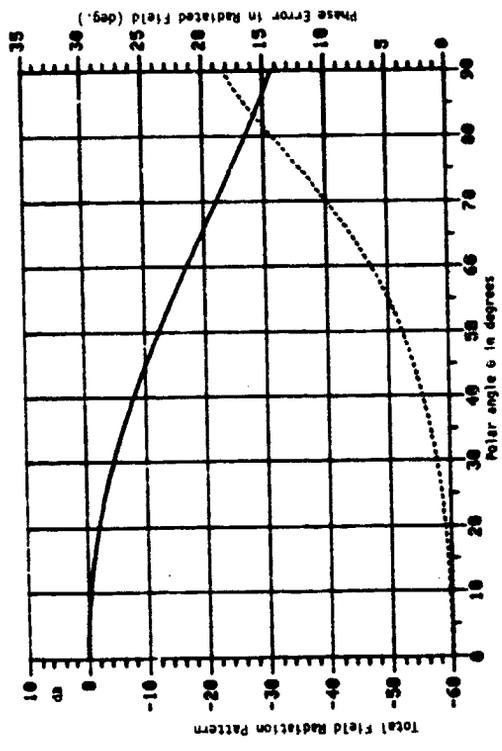

Fig. 2.6c b = 1.7 cm., ϕ = 0°

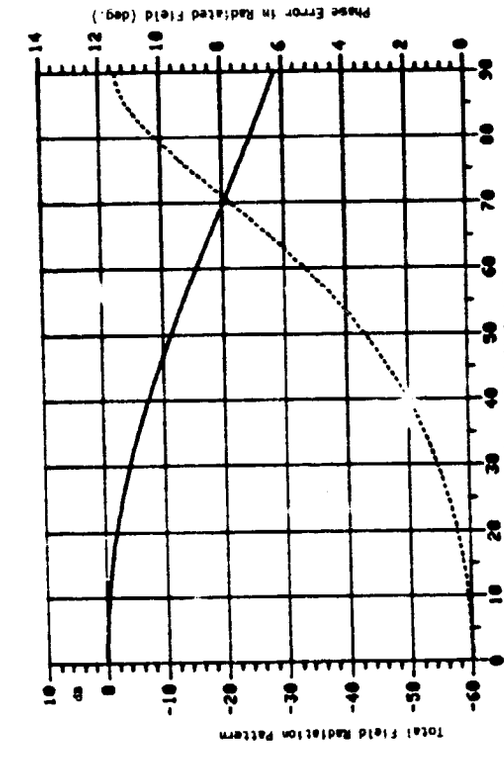

Fig. 2.6d b = 1.8 cm., ϕ = 0°

Figure 2.6, Dual-mode circular waveguide radiation patterns (optimum modeing ratio).

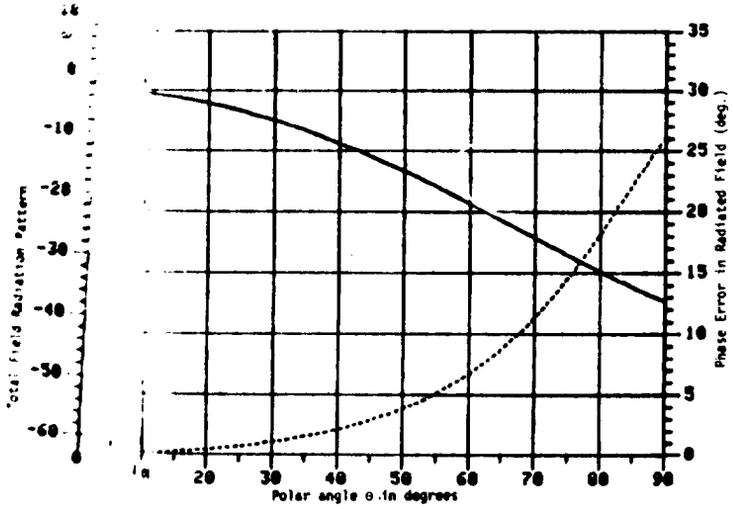

Fig. 2.6e b = 1.9 cm., ϕ = 0°

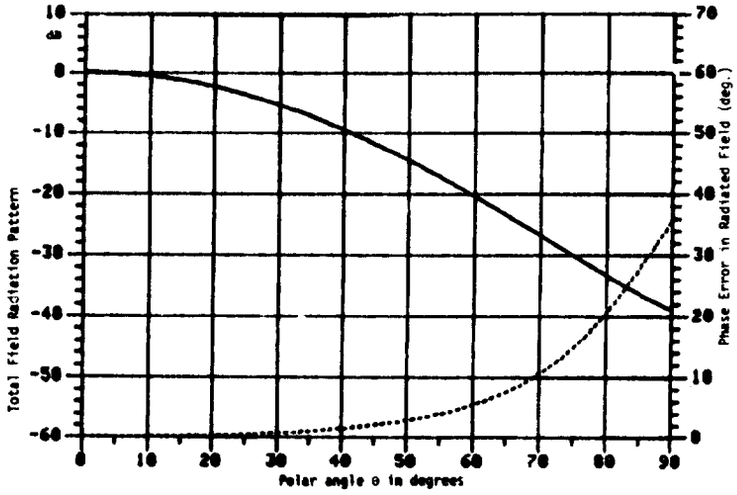

Fig. 2.6f b = 2 cm., ϕ = 0°

ure 2.6, (cont.) Dual-mode circular waveguide radiation patterns (optimum modeing ratio).

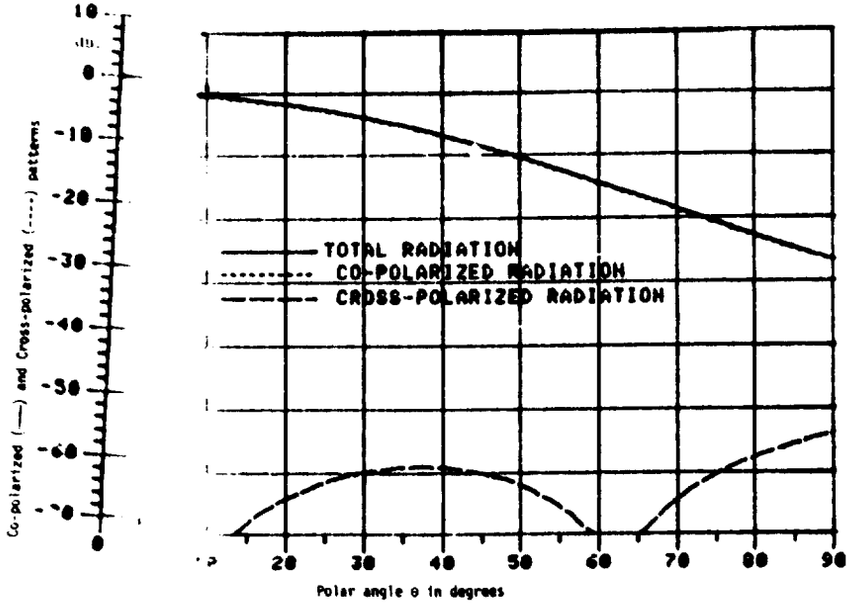

2.7a b = 1.6 cm., ϕ = 45°

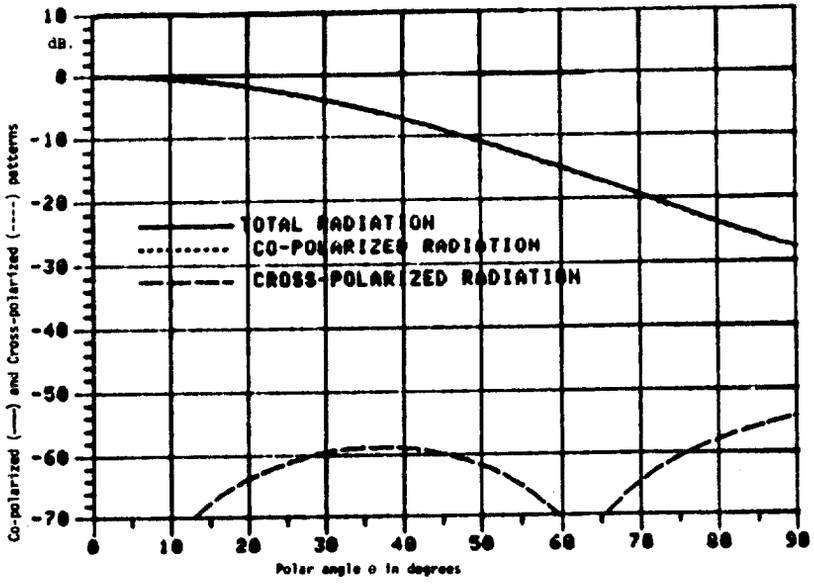

Fig. 2.7b b = 1.65 cm., ϕ = 45°

ure 2.7, Dual-mode circular waveguide radiation patterns (optimum modeing ratio).

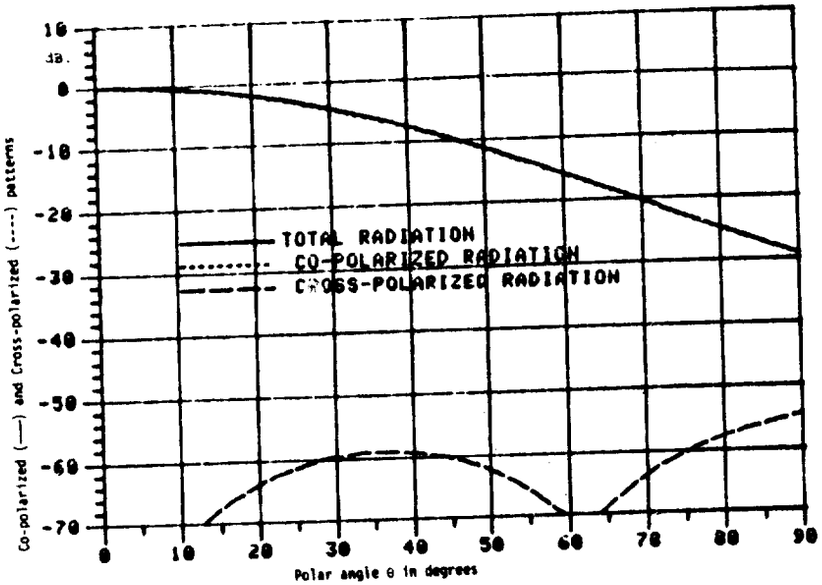

Fig. 2.7c b = 1.7 cm., ϕ = 45°

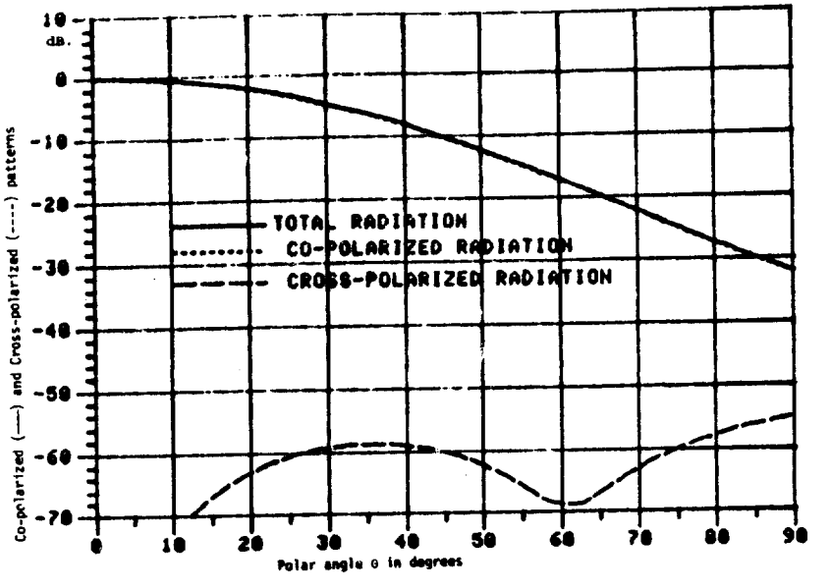

Fig. 2.7d b = 1.8 cm., ϕ = 45°

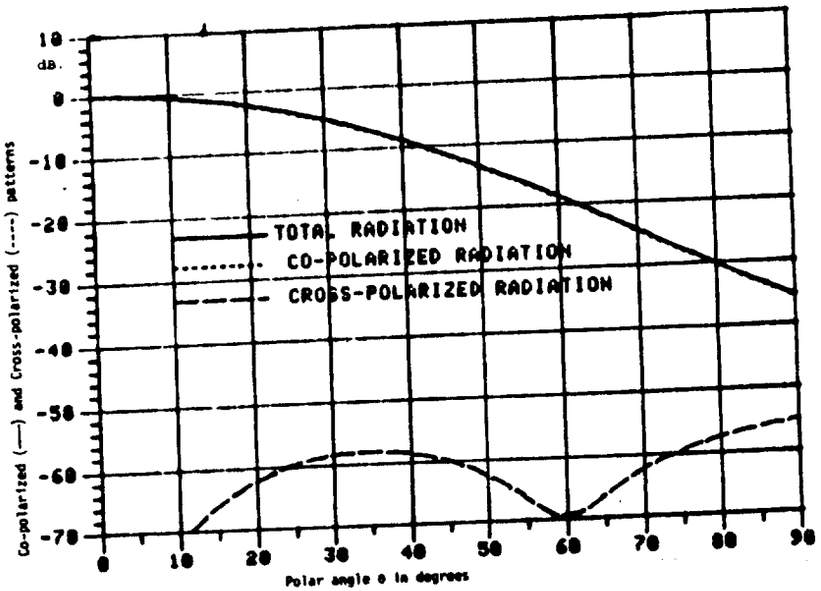

Fig. 2.7e b = 1.9 cm., ϕ = 45°

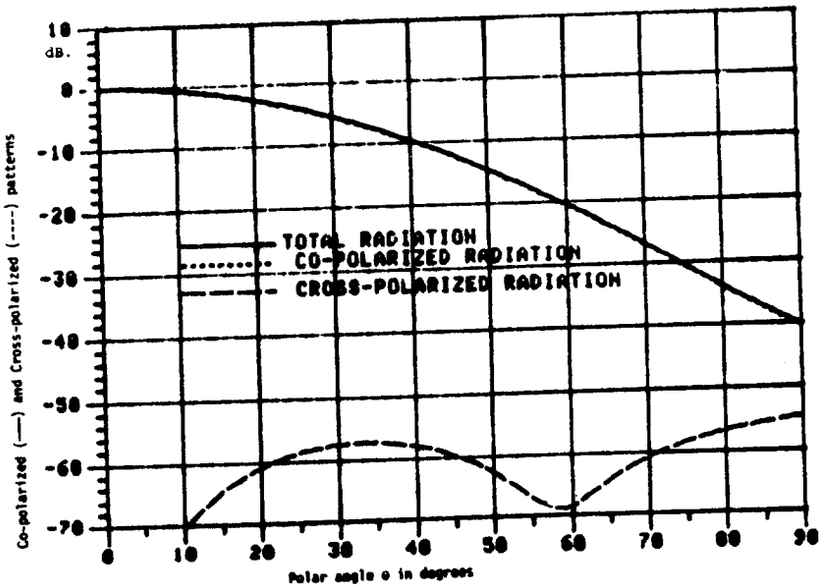

Fig. 2.7f b = 2 cm., ϕ = 45°

Figure 2.7, (cont.) Dual-mode circular waveguide radiation patterns (optimum modeing ratio).

The ratio of the TE_{11} to TM_{11} incident mode amplitudes at the aperture is given by

$$\frac{TE_{11}}{TM_{11}} = \frac{(e^{j\theta_2} - S'_{24}\Gamma_{12}e^{-j\theta_1} - S'_{44}\Gamma_{22}e^{-j\theta_2})S'_{12} + (S'_{24}\Gamma_{22}e^{-j\theta_2} + S'_{22}\Gamma_{12}e^{-j\theta_1})S'_{14}}{(S'_{24}\Gamma_{11}e^{-j\theta_1} + S'_{44}\Gamma_{12}e^{-j\theta_2})S'_{12} + (e^{j\theta_1} - S'_{24}\Gamma_{12}e^{-j\theta_2} - S'_{22}\Gamma_{11}e^{-j\theta_1})S'_{14}} \tag{2.2}$$

where $\theta_1 = \beta_{21}T$ and $\theta_2 = \gamma_{21}T$. The S'_{ij} depend on the parameter S as given by (2.1).

Figures 2.8-2.10 show the minimum cross-polarization in dB. as a function of the inner guide radius a for a given value of outer guide radius b, and the corresponding best values for the parameters S and T Note that unless a is above a certain minimum value the smallest cross-polarization obtained is not as low as can be achieved, e.g. in Fig. 2.8, a must be greater than 1.28 cm. for b = 1.6 cm. in order to obtain a cross-polarization as low as -58 dB. There are two solutions for S and T shown in the figures - the second solution being indicated by the dotted curves. For a pair of values for a and b that yield minimum cross-polarization the figures give the optimum values for S and T. In the figures a and b are in cm. and the data applies for a frequency of 12 ghz. but may be scaled for other frequencies.

In order to show the sensitivity of the cross-polarization to changes in S and T, contour plots of cross-polarization in the S-T plane for various a and b values were generated. These are shown in Fig's. 2.11a-2.11ℓ for b = 1.6 cm., in Fig's. 2.12a-f for b = 1.7 cm. and Fig's. 2.13a-d for b = 1.8 cm. Note that for b = 1.8 cm. the minimum cross-polarization

cannot be achieved without increasing a beyond 1.45 cm. which would then allow the TM_{11} mode to propagate in the smaller waveguide. These figures also show the minimum cross-polarization that can be obtained for a given pair of a and b values. For example, Fig. 2.11a shows that with a = 1 cm., b = 1.6 cm. the minimum cross-polarization is only -32.1 dB. For optimum cross-polarization a must be increased to around 1.3 cm. as shown in Fig.2.11e (see also Fig. 2.8).

2.6 COAXIAL FEED PERFORMANCE - THEORETICAL

The minimum cross-polarization at a particular frequency for the dual-mode coaxial feed was shown to be around -58dB. in the previous section. In order for this feed to be useful for a satellite system it must have a reasonable bandwidth. In order to obtain information on the bandwidth the following quantities: maximum cross-polarization, maximum phase error in radiation pattern, and the input reflection coefficient $|S_{11}|$ were evaluated as a function of the percent deviation in frequency from the design value of 12 ghz. This data is given in Figures 2.14a through 14p for various optimum feeds with different a and b values.† The bandwidth will be chosen as the frequency band over which the cross-polarization remains below -30dB. On this basis the bandwidth is in the range of 4.5 to 5 percent. The curves indicate that the cross-polarization, input reflection coefficient, and phase error increase more rapidly with frequency below the design value than for frequencies above the design value. Over the bandwidth, as defined above, the input reflection coefficient remains below 0.05 corresponding to a VSWR of 1.1. Hence the feed does have a very good impedance match to the input waveguide.

---

†In these figures A and B are the waveguide radii. A,B,S, and T are in cm.

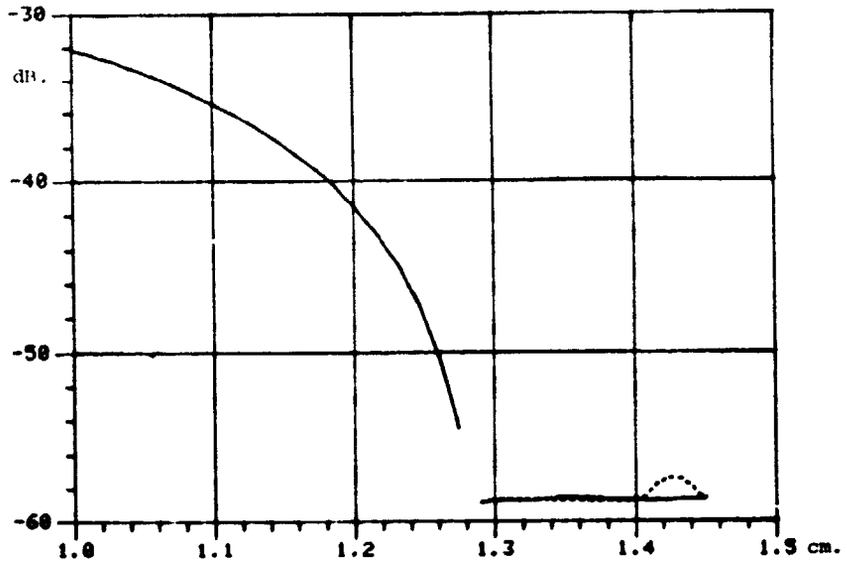

Fig. 2.8a Cross-polarization vs. a for b = 1.6 cm.

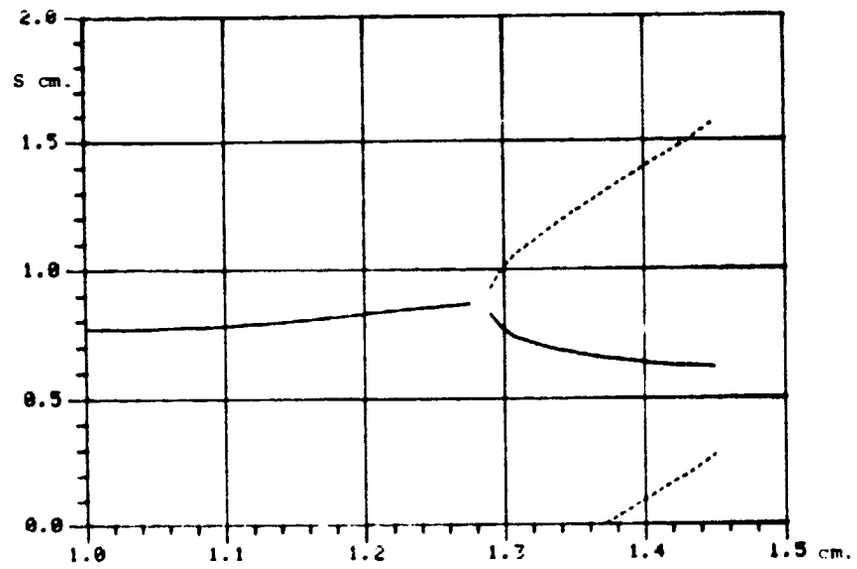

Fig. 2.8b S vs. a for b = 1.6 cm.

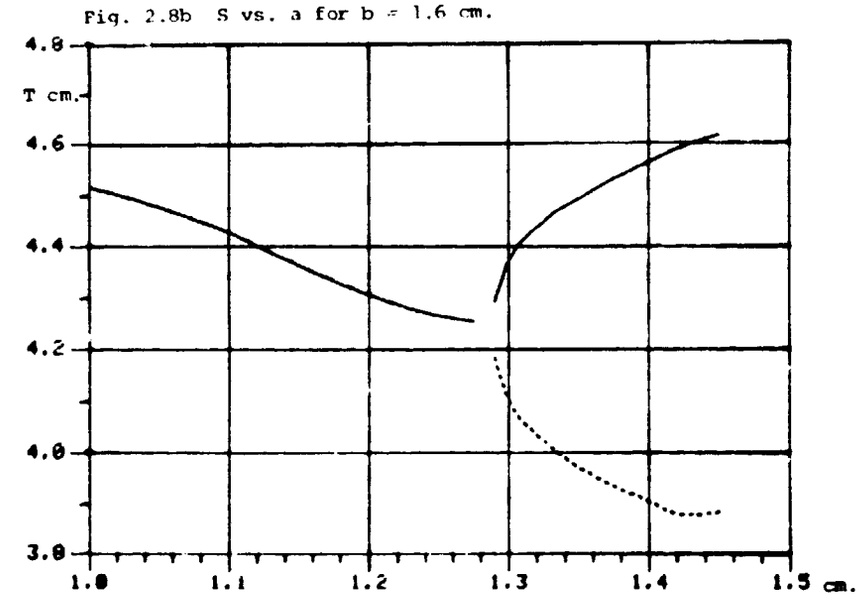

Fig. 2.8c T vs. a for b = 1.6 cm.

Figure 2.8. Optimum feed parameters for b = 1.6 cm.

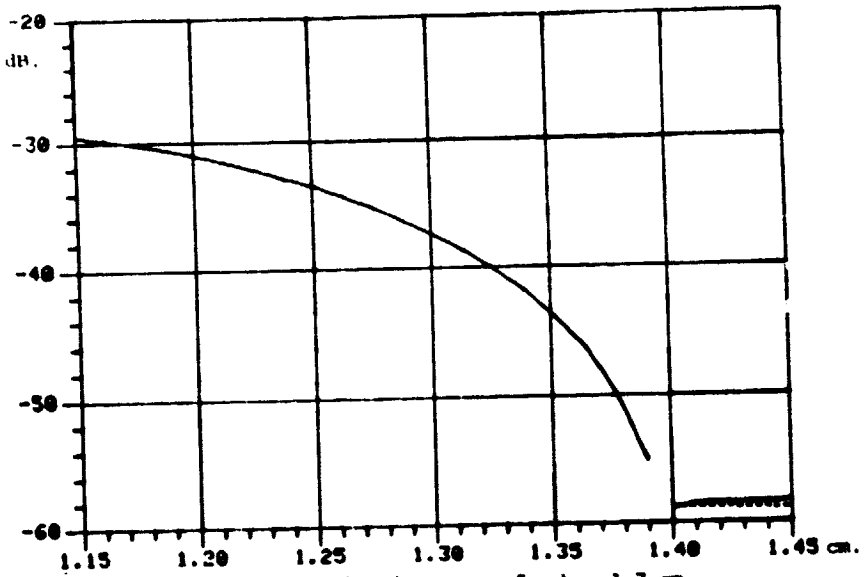

Fig. 2.9a Cross-polarization vs. a for b = 1.7 cm.

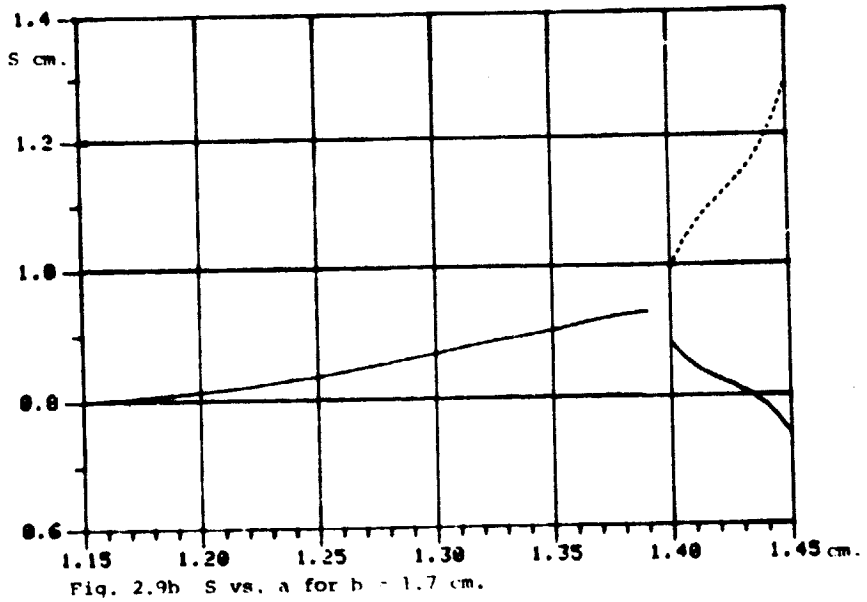

Fig. 2.9b S vs. a for b = 1.7 cm.

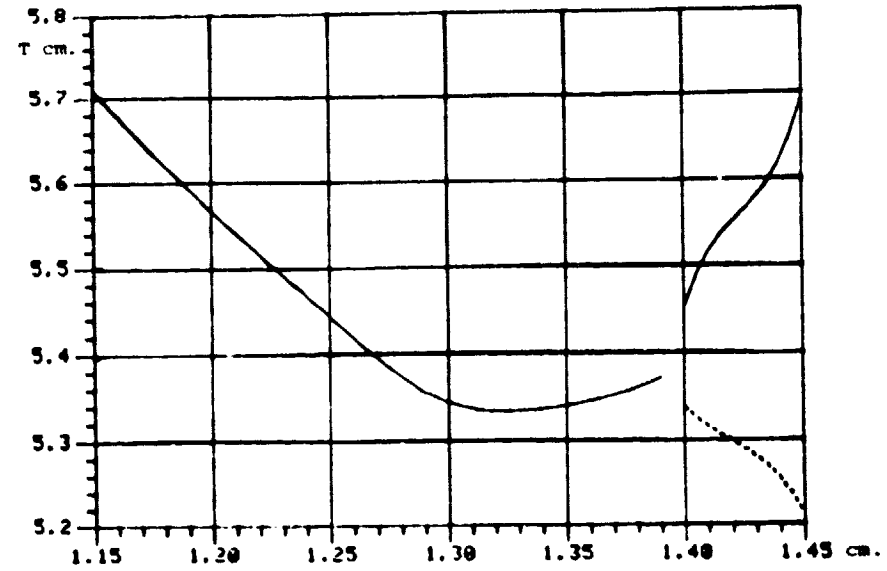

Fig. 2.9c T vs. a for b = 1.7 cm.

Figure 2.9. Optimum feed parameters for b = 1.7 cm.

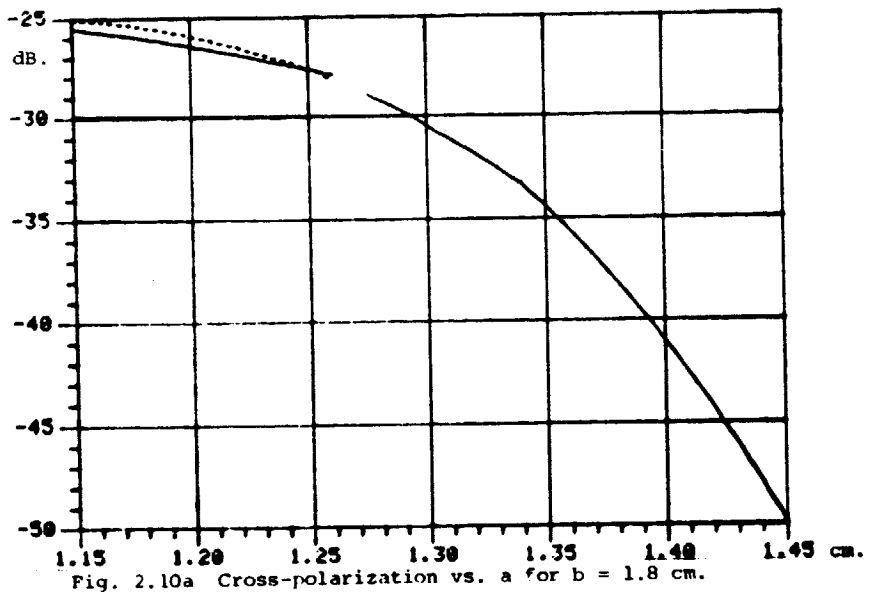

Fig. 2.10a Cross-polarization vs. a for b = 1.8 cm.

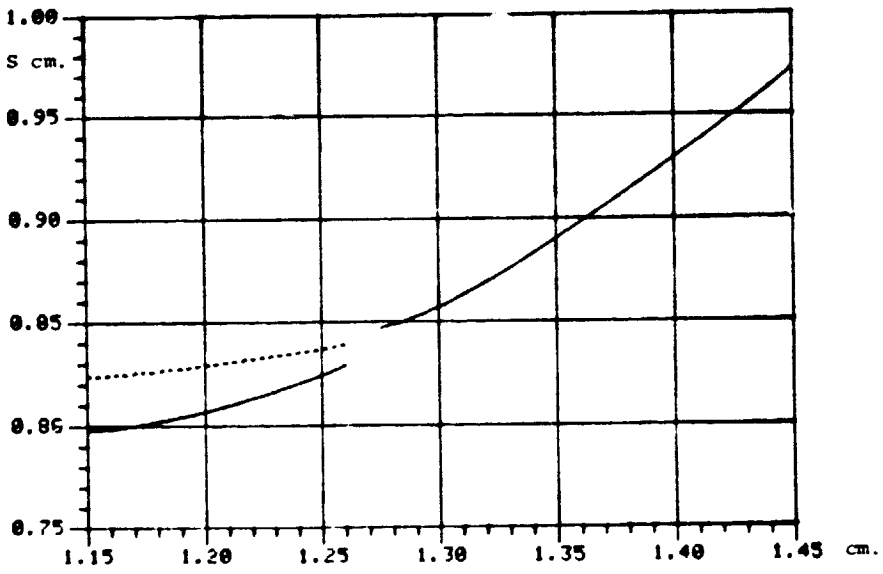

Fig. 2.10b S vs. a for b = 1.8 cm.

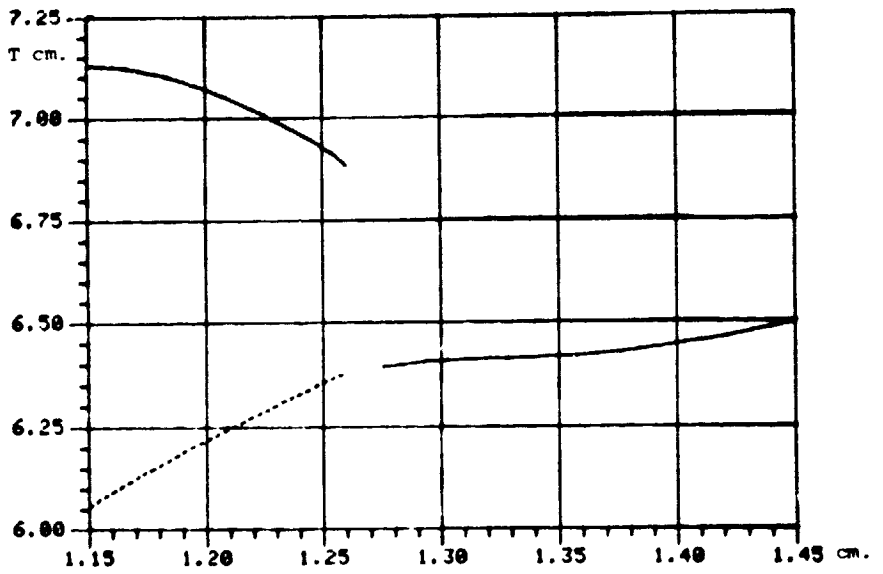

Fig. 2.10c T vs. a for b = 1.8 cm.

Figure 2.10, Optimum feed parameters for b = 1.8 cm.

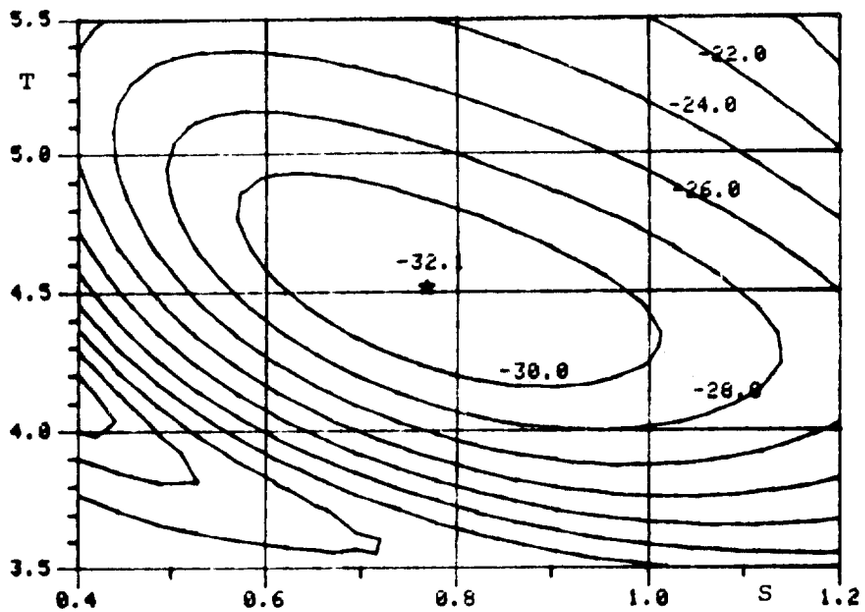

Fig. 2.11a Cross-polarization for a = 1 cm., b = 1.6 cm.

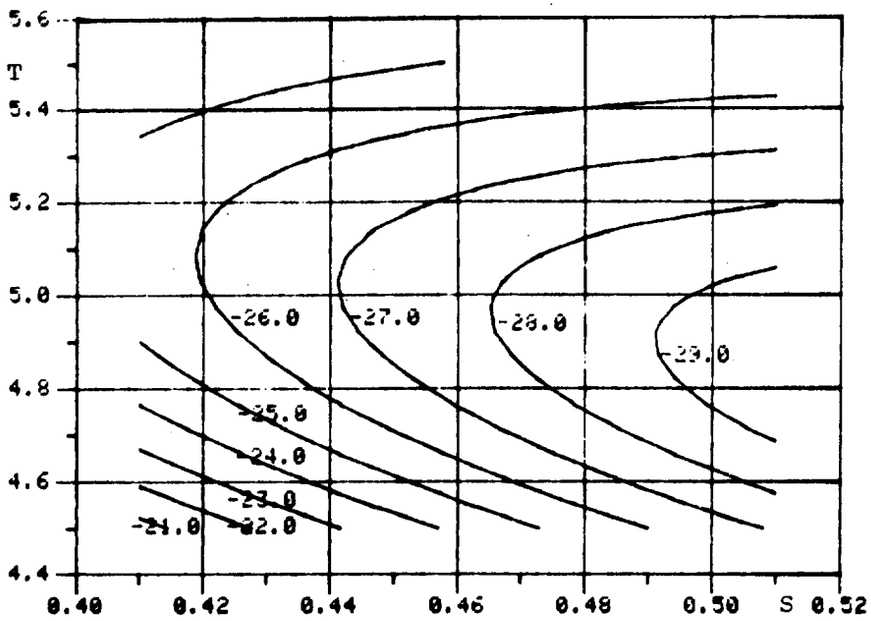

Fig. 2.11b Cross-polarization for a=1.07 cm., b=1.6 cm.

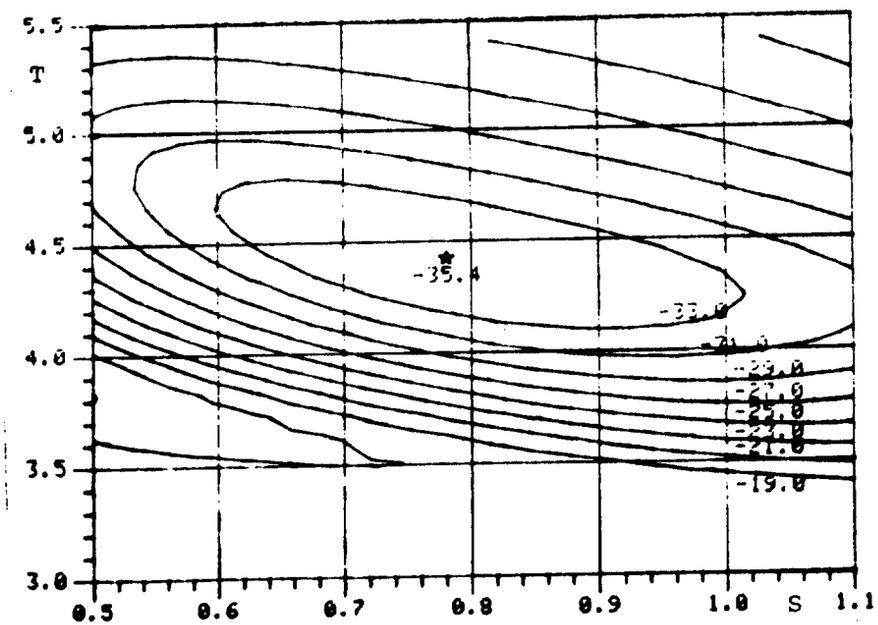

Fig. 2.11c Cross-polarization for a=1.1 cm., b=1.6 cm.

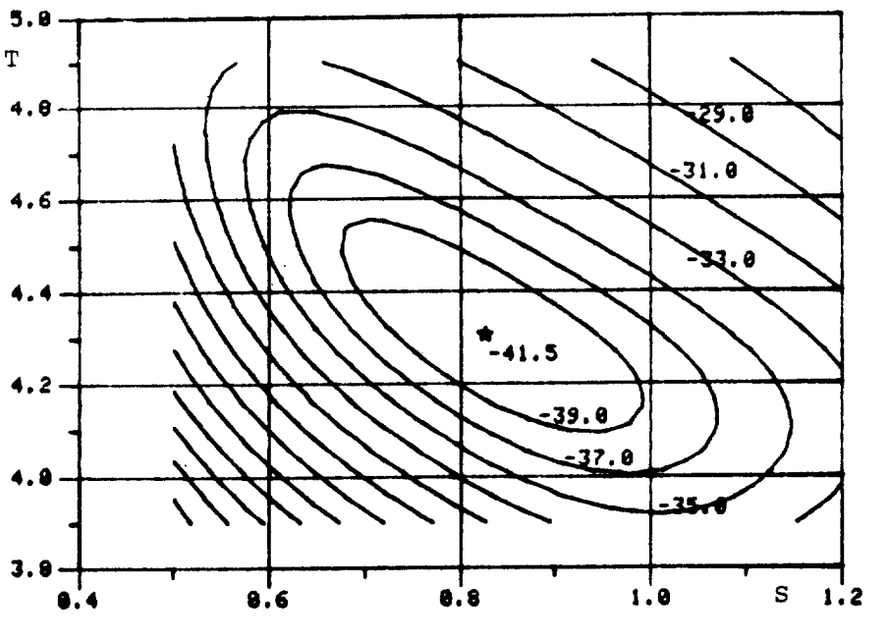

Fig. 2.11d Cross-polarization for a=1.2 cm., b=1.6 cm.

Figure 2.11, Cross-polarization of dual-mode feed as a function of S and T.

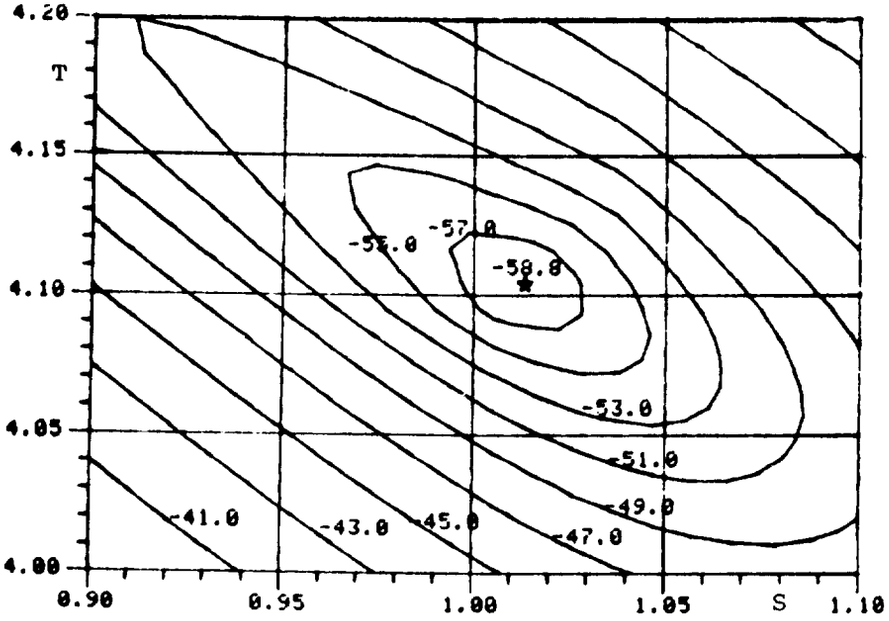

Fig. 2.11e Cross-polarization for a=1.3 cm., b=1.6 cm.

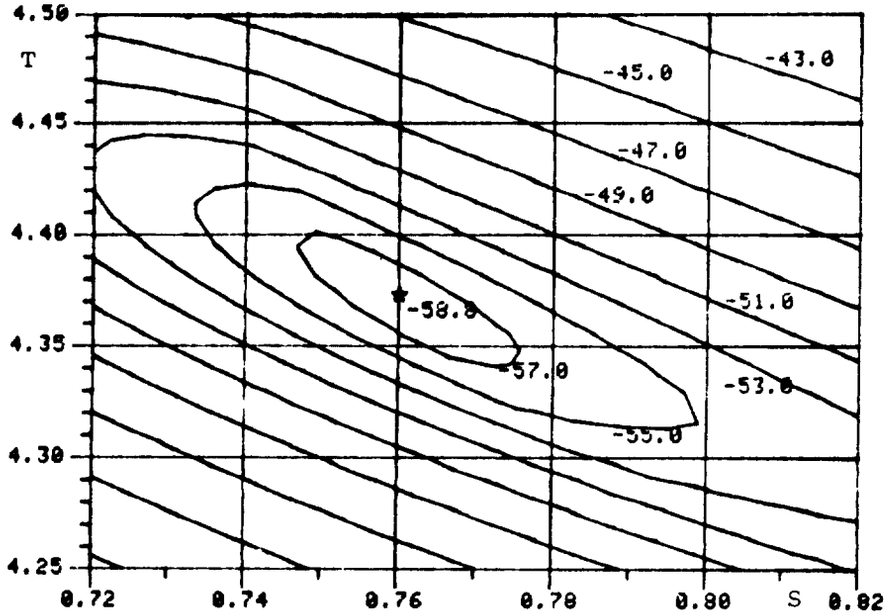

Fig. 2.11f Cross-polarization for a=1.3 cm., b=1.6 cm.

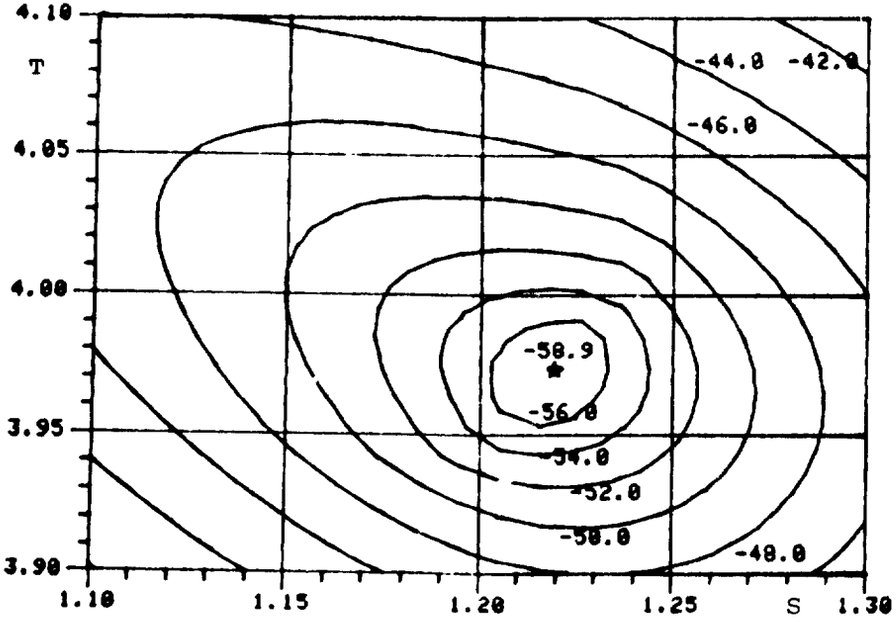

Fig. 2.11g Cross-polarization for a=1.35 cm., b=1.6 cm.

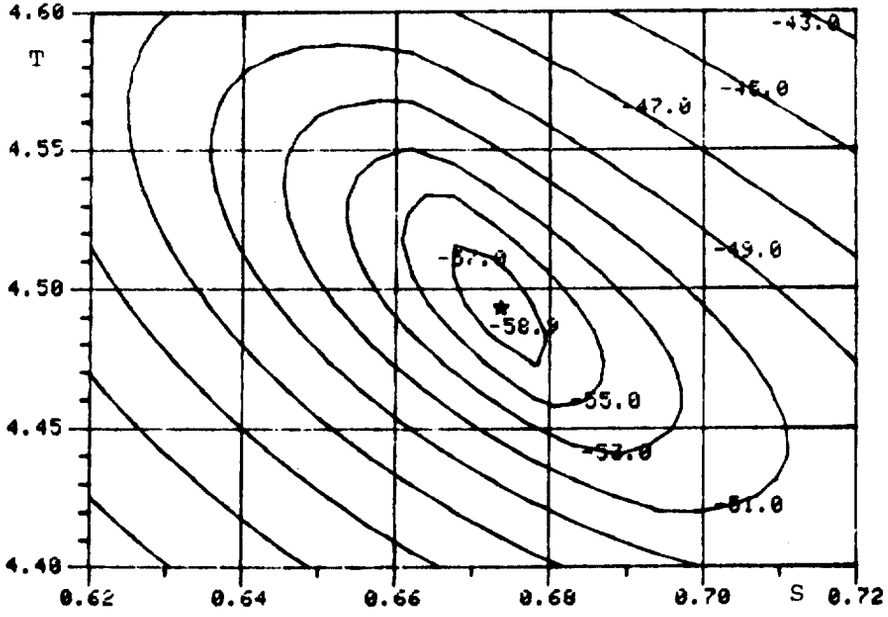

Fig. 2.11h Cross-polarization for a=1.35 cm., b=1.6 cm.

Figure 2.11, (cont.) Cross-polarization of dual-mode feed as a function of S and T.

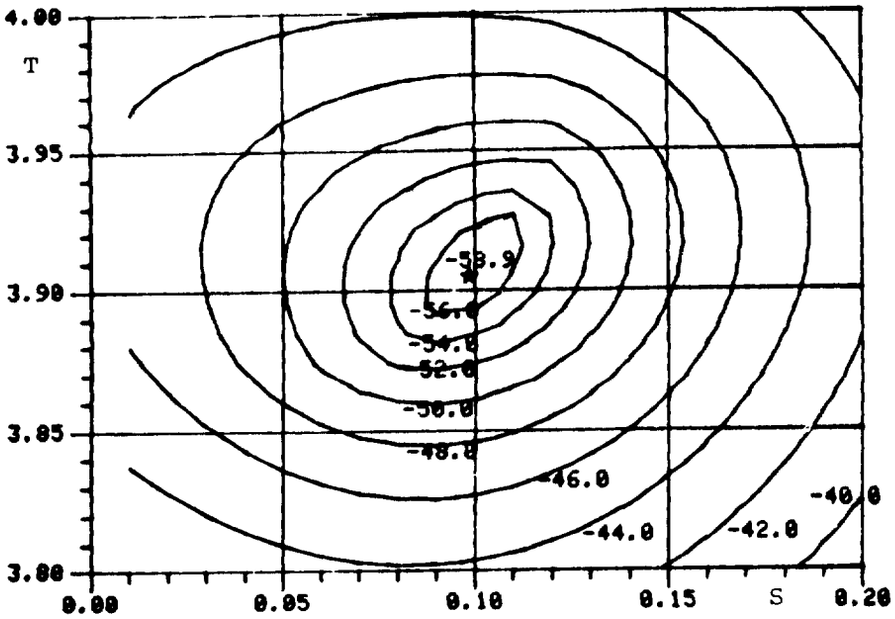

Fig. 2.11i Cross-polarization for a=1.4 cm., b=1.6 cm.

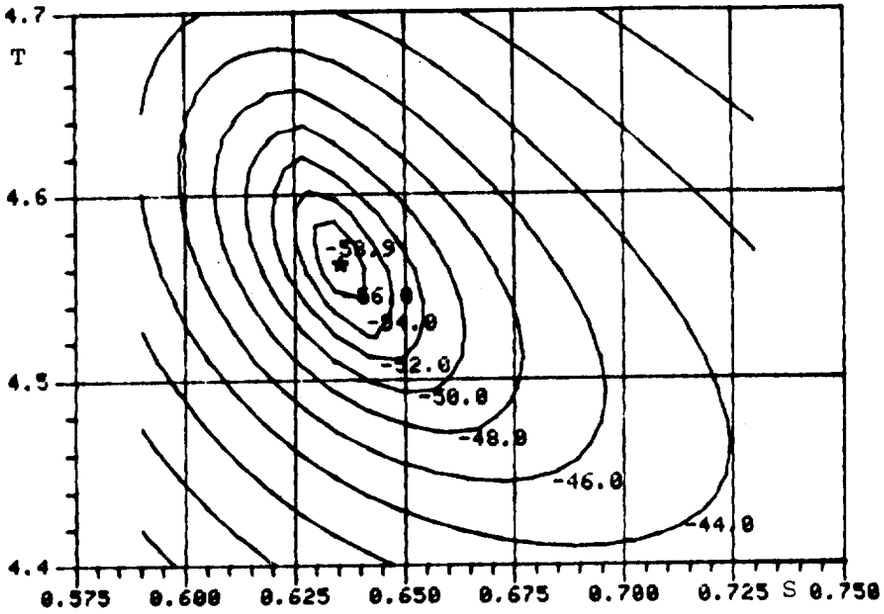

Fig. 2.11j Cross-polarization for a=1.4 cm., b=1.6 cm.

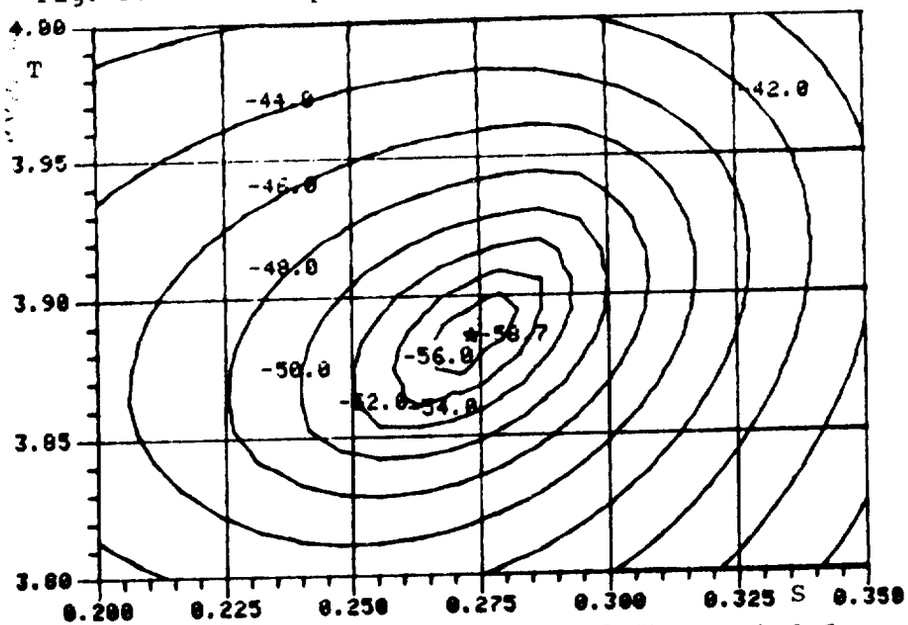

Fig. 2.11k Cross-polarization for a=1.45 cm., b=1.6 cm.

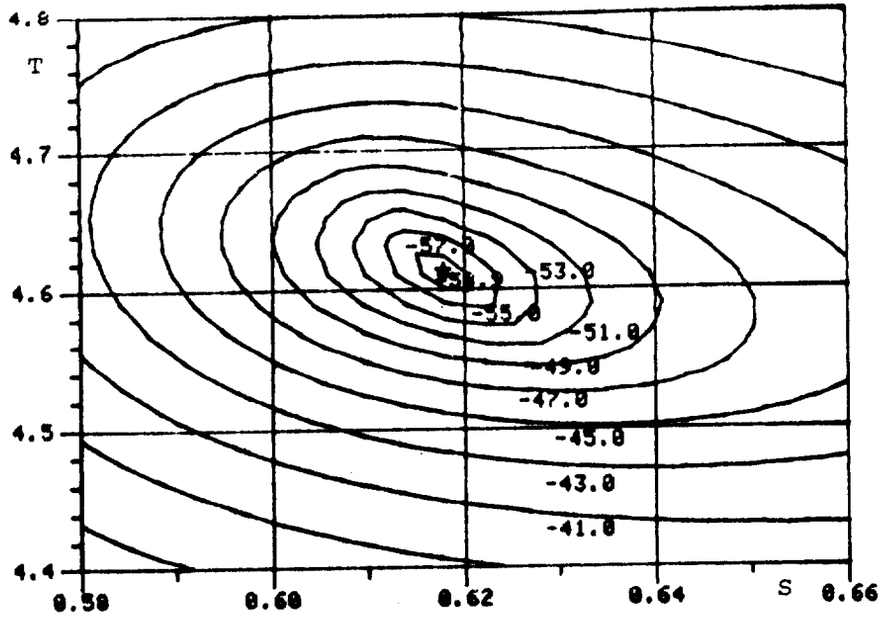

Fig. 2.11ℓ Cross-polarization for a=1.45 cm., b=1.6 cm.

Figure 2.11, (cont.) Cross-polarization of dual-mode feed as a function of S and T.

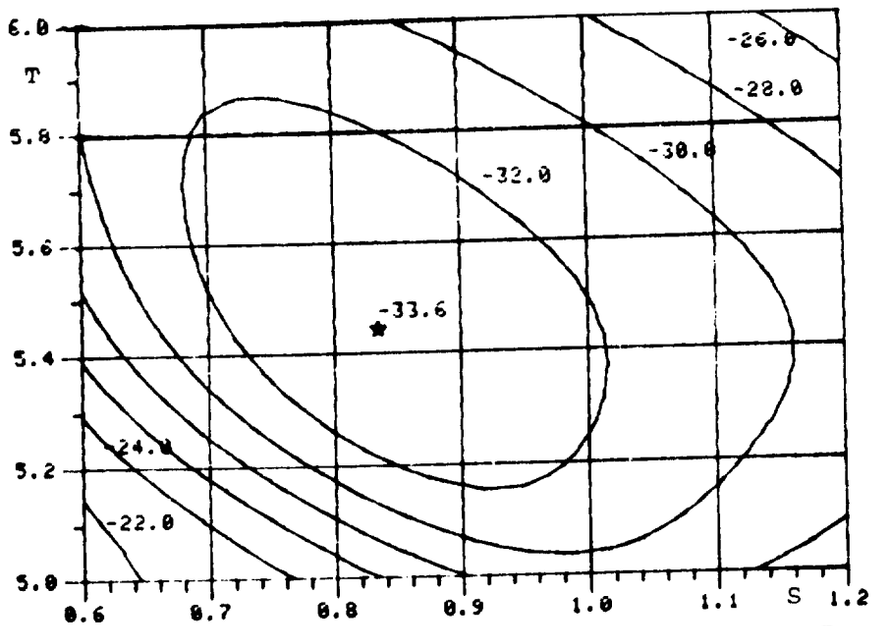

Fig. 2.12a Cross-polarization for a=1.25 cm., b=1.7 cm.

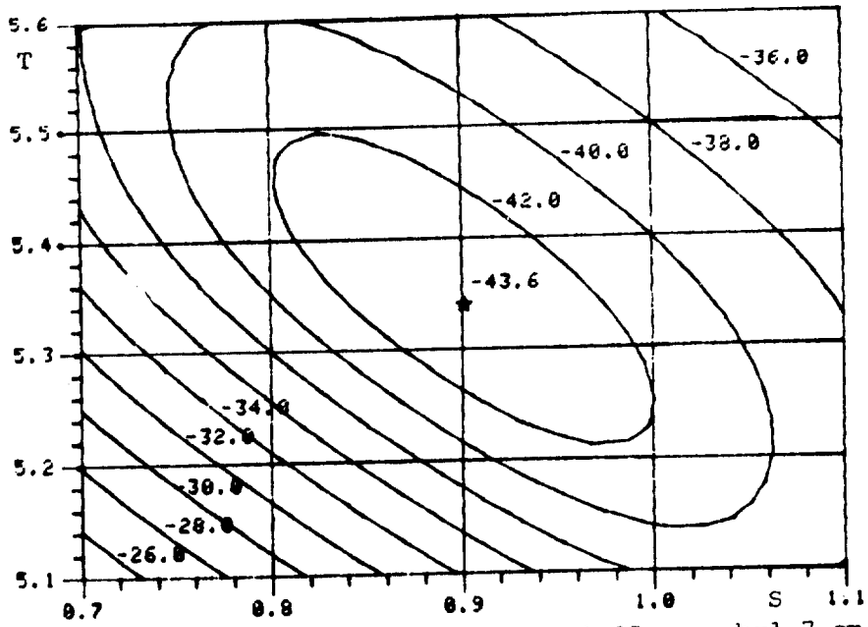

Fig. 2.12b Cross-polarization for a=1.35 cm., b=1.7 cm.

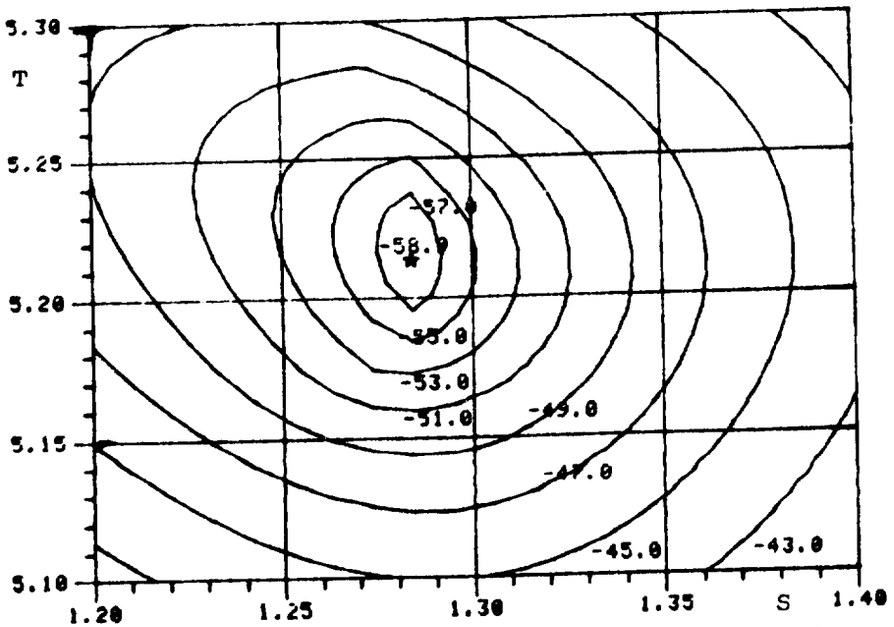

Fig. 2.12c Cross-polarization for a=1.45 cm., b=1.7 cm.

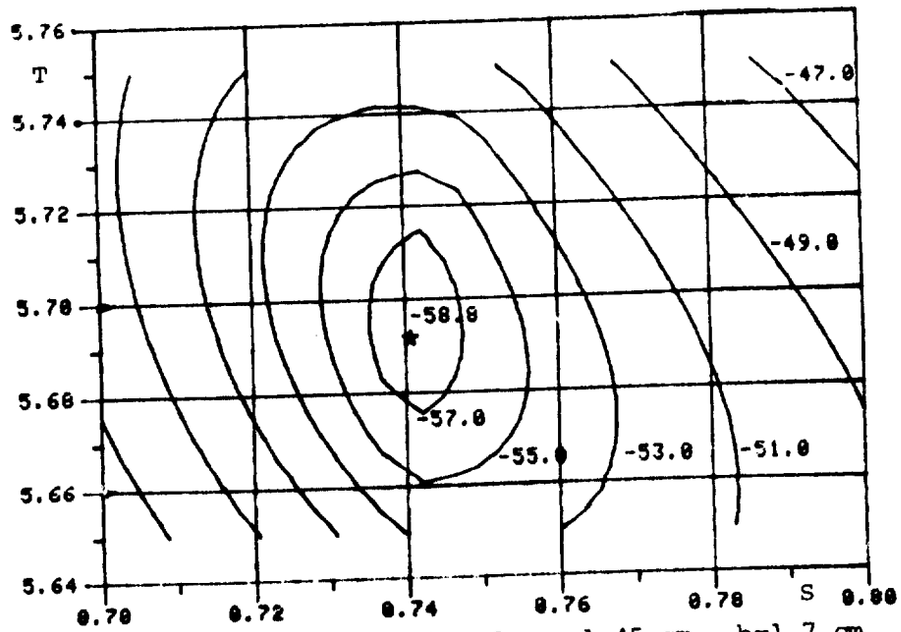

Fig. 2.12d Cross-polarization for a=1.45 cm., b=1.7 cm.

Figure 2.12, Cross-polarization of dual-mode feed as a function of S and T.

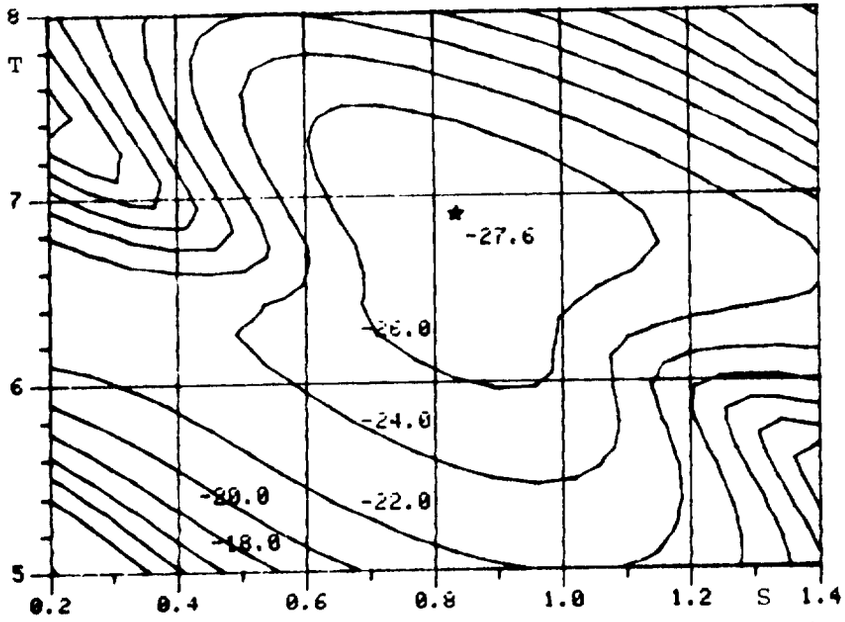

Fig. 2.13a Cross-polarization for a=1.25 cm., b=1.8 cm.

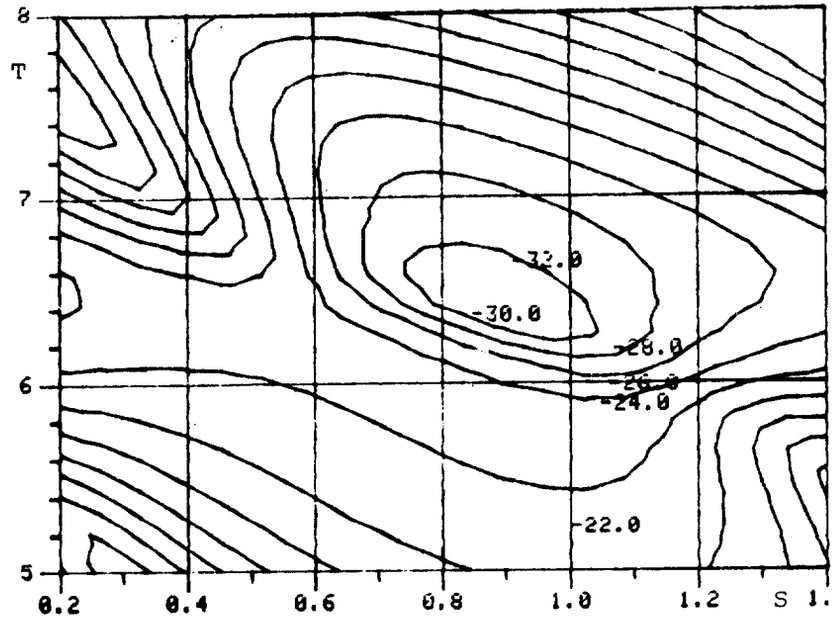

Fig. 2.13b Cross-polarization for a=1.35 cm., b=1.8 cm.

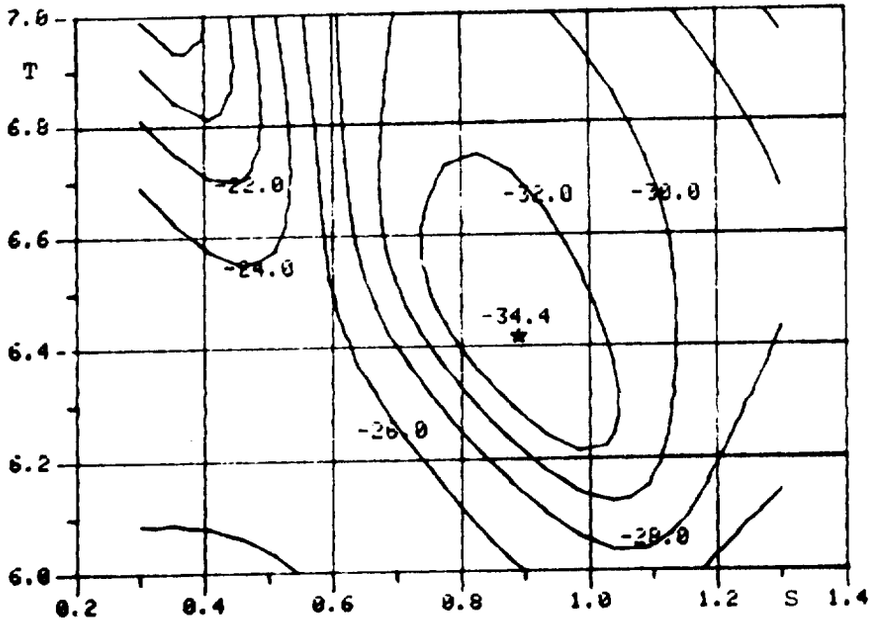

Fig. 2.13c Cross-polarization for a=1.35 cm., b=1.8 cm.

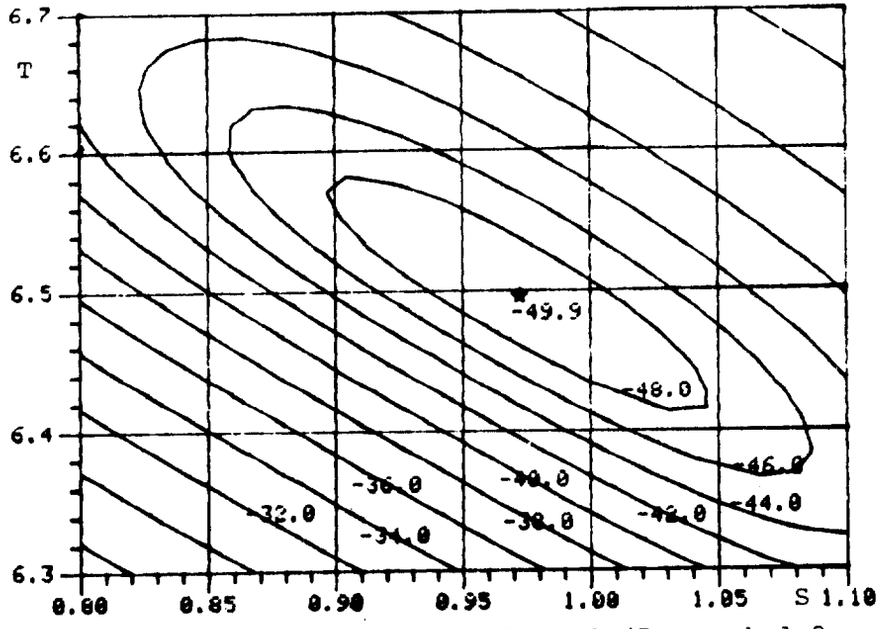

Fig. 2.13d Cross-polarization for a=1.45 cm., b=1.8 cm.

Figure 2.13, Cross-polarization of dual-mode feed as a function of S and T.

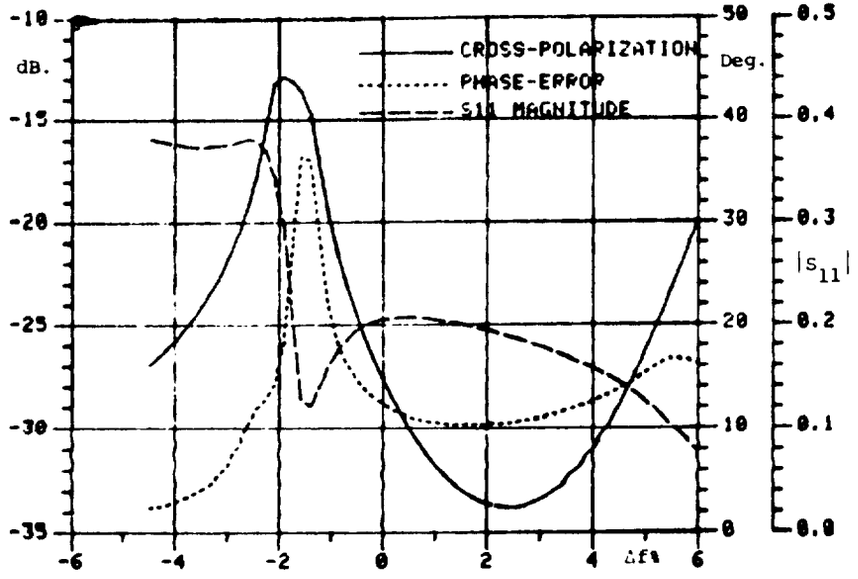

Fig. 2.14a A= 1.07 B= 1.60 S= 0.4600 T= 5.0000

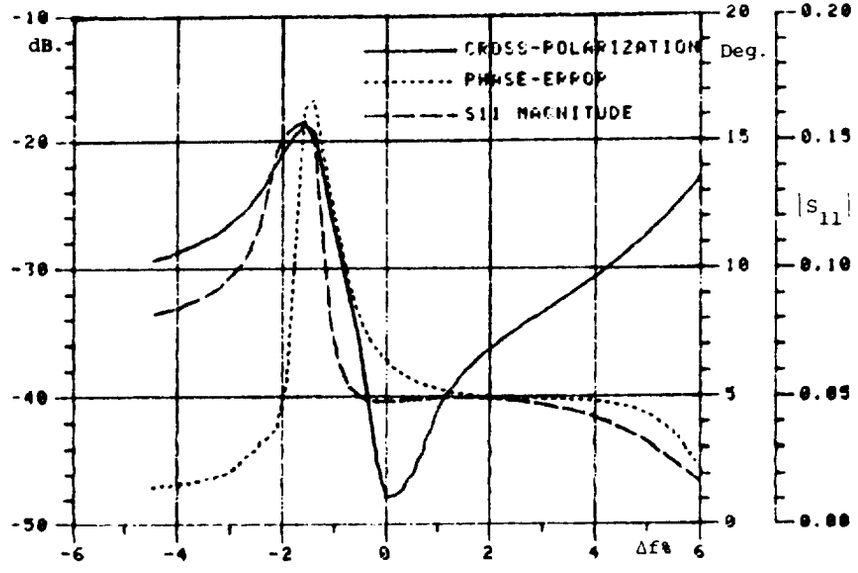

Fig. 2.14b A= 1.25 B= 1.60 S= 0.8500 T= 4.2640

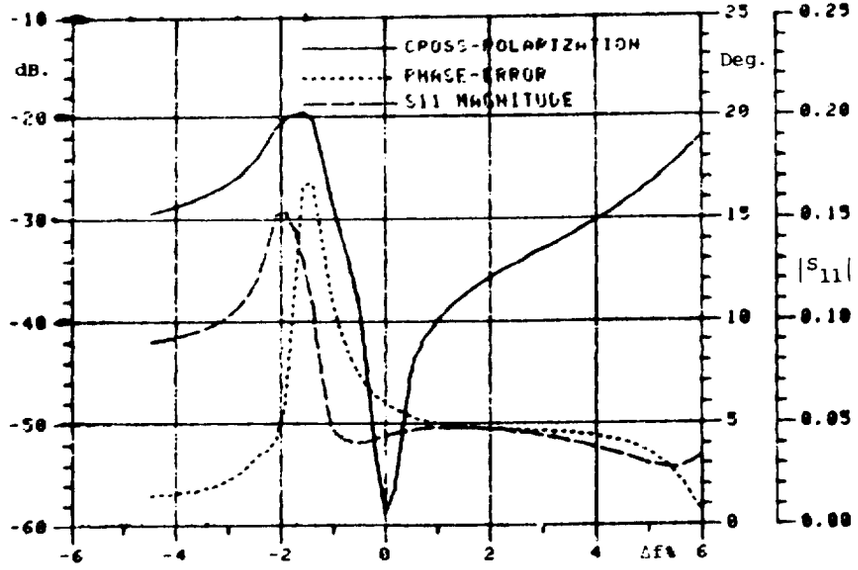

Fig. 2.14c A= 1.30 B= 1.60 S= 0.7600 T= 4.3720

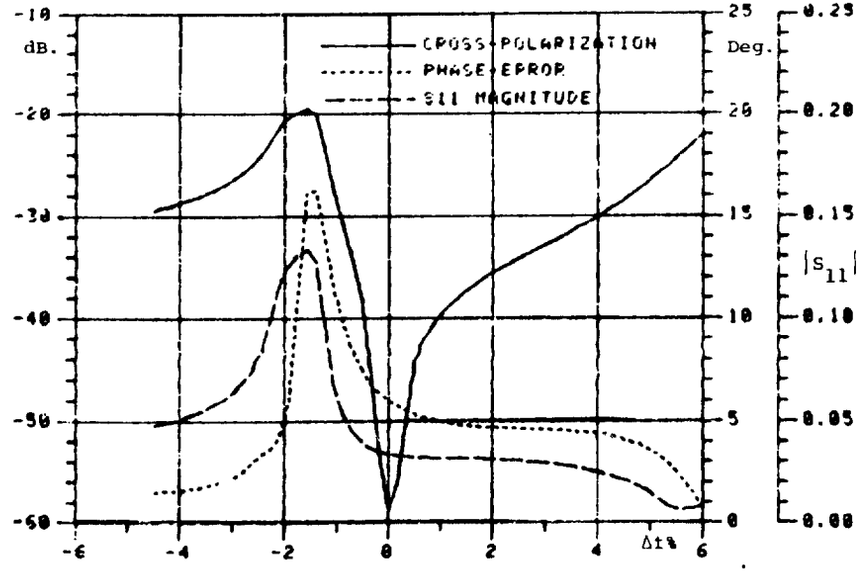

Fig. 2.14d A= 1.30 B= 1.60 S= 1.0120 T= 4.1020

Figure 2.14, Dual-mode feed characteristics as a function of frequency.

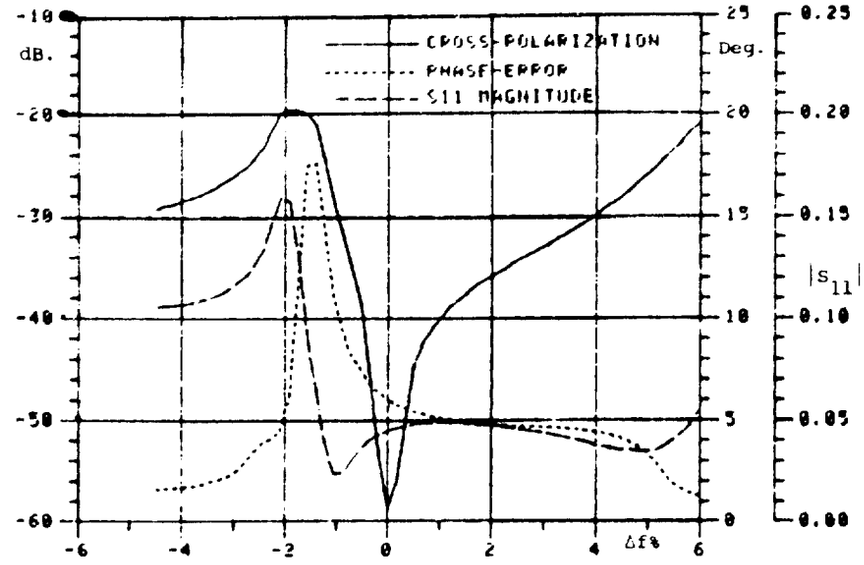

Fig. 2.14e A= 1.35 B= 1.60 S= 0.6730 T= 4.4930

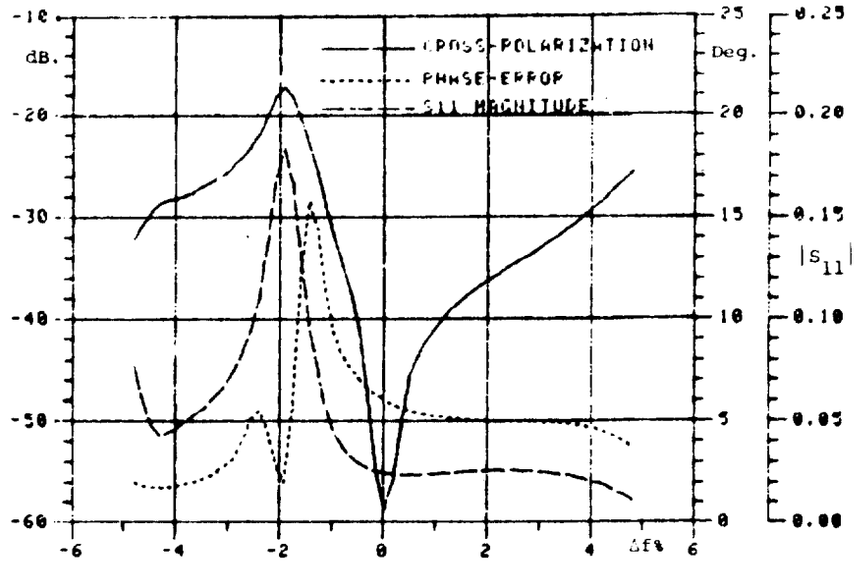

Fig. 2.14f A= 1.35 B= 1.60 S= 1.2200 T= 3.9720

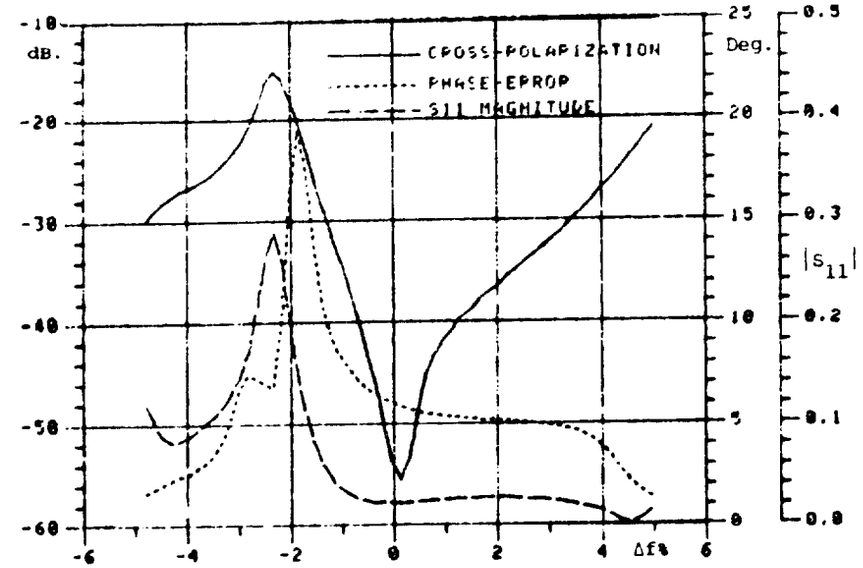

Fig. 2.14g A= 1.40 B= 1.69 S= 0.1000 T= 3.9050

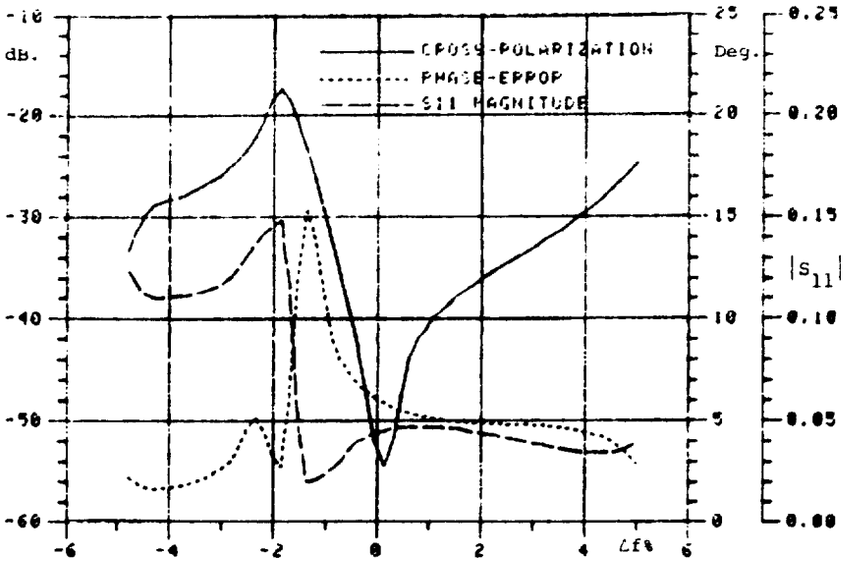

Fig. 2.14h A= 1.40 B= 1.60 S= 0.6350 T= 4.0650

Figure 2.14, (cont.) Dual-mode feed characteristics as a function of frequency.

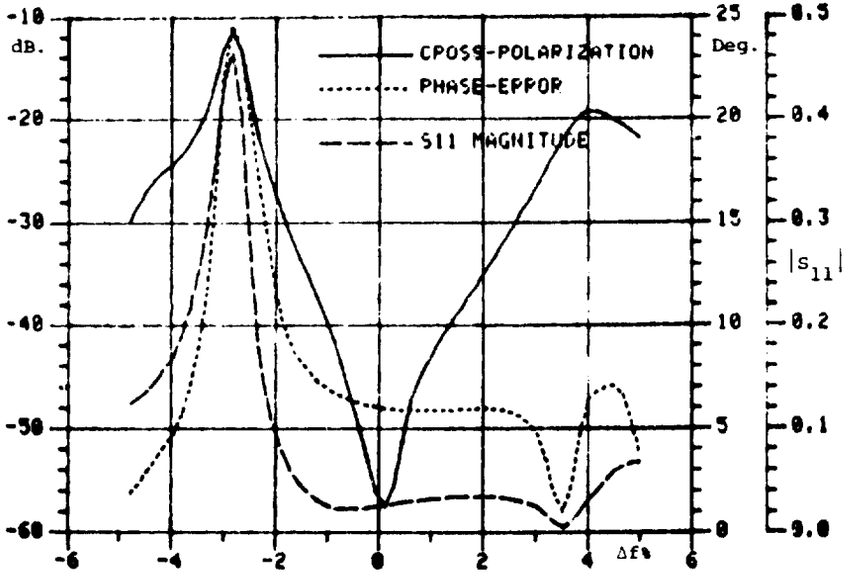

Fig. 2.14i A= 1.45 B= 1.60 S= 0.2730 T= 3.0840

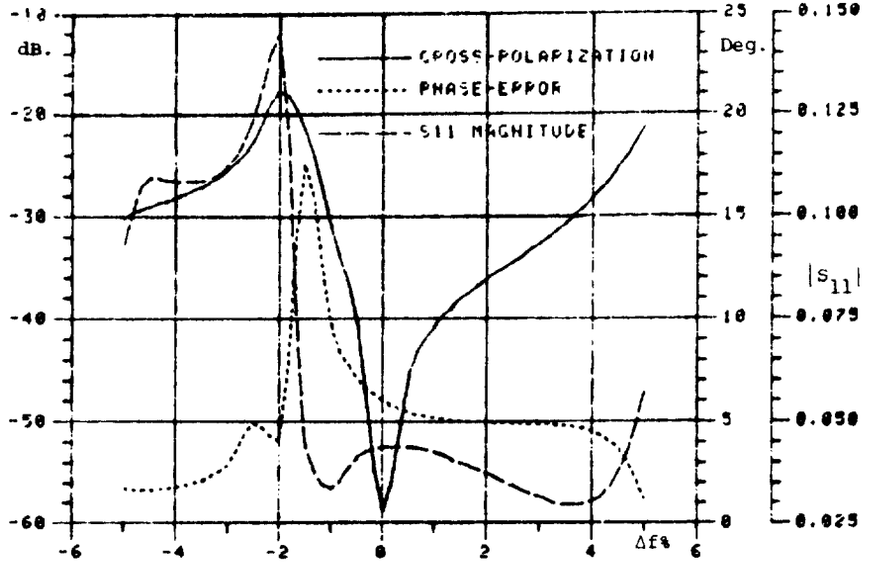

Fig. 2.14j A= 1.45 B= 1.60 S= 0.6170 T= 4.6160

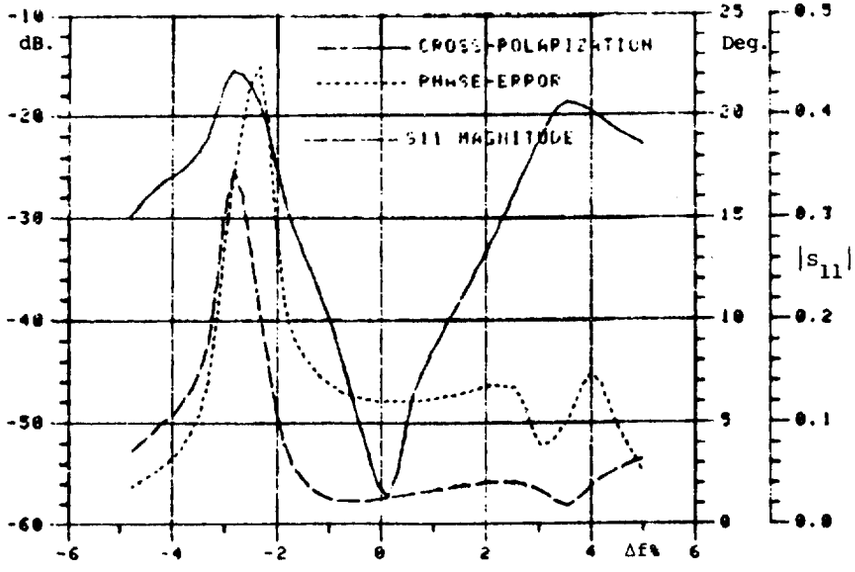

Fig. 2.14k A= 1.45 B= 1.60 S= 1.5600 T= 3.0840

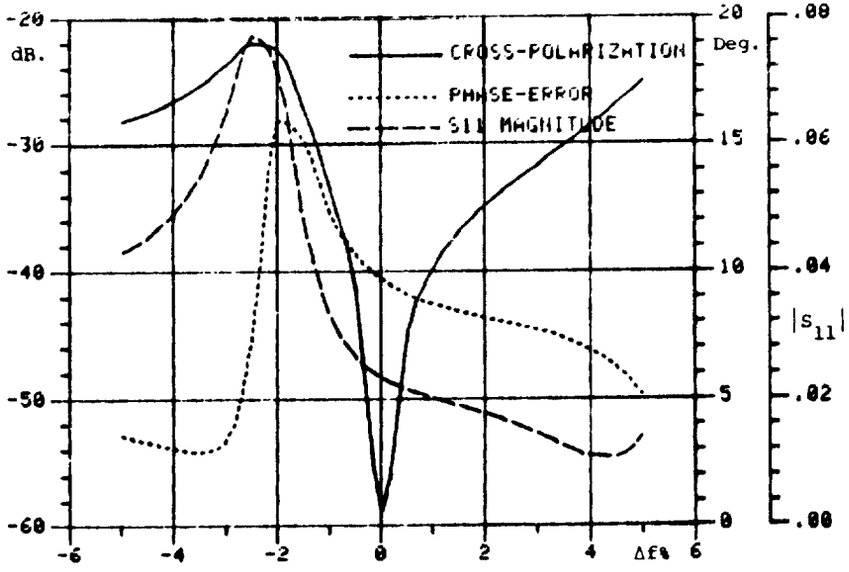

Fig. 2.14ℓ A= 1.40 B= 1.70 S= 0.8790 T= 5.4510

Figure 2.14, (cont.) Dual-mode feed characteristics as a function of frequency.

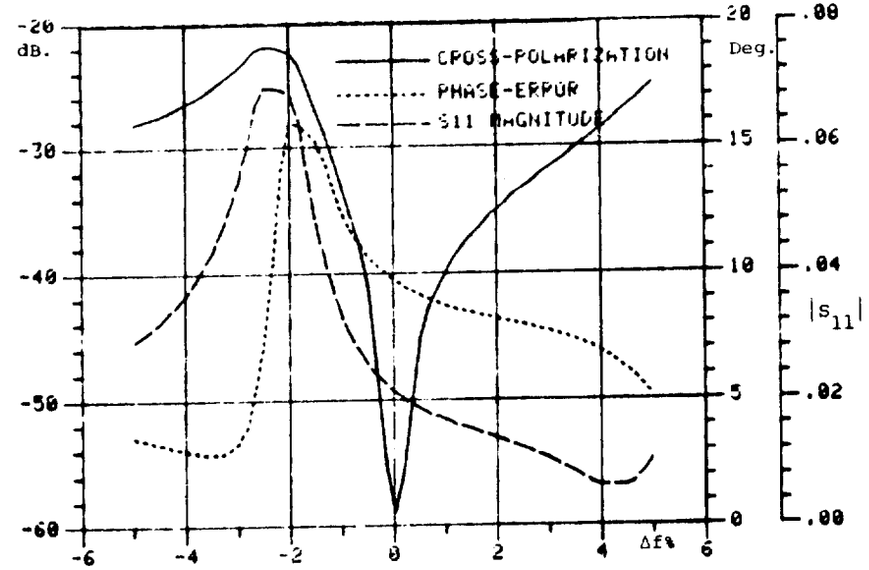

Fig. 2.14m A= 1.40 B= 1.70 S= 0.9930 T= 5.3380

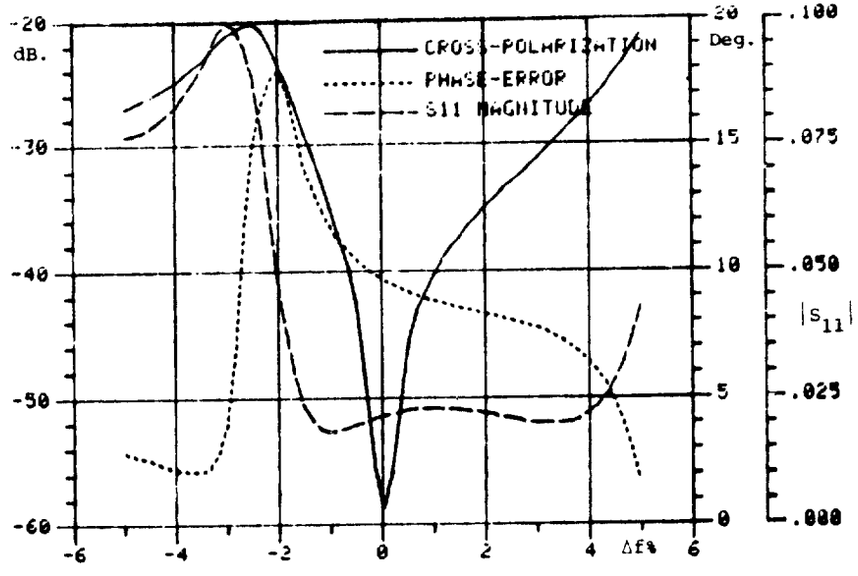

Fig. 2.14n A= 1.45 B= 1.70 S= 0.7400 T= 5.6920

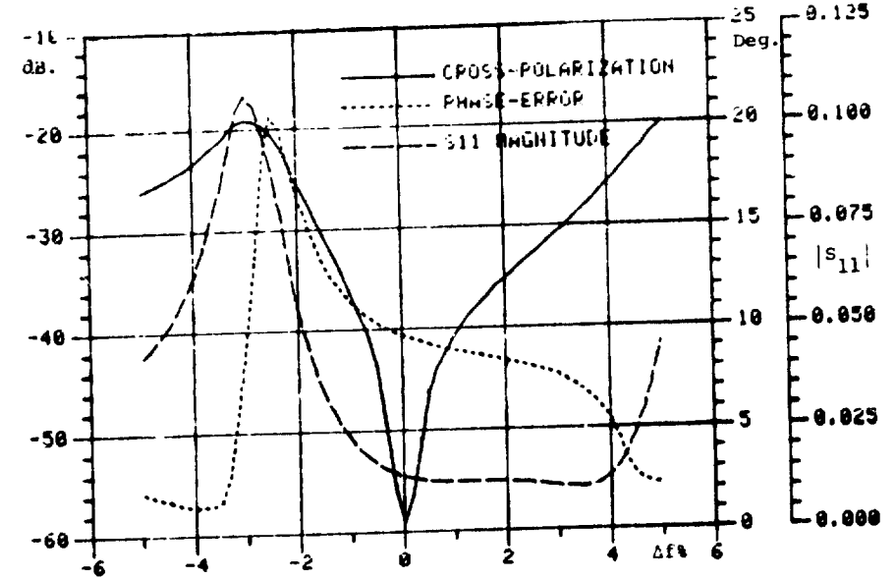

Fig. 2.14o A= 1.45 B= 1.70 S= 1.2040 T= 5.2140

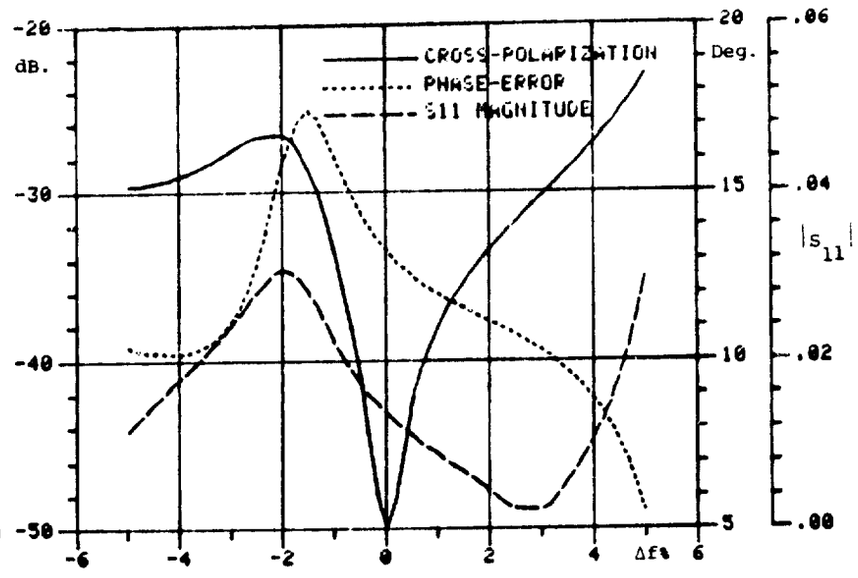

Fig. 2.14p A= 1.45 B= 1.80 S= 0.9720 T= 6.4970

Figure 2.14, (cont.) Dual-mode feed characteristics as a function of frequency

The phase error (departure from a spherical phase front) in the radiation pattern is also negligible, typically less than 10° over the band.

The efficiency of the feed depends on the f/D ratio of the paraboloid reflector it is used with. Figures 2.15a-h show the illumination efficiency, spillover efficiency, and total efficiency for various f/D ratios as a function of the outer waveguide radius b. The data is not applicable for b greater than 2.12 cm. at which point the TE_{12} mode begins to propagate. For these feeds the computed phase error loss and cross-polarization loss was entirely negligible being less than 0.25%. With an f/D ratio of 0.33 the efficiency is 57% for b = 1.6 cm. but rises to 68% with f/D increased to 0.4. The maximum attainable efficiency is around 78% for b = 1.85 cm. and an f/D ratio of 0.6 (see Fig. 2.15h). The maximum efficiency arises from the competition between a rising illumination efficiency and a decreasing spillover efficiency.

The efficiency that can be realized in practice depends on how much aperture field taper is required to obtain sidelobes of a given specified maximum value. Figures 2.16a-b show the first and second sidelobe levels as a function of f/D for b = 1.6 cm. and 1.7 cm. The interesting feature in these curves is that as f/D increases the aperture field taper decreases causing the main lobe to become narrower and causing the first sidelobe to essentially disappear by merging with the main lobe. The second sidelobe then becomes dominant. A further increase in f/D reestablishes the first sidelobe as the dominant one. This behavior can be understood by examining Fig. 2.17 which shows the angular position of the first two sidelobes and the first two nulls as a function of f/D.

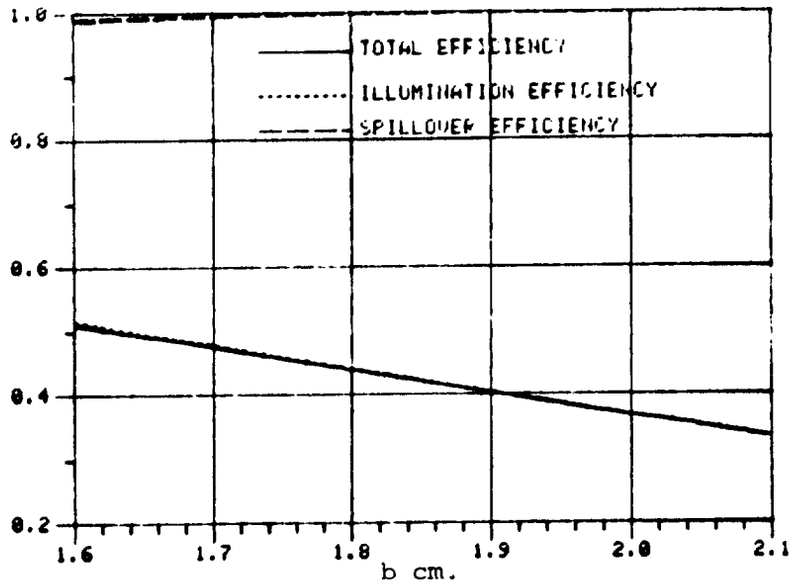

Fig. 2.15a FOCAL LENGTH/DIAMETER RATIO= 0.30 (THETA0= 79.6)

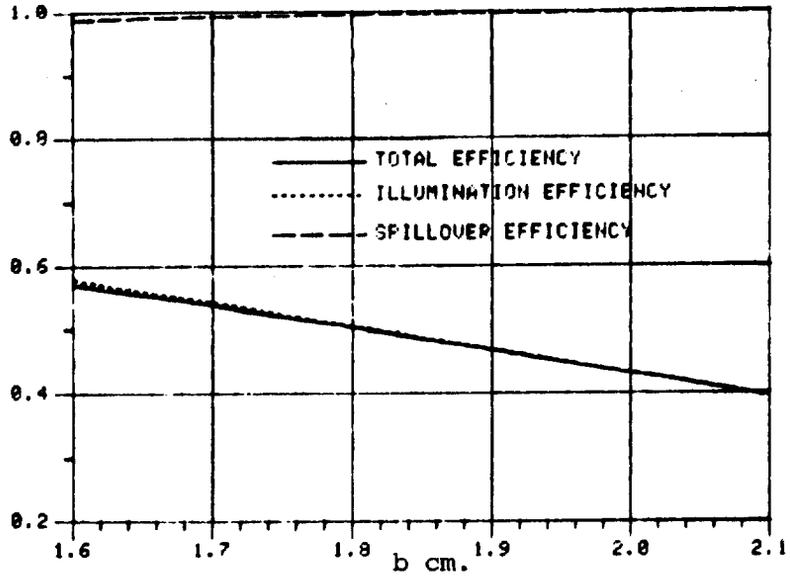

Fig. 2.15b FOCAL LENGTH/DIAMETER RATIO= 0.33 (THETA0= 74.3)

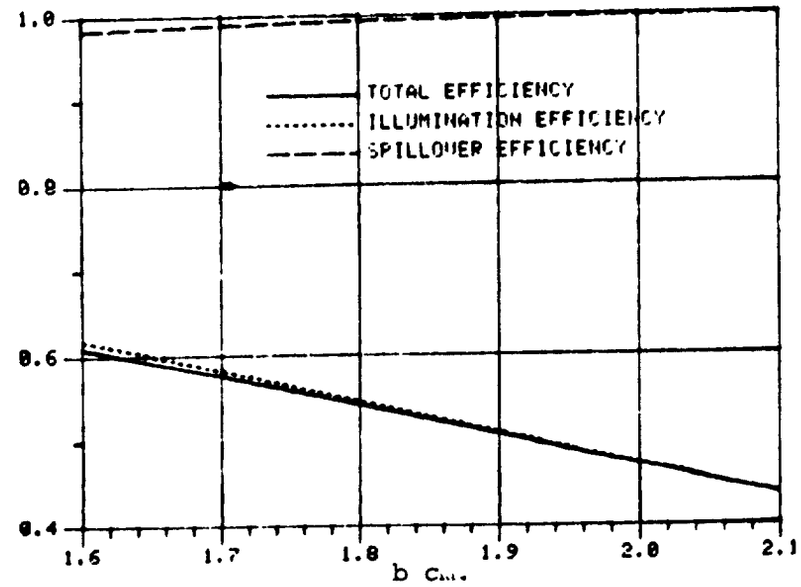

Fig. 2.15c FOCAL LENGTH/DIAMETER RATIO= 0.35 (THETA0= 71.1)

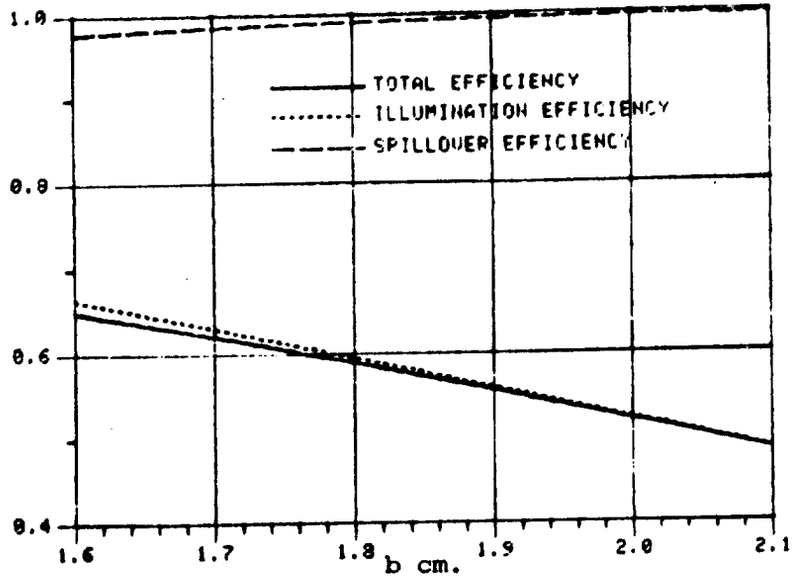

Fig. 2.15d FOCAL LENGTH/DIAMETER RATIO= 0.38 (THETA0= 67.4)

Figure 2.15, Paraboidal antenna efficiency for different f/D ratios.

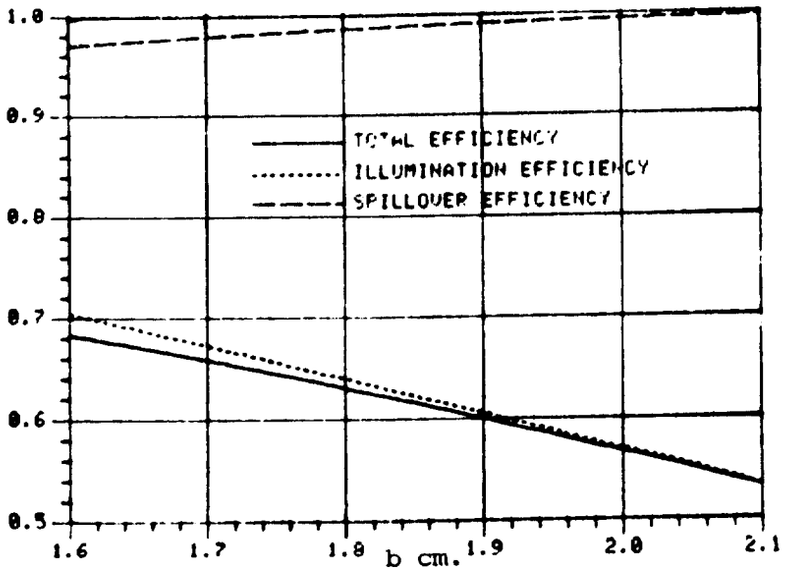

Fig. 2.15e FOCAL LENGTH/DIAMETER RATIO= 0.40 (THETA0= 64.0)

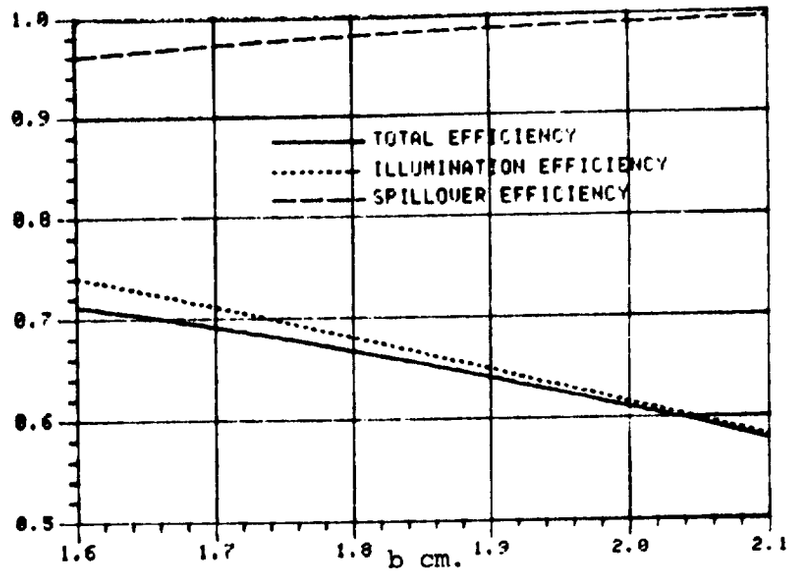

Fig. 2.15f FOCAL LENGTH/DIAMETER RATIO= 0.43 (THETA0= 60.9)

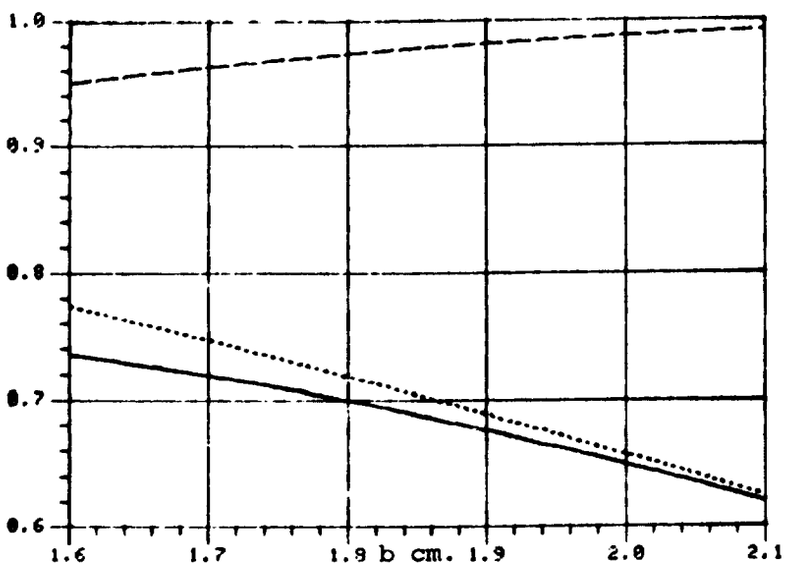

Fig. 2.15g FOCAL LENGTH/DIAMETER RATIO= 0.45 (THETA0= 58.1)

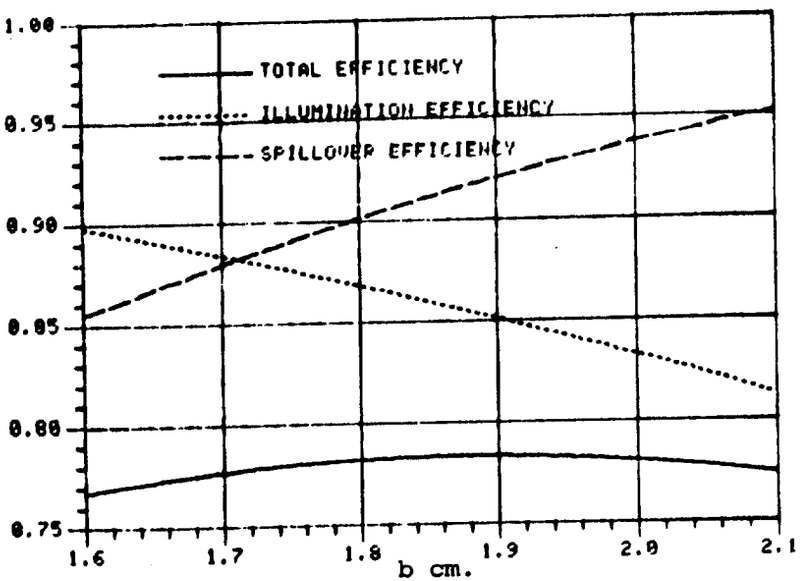

Fig. 2.15h FOCAL LENGTH/DIAMETER RATIO= 0.60 (THETA0= 45.2)

Figure 2.15, (cont.) Paraboidal antenna efficiency for different f/D ratios.

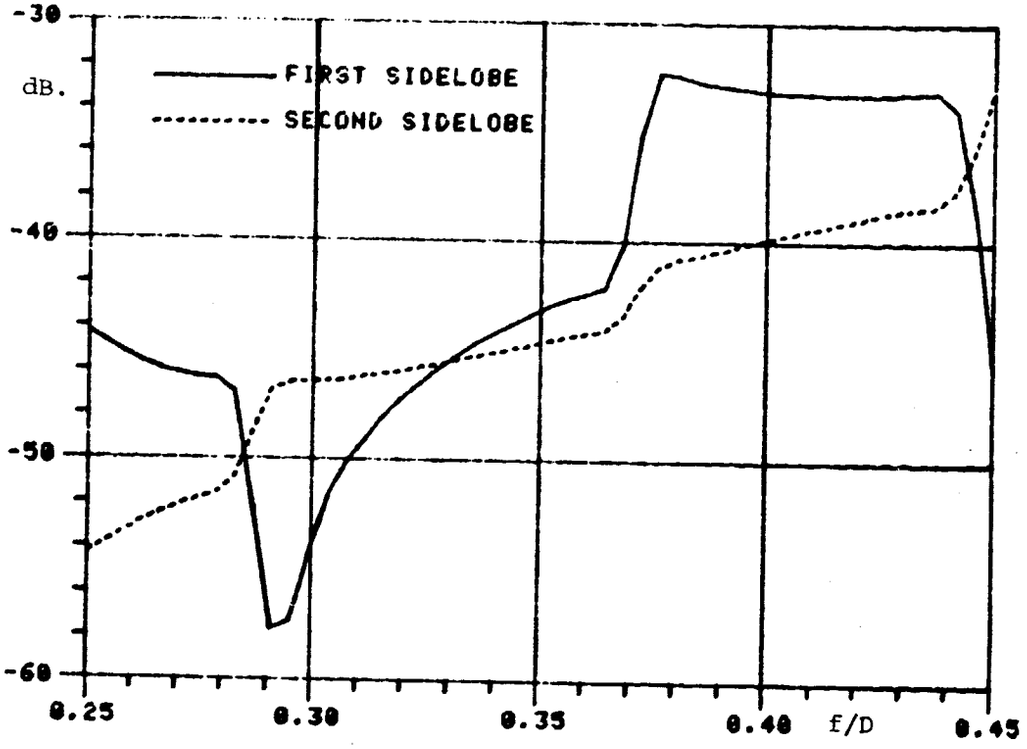

B= 1.70 DISH DIAMETER= 1.22 meter

Fig. 2.16a Sidelobe levels vs. f/D.

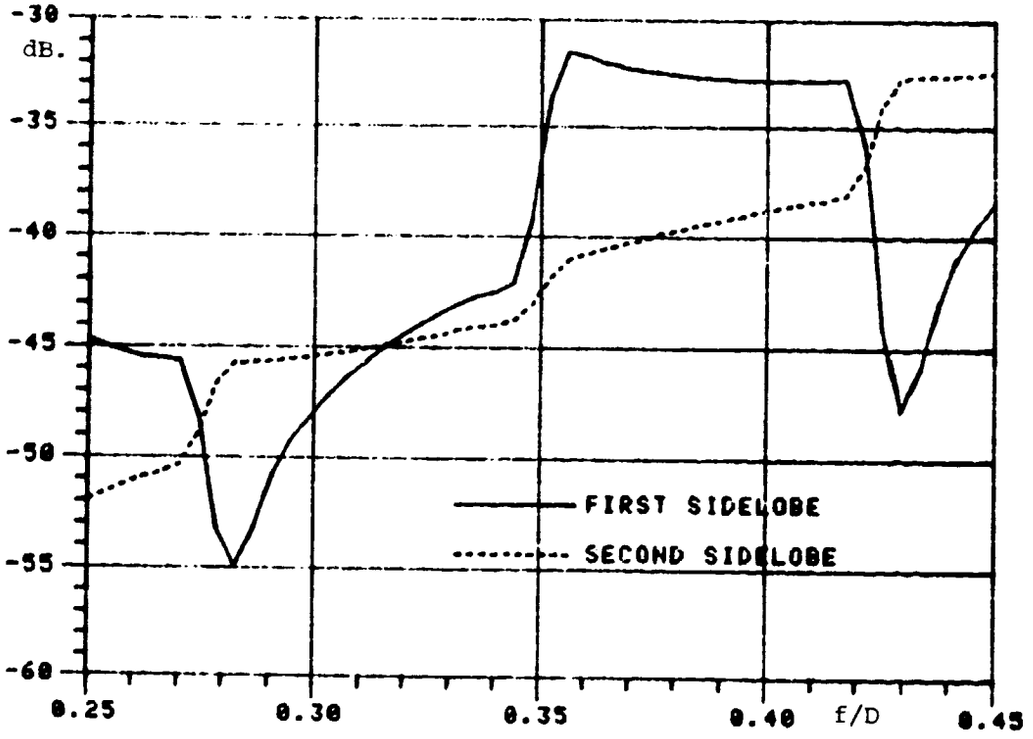

B= 1.60 DISH DIAMETER= 1.22 meter

Fig. 2.16b Sidelobe levels vs. f/D.

Figure 2.16, Sidelobe characteristics for paraboloidal reflector

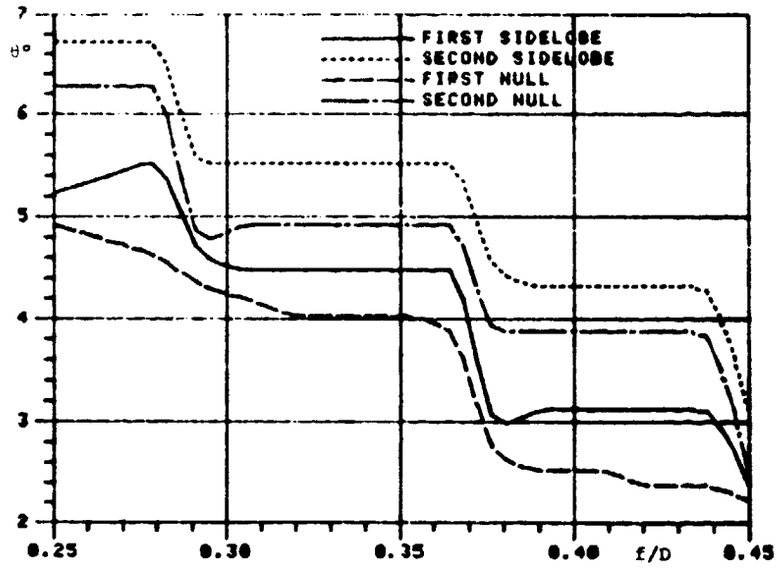

B= 1.70 DISH DIAMETER= 1.22 meter

Figure 2.17, Sidelobe and null positions vs. f/D.

If the criterion of sidelobes below -30dB. is chosen then Fig's. 2.16a-b show that this can be met with f/D ratios as large as 0.45. This means that efficiencies as large as 70% or more can be realized. If the criterion is -35dB. sidelobes in order to allow for some increase in sidelobe level due to feed blockage and scatter from the feed supports then f/D is restricted to about 0.35 for b = 1.6 cm. and to 0.37 for b = 1.7 cm. which corresponds to an efficiency of around 60%. The efficiency curves were computed using the formulas given in Chapter 1.

Typical radiation patterns for a 1.22 meter (4 foot) paraboloid of different f/D ratios and for b = 1.6 and 1.7 cm. are shown in Figures 2.18 and 2.19. The series of figures such as Figures 2.18a-2.18e show the formation of sidelobes as the aperture field taper is reduced with increasing f/D ratios. In Fig. 2.18a where f/D = 0.3 the main lobe has a broad shoulder beginning at about the -30 dB. level and having a half

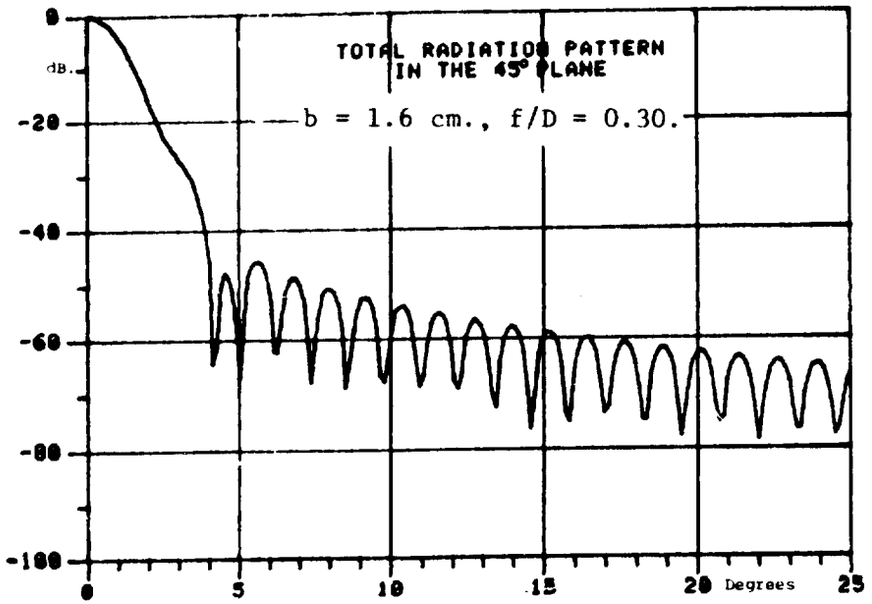

Figure 2.18a, Reflector radiation pattern.

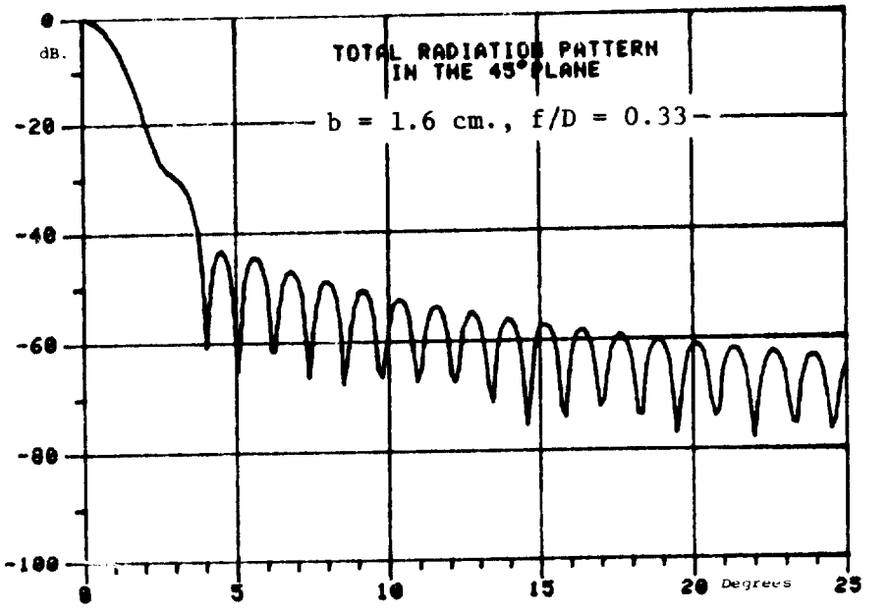

Figure 2.18b, Reflector radiation pattern.

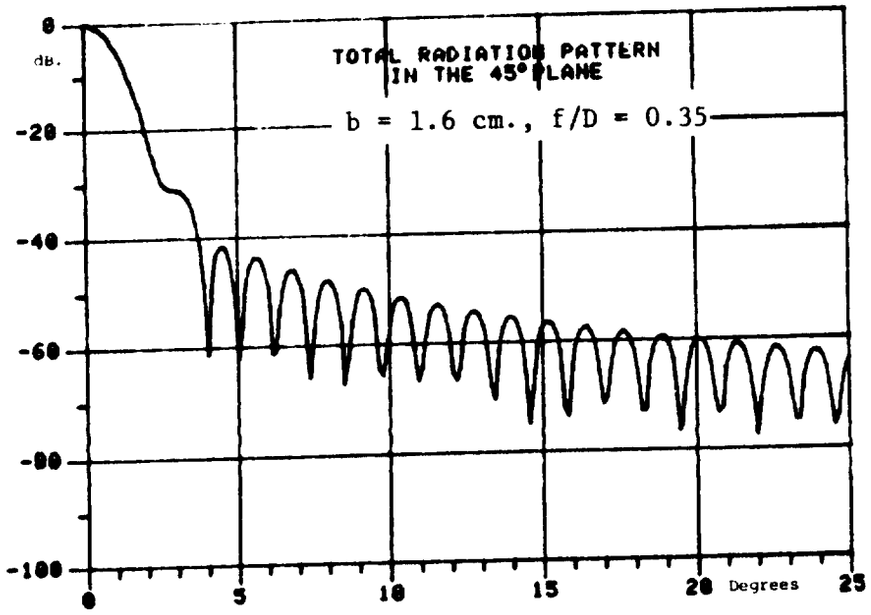

Figure 2.18c, Reflector radiation pattern.

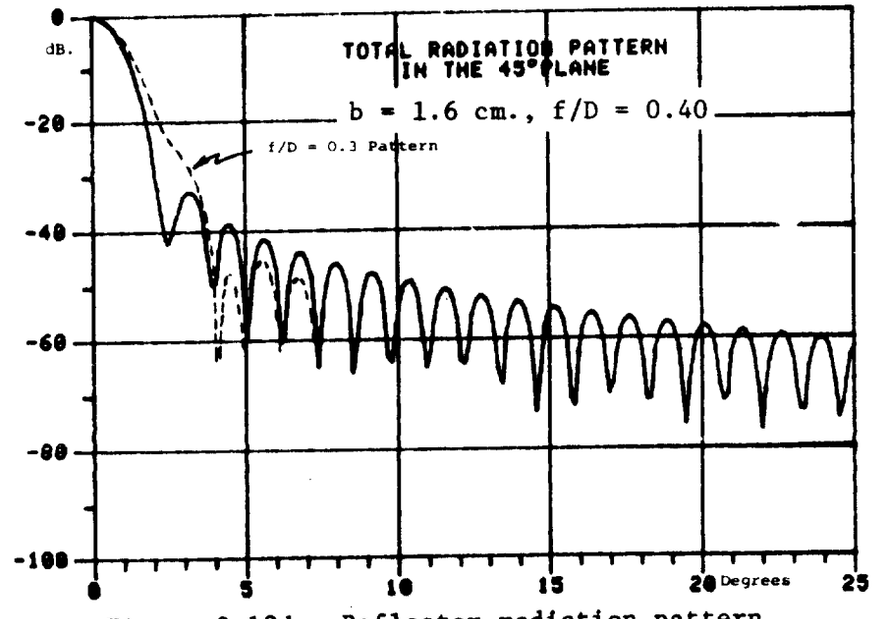

Figure 2.18d, Reflector radiation pattern.

Figure 2.18, Reflector radiation patterns as a function of f/D, D = 1.22 m.

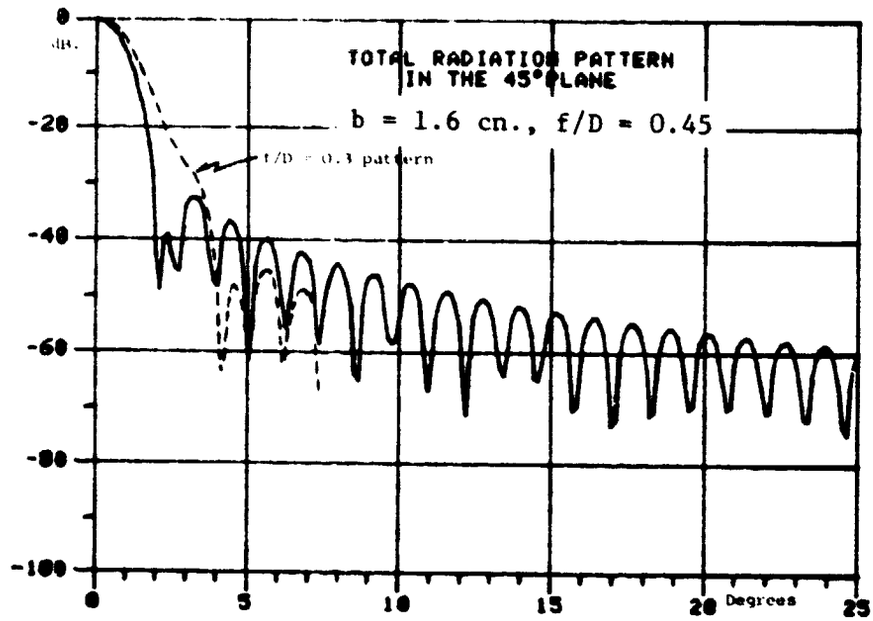

Figure 2.18e, Reflector radiation pattern

Figure 2.18, Reflector radiation patterns as a function of f/D, D = 1.22 m.

angular width of 4° at the -40 dB. level. The next series of four figures shows this shoulder moving away and becoming a distinct sidelobe with a relative height of -33 dB. at $\theta = 3.5°$ when f/D = 0.4. For f/D = 0.45 a new sidelobe at 2.5° begins to form. With f/D = 0.3 the -33 dB. level is also at about $\theta = 3.5°$ but is part of the shoulder of the main lobe. The f/D = 0.3 corresponds to an aperture efficiency of 52% while f/D = 0.4 corresponds to an aperture efficiency of 68%. If the pattern is measured in terms of the envelope the f/D = 0.4 pattern is better than the f/D = 0.3 pattern down to the -40 dB. level. The b = 1.7 cm. case is similar. These figures thus show that for a given feed and reflector there is an optimum f/D ratio that will give the best aperture efficiency along with the best pattern envelope characteristic. The envelope provides a good measure of the interference rejection characteristics of the overall pattern. A main lobe with a broad shoulder yet with small sidelobes is not as good as a narrow main lobe

with a higher first sidelobe level as long as the sidelobe level is below that of the shoulder.

The patterns shown in Fig's. 2.18-2.19 are in the $\phi = 45°$ plane but because of the very low cross-polarization the patterns are essentially the same in all planes. Figure 2.20a shows the co-polarized pattern, the total pattern, and the contribution from the z-component of current on the paraboloid. The field from the cross-polarized field of the feed is below -100 dB. Figure 2.20b shows the various contributions to the cross-polarized field in the 45° plane. The cross-polarized component due to the z-component of current is comparable in value to that due to the cross-polarized radiation from the feed for an optimum feed.

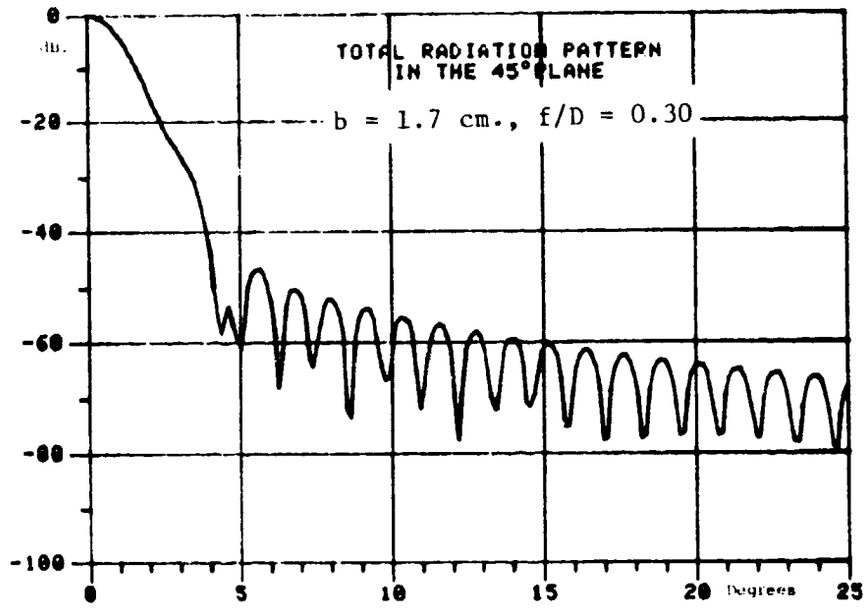

Figure 2.19a, Reflector radiation pattern

Figure 2.19, Reflector radiation patterns as a function of f/D, D = 1.22 m.

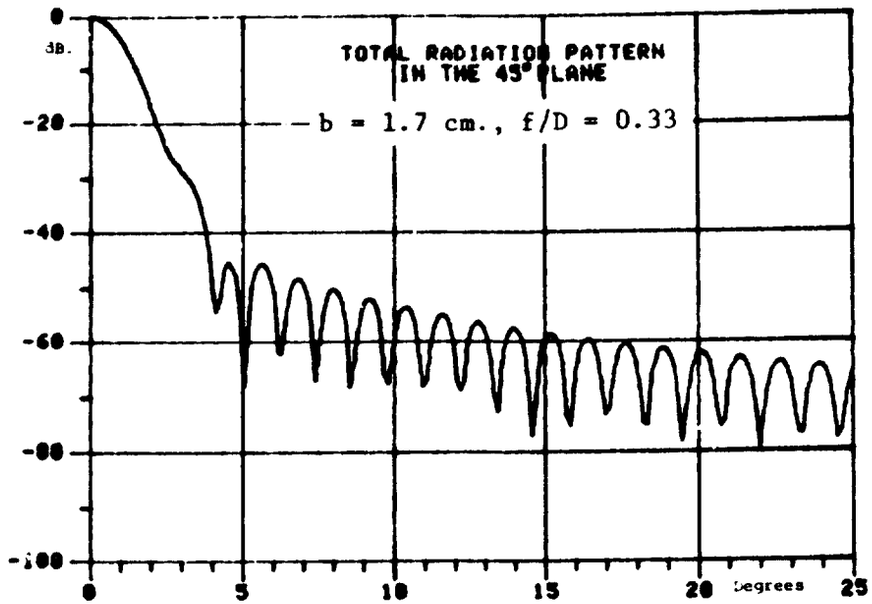

Figure 2.19b, Reflector radiation pattern

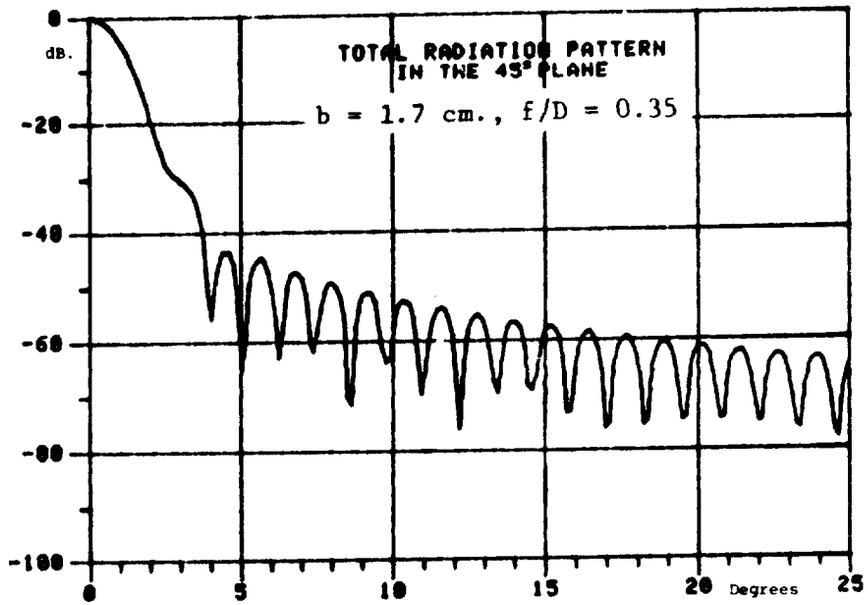

Figure 2.19c, Reflector radiation pattern

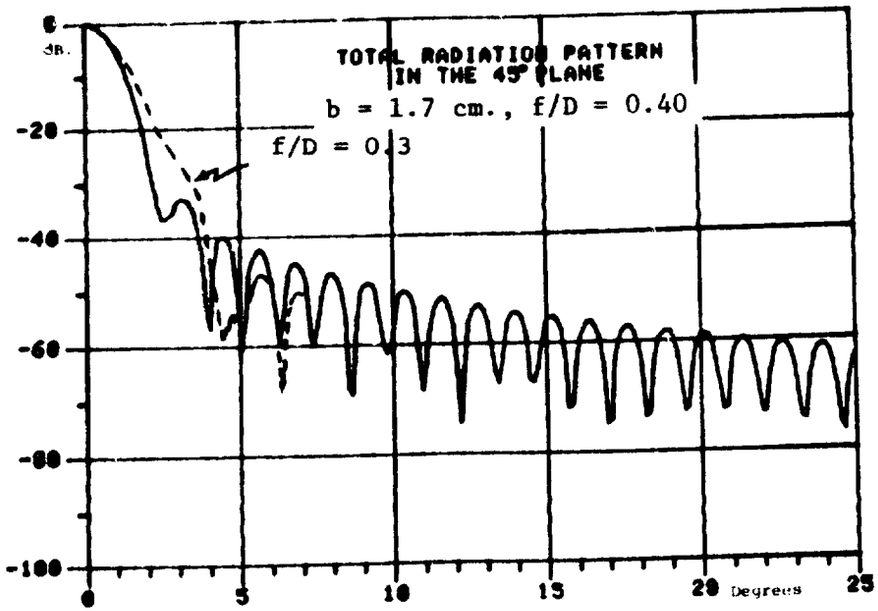

Figure 2.19d, Reflector radiation pattern

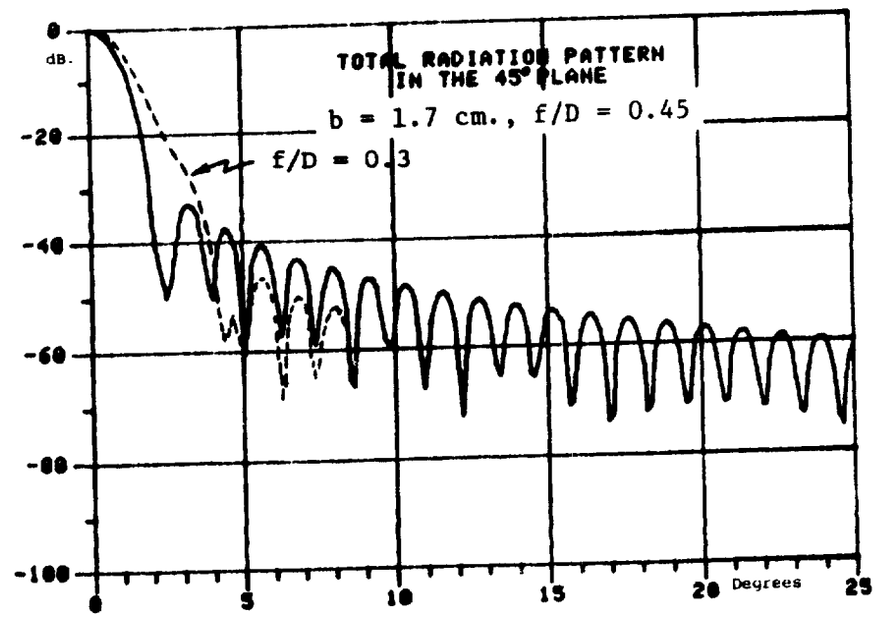

Figure 2.19e, Reflector radiation pattern

Figure 2.19, Reflector radiation patterns as a function of f/D, D = 1.22 m.

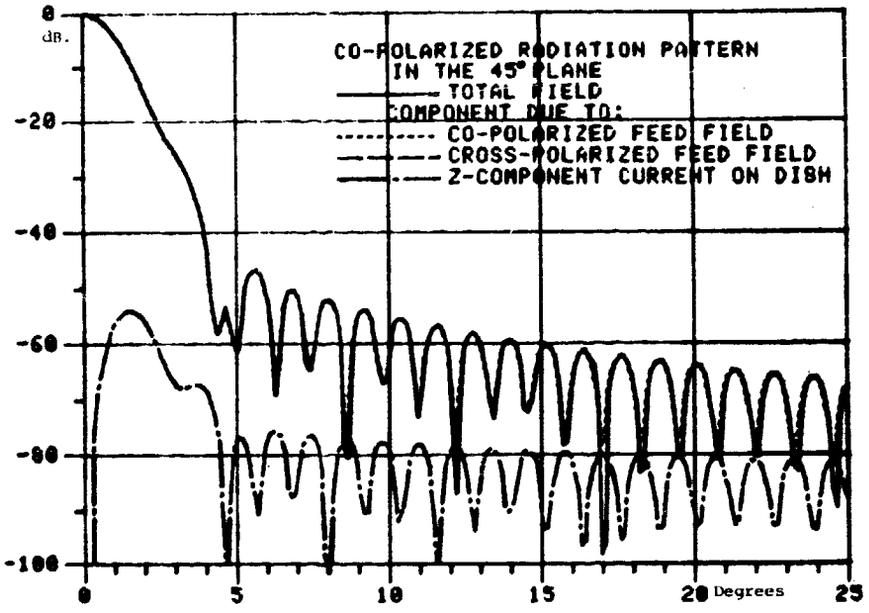

Figure 2.20a, Reflector co-polarized radiation patterns for b = 1.7 cm., f/D = 0.30, D = 1.22 m.

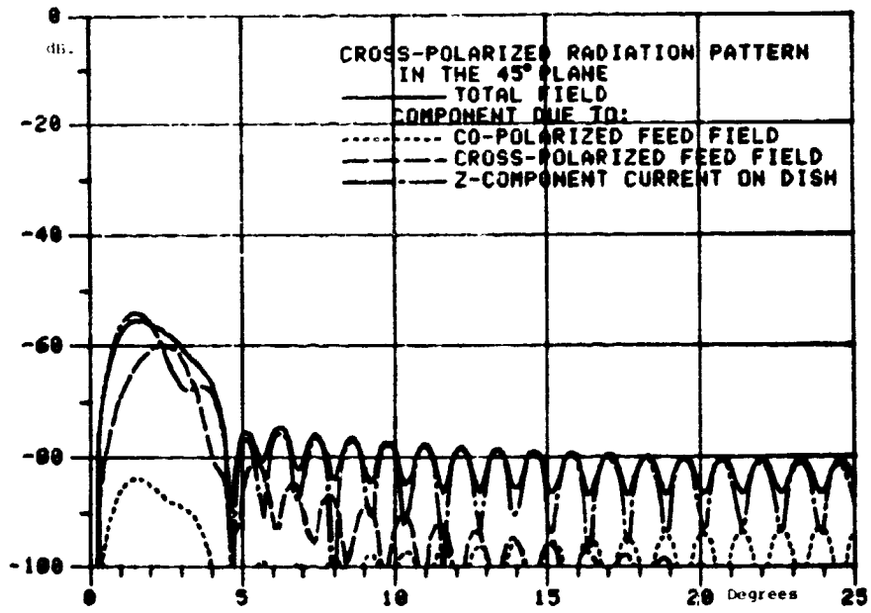

Figure 2.20b, Reflector cross-polarized radiation pattern for b = 1.7 cm., f/D = 0.30, D = 1.22 m.

Figure 2.20, Reflector co- and cross-polarized radiation patterns.

2.7 COAXIAL FEED PERFORMANCE - EXPERIMENTAL

Two long-cup dual-mode coaxial feeds were built and their radiation patterns and cross-polarization properties measured. One of the feeds was not an optimum design since it was constructed from design data that, unfortunately, was in error due to a sign error in the aperture TE_{11} to TM_{11} mode coupling coefficient. This feed was scaled to operate at a center frequency of 10.1 ghz. However, based on the corrected design data the lowest cross-polarization should occur around 10.3 ghz. The data shown in Figure 2.11b applies to this feed, as does the data in Figure 2.14a. The theory predicts a minimum cross-polarization of -34 dB. and a 5% bandwidth over which the cross-polarization should remain below -25 dB. This sub-optimum feed was also tested with a 1.22 meter diameter fiber glass paraboloid with f/D = 0.33. For the sub-optimum feed a = 1.27 cm., b = 1.905 cm. (see Fig.3.1)

The co-polarized and cross-polarized radiation patterns in the 45° plane for the sub-optimum feed are shown in Figures 2.21a through 2.21f and cover the frequency range from 9.9 ghz. to 10.6 ghz. At 9.9 ghz. the measured cross-polarization was -18 dB., at 10 ghz. it was -28 dB., while at the design center frequency of 10.1 ghz. it was -34 dB. At 10.3 ghz. the measured cross-polarization was -35 dB. which is somewhat better than the theory predicted. At 10.5 ghz. the cross-polarization was found to be -28 dB. and rose to only -24 dB. at 10.6 ghz. The measurements were made on an indoor antenna range with the feed and transmitting horns separated by 0.7 meter. The transmitting horn was approximately 5 cm. by 8 cm. Spurious reflections from the ceiling and walls were calculated to be below -40 dB. It was, however, found that some interference between the transmitting and receiving horn mounting structures was present and limited the ability to measure very low cross-polarization levels with good accuracy.

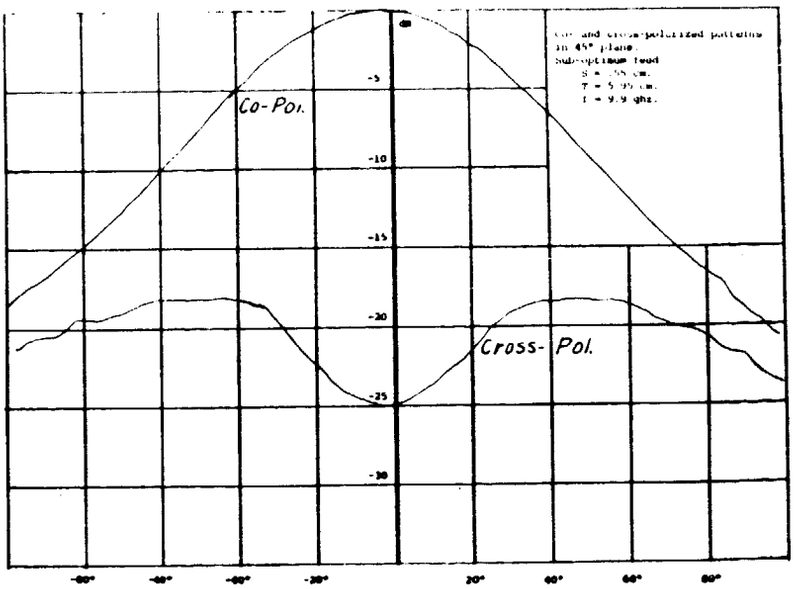

Figure 2.21a - 45° plane radiation patterns for sub-optimum feed at 9.9 ghz.

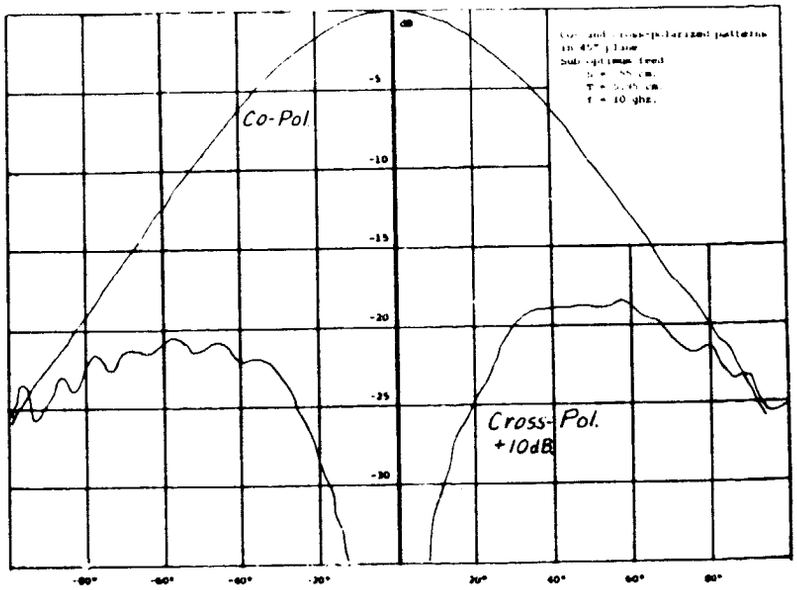

Figure 2.21b - 45° plane radiation patterns for sub-optimum feed at 10 ghz.

Figure 2.21, Radiation patterns for sub-optimum feed.

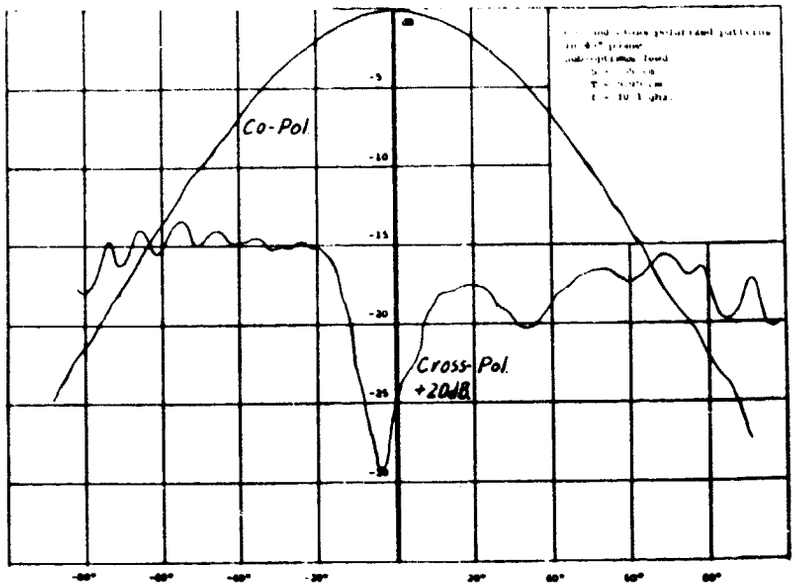

Figure 2.21c - 45° plane radiation patterns for sub-optimum feed at 10.1 ghz.

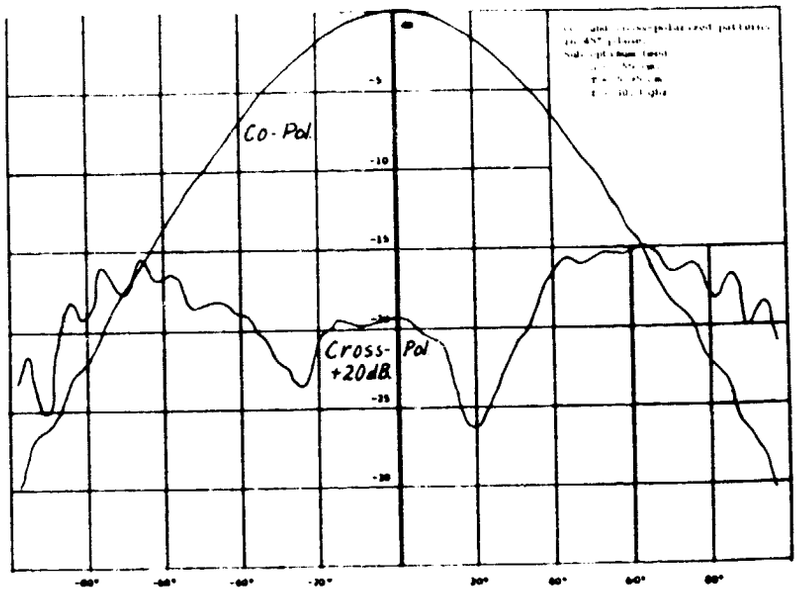

Figure 2.21d - 45° plane radiation patterns for sub-optimum feed at 10.3 ghz.

Figure 2.21, (cont.) Radiation patterns for sub-optimum feed.

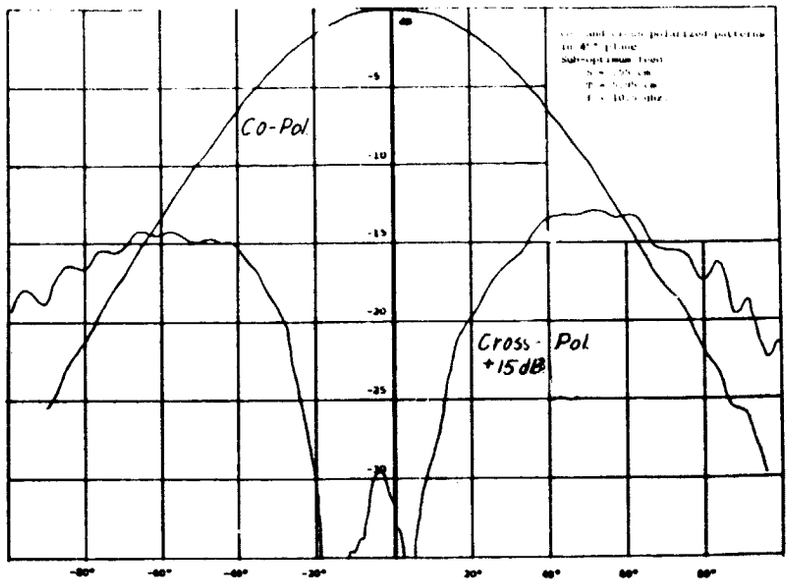

Figure 2.21e - 45° plane radiation patterns for sub-optimum feed at 10.5 ghz.

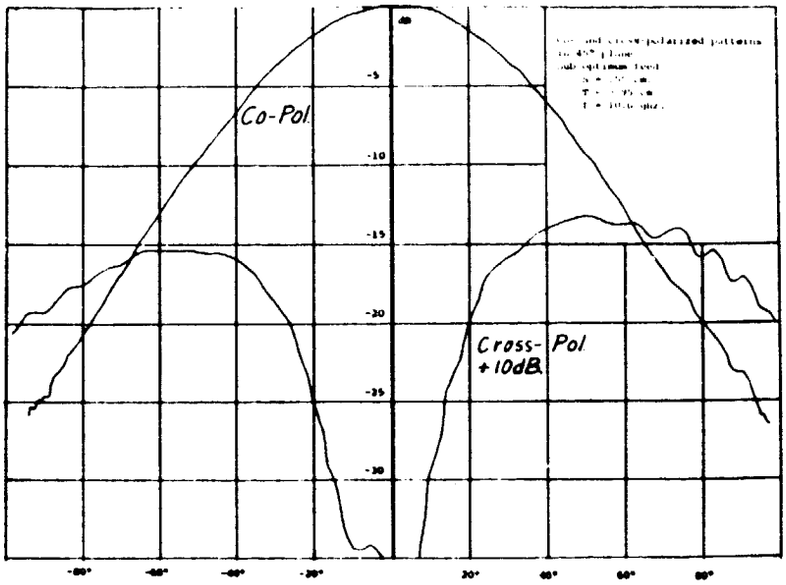

Figure 2.21f - 45° plane radiation patterns for sub-optimum feed at 10.6 ghz.

Figure 2.21, (cont.) Radiation patterns for sub-optimum feed.

Figure 2.22 shows the E- and H-plane patterns superimposed on the 45° plane co-polarized pattern at 10.1 ghz. Equal E- and H-plane patterns were not achieved, which is in accord with the theory. Nevertheless the radiation pattern for this sub-optimum feed does have quite good rotational symmetry at the design frequency.

When the sign error was discovered new design data was generated and an optimum feed was built for operation at 10.1 ghz. This optimum design corresponds to the feed that is characterized by the data shown in Figures 2.11f and 2.14c. The theory predicts a cross-polarization below -30 dB. over a 5% bandwidth extending from 10 ghz. to 10.5 ghz. The front section

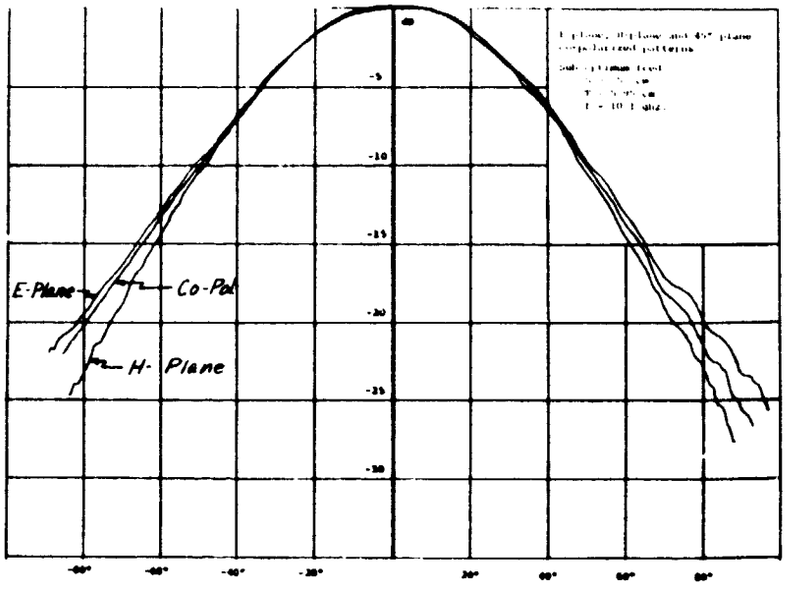

Figure 2.22 - Comparison E-plane, H-plane, and 45° plane co-polarized patterns for sub-optimum feed at 10.1 ghz.

of the feed employed a small tapered horn section as shown in Figure 2.23. The outer cup and inner section were also tapered to a sharp edge so as to be more nearly like the infinitely thin waveguides for which the theory is applicable.

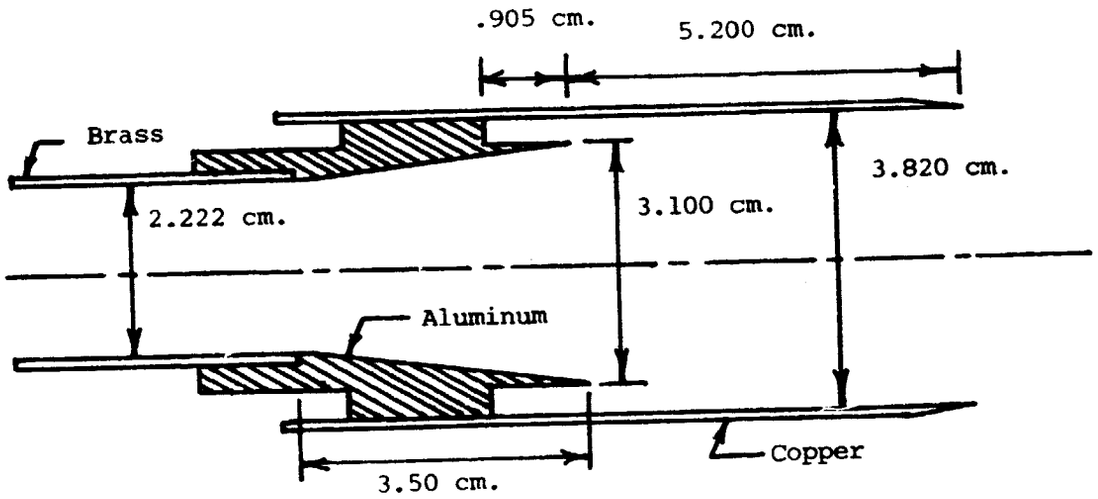

Figure 2.23 - Optimum Feed Configuration.

The E- and H-plane patterns and the co- and cross-polarized 45° plane patterns for the optimum feed are shown in Figures 2.24a through 2.24f. It can be seen that in the frequency range 10 ghz. to 10.5 ghz. the pattern has very good rotational symmetry and the measured cross-polarization was below -27 dB. At the design frequency the measured cross-polarization was below -40 dB. on one side and below -38 dB. on the other side of boresight. At 9.9 ghz. and 10.7 ghz. the E- and H-plane patterns are no longer equal and the cross-polarization has risen to - 25dB. and -16 dB. respectively. Overall there is very good correlation of the experimental data with the theoretical predictions. It thus appears that the theoretical design data can be used for design purposes without modification. The inability to measure a cross-

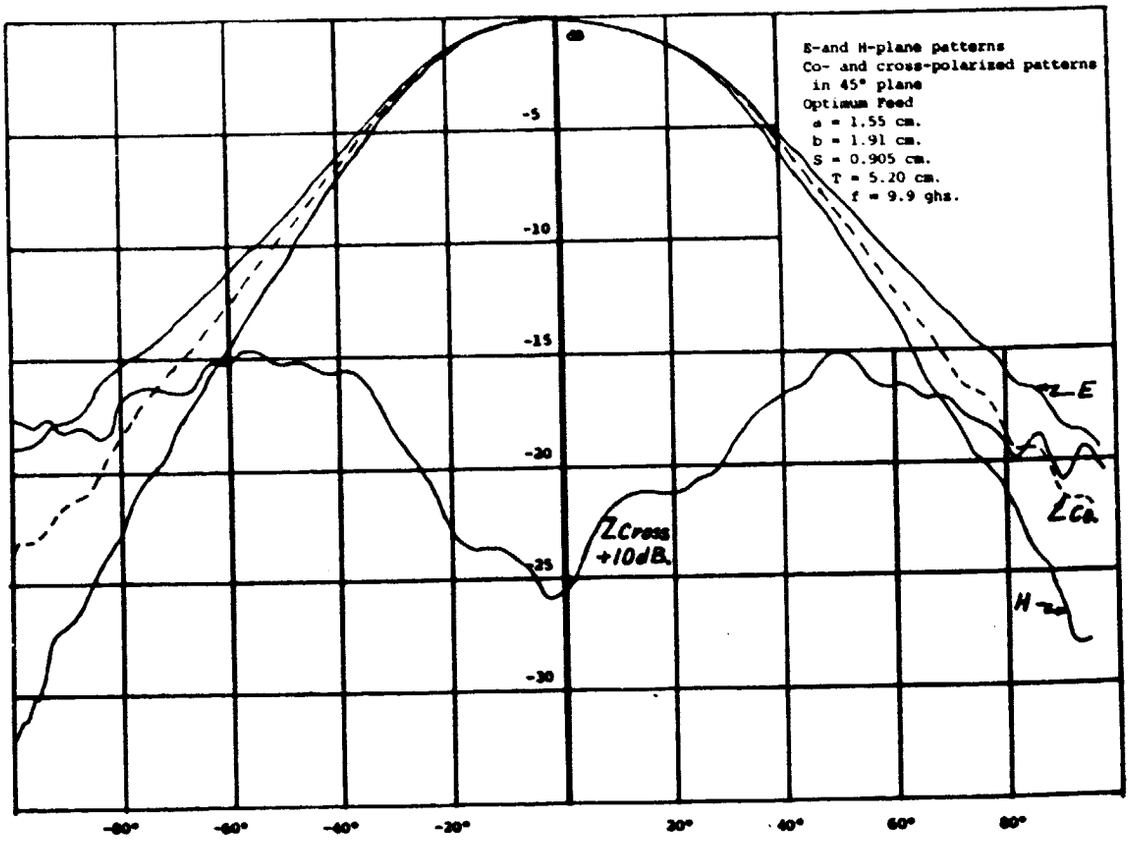

Figure 2.24a - Radiation patterns for optimum feed at 9.9 ghz.

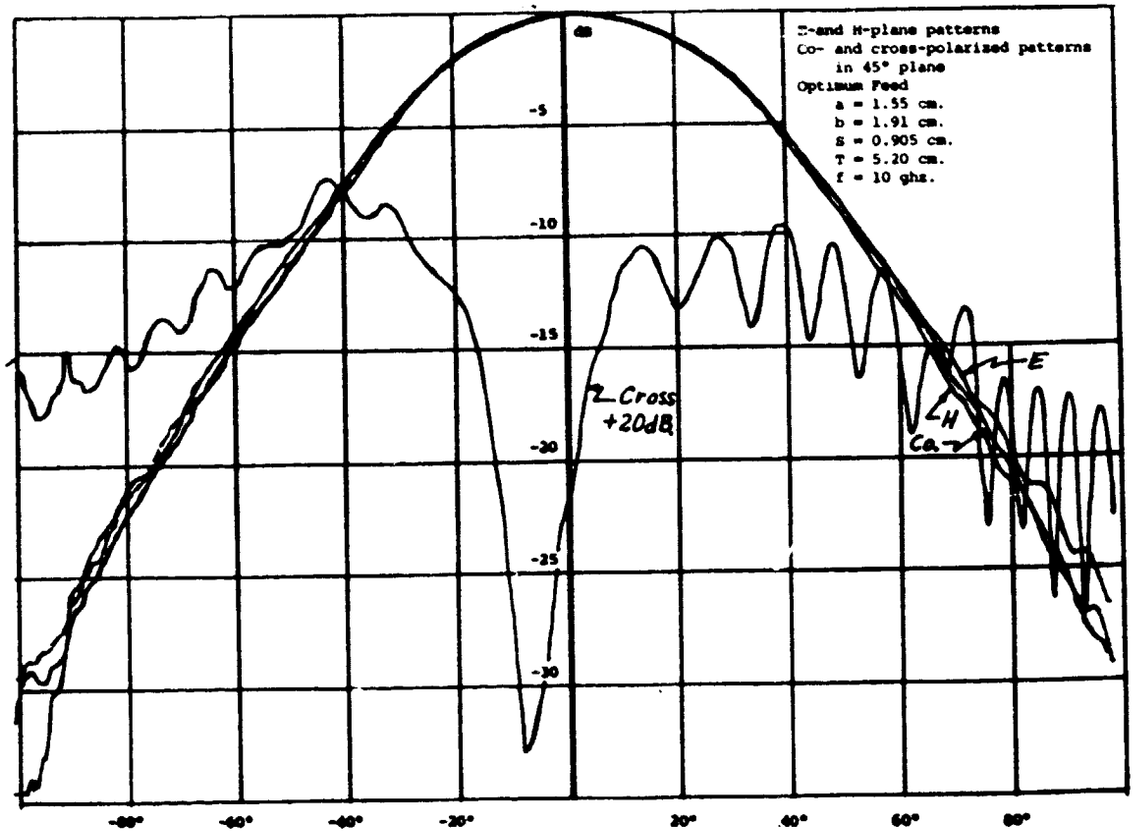

Figure 2.24b - Radiation patterns for optimum feed at 10 ghz.

Figure 2.24, Radiation patterns for optimum feed.

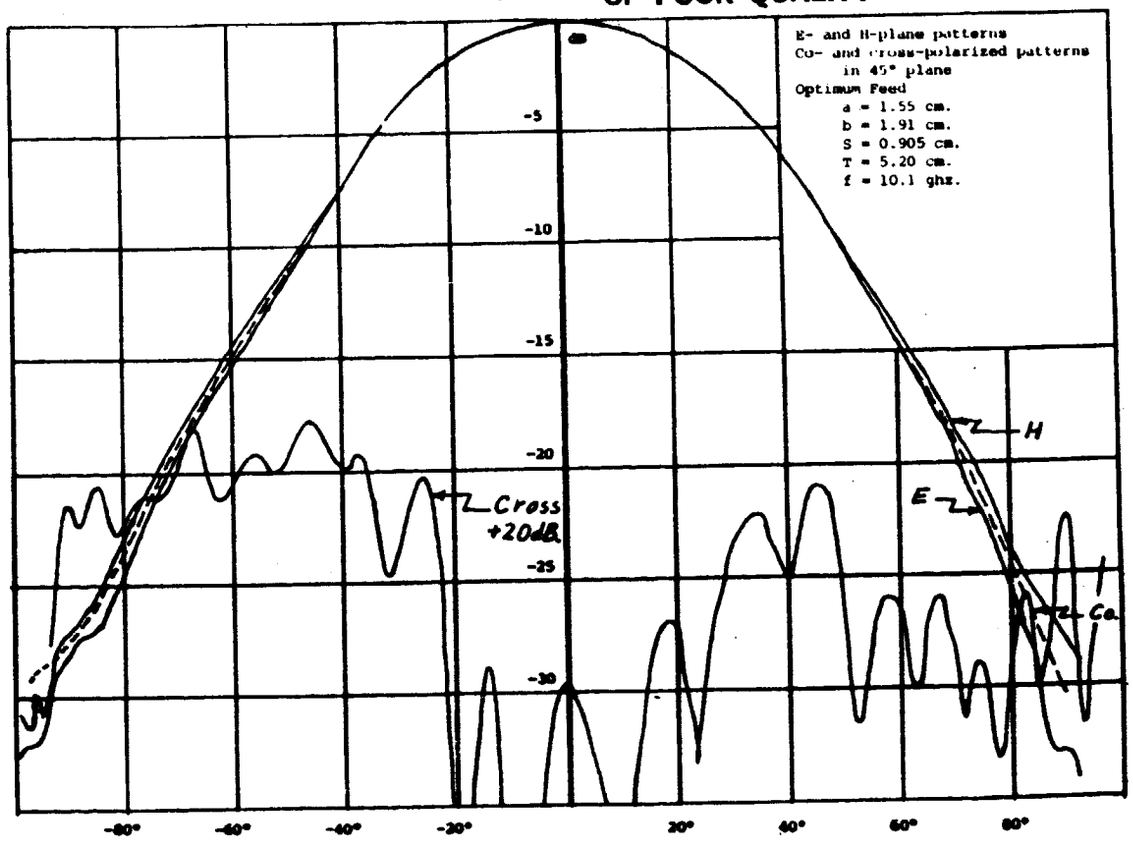

Figure 2.24c - Radiation patterns for optimum feed at 10.1 ghz.

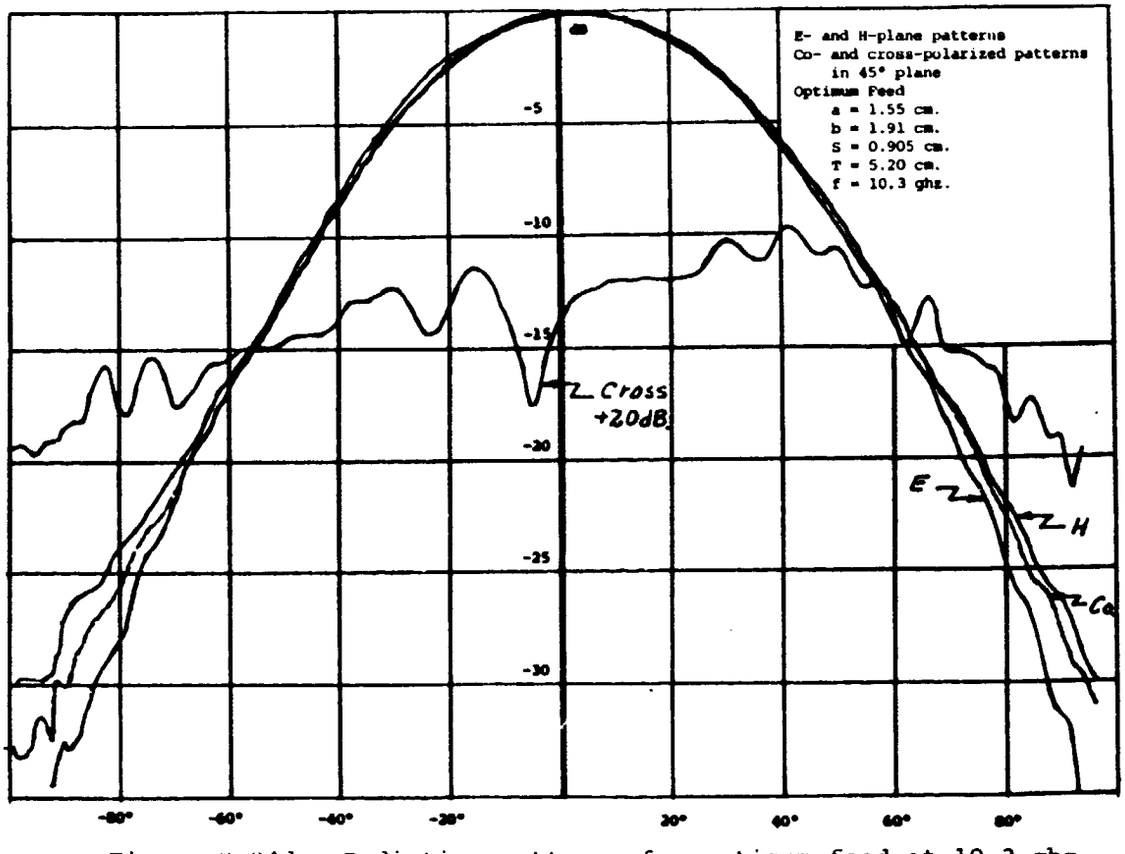

Figure 2.24d - Radiation patterns for optimum feed at 10.3 ghz.

Figure 2.24, Radiation patterns for optimum feed.

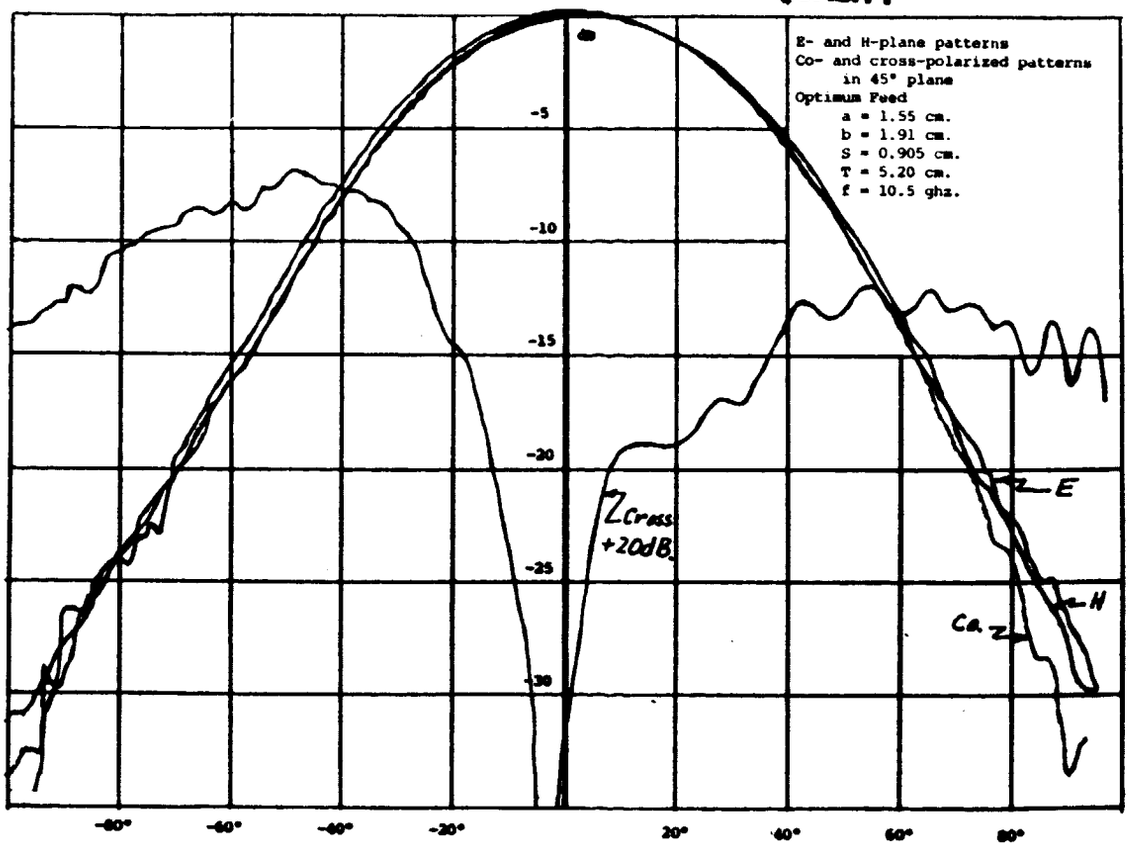

Figure 2.24e - Radiation patterns for optimum feed at 10.5 ghz.

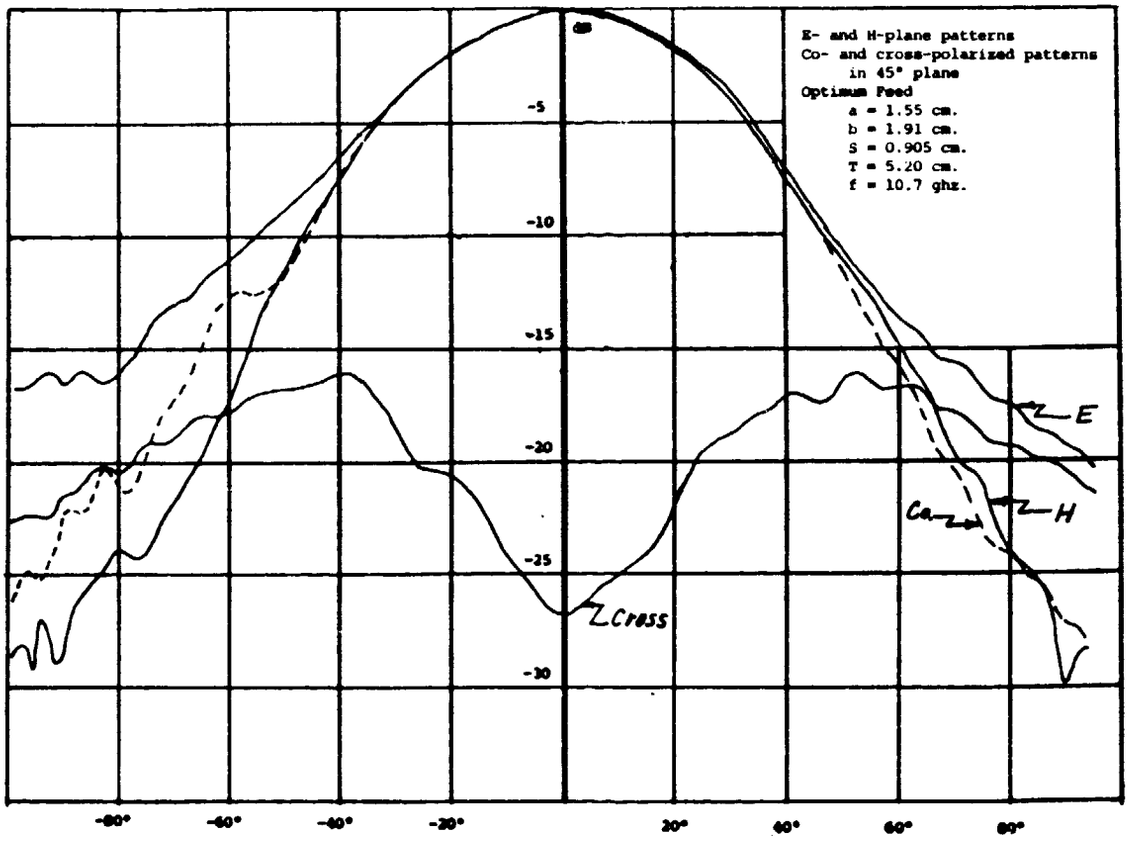

Figure 2.24f - Radiation patterns for optimum feed at 10.7 ghz.

Figure 2.24, Radiation patterns for optimum feed.

polarization as low as -58 dB. at the design center frequency is believed to be due to spurious reflections as well as various small imperfections in the feed.

2.8 PARABOLOIDAL RADIATION PATTERNS

The sub-optimum feed was used to illuminate a 1.22 meter diameter paraboloid with f/D = 0.33. The E- and H-plane patterns as well as the 45° plane co- and cross-polarized patterns were measured.† It was found experimentally that when the four feed support rods were located in the E- and H-planes as shown in Figure 2.25a that the sidelobe level was much higher than predicted, of order -22 dB. to -26 dB. By placing the support rods in the 45° planes as shown in Figure 2.25b the sidelobes remained below -30 dB. In general scatter from the support rods and blockage by the feed makes it difficult to obtain close correlation between measured patterns and theoretical patterns below the -30 dB. level. For this study the objective was to verify that by using sufficient aperture tapering the first two sidelobes could be kept below -30 dB. and the remaining sidelobes below -40 dB. The objective with regard to the first two sidelobes was met but because of scatter it was found that the remaining sidelobes were not always below -40 dB. There also was a limitation of 40 dB. dynamic range for the measurement equipment used.

The measured radiation patterns at 10.3 ghz. with the support rods in the E- and H-planes are shown in Figures 2.26 a-c. It is clear that scatter from the support rods is producing a lot of fill in radiation below the -30 dB. level in addition to producing high sidelobe peaks.

---

†The lack of time did not permit these measurements to be repeated using the optimum feed.

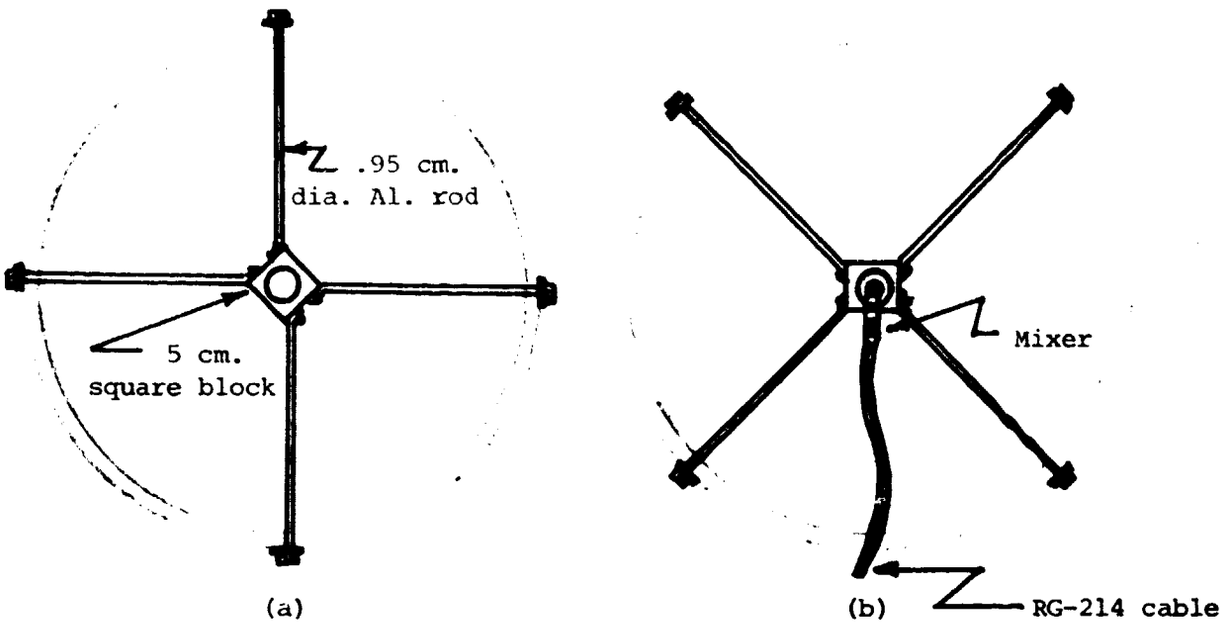

Figure 2.25 - Feed support structure for paraboloid antenna

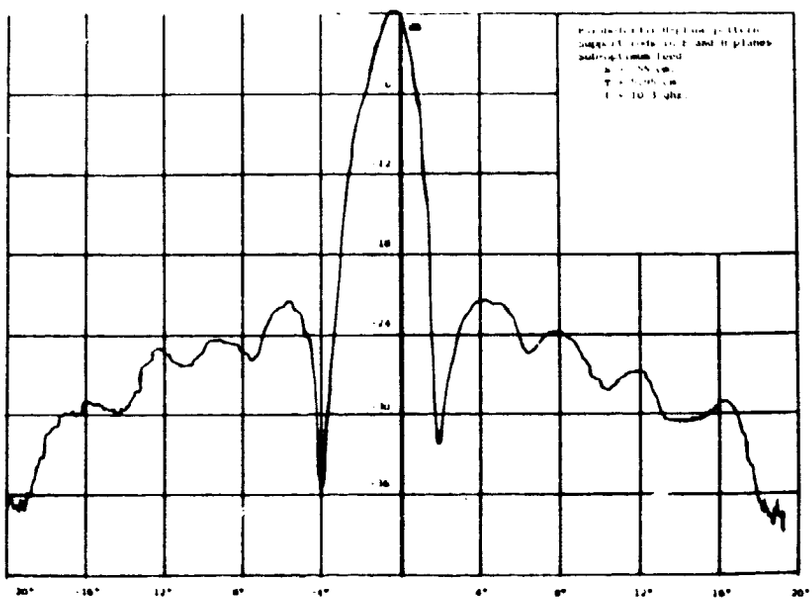

Figure 2.26a - H-plane pattern of 1.22 meter paraboloid illuminated with sub-optimum feed.

Figure 2.26, Radiation patterns for paraboloid illuminated with a sub-optimum feed, f/D = 0.33.

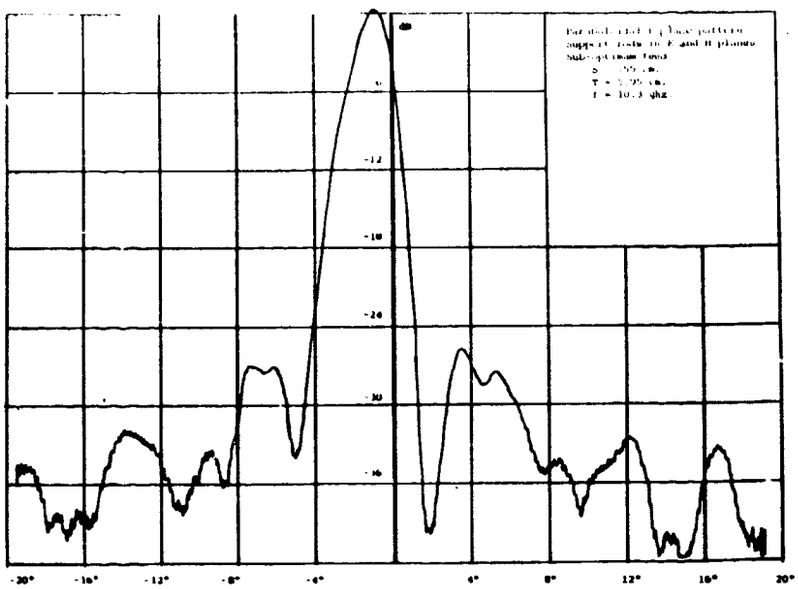

Figure 2.26b - E-plane pattern of 1.22 meter paraboloid illuminated with sub-optimum feed.

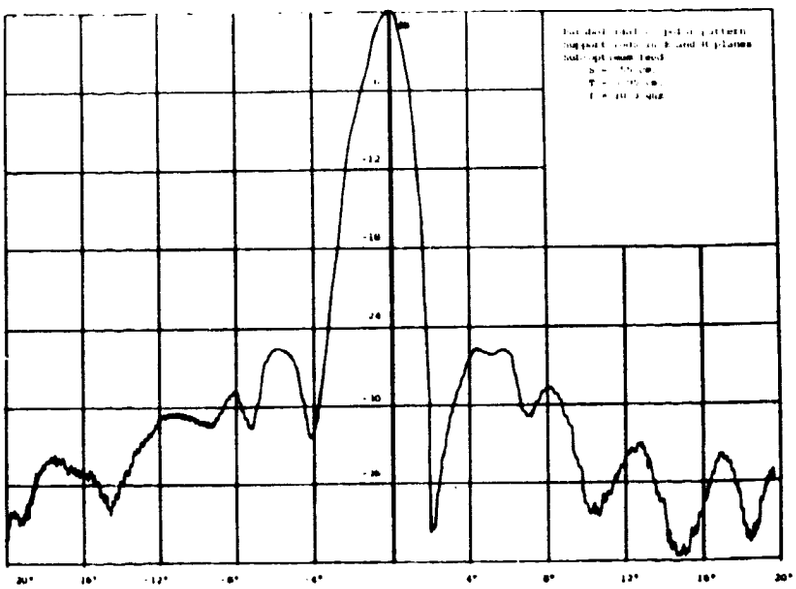

Figure 2.26c - 45° plane co-polarized pattern of 1.22 meter paraboloid illuminated with sub-optimum feed.

Figure 2.26, Radiation patterns for paraboloid illuminated with a sub-optimum feed, f/D = 0.33.

The measured radiation patterns over the frequency range 9.9 ghz. to 10.5 ghz. and with the support rods in the 45° plane are shown in Figures 2.27a-k. The measured peak cross-polarization at 10.1 ghz. and 10.3 ghz. was -31 dB. while at 10.5 ghz. it was -27 dB. The cross-polarization level correlates well with that of the feed. When the E-plane, H-plane, and 45° plane co-polarized patterns are superimposed they are found to be essentially identical down to the -24 dB. level over the frequency range 10 ghz. to 10.5 ghz. Thus the good circular symmetry of the feed radiation pattern is verified. The theoretical pattern is 4.25° wide at the -20 dB. level at 12 ghz. which corresponds to a pattern 5° wide at the -20 dB. level at 10.1 ghz. for the same 1.22 meter diameter reflector. The measured patterns are also 5° wide at the -20 dB. level in accordance with the theoretical predictions.

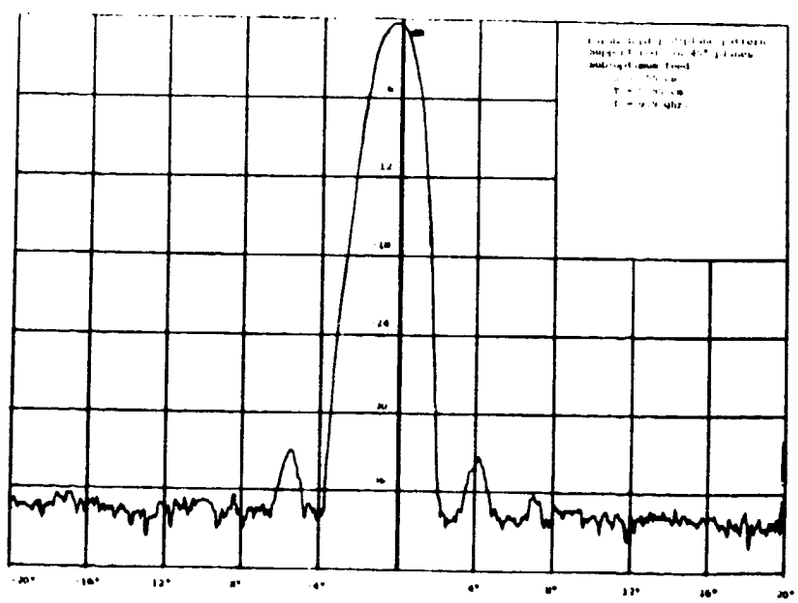

Figure 2.27a - H-plane pattern of 1.22 meter paraboloid illuminated with sub-optimum feed.

Figure 2.27, Radiation patterns for paraboloid illuminated with a sub-optimum feed, f/D = 0.33.

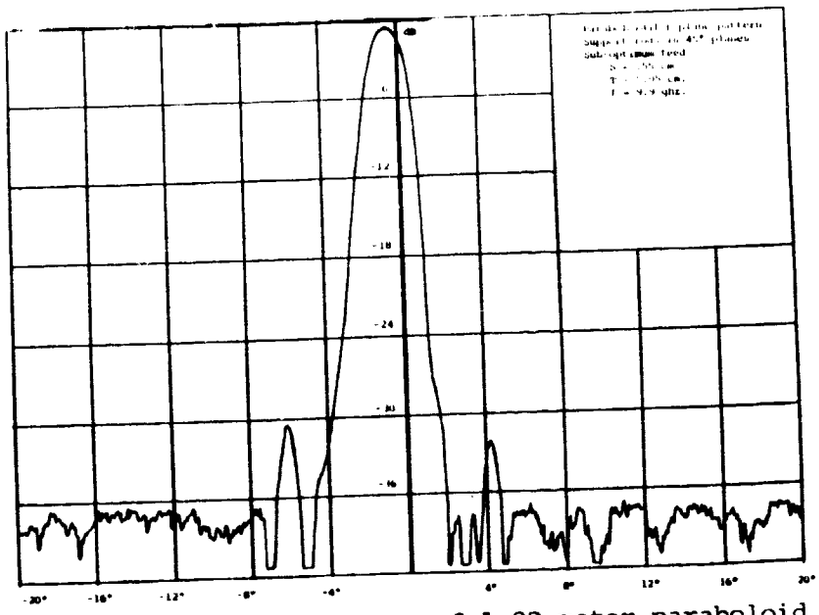

Figure 2.27b - E-plane pattern of 1.22 meter paraboloid illuminated with sub-optimum feed.

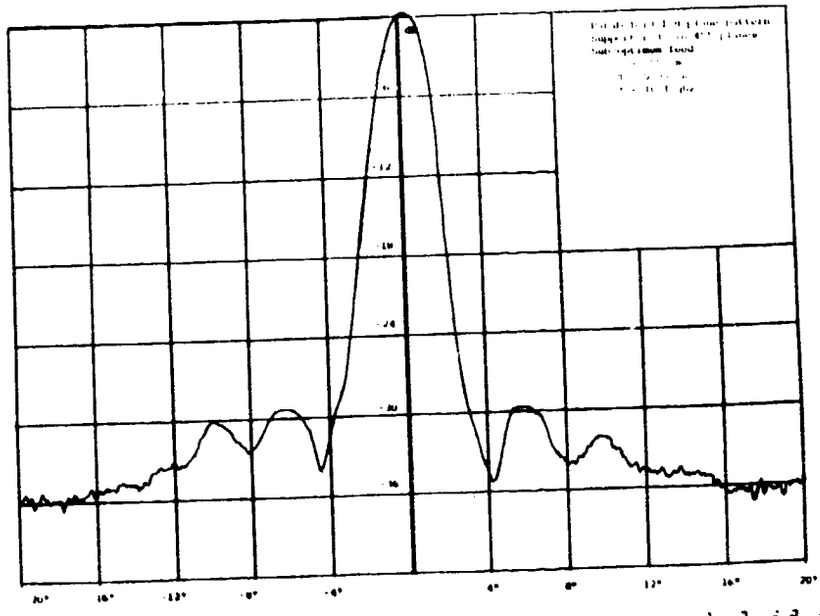

Figure 2.27c - H-plane pattern of 1.22 meter paraboloid illuminated with sub-optimum feed.

Figure 2.27, Radiation patterns for paraboloid illuminated with a sub optimum feed, f/D = 0.33.

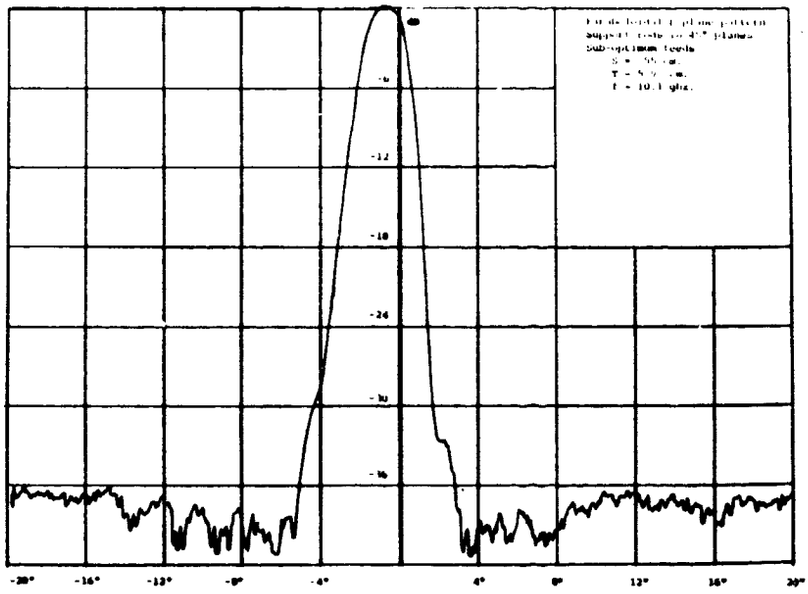

Figure 2.27d - E-plane pattern with 1.22 meter paraboloid illuminated with sub-optimum feed

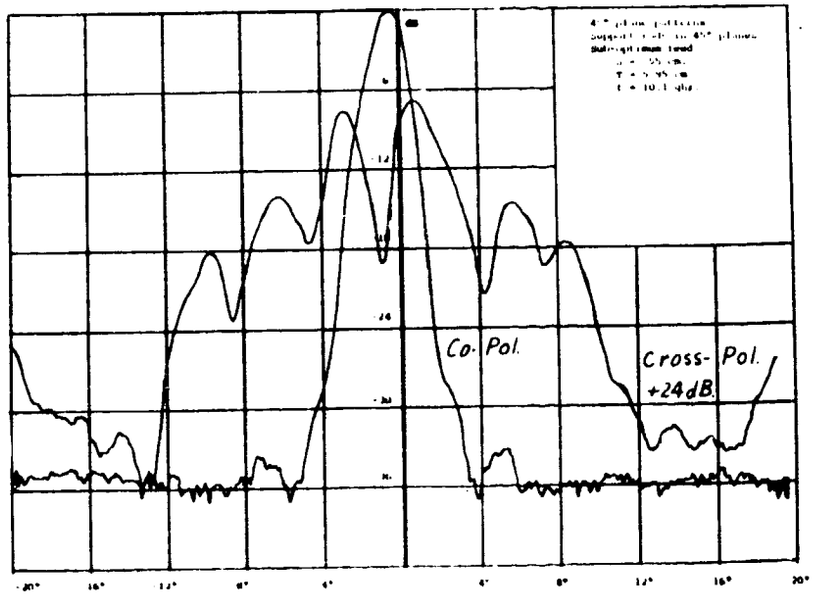

Figure 2.27e - Co- and cross-polarized 45° plane patterns of paraboloid illuminated with sub-optimum feed.

Figure 2.27, Radiation patterns for paraboloid illuminated with a sub-optimum feed, f/D = 0.33.

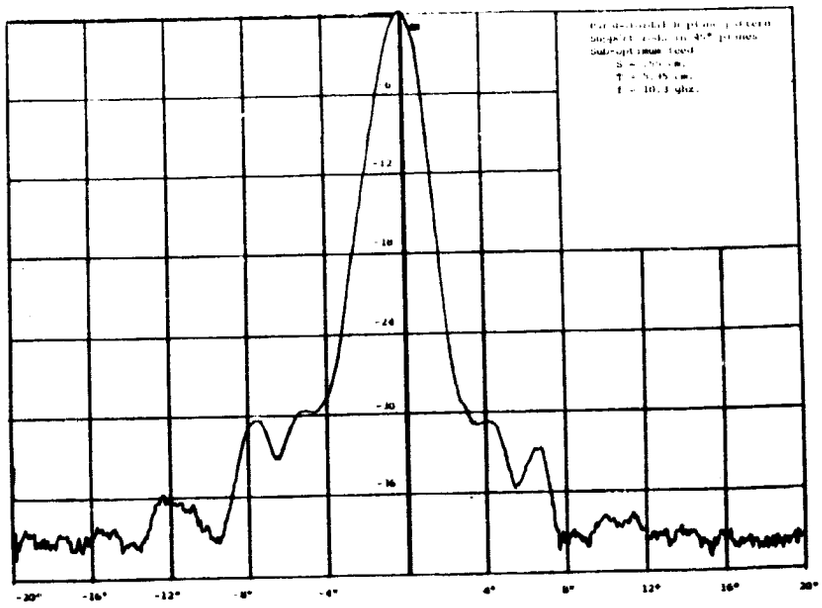

Figure 2.27f - H-plane pattern of 1.22 meter paraboloid illuminated with sub-optimum feed.

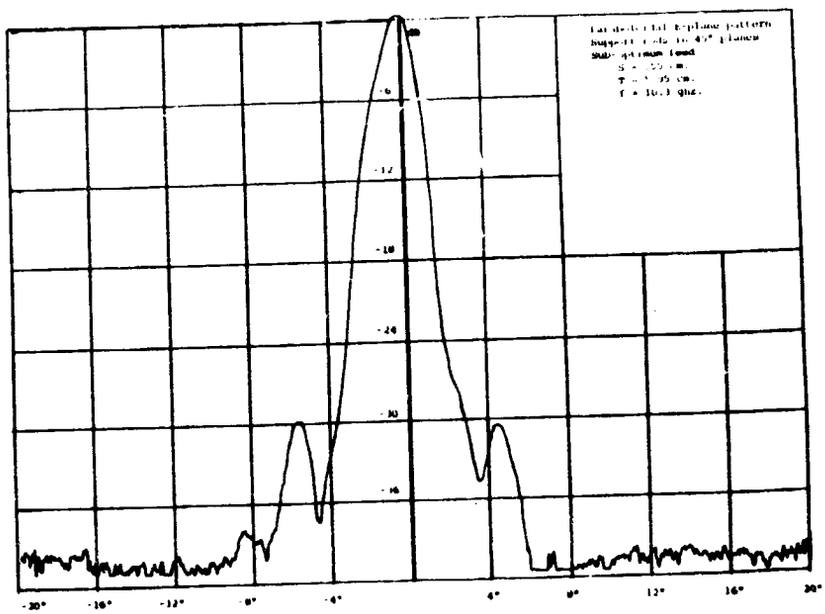

Figure 2.27g E-plane pattern of 1.22 meter paraboloid illuminated with sub-optimum feed

Figure 2.27, Radiation patterns for paraboloid illuminated with a sub-optimum feed, f/D = 0.33.

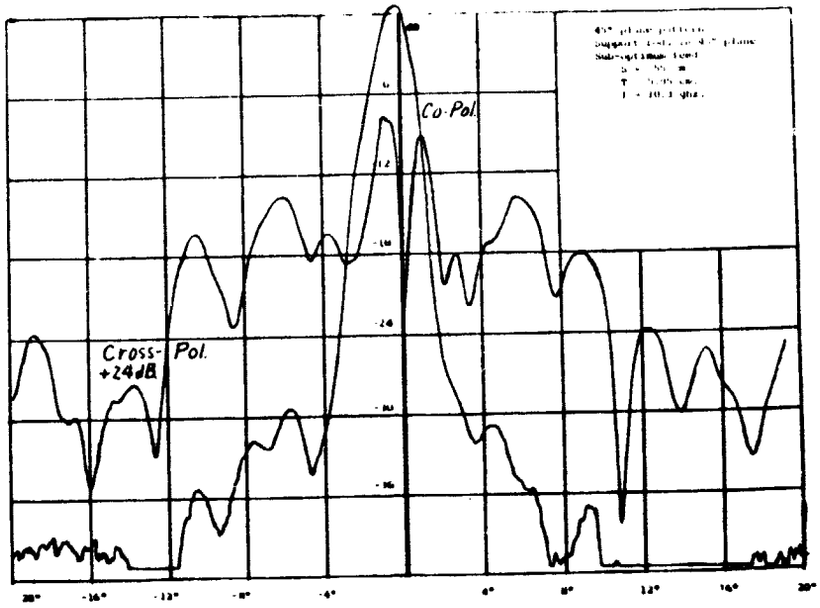

Figure 2.27h - Co- and cross-pclarized 45° plane patterns of paraboloid illuminated with sub-optimum feed.

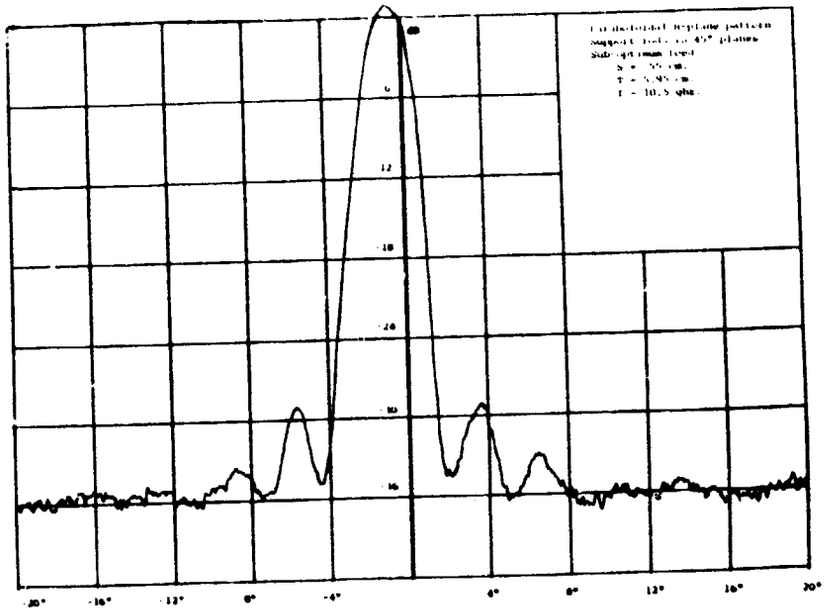

Figure 2.27i - H-plane pattern of 1.22 meter paraboloid illuminated with sub-optimum feed.

Figure 2.27, Radiation patterns for paraboloid illuminated with a sub-optimum feed, f/D = 0.33.

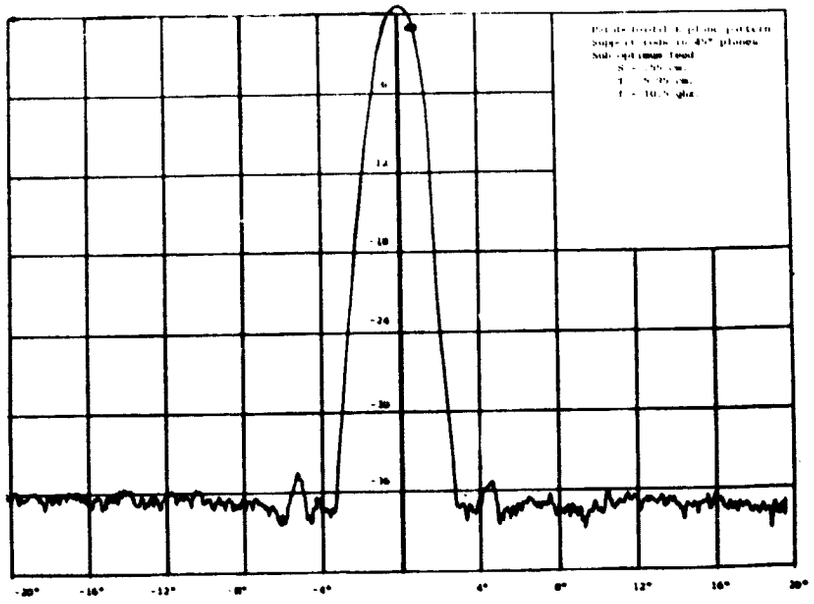

Figure 2.27j - E-plane pattern of 1.22 meter paraboloid illuminated with sub-optimum feed.

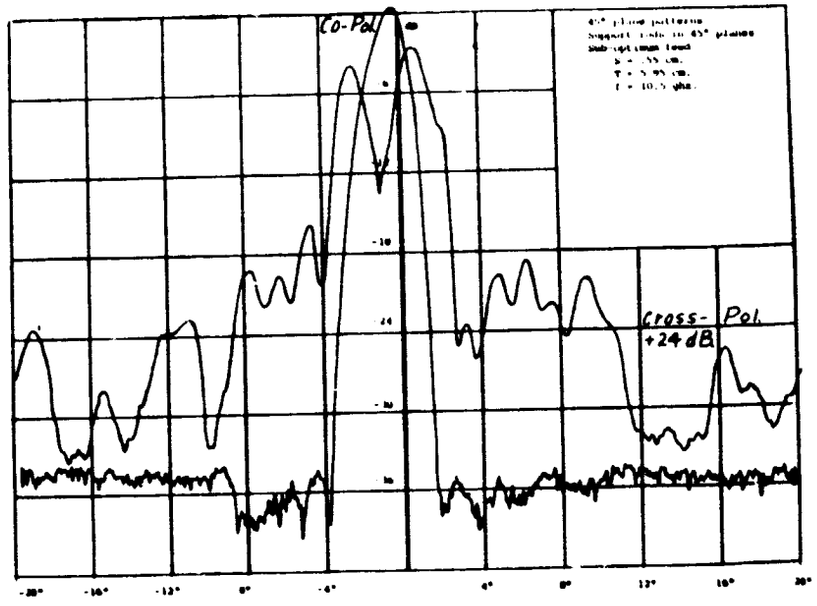

Figure 2.27k - Co- and cross-polarized 45° plane patterns of paraboloid illuminated with sub-optimum feed.

Figure 2.27, Radiation patterns for paraboloid illuminated with a sub-optimum feed, f/D = 0.33

CHAPTER 3

THE SHORT-CUP COAXIAL FEED

3.1 INTRODUCTION

The short-cup coaxial feed shown in Figure 3.1 was investigated by Kumar (Kumar, 1978). The experimentally optimized feed had the following parameters: a = 1.3 cm., b = 3.075 cm., S = 1.6 cm., and T = 0 cm. This feed produced a cross-polarization of -31 dB. at 8 ghz. and 8.5 ghz., -30 dB. at 9 ghz., and -26 dB at 9.5 ghz.

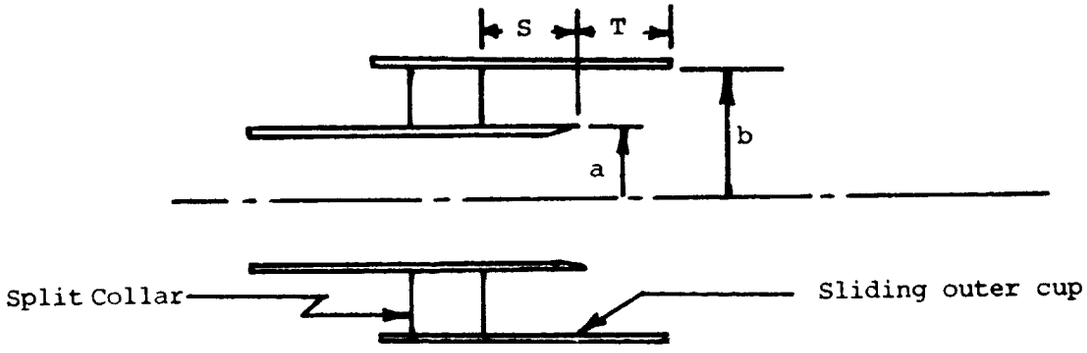

Figure 3.1 - Short-cup coaxial feed

A similar feed was built and the position of the split collar and outer waveguide were varied (S and T parameters) so as to obtain equal E- and H-plane patterns. The waveguide radii used were a = 1.27 cm. and b = 2.54 cm. Since T is small and b is quite large the aperture is excited by TE_{11}, TM_{11}, TE_{12}, TM_{12} circular waveguide modes when T is non-zero. When T is zero the aperture is excited by the TE_{11} mode in the inner guide and by the TE_{11}, TM_{11}, plus higher order TE_{1m} and TM_{1m} modes in the coaxial region. The theoretical analysis of this type of feed is thus much more difficult to carry out than is the case for the dual-mode feed.

By experimental adjustment of the S and T parameters good symmetry between the E- and H-plane patterns can be obtained over a 10-15% frequency band. A cross-polarization of -30 dB. or better can be obtained. The ultimate theoretical minimum cross-polarization and optimum feed parameters have not been determined. It would be desirable to carry out such an analysis since the short-cup feed does appear to have at least twice the bandwidth that the long-cup dual-mode feed does.

3.2 SHORT-CUP COAXIAL FEED - RADIATION PATTERNS

For the chosen a and b parameters, namely a = 1.27 cm., b = 2.54 cm., the best patterns were obtained with S = 1.27 cm., T = 0 cm. Measurements made on a feed with S = 0.95 cm. and T = 0.32 cm. gave almost as good results for the cross-polarization and thus indicates that the S parameter is not very critical. The measured peak cross-polarization as a function of frequency is listed below for S = 1.27 cm., T = 0 cm.

Frequency	Maximum Cross-Polarization
8.5 ghz.	- 10 dB.
9 ghz.	- 31 dB.
9.5 ghz.	- 28 dB.
10 ghz.	- 27 dB.
10.5 ghz.	- 27 dB.
11 ghz.	- 12 dB.

The E-plane, H-plane, and 45° plane co-polarized and cross-polarized patterns at 9, 9.5, 10, and 10.5 ghz. are shown in Figures 3.2a-d. The E- and H-plane patterns exhibit a high degree of symmetry and based

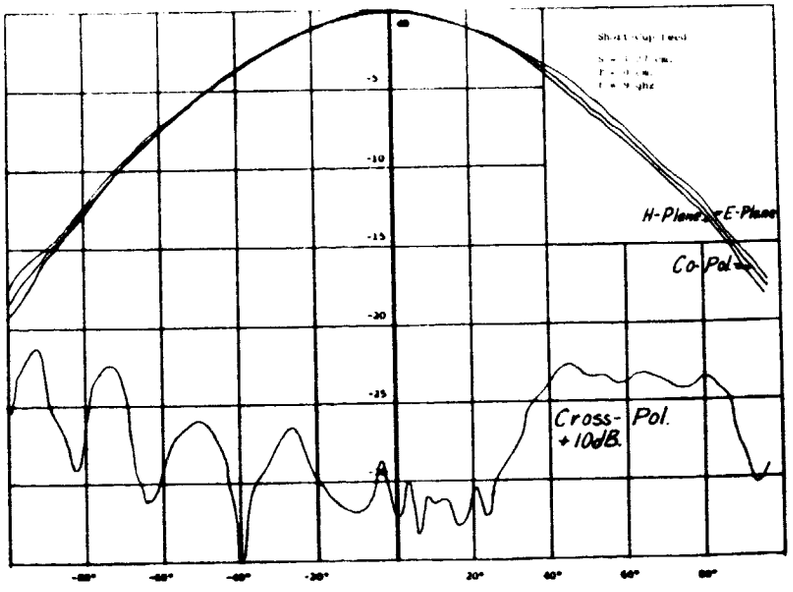

Figure 3.2a - E-plane, H-plane, and 45° plane co- and cross-polarized patterns for short-cup feed.

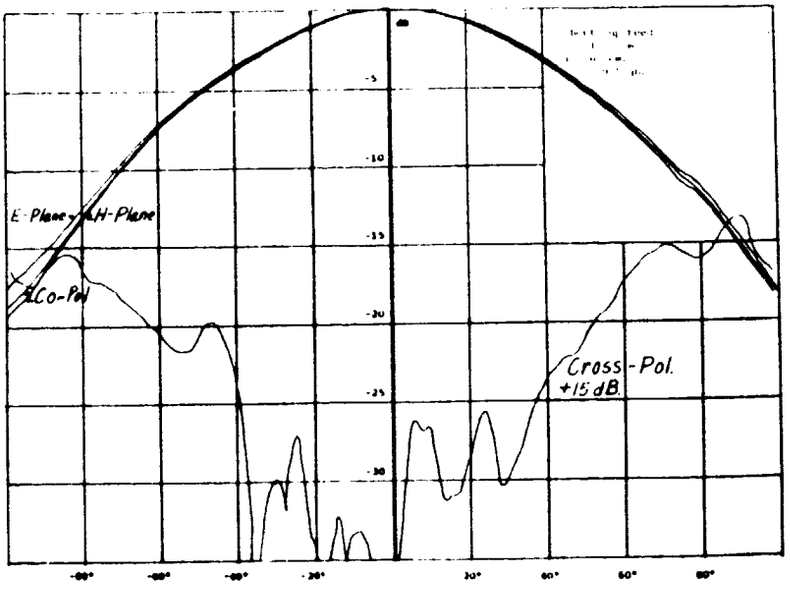

Figure 3.2b - E-plane, H-plane, and 45° plane co- and cross-polarized patterns for short-cup feed.

Figure 3.2, Radiation patterns for short-cup feed.

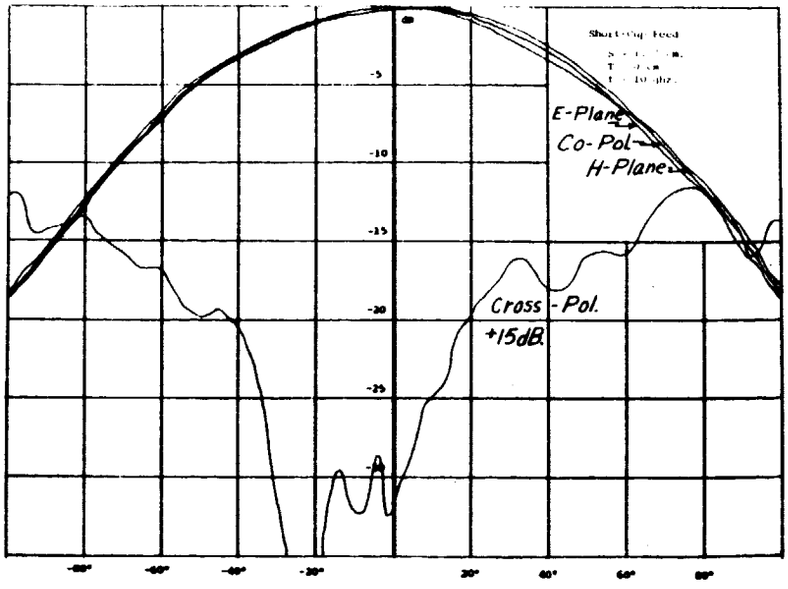

Figure 3.2c - E-plane, H-plane, and 45° plane co- and cross-polarized patterns for short-cup feed.

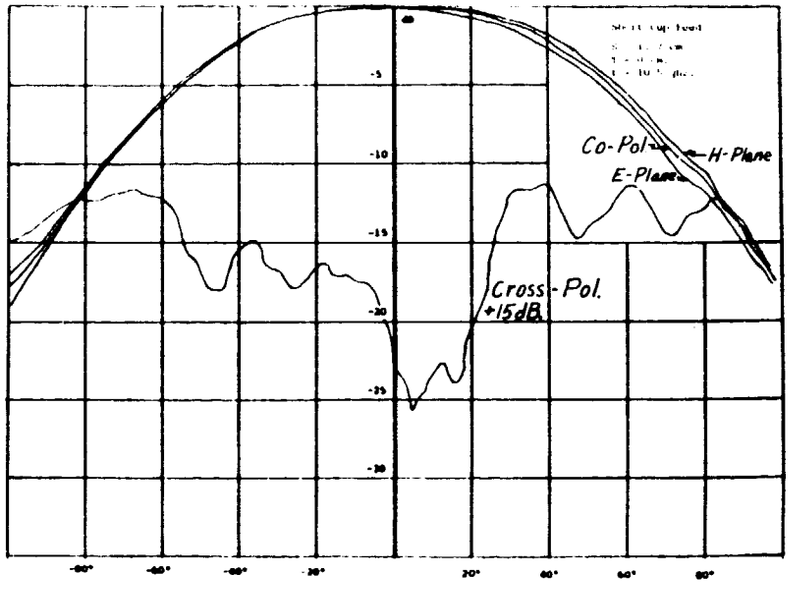

Figure 3.2d - E-plane, H-plane, and 45° plane co- and cross-polarized patterns for short-cup feed.

Figure 3.2, Radiation patterns for short-cup feed.

on this symmetry the cross-polarization should have been smaller than was measured. The cross-polarization in dB. is given by 20 log $|E-H|/2$ where $|E-H|$ is the difference in the E- and H-plane normalized pattern amplitudes. A difference of 1/2 dB. at the -15 dB. level corresponds to a cross-polarization of -45.5 dB. when there is no phase error in the radiation patterns. When there is a phase difference in the E- and H-plane patterns the cross-polarization will be larger. This is probably the reason why the measured cross-polarization was larger than expected from a consideration of the E- and H-plane amplitude patterns alone. It was also noted during the measurements that placing absorber material behind the feed resulted in lower cross-polarization being measured. There apparently was significant interaction between the transmitting horn and the feed which were spaced only 0.7 meter apart.

A noteable feature of the short-cup coaxial feed is that even though the aperture is larger than that of the long-cup dual-mode feed the radiation pattern is very close to that of the circular waveguide alone. This seems to indicate that the modes in the coaxial region are weakly excited. Measurements of the cross-polarization of the circular waveguide alone with the same inner radius a = 1.27 cm. gave a peak cross-polarization of -25 dB. at 9.5 ghz., -30 dB. at 10.5 ghz., and -14 dB. at 11 ghz. In view of these features of the circular waveguide alone it can be expected that only relatively small amplitude modes in the coaxial region will be needed to improve the cross-polarization properties.

3.3 PARABOLOIDAL RADIATION PATTERNS - SHORT-CUP FEED

A 1.22 meter diameter paraboloidal reflector with f/D was illuminated with the short-cup feed and the E- and H-plane as well as the 45° plane co- and cross-polarized patterns measured. These patterns are shown in Figures 3.3a-i for frequencies 9.5 ghz., 10 ghz. and 10.5 ghz. The cross-

polarization was not as good as for the long-cup feed, possibly because of more interaction of the back radiation of the feed with the feed support structure (the long-cup feed is more directional). The measured peak cross-polarization was -28 dB. at 9.5 ghz., -21 dB. at 10 ghz., and -19 dB. at 10.5 ghz. These values are considerably larger than would be expected based on the cross-polarization levels of the feed. It is presumably caused by the feed support structure and its interaction with the radiation from the feed.

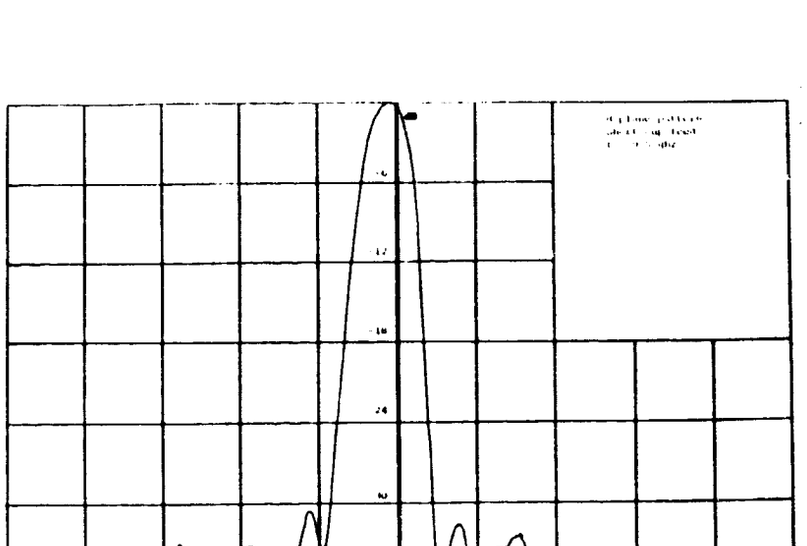

Figure 3.3a - H-plane pattern for paraboloidal reflector illuminated with short-cup feed.

Figure 3.3, Radiation patterns of paraboloidal reflector illuminated with the short-cup feed.

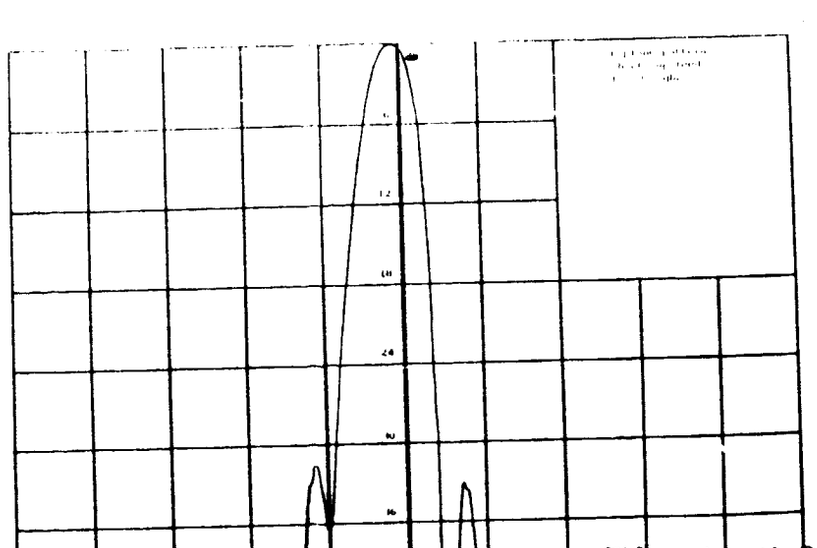

Figure 3.3b - E-plane pattern for paraboloidal reflector illuminated with short-cup feed.

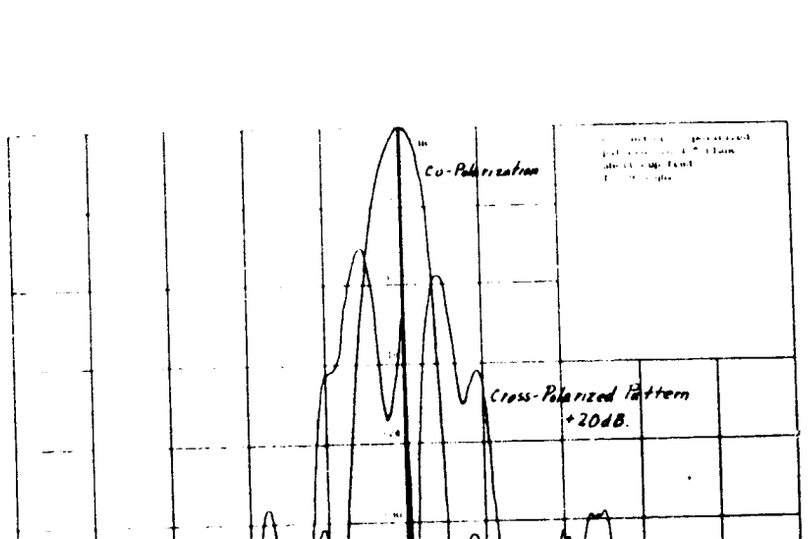

Figure 3.3c - 45° plane co- and cross-polarized patterns for paraboloidal reflector illuminated with short-cup feed.

Figure 3.3, Radiation patterns of paraboloidal reflector illuminated with the short-cup feed.

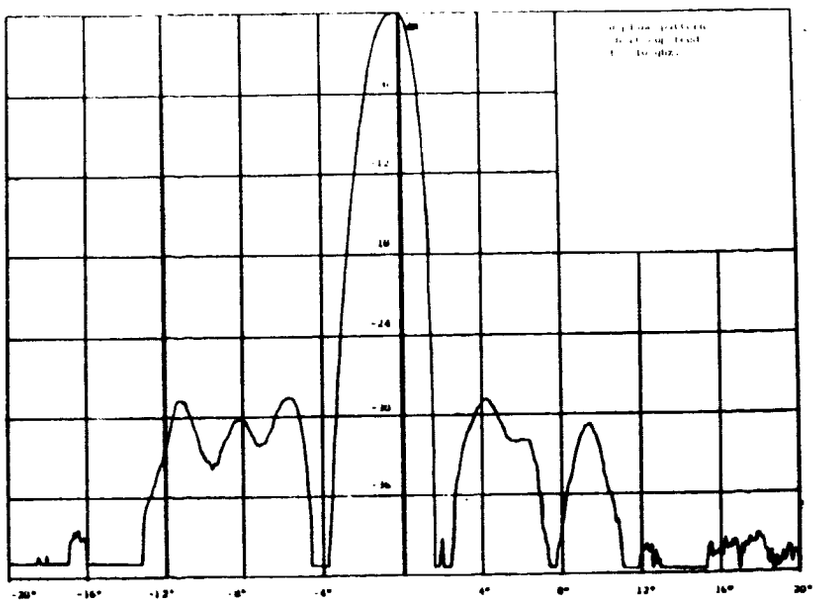

Figure 3.3d - H-plane pattern for paraboloidal reflector illuminated with short-cup feed.

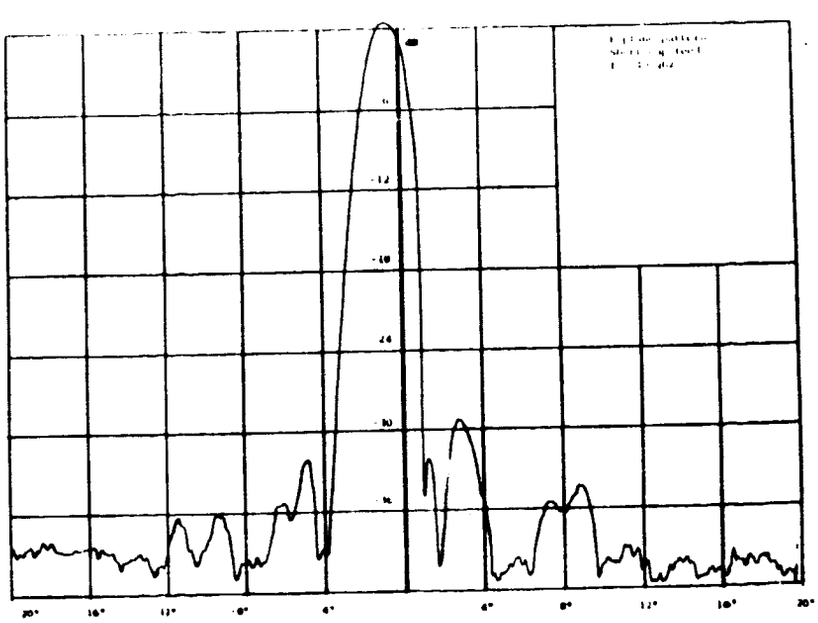

Figure 3.3e - E-plane pattern for paraboloidal reflector illuminated with short-cup feed.

Figure 3.3, Radiation patterns of paraboloidal reflector illuminated with the short-cup feed.

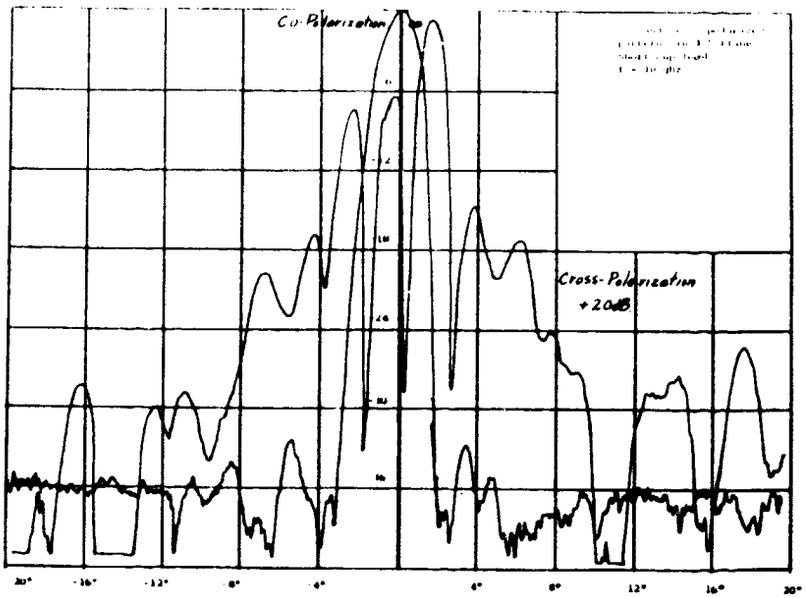

Figure 3.3f - 45° plane co- and cross-polarized patterns for paraboloidal reflector illuminated with short-cup feed.

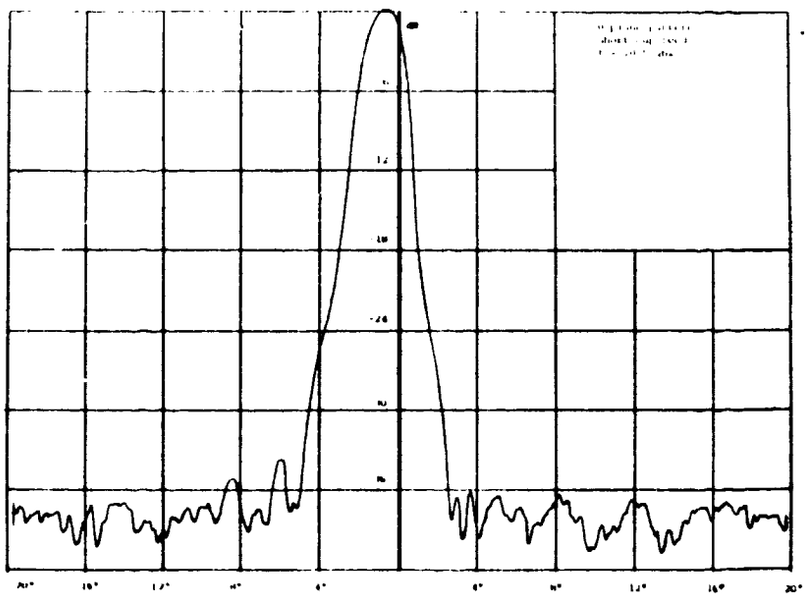

Figure 3.3g - H-plane pattern for paraboloidal reflector illuminated with short-cup feed.

Figure 3.3, Radiation patterns of paraboloidal reflector illuminated with the short-cup feed.

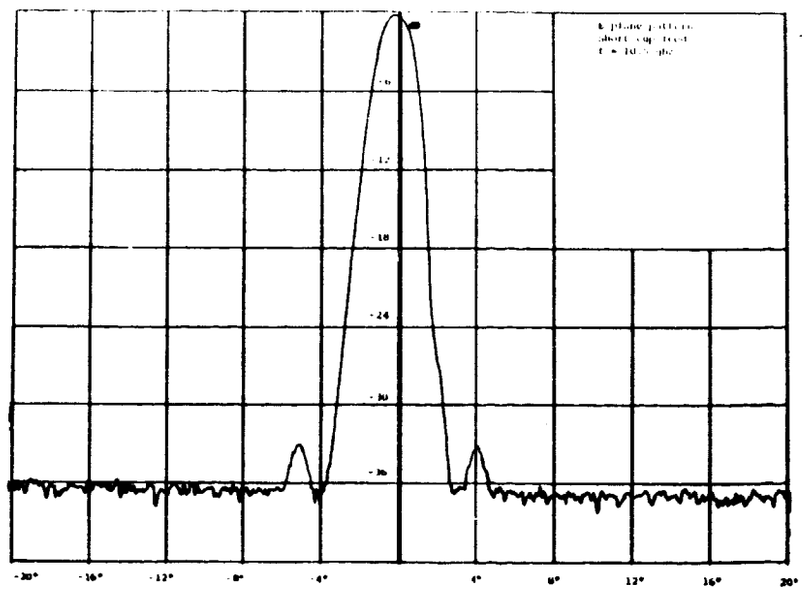

Figure 3.3h - E-plane pattern for paraboloidal reflector illuminated with short-cup feed.

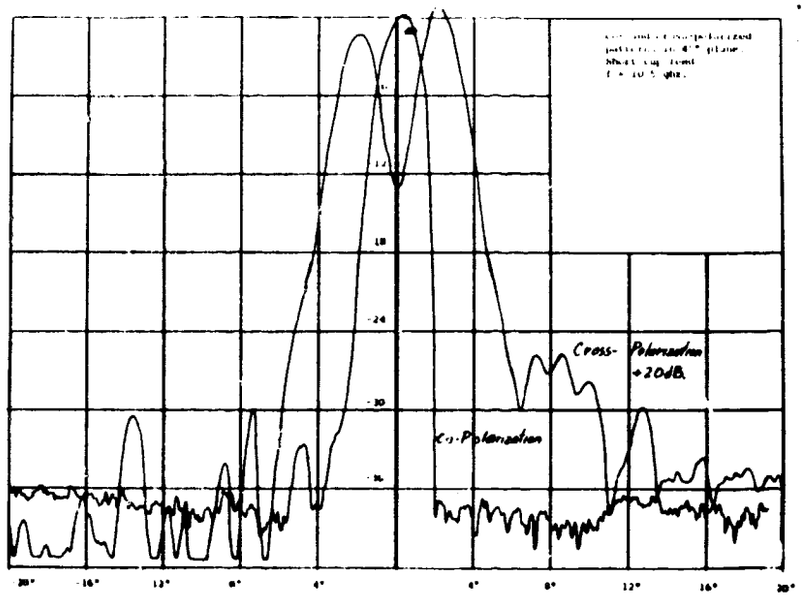

Figure 3.3i - 45° plane co- and cross-polarized patterns for paraboloidal reflector illuminated with short-cup feed.

Figure 3.3, Radiation patterns of paraboloidal reflector illuminated with the short-cup feed.

CHAPTER 4

CONCLUSIONS AND RECOMMENDATIONS

The major findings of this study are:

- A long-cup dual-mode feed can be optimized to have a center frequency cross-polarization peak as low as -58 dB.
- Over a 5% bandw dth the dual-mode feed has a cross-polarization peak below -30 dB., a phase error of less than 10°, and an input VSWR of order 1.1.
- The dual-mode feed, when used to illuminate a 1.22 meter paraboloidal reflector with f/D of around 0.4, will result in sidelobes below -30 dB. and an aperture efficiency of over 70%. The peak cross-polarization level will be comparable to that of the feed.
- The short-cup coaxial feed can be optimized to produce low cross-polarization (or order -30 dB. or less) over a 10-15% bandwidth.
- For prime focus antennas designed for sidelobes and cross-polarization below -30 dB. one must pay careful attention to the feed support structure in order to achieve the desired characteristics.

Some of the recommendations for future work are:

- Derive analytical solutions for the short-cup coaxial feed and optimum design data. This feed has the advantage that the bandwidth appears to be 10-15%.
- Develop optimum feed support structures in order to achieve low cross-polarization and sidelobe levels.
- It would be desirable to repeat the cross-polarization measurements on an antenna range that was carefully designed so as to enable field strengths 60 dB. below the radiation maximum to be measured.

2 OF 2

31585

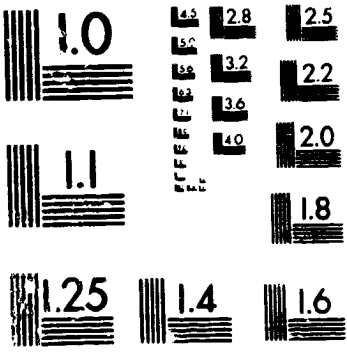

MICROCOPY RESOLUTION TEST CHART
NATIONAL BUREAU OF STANDARDS
STANDARD REFERENCE MATERIAL 1010a
(ANSI and ISO TEST CHART No. 2)

REFERENCES

Clarricoats, P.J.B., and G. R. Poulton. High Efficiency Microwave Reflector Antennas - A Review, Proc. IEEE, Vol. 65, pp. 1470-1504, Oct. 1977.

Hansen, J.E., and L. Shafai. Cross-polarized Radiation from Waveguides and Narrow Angle Horns, Elec. Letters, Vol. 13, pp. 313-315, 1977.

Hockham, G.A. Investigation of a 90° Corrugated Horn, Elec. Letters, Vol. 12, pp. 199-201, 1976.

James, G.L. Radiation Properties of 90° Concial Horns. Elec. Letters, Vol. 13, pp. 293-294, 1977.

James, G.L., and C. J. Greene. Effect of Wall Thickness on Radiation from Circular Waveguides, Elec. Letters, Vol. 14, pp. 90-91, 1978.

Johnson, T. W., and D. L. Moffatt. Electromagnetic Scattering by Open Circular Waveguides, Tech. Rept. No. 710816-9, Electro-Science Laboratory, The Ohio State University, Dec. 1980.

Kay, A. F. The Scalar Feed, U. S. Air Force Cambridge Res. Labs., Rept. No. 62-347, March 1964.

Koch, G. F. Coaxial Feeds for High Aperture Efficiency and Low Spillover for Paraboloidal Reflector Antennas, IEEE Trans., Vol. AP-21, pp. 164-169, March 1973.

Kouznetsov, V. Sidelobe Reduction in Circular Aperture Antennas, European Antenna Conference Digest, London, 1978.

Kumar, A. Experimental Study of a Dielectric Rod Enclosed by a Waveguide for Use as a Feed, Elec. Letters, Vol. 12, pp. 666-668, Dec. 1976.

Kumar, A. Reduce Cross-Polarization in Reflector Type Antennas, Microwaves, Vol. 17, pp. 48-51, March, 1978.

Kumar, A. Waveguide Feed Reduces Cross-Polarization Levels, Microwave Journal, Vol. 21, pp. 86-88, March 1978.

Ludwig, A. C. Antenna Feed Efficiency, Space Programs Summary 37-26, Vol. IV, pp. 200-208, 1965, Jet Prop. Lab., CIT, Pasadena, Calif.

Ludwig, A. C. The Definition of Cross-Polarization, IEEE Trans., Vol. AP-21, pp. 116-119, Jan. 1973.

Potter, P. D. A New Horn Antenna With Suppressed Sidelobes and Equal Beamwidths, Microwave Journal, Vol. 6, pp. 71-78, 1963.

Satoh, T. Dielectric-Loaded Horn Antenna, IEEE Trans., Vol. AP-20, pp. 199-201, 1972.

Scheffer, H. Improvements in the Development of Coaxial Feeds for Parabolical Reflector Antennas, 5'th European Microwave Conference, Hamburg, Germany, Sept. 1975.

Schilling, H. Dual-Mode Coaxial Feed for Parabolic Antennas, Ph.D. Thesis, Dept. of Electrical Engineering and Applied Physics, Case Western Reserve University, 1982.

Silver, S. Microwave Antenna Theory and Design, McGraw-Hill Book Co. New York, 1949.

Thomas, B. MacA. Theoretical Performance of Prime-Focus Paraboloids Using Hybrid-Mode Feeds, Proc. IEE, Vol. 118, pp. 1539-1549, 1971.

Weinstein, L. A. The Theory of Diffraction and the Factrorization Method, Golem Press, Boulder, Colo., 1969.

Wood, P. J. Reflector Antenna Analysis and Design, Peregrinus Ltd., England, 1980.

APPENDIX A

SCATTERING MATRIX FOR BIFURCATION JUNCTION

The first step in determing the optimum feed dimensions is to solve the problem of mode coupling in the bifurcated waveguide shown in Figure A1. This problem can be formulated as follows: (1) Express the transverse electric and magnetic fields at the junction in terms of a series expansion involving the TE_{1n} and TM_{1n} modes in each waveguide. (2) Make the transverse fields continuous across the junction. (3) From the continuity conditions use Fourier analysis to obtain algebraic equations for the mode amplitudes. (4) Solve the infinite set of equations by the residue calculus technique.

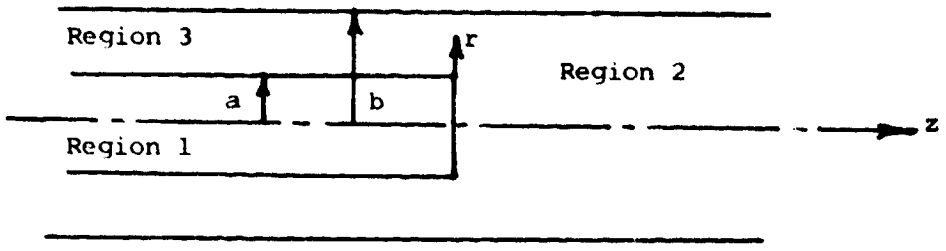

Figure A1 - Birfurcated circular waveguide showing the three different waveguide regions.

The following notation will be used:

1. Transverse electric field of TE_{1n} modes in regions 1, 2, 3 is

$\vec{e}_{1n}$, $\vec{e}_{2n}$, $\vec{e}_{3n}$.

2. Transverse electric field of TM_{1n} modes in regions 1,2,3 is $\vec{E}_{1n}$, $\vec{E}_{2n}$, $\vec{E}_{3n}$.

3. TE_{1n} mode amplitudes in regions 1,2,3 are $a_n^{\pm}$, $b_n^{\pm}$, and $c_n^{\pm}$ where + stands for incident wave and - for reflected or scattered wave.

4. TM_{1n} mode amplitudes in regions 1,2,3 are $A_n^{\pm}$, $B_n^{\pm}$, and $C_n^{\pm}$.

5. TE_{1n} propagation constants in regions 1,2,3 are β_{1n}, β_{2n}, β_{3n}.

6. TM_{1n} propagation constants in regions 1,2,3 are γ_{1n}, γ_{2n}, γ_{3n}.

7. Cutoff wave numbers for TE_{1n} modes in the three regions are k_{1n}, k_{2n}, k_{3n}.

8. Cutoff wave numbers for TM_{1n} modes in the three regions are ℓ_{1n}, ℓ_{2n}, ℓ_{3n}.

It will be assumed that only the TE_{11} mode can propagate in regions 1 and 3 while both TE_{11} and TM_{11} modes can propagate in region 2. It is also assumed that propagating modes are incident in all three regions.

The equations expressing the continuity of the transverse electric field in the $z = 0$ plane is

$$(b_1^+ + b_1^-)\vec{e}_{21} + (B_1^+ + B_1^-)\vec{E}_{21} + \sum_{n=2}^{\infty} (b_n^- \vec{e}_{2n} + B_n^- \vec{E}_{2n})$$

$$= \begin{cases} (a_1^+ + a_1^-)\vec{e}_{11} + A_1^- \vec{E}_{11} + \sum_{n=2}^{\infty} (a_n^- \vec{e}_{1n} + A_n^- \vec{E}_{1n}), & 0 < r < a \\ (c_1^+ + c_1^-)\vec{e}_{31} + C_1^- \vec{E}_{31} + \sum_{n=2}^{\infty} (c_n^- \vec{e}_{3n} + C_n^- \vec{E}_{3n}), & a < r < b \end{cases} \qquad (A1)$$

The equation that expresses the continuity of the transverse magnetic field at $z = 0$ is

$$(b_1^+ - b_1^-)\hat{\beta}_{21}\vec{e}_{21} + (B_1^+ - B_1^-)\hat{\gamma}_{21}^{-1}\vec{E}_{21} - \sum_{n=2}^{\infty}(b_n^-\hat{\beta}_{2n}\vec{e}_{2n} + B_n^-\hat{\gamma}_{2n}^{-1}\vec{E}_{2n})$$

$$= \begin{cases} (-a_1^+ + a_1^-)\hat{\beta}_{11}\vec{e}_{11} + A_1^-\hat{\gamma}_{11}^{-1}\vec{E}_{11} + \sum_{n=2}^{\infty}(a_n^-\hat{\beta}_{1n}\vec{e}_{1n} + A_n^-\hat{\gamma}_{1n}^{-1}\vec{E}_{1n}), & 0 < r < a \\ (-c_1^+ + c_1^-)\hat{\beta}_{31}\vec{e}_{31} + C_1^-\hat{\gamma}_{31}^{-1}\vec{E}_{31} + \sum_{n=2}^{\infty}(c_n^-\hat{\beta}_{3n}\vec{e}_{3n} + C_n^-\hat{\gamma}_{3n}^{-1}\vec{E}_{3n}), & a < r < b \end{cases} \quad \text{(A2)}$$

The waveguide modes are normalized such that power flow is given by $1/2\,|a_n^+|^2$, $1/2\,|A_n^+|^2$, etc. In (2) $\hat{\beta}_{21} = \beta_{21}/k_o$, $\hat{\gamma}_{21} = \gamma_{21}/k_o$ etc.

Thus we have

$$\int_0^a \int_0^{2\pi} \vec{e}_{1n} \cdot \vec{e}_{1n}\, r\, dr\, d\phi = \frac{k_o Z_o}{\beta_{1n}} \quad \text{(A3a)}$$

$$\int_0^a \int_0^{2\pi} \vec{E}_{1n} \cdot \vec{E}_{1n}\, r\, dr\, d\phi = \frac{\gamma_{1n} Z_o}{k_o} \quad \text{(A3b)}$$

$$\int_0^b \int_0^{2\pi} \vec{e}_{2n} \cdot \vec{e}_{2n}\, r\, dr\, d\phi = \frac{k_o Z_o}{\beta_{2n}} \quad \text{(A3c)}$$

$$\int_0^b \int_0^{2\pi} \vec{E}_{2n} \cdot \vec{E}_{2n}\, r\, dr\, d\phi = \frac{\gamma_{2n} Z_o}{k_o} \quad \text{(A3d)}$$

$$\int_0^b \int_a^{2\pi} \vec{e}_{3n} \cdot \vec{e}_{3n}\, r\, dr\, d\phi = \frac{k_o Z_o}{\beta_{3n}} \quad \text{(A3e)}$$

$$\int_0^b \int_a^{2\pi} \vec{E}_{3n} \cdot \vec{E}_{3n}\, r\, dr\, d\phi = \frac{\gamma_{3n} Z_o}{k_o} \quad \text{(A3f)}$$

where $k_o = 2\pi/\lambda_o$ and $Z_o = (\mu_o/\epsilon_o)^{1/2}$.

We now introduce the following mode coupling coefficients:

$$\int_0^{2\pi}\int_0^{a} \vec{e}_{1n}\cdot\vec{e}_{2m}\, r\, dr\, d\phi = f_{nm} \tag{A4a}$$

$$\int_0^{2\pi}\int_0^{a} \vec{e}_{1n}\cdot\vec{E}_{2m}\, r\, dr\, d\phi = \alpha_{nm} \tag{A4b}$$

$$\int_0^{2\pi}\int_0^{a} \vec{E}_{1n}\cdot\vec{e}_{2m}\, r\, dr\, d\phi = \delta_{nm} = 0 \tag{A4c}$$

$$\int_0^{2\pi}\int_0^{a} \vec{E}_{1n}\cdot\vec{E}_{2m}\, r\, dr\, d\phi = F_{nm} \tag{A4d}$$

$$\int_0^{2\pi}\int_a^{b} \vec{e}_{3n}\cdot\vec{e}_{2m}\, r\, dr\, d\phi = g_{nm} \tag{A4e}$$

$$\int_0^{2\pi}\int_a^{b} \vec{e}_{3n}\cdot\vec{E}_{2m}\, r\, dr\, d\phi = \nu_{nm} \tag{A4f}$$

$$\int_0^{2\pi}\int_a^{b} \vec{E}_{3n}\cdot\vec{e}_{2m}\, r\, dr\, d\phi = \mu_{nm} = 0 \tag{A4g}$$

$$\int_0^{2\pi}\int_a^{b} \vec{E}_{3n}\cdot\vec{E}_{2m}\, r\, dr\, d\phi = G_{nm} \tag{A4h}$$

The normalized mode functions are given by

$$\vec{e}_{1n} = \frac{\vec{a}_z \times \nabla_t J_1(k_{1n} r)\cos\phi}{\sqrt{\frac{\pi}{2}\,(k_{1n}^2 a^2 - 1)\; J_1(k_{1n} a)}} \left(\frac{k_o Z_o}{\beta_{1n}}\right)^{1/2} \tag{A5a}$$

where $d\,J_1(k_{1n}r)/d(k_{1n}r) = J_1'(k_{1n}r) = 0$ at $r = a$.

$$\vec{E}_{1n} = \frac{\nabla_t J_1(\ell_{1n} r)\sin\phi}{\sqrt{\frac{\pi}{2}}\,\ell_{1n}\, a\, J_1'(\ell_{1n} a)} \left(\frac{\gamma_{1n} Z_o}{k_o}\right)^{1/2} \qquad \text{(A5b)}$$

where $J_1(\ell_{1n} a) = 0.$

$$\vec{e}_{2n} = \frac{\vec{a}_z \times \nabla_t J_1(k_{2n} r)\cos\phi}{\sqrt{\frac{\pi}{2}(k_{2n}^2 b^2 - 1)}\; J_1(k_{2n} b)} \left(\frac{k_o Z_o}{\beta_{2n}}\right)^{1/2} \qquad \text{(A5c)}$$

where $J_1'(k_{2n} b) = 0.$

$$\vec{E}_{2n} = \frac{\nabla_t J_1(\ell_{2n} r)\sin\phi}{\sqrt{\frac{\pi}{2}}\,\ell_{2n} b\, J_1'(\ell_{2n} b)} \left(\frac{\gamma_{2n} Z_o}{k_o}\right)^{1/2} \qquad \text{(A5d)}$$

where $J_1(\ell_{2n} b) = 0$

$$\vec{e}_{3n} = \frac{\vec{a}_z \times \nabla_t Z_1(k_{3n} r)\cos\phi}{\sqrt{\frac{\pi}{2}}\left[(k_{3n}^2 b^2 - 1) Z_1^2(k_{3n} b) - (k_{3n}^2 a^2 - 1) Z_1^2(k_{3n} a)\right]^{1/2}} \left(\frac{k_o Z_o}{\beta_{3n}}\right)^{1/2} \qquad \text{(A5e)}$$

where $Z_1(k_{3n} r) = J_1'(k_{3n} a) Y_1(k_{3n} r) - Y_1'(k_{3n} a) J_1(k_{3n} r)$ and

$Z_1'(k_{3n} a) = Z_1'(k_{3n} b) = 0.$

$$\vec{E}_{3n} = \frac{\nabla_t W_1(\ell_{3n} r)\sin\phi}{\sqrt{\frac{\pi}{2}}\left[(\ell_{3n} b W_1'(\ell_{3n} b))^2 - (\ell_{3n} a\, W_1'(\ell_{3n} a))^2\right]^{1/2}} \left(\frac{\gamma_{3n} Z_o}{k_o}\right)^{1/2} \qquad \text{(A5f)}$$

where $W_1 = J_1(\ell_{3n} a) Y_1(\ell_{3n} r) - Y_1(\ell_{3n} a) J_1(\ell_{3n} r)$

and $W_1(\ell_{3n} a) = W_1(\ell_{3n} b) = 0.$

The derivation of the normalization constants will be illustrated for (A5e) and (A5f). Consider (A5e) first for which

$$I = \int_a^b \int_0^{2\pi} (\vec{a}_z \times \nabla_t Z_1 \cos\phi) \cdot (\vec{a}_z \times \nabla_t Z_1 \cos\phi)\, r\, dr\, d\phi$$

$$= \int_a^b \int_0^{2\pi} \left[\left(\frac{dZ_1}{dr} \cos\phi \right)^2 + \left(\frac{Z_1}{r} \sin\phi \right)^2 \right] r\, dr\, d\phi$$

$$= \pi \int_a^b \left[\left(\frac{dZ_1}{dr} \right)^2 r + \frac{Z_1^2}{r} \right] dr$$

$$= \pi\, Z_1 r\, \frac{dZ_1}{dr} \Bigg|_a^b + \int_a^b \left(\frac{Z_1^2}{r} - Z_1 \frac{d}{dr} r \frac{dZ_1}{dr} \right) dr$$

upon integrating by parts once. Now $Z_1' = 0$ at $r = a,b$ and $\frac{d}{dr} d \frac{dZ_1}{dr} = Z_1 \left(\frac{1}{r} - k_{3n}^2 r \right)$ so

$$I = \pi \int_a^b k_{3n}^2 Z_1^2\, r\, dr = \frac{\pi}{2} k_{3n}^2 r^2 \left[(Z_1')^2 + \left(1 - \frac{1}{k_{3n}^2 r^2} \right) Z_1^2 \right] \Bigg|_a^b$$

$$= \frac{\pi}{2} \left[(k_{3n}^2 b^2 - 1) Z_1^2 (k_{3b} b) - (k_{3n}^2 a^2 - 1) Z_1^2 (k_{3n} a) \right]$$

By using this result along with (A3e) we obtain (A5e).

For (A5f) we have

$$I = \int_a^b \int_0^2 \left[\left(\frac{dW_1}{dr} \sin\phi \right)^2 + \left(\frac{W_1 \cos\phi}{r} \right)^2 \right] r\, dr\, d\phi$$

$$= \pi \int_a^b \left[\left(\frac{dW_1}{dr} \right)^2 + \left(\frac{W_1}{r} \right)^2 \right] r\, dr$$

This is the same integral as evaluated earlier with the exception that now $W_1 = 0$ at $r = a,b$ so

$$I = \frac{\pi}{2} [\ell_{3n} b\, W_1'(\ell_{3n} b)]^2 - \frac{\pi}{2} [\ell_{3n} a\, W_1'(\ell_{3n} a)]^2$$

Let $U(kr)$ and $V(\ell r)$ be solutions of the following Bessel differential equations:

$$\frac{d}{dr} r \frac{dU}{dr} + (k^2 r - \frac{1}{r}) U = 0$$

$$\frac{d}{dr} r \frac{dV}{dr} + (\ell^2 r - \frac{1}{r}) V = 0$$

The mode coupling coefficients involve three integrals of the following type (after integration over ϕ):

$$I_1 = \int [r \frac{dU(k_i r)}{dr} \frac{dU(k_2 r)}{dr} + \frac{U(k_i r) U(k_2 r)}{r}] dr, \text{ TE to TE coupling}$$

$$I_2 = \int [r \frac{dV(\ell_i r)}{dr} \frac{dV(\ell_2 r)}{dr} + \frac{V(\ell_i r) V(\ell_2 r)}{r}] dr, \text{ TM to TM coupling}$$

$$I_3 = \int [U(kr) \frac{dV(\ell r)}{dr} + V(\ell r) \frac{dU(kr)}{dr}] dr, \text{ TE to TM coupling}$$

I_1 and I_2 are evaluated the same way. An integration by parts gives

$$I_1 = rU(k_i r) \frac{dU(k_2 r)}{dr} + \int [\frac{U(k_i r) U(k_2 r)}{r} - U(k_i r) \frac{d}{dr} r \frac{dU(k_2 r)}{dr}] dr$$

Now use the differe[illegible]l equation to obtain

$$I_1 = rU(k_i r)\frac{dU(k_2 r)}{dr} + k_2^2 \int U(k_i r)U(k_2 r)\, r\, dr$$

$$= r\,U(k_i r)\frac{dU(k_2 r)}{dr} + \frac{k_2^2 r}{k_i^2 - k_2^2}\left[k_2 U'(k_2 r)U(k_i r) - k_i U'(k_i r)U(k_2 r)\right]$$

$$= \frac{k_i k_2 r}{k_i^2 - k_2^2}\left[k_i U(k_i r)U'(k_2 r) - k_2 U(k_2 r)U'(k_i r)\right] \qquad \text{(A6a)}$$

For I_3 an integration by parts of one term gives $I_3 = U(kr)V(\ell r)$ (A6b)

By using the above results the following expressions for the mode coupling coefficients are obtained:

$$f_{nm} = \frac{2 Z_o k_{1n}^2 k_{2m} k_o a}{(k_{1n}^2 - k_{2m}^2)(\beta_{1n}\beta_{2m})^{1/2}} \frac{J_1'(k_{2m}a)}{[(k_{1n}^2 a^2 - 1)(k_{2m}^2 b^2 - 1)]^{1/2} J_1(k_{2m}b)} \qquad \text{(A7a)}$$

$$\alpha_{nm} = 2Z_o \left(\frac{\gamma_{2m}}{\beta_{1n}}\right)^{1/2} \frac{J_1(\ell_{2m}a)}{\ell_{2m} b (k_{1n}^2 a^2 - 1)^{1/2} J_1'(\ell_{2m}b)} \qquad \text{(A7b)}$$

$$F_{nm} = -\frac{2Z_o(\gamma_{1n}\gamma_{2m})^{1/2}\, \ell_{2m} a\, J_1(\ell_{2m}a)}{(\ell_{1n}^2 - \ell_{2m}^2) k_o ab\, J_1'(\ell_{2m}b)} \qquad \text{(A7c)}$$

$$g_{nm} = \frac{-2k_o a\, Z_o\, k_{3n}^2 k_{2m}\, Z_1(k_{3n}a)\, J_1'(k_{2m}a)}{[(\beta_{3n}\beta_{2m})(k_{2m}^2 b^2 - 1)]^{1/2}\,[(k_{3n}^2 b^2 - 1) Z_1^2(k_{3n}b) - (k_{3n}^2 a^2 - 1) Z_1^2(k_{3n}a)]^{1/2} J_1(k_{2m}b)}$$

$$\times \frac{1}{k_{3n}^2 - k_{2m}^2} \qquad \text{(A7d)}$$

$$\nu_{nm} = -2Z_o \left(\frac{\gamma_{2m}}{\beta_{3n}}\right)^{1/2} \frac{Z_1(k_{3n}a) J_1(\ell_{2m}a)}{\ell_{2m} b J_1'(\ell_{2m}b)\,[(k_{3n}^2 b^2 - 1) Z_1^2(k_{3n}b) - (k_{3n}^2 a^2 - 1) Z_1^2(k_{3n}a)]^{1/2}}$$

(A7e)

$$G_{nm} = \frac{2Z_o(\gamma_{3n}\gamma_{2m})^{1/2}\ell_{2m}a \; W_1'(\ell_{3n}a)\; J_1(\ell_{2m}a)}{k_o b(\ell_{3n}^2-\ell_{2m}^2)J_1'(\ell_{2m}b)[b^2W_1'^2(\ell_{3n}b) - a^2W_1'^2(\ell_{3n}a)]^{1/2}} \qquad \text{(A7f)}$$

The equations for finding the amplitude coefficients are obtained from (A1) and (A2) by scalar multiplying by $\vec{e}_{1n}$ and $\vec{E}_{1n}$ and integrating over r from 0 to a and over ϕ from 0 to 2π and then by scalar multiplying by $\vec{e}_{3n}$ and $\vec{E}_{3n}$ and integrating from r = a to b and over ϕ from 0 to 2π . The results are:

$$\frac{k_o Z_o}{\beta_{1n}}(a_n^+ \delta_{1n} + a_n^-) = \sum_{m=1}^{\infty}[(b_m^+\delta_{1m} + b_m^-)f_{nm} + (B_m^+\delta_{1m} + B_m^-)\alpha_{nm}] \qquad \text{(A8a)}$$

$$A_n^- \frac{\gamma_{1n}Z_o}{k_o} = \sum_{m=1}^{\infty}(B_m^+\delta_{1m} + B_m^-)F_{nm} \qquad \text{(A8b)}$$

$$\frac{k_o Z_o}{\beta_{3n}}(c_n^+ \delta_{1n} + c_n^-) = \sum_{m=1}^{\infty}[(b_m^+\delta_{1n} + b_m^-)g_{nm} + (B_m^+\delta_{1n} + B_m^-)\nu_{nm}] \qquad \text{(A8c)}$$

$$C_n^- \frac{\gamma_{3n}Z_o}{k_o} = \sum_{m=1}^{\infty}(B_m^+\delta_{1m} + B_m^-)G_{nm} \qquad \text{(A8d)}$$

$$(-a_n^+\delta_{1n} + a_n^-)k_o Z_o = \sum_{m=1}^{\infty}[(b_m^+\delta_{1m} - b_m^-)\beta_{2m}f_{nm} + (B_m^+\delta_{1m} - B_m^-)\gamma_{2m}^{-1}\alpha_{nm}k_o^2] \qquad \text{(A8e)}$$

$$\frac{A_n^- Z_o}{k_o} = \sum_{m=1}^{\infty}(B_m^+\delta_{1m} - B_m^-)\gamma_{2m}^{-1}F_{nm} \qquad \text{(A8f)}$$

$$(-c_n^+\delta_{1n} + c_n^-)k_o Z_o = \sum_{m=1}^{\infty}[(b_m^+\delta_{1m} - b_m^-)\beta_{2m}g_{nm} + (B_m^+\delta_{1m} - B_m^-)\gamma_{2m}^{-1}\nu_{nm}k_o^2] \qquad \text{(A8g)}$$

$$\frac{C_n^- Z_o}{k_o} = \sum_{m=1}^{\infty}(B_m^+\delta_{1m} - B_m^-)\gamma_{2m}^{-1}G_{nm} \qquad \text{(A8h)}$$

In these equations n = 1,2,3,--- and δ_{ij} equals zero except when i=j.

A summary of the solution procedure is given below. The starting point is the set of equations (A8).

Define new amplitude coefficients as follows:

$$\hat{a}_n = \frac{a_n \sqrt{\beta_{1n}(k_{1n}^2 a^2 - 1)}}{2k_{1n}^2}, \quad \text{(A9a)} \qquad \hat{b}_m = \frac{b_m k_{2m} a J_1'(k_{2m} a)}{\sqrt{\beta_{2m}(k_{2m}^2 b^2 - 1)}\, J_1(k_{2m} b)} \quad \text{(A9b)}$$

$$\hat{c}_n = \frac{-c_n \beta_{3n}^{1/2} \left[(k_{3n}^2 b^2 - 1) Z_1^2(k_{3n} b) - (k_{3n}^2 a^2 - 1) Z_1^2(k_{3n} a)\right]^{1/2}}{2k_{3n}^2 Z_1(k_{3n} a)} \quad \text{(A9c)}$$

$$\hat{B}_m = \frac{B_m \gamma_{2m}^{1/2} J_1(\ell_{2m} a)}{\ell_{2m} b J_1'(\ell_{2m} b)}, \quad \text{(A9d)} \qquad \hat{A}_n = \frac{-k_o^2 ab A_n}{2 \gamma_{1n}^{1/2}} \quad \text{(A9e)}$$

$$\hat{C}_n = \frac{C_n k_o^2 ab \left[(b/a)^2 W_1'^2(\ell_{3n} b) - W_1'^2(\ell_{3n} a)\right]^{1/2}}{2 \gamma_{3n}^{1/2} W_1'(\ell_{3n} a)} \quad \text{(A9f)}$$

In terms of these new coefficients the system of equations become:

$$\hat{a}_n^+ \delta_{1n} + \hat{a}_n^- = \sum_{m=1}^{\infty} \left[\frac{(\hat{b}_m^+ \delta_{1m} + \hat{b}_m^-) \beta_{1n}}{\beta_{2m}^2 - \beta_{1n}^2} + \frac{(\hat{B}_m^+ \delta_{1m} + \hat{B}_m^-)}{k_o k_{1n}^2} \beta_{1n} \right] \quad \text{(A10a)}$$

$$\hat{A}_n^- \delta_{1n} = \sum_{m=1}^{\infty} (\hat{B}_m^+ \delta_{1m} + \hat{B}_m^-) \frac{\ell_{2m}^2 ab k_o^2}{\gamma_{2m}^2 - \gamma_{1n}^2} \quad \text{(A10b)}$$

$$\hat{c}_n^+ \delta_{1n} + \hat{c}_n^- = \sum_{m=1}^{\infty} \left[\frac{(\hat{b}_m^+ \delta_{1m} + \hat{b}_m^-) \beta_{3n}}{\beta_{2m}^2 - \beta_{3n}^2} + \frac{(\hat{B}_m^+ \delta_{1m} + \hat{B}_m^-)}{k_o k_{3n}^2} \beta_{3n} \right] \quad \text{(A10c)}$$

$$\hat{C}_n^- \gamma_{3n} = \sum_{m=1}^{\infty} \frac{(\hat{B}_m^+ \delta_{1m} + \hat{B}_m^-)\, k_o^2\, \ell_{2n}^2 ab}{\gamma_{2m}^2 - \gamma_{3n}^2} \qquad \text{(A10d)}$$

$$(-\hat{a}_n^+ \delta_{1n} + \hat{a}_n^-) = \sum_{m=1}^{\infty} \left[\frac{(\hat{b}_m^+ \delta_{1m} - \hat{b}_m^-)\, \beta_{2m}}{\beta_{2m}^2 - \beta_{1n}^2} + (\hat{B}_m^+ \delta_{1m} - \hat{B}_m^-) \frac{k_o}{\gamma_{2m} k_{1n}^2} \right] \qquad \text{(A10e)}$$

$$\hat{A}_n^- \gamma_{1n} = \sum_{m=1}^{\infty} \left[(\hat{B}_m^+ \delta_{1m} - \hat{B}_m^-) \frac{\gamma_{1n}}{\gamma_{2m}} \frac{\ell_{2m} ab\, k_o^2}{\gamma_{2m}^2 - \gamma_{1n}^2} \right] \qquad \text{(A10f)}$$

$$(-\hat{c}_n^+ \delta_{1n} + \hat{c}_n^-) = \sum_{m=1}^{\infty} \left[\frac{(\hat{b}_m^+ \delta_{1m} - \hat{b}_m^-)\, \beta_{2m}}{\beta_{2m}^2 - \beta_{3n}^2} + (\hat{B}_m \delta_{1m} - \hat{B}_m^-) \frac{k_o}{\gamma_{2m} k_{3n}^2} \right] \qquad \text{(A10g)}$$

$$\hat{C}_n^- \gamma_{3n} = \sum^{\infty} (\hat{B}_m^+ \delta_{1m} - \hat{B}_m^-) \frac{k_o^2 \gamma_{3n}}{\gamma_{2m}} \frac{\ell_{2m}^2 ab}{\gamma_{2m}^2 - \gamma_{3n}^2} \qquad \text{(A10h)}$$

From the above equations, we now generate a new system of equations as follows:

(A10a) + (A10e) gives

$$2\hat{a}_n^- = \sum_{m=1}^{\infty} \left[\frac{\hat{b}_m^+ \delta_{1m}}{\beta_{2m} - \beta_{1n}} - \frac{\hat{b}_m^-}{\beta_{2m} + \beta_{1n}} + \hat{B}_m^+ \delta_{1m} \frac{\left(\frac{\beta_{1n}}{k_o} + \frac{k_o}{\gamma_{2m}} \right)}{k_{1n}^2} + \hat{B}_m^- \frac{\left(\frac{\beta_{1n}}{k_o} - \frac{k_o}{\gamma_{2m}} \right)}{k_{1n}^2} \right] \qquad \text{(A11a)}$$

(A10a)-(A10e) gives

$$2\hat{a}_n^+ \delta_{1n} = \sum_{m=1}^{\infty} \left[\frac{-\hat{b}_m^+ \delta_{1m}}{\beta_{2m} + \beta_{1n}} + \frac{\hat{b}_m^-}{\beta_{2m} - \beta_{1n}} + \frac{\hat{B}_m^+ \delta_{1m} \left(\frac{\beta_{1n}}{k_o} - \frac{k_o}{\gamma_{2m}} \right)}{k_{1n}^2} + \hat{B}_m^- \frac{\left(\frac{\beta_{1n}}{k_o} + \frac{k_o}{\gamma_{2m}} \right)}{k_{1n}^2} \right] \qquad \text{(A11b)}$$

(A10c) $\pm$ (A10g) gives

$$2\hat{c}_n^- = \sum_{m=1}^{\infty} \left[\frac{b_m^+ \delta_{1m}}{\beta_{2m}-\beta_{3n}} - \frac{b_m^-}{\beta_{2m}+\beta_{3n}} + \hat{B}_m^+ \delta_{1m} \frac{\left(\frac{\beta_{3n}}{k_o} + \frac{k_o}{\gamma_{2m}}\right)}{k_{3n}^2} + \hat{B}_m^- \frac{\left(\frac{\beta_{3n}}{k_o} - \frac{k_o}{\gamma_{2m}}\right)}{k_{3n}^2} \right] \tag{A11c}$$

$$2\hat{c}_n^+ \delta_{1n} = \sum_{m=1}^{\infty} \left[\frac{-\hat{b}_m^+ \delta_{1m}}{\beta_{2m}+\beta_{3n}} + \frac{\hat{b}_m}{\beta_{2m}-\beta_{3n}} + \hat{B}_m^+ \delta_{1m} \frac{\left(\frac{\beta_{1n}}{k_o} - \frac{k_o}{\gamma_{2m}}\right)}{k_{3n}^2} + \hat{B}_m^- \frac{\left(\frac{\beta_{3n}}{k_o} + \frac{k_o}{\gamma_{2m}}\right)}{k_{3n}^2} \right] \tag{A11d}$$

(A10b) $\pm$ (A10f) gives

$$2\hat{A}_n^- \gamma_{1n} = \sum_{m=1}^{\infty} \left[\frac{\hat{B}_m^+ \delta_{1m} \ell_{2m}^2 \, ab \, k_o^2}{\gamma_{2m}(\gamma_{2m}-\gamma_{1n})} + \frac{\hat{B}_m^- \ell_{2m}^2 \, ab \, k_o^2}{\gamma_{2m}(\gamma_{2m}+\gamma_{1n})} \right] \tag{A11e}$$

$$0 = \sum_{m=1}^{\infty} \left[\frac{\hat{B}_m^+ \delta_{1m} \ell_{2m}^2 \, ab \, k_o^2}{\gamma_{2m}(\gamma_{2m}+\gamma_{1n})} + \frac{\hat{B}_m^- \ell_{2m}^2 \, ab \, k_o^2}{\gamma_{2m}(\gamma_{2m}-\gamma_{1n})} \right] \tag{A11f}$$

(A10d) $\pm$ (A10h) gives

$$2\hat{C}_n^- \gamma_{3n} = \sum_{m=1}^{\infty} \left[\frac{\hat{B}_m^+ \delta_{1n} \ell_{2m}^2 \, ab \, k_o^2}{\gamma_{2m}(\gamma_{2m}-\gamma_{3n})} + \frac{\hat{B}_m^- \ell_{2m}^2 \, ab \, k_o^2}{\gamma_{2m}(\gamma_{2m}+\gamma_{3n})} \right] \tag{A11g}$$

$$0 = \sum_{m=1}^{\infty} \left[\frac{\hat{B}_m^+ \delta_{1m} \ell_{2m}^2 \, ab \, k_o^2}{\gamma_{2m}(\gamma_{2m}+\gamma_{3n})} + \frac{\hat{B}_m^- \ell_{2m}^2 \, ab \, k_o^2}{\gamma_{2m}(\gamma_{2m}-\gamma_{3n})} \right] \tag{A11h}$$

Consider a function $Q_1(w)$ with poles at $w = \gamma_{2m}, -\gamma_{21}$, and with zeroes at γ_{1n}, γ_{3n}.

Let $\hat{\hat{B}}_m = \hat{B}_m \ell_{2m}^2 \, ab \, k_o^2/\gamma_{2m}$.

The contour integral over a closed circle C of infinite radius gives

(residue evaluation)

$$\frac{1}{2\pi j}\oint_C \frac{Q_1\,dw}{w-\gamma_{1n}} = \sum_{m=1}^{\infty} \frac{\text{Res } Q_1 \text{ at } \gamma_{2m}}{\gamma_{2m}-\gamma_{1n}} - \frac{\text{Res } Q_1 \text{ at } -\gamma_{21}}{\gamma_{21}+\gamma_{1n}} \qquad \text{(A12f)}$$

$$\frac{1}{2\pi j}\oint_C \frac{Q_1\,dw}{w+\gamma_{1n}} = \sum_{m=1}^{\infty} \frac{\text{Res } Q_1 \text{ at } \gamma_{2m}}{\gamma_{2m}+\gamma_{1n}} - \frac{\text{Res } Q_1 \text{ at } -\gamma_{21}}{\gamma_{21}-\gamma_{1n}} + Q_1(-\gamma_{1n}) \qquad \text{(A12e)}$$

Examination of these equations with respect to (A11f) and (A11e) shows that

$$\hat{B}_m^- = \text{Res } Q_1 \text{ at } \gamma_{2m}, \qquad \hat{\hat{B}}_m^+ \delta_{1m} = -\text{Res } Q_1 \text{ at } -\gamma_{21}, \qquad 2\hat{A}_n^- \gamma_{1n} = -Q_1(-\gamma_{1n})$$

Likewise

$$\frac{1}{2\pi j}\oint_C \frac{Q_1\,dw}{w \pm \gamma_{3n}} \text{ will solve (A11g), (A11h) with } 2\hat{C}_n^- \gamma_{3n} = -Q_1(-\gamma_{3n})$$

The construction of $Q_1(w)$ will be given later.

The set of equations (A11e), (A11f) and (A11g) and (A11h) are of the form that occur in bifurfacted parallel plate waveguides so the solution procedure was well known. The function Q_1 will contain two arbitrary constants - as dictated by the edge conditions, but only one incident mode amplitude is specified, namely $\hat{\hat{B}}_1^+$. Thus Q_1 is not completely known and must still be determined in part by the remaining equations in the set (A11). Equations (A11a), (A11b), (A11c), and (A11d) are not of the type encountered before. It was only when we discovered how to express these equations as a contour integral

involving another function $Q_2(w)$ and how to relate Q_1 and Q_2 that the whole system of equations could be solved. The procedure is summarized below.

(A11a) and (A11b) can be written as

$$2\hat{a}_n^- = \sum_{m=1}^{\infty} \left[\frac{\hat{b}_m^+ \delta_{1m}}{\beta_{2m}-\beta_{1n}} - \frac{\hat{b}_m^-}{\beta_{2m}+\beta_{1n}} + \frac{\hat{\hat{B}}_m^+ \delta_{1m} (\gamma_{2m}\beta_{1n}+k_o^2)}{k_o^3 ab\,(k_o^2-\gamma_{2m}^2)\,k_{1n}^2} + \frac{\hat{\hat{B}}_m^- (\gamma_{2m}\beta_{1n}-k_o^2)}{k_o^3 ab\,(k_o^2-\gamma_{2m}^2)k_{1n}^2} \right] \quad \text{(A13a)}$$

$$-2\hat{a}_n^+\delta_{1n} = \sum_{m=1}^{\infty} \left[\frac{\hat{b}_m^+\delta_{1m}}{\beta_{2m}+\beta_{1n}} - \frac{\hat{b}_m^-}{\beta_{2m}-\beta_{1n}} - \frac{\hat{\hat{B}}_m^+\delta_{1m} (\gamma_{2m}\beta_{1n}-k_o^2)}{k_o^3 ab\,(k_o^2-\gamma_{2m}^2)k_{1n}^2} - \frac{\hat{\hat{B}}_m^- (\gamma_{2m}\beta_{1n}+k_o^2)}{k_o^3 ab(k_o^2-\gamma_{2m}^2)k_{1n}^2} \right] \quad \text{(A13b)}$$

Introduce $\dfrac{Q_2(w)}{w^2-k_o^2}$ with Q_2 having poles at β_{2m}, $-\beta_{21}$ and zeroes at β_{1n}, β_{3n} but not at β_{11}, β_{31}. Then consider the residue evaluation of the following integral.

$$\frac{1}{2\pi j} \oint_C \left[\frac{Q_2}{(w^2-k_o^2)(w-\beta_{1n})} + \frac{Q_1(w)\,(\beta_{1n}w+k_o^2)}{k_o^3 ab\, k_{1n}^2 (k_o^2-w^2)} \right] dw$$

$$= \sum_{m=1}^{\infty} \frac{\text{Res } Q_2 \text{ at } \beta_{2m}}{(\beta_{2m}^2-k_o^2)(\beta_{2m}-\beta_{1n})} - \frac{\text{Res } Q_2 \text{ at } -\beta_{21}}{(\beta_{21}^2-k_o^2)(\beta_{21}+\beta_{1n})} + \sum_{m=1}^{\infty} \frac{\text{Res } Q_1 \text{ at } \gamma_{2m} (\beta_{1n}\gamma_{2m}+k_o^2)}{k_o^3 ab\,(k_o^2-\gamma_{2m}^2)k_{1n}^2}$$

$$+ \frac{Q_2(\beta_{11})\,\delta_{1n}}{\beta_{11}^2-k_o^2} - \frac{\text{Res } Q_1 \text{ at } -\gamma_{21}\,(\beta_{1n}\gamma_{21}-k_o^2)}{k_o^3 ab\,(k_o^2-\gamma_{21}^2)\,k_{1n}^2} = 0$$

provided $$\frac{Q_2(\pm k_o)}{\pm k_o - \beta_{1n}} = \frac{Q_1(\pm k_o)\ (\pm \beta_{1n} + k_o)}{k_o^2 ab\ (k_o - \beta_{1n})(k_o + \beta_{1n})}$$

or $$Q_2(k_o) = \frac{Q_1(k_o)}{k_o^2\ ab}\ , \qquad Q_2(-k_o) = \frac{-Q_1(-k_o)}{k_o^2\ ab}$$

The residues at the poles $\pm k_o$ must cancel and this relates Q_1 to Q_2.

We also have

$$\hat{b}_m^- = \frac{\text{Res } Q_2 \text{ at } \beta_{2m}}{\beta_{2m}^2 - k_o^2}\ , \quad \hat{b}_m^+ = \frac{\text{Res } Q_2 \text{ at } -\beta_{21}}{\beta_{21}^2 - k_o^2}\ , \quad -2\hat{a}_1^+ = \frac{Q_2(\beta_{11})}{\beta_{11}^2 - k_o^2}$$

$$\hat{B}_m^- = \text{Res } Q_1 \text{ at } \gamma_{2m}\ , \quad \hat{B}_m^+ \delta_{1m} = -\text{Res } Q_1 \text{ at } -\gamma_{21}$$

Thus we see that the above solves (A13b). Consider next

$$\frac{1}{2\pi j} \oint_C \left[\frac{Q_2}{(w^2 - k_o^2)(w + \beta_{1n})} - \frac{Q_1(\beta_{1n} w - k_o^2)}{k_o^3 ab\ k_{1n}^2\ (k_o^2 - w^2)} \right] dw$$

$$= \sum_{m=1}^{\infty} \frac{\text{Res } Q_2 \text{ at } \beta_{2m}}{(\beta_{2m}^2 - k_o^2)(\beta_{2m} + \beta_{1n})} - \frac{\text{Res } Q_2 \text{ at } -\beta_{21}}{(\beta_{21}^2 - k_o^2)(\beta_{21} - \beta_{1n})} + \frac{Q_2(-\beta_{1n})}{(\beta_{1n}^2 - k_o^2)}$$

$$+ \sum_{m=1}^{\infty} \frac{-\text{Res } Q_1 \text{ at } \gamma_{2m}\ (\gamma_{2m}\beta_{1n} - k_o^2)}{k_o^3 ab\ k_{1n}^2\ (k_o^2 - \gamma_{2m}^2)} + \frac{\text{Res } Q_1 \text{ at } -\gamma_{21}(\gamma_{21}\beta_{1n} + k_o^2)}{k_o^3 ab\ k_{1n}^2\ (k_o^2 - \gamma_{21}^2)} = 0$$

$$= \sum_{m=1}^{\infty} \frac{\hat{b}_m^-}{\beta_{2m}+\beta_{1n}} - \frac{\hat{b}_m^+ \delta_{1m}}{\beta_{21}-\beta_{1n}} + \frac{Q_2(-\beta_{1n})}{\beta_{1n}^2 - k_o^2}$$

$$+ \sum_{m=1}^{\infty} - \frac{\hat{B}_m^- (\gamma_{2m}\beta_{1n}-k_o^2)}{k_o^3 ab\, k_{1n}^2 (k_o^2-\gamma_{2m}^2)} - \frac{\hat{B}_m^+ \delta_{1m} (\gamma_{21}\beta_{1n}+k_o^2)}{k_o^3 ab\, k_{1n}^2 (k_o^2-\gamma_{21}^2)}$$

Thus $2\hat{a}_n^- = \frac{Q_2(-\beta_{1n})}{\beta_{1n}^2 - k_o^2}$.

Again we require the residues at $\pm k_o$ to cancel, thus

$$\frac{Q_2(\pm k_o)}{\pm k_o+\beta_{1n}} = - \frac{Q_1(\pm k_o)(\pm\beta_{1n}k_o-k_o^2)}{k_o^3 ab(k_o-\beta_{1n})(k_o+\beta_{1n})}$$

or

$$Q_2(k_o) = - \frac{Q_1(k_o)k_o(\beta_{1n}-k_o)}{k_o^3 ab\,(k_o-\beta_{1n})} = \frac{Q_1(k_o)}{k_o^2 ab}$$

and

$$Q_2(-k_o) = \frac{(\beta_{1n}-k_o)(-Q_1(-k_o))(-\beta_{1n}-k_o)}{k_o^2 ab\,(k_o-\beta_{1n})(k_o+\beta_{1n})} = \frac{-Q_1(-k_o)}{k_o^2 ab}$$

This is consistent with the previous relationship derived for Q_1 and Q_2. Hence the above solves (A13b).

We can also find $2\hat{c}_n^- = \frac{Q_2(-\beta_{3n})}{\beta_{3n}^2-k_o^2}$ and $-2\hat{c}_1^+ = \frac{Q_2(\beta_{31})}{\beta_{31}^2-k_o^2}$

From a study of the edge conditions we find that Q_2 has four unknown constants. Thus Q_1 and Q_2 together contain 6 constants which can be determined in terms of the 4 incident mode amplitudes and the two relations between Q_1 and Q_2.

The function $Q_1(w)$ is given by

$$Q_1(w) = \prod_{n=1}^{\infty} \frac{(1-w/\gamma_{1n})\ (1-w/\gamma_{3n})}{(1-w/\gamma_{2n})} \frac{h(w)}{w+\gamma_{21}} (K_1 + K_2 w) \qquad \text{(A14)}$$

with

$$h(w) = \exp\ [-\frac{jw}{\pi}\ (a\ \ell n\ \frac{a}{b} - c\ \ell n\ \frac{b}{c}\ )]$$

Let $P_1(w)$ be the infinite product in (A14) and let $\tilde{P}_1(w) = P_1(s)h(w)$ so that

$$Q_1(w) = \frac{\tilde{P}_1(w)\ (K_1 + K_2 w)}{w + \gamma_{21}} \qquad \text{(A15)}$$

The function Q_1 has poles at $w = \gamma_{2m}, -\gamma_{21}$, $m = 1,2,----$ and zeroes at $w = \gamma_{1n}, \gamma_{3n}$, $n = 1,2,----$ and has algebraic behavior like $w^{-1/2}$ as $|w| \to \infty$.

The function $Q_2(w)$ has poles at $w = \beta_{2m}, -\beta_{21}$, $n = 1,2,----$, has zeroes at $w = \beta_{1n}, \beta_{3n}$, $n = 2,3,----$ and behaves like $w^{1/2}$ as $|w| \to \infty$. This function is given by

$$Q_2(w) = \frac{\tilde{P}_2(w)}{w + \beta_{21}} (R_1 + R_2 w + R_3 w^2 + R_4 w^3) \qquad \text{(A16)}$$

where $\tilde{P}_2 = P_2\ h$, R_i are constants, and

$$P_2(w) = \prod_{n=2}^{\infty} \frac{(1-w/\beta_{1n})(1-w/\beta_{3n})}{(1-w/\beta_{2n})} \frac{1}{(1-w/\beta_{21})} \qquad \text{(A17)}$$

With reference to the scattering matrix parameters S_{ij} the subscripts are chosen as follows (see Fig. A2). 1 refers to TE_{11} mode in region 1, amplitude is a_1, propagation constant is β_{11}. 2 refers to TE_{11} mode in region 2, amplitude is b_1, propagation constant β_{21}. 3 refers to TE_{11} mode in region 3, amplitude c_1, propagation constant β_{31}. 4 refers to TM_{11} mode in region 2, amplitude B_1, propagation constant γ_{21}. The scattering matrix equation is

$$\begin{bmatrix} a_1^- \\ b_1^- \\ c_1^- \\ B_1^- \end{bmatrix} = [S_{ij}] \begin{bmatrix} a_1^+ \\ b_1^+ \\ c_1^+ \\ B_1^+ \end{bmatrix} \qquad \text{(A18)}$$

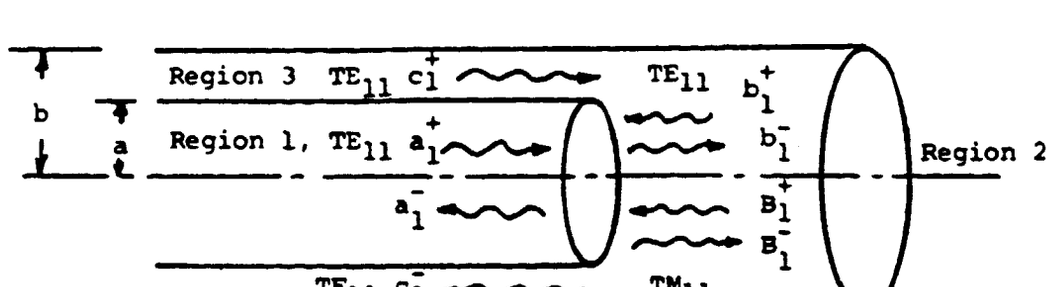

Figure A2 - Bifurcated circular waveguide.

In order to find expression for the S_{ij} four special cases are considered:

I. $a_1^+ = 1, \quad b_1^+ = c_1^+ = B_1^+ = 0$

$S_{11} = a_1^-, \quad S_{21} = b_1^-, \quad S_{31} = c_1^-, \quad S_{41} = B_1^-$

II. $b_1^+ = 1, \quad a_1^+ = c_1^+ = B_1^+ = 0$

$S_{12} = a_1^-, \quad S_{22} = b_1^-, \quad S_{32} = c_1^-, \quad S_{42} = B_1^-$

III. $c_1^+ = 1, \quad a_1^+ = b_1^+ = B_1^+ = 0$

$S_{13} = a_1^-, \quad S_{23} = b_1^-, \quad S_{33} = c_1^-, \quad S_{43} = B_1^-$

IV. $B_1^+ = 1, \quad a_1^+ = b_1^+ = c_1^+ = 0$

$S_{14} = a_1^-, \quad S_{24} = b_1^-, \quad S_{34} = c_1^-, \quad S_{44} = B_1^-$

The required equations are summarized below (notation and parameters are given in earlier progress reports).

$$a_1^+ = \hat{f}_{n=1}\hat{a}_1^+ = \frac{\hat{f}_{n=1}}{a\,k_{11}^2}\,Q_2(\beta_{11})$$

$$b_1^+ = \hat{b}_1^+/\hat{f}_{m=1} = -\frac{\text{Residue } Q_2 \text{ at } -\beta_{21}}{\hat{f}_{n=1}\,k_{21}^2}$$

$$c_1^+ = \hat{c}_1^+\,\hat{g}_{n=1} = \frac{\hat{g}_{n=1}\,Q_2(\beta_{31})}{2\,k_{31}^2}$$

$$B_1^+ = \hat{B}_1^+/\hat{\alpha}_{n=1} = \frac{\gamma_{21}\,\hat{B}_1^+}{\ell_{21}^2 k_o^2 ab\,\hat{\alpha}_{m=1}} = \frac{-\gamma_{21}\,\text{Residue } Q_1 \text{ at } -\gamma_{21}}{\ell_{21}^2\,k_o^2\,ab\,\hat{\alpha}_{m=1}}$$

$$a_1^- = \hat{f}_{n=1}\,\hat{a}_1^- = -\frac{\hat{f}_{n=1}\,Q_2(-\beta_{11})}{2\,k_{11}^2}$$

$$b_1^- = \hat{b}_1^-/\hat{f}_{m=1} = -\frac{\text{Residue } Q_2 \text{ at } \beta_{21}}{k_{21}^2\,\hat{f}_{m=1}}$$

$$c_1^- = \hat{g}_{n=1}\,\hat{c}_1^- = -\frac{\hat{g}_{n=1}\,Q_2(-\beta_{21})}{2\,k_{31}^2}$$

$$B_1^- = \frac{\gamma_{21}}{\ell_{21}^2 k_o^2 ab \hat{\alpha}_{m=1}} \qquad \hat{B}_1^- = \frac{\gamma_{21} \text{ Residue } Q_1 \text{ at } \gamma_{21}}{\ell_{21}^2 k_o^2 ab \hat{\alpha}_{m=1}}$$

$$Q_2(k_o) = \frac{Q_1(k_o)}{k_o^2 ab}, \qquad Q_2(-k_o) = -\frac{Q_1(-k_o)}{k_o^2 ab}$$

Case I

From the conditions $b_1^+ = c_1^+ = 0$ we see that Q_2 has a zero at β_{31} and no pole at $-\beta_{21}$. Since $B_1^+ = 0$ also we require that Q_1 does not have a pole at $-\gamma_{21}$. Hence

$$Q_1 = \tilde{P}_1 K_1, \quad Q_2 = \tilde{P}_2 (1 - w/\beta_{31}) (R_1 + R_2 w)$$

The equations that determine K_1, R_1, and R_2 are

$$\frac{\hat{f}_{n=1} \tilde{P}_2(\beta_{11})}{2 k_{11}^2} (1 - \frac{\beta_{11}}{\beta_{31}}) (R_1 + R_2\beta_{11}) = 1 \qquad \text{(A19a)}$$

$$\mp \frac{K_1 \tilde{P}_1(\pm k_o)}{k_o^2 ab} + \tilde{P}_2(\pm k_o)(1 \mp \frac{k_o}{\beta_{31}})(R_1 \pm R_2 k_o) = 0 \qquad \text{(A19b,c)}$$

The matrix elements S_{i1} are given by:

$$S_{11} = -\frac{\hat{f}_{n=1}}{2k_{11}^2} \tilde{P}_2(-\beta_{11})(1 + \frac{\beta_{11}}{\beta_{31}})(R_1 - R_2\beta_{11}) \qquad \text{(A20a)}$$

$$S_{21} = -\frac{1}{k_{21}^2 \hat{f}_{m=1}} (1 - \frac{\beta_{21}}{\beta_{31}}) (R_1 + R_2\beta_{21}) \text{ Residue } \tilde{P}_2 \text{ at } \beta_{21} \qquad \text{(A20b)}$$

$$S_{31} = -\frac{\hat{g}_{n=1}}{k_{31}^2} \tilde{P}_2(-\beta_{31})(R_1 - R_2\beta_{31}) \qquad \text{(A20c)}$$

$$S_{41} = \frac{\gamma_{21}K_1}{\ell_{21}^2 k_o^2 ab\, \hat{a}_{m=1}} \quad \text{Residue } \tilde{P}_1 \text{ at } \gamma_{21} \qquad \text{(A20d)}$$

Case II

From $a_1^+ = c_1^+ = 0$ we get that Q_2 has zeroes at $w = \beta_{11}$ and β_{31}.

From $B_1^+ = 0$ we get that Q_1 has no pole at $w = -\gamma_{21}$

$$Q_1 = K_1\tilde{P}_1 \quad , \quad Q_2 = \frac{\tilde{P}_2(1-w/\beta_{11})(1-w/\beta_{31})}{w+\beta_{21}}(R_1 + R_2 w)$$

The equations that determine K_1, R_1 and R_2 are:

$$-\frac{\tilde{P}_2(-\beta_{21})}{k_{21}^2 \hat{f}_{m=1}}\left(1+\frac{\beta_{21}}{\beta_{11}}\right)\left(1+\frac{\beta_{21}}{\beta_{31}}\right)(R_1 - R_2\beta_{21}) = 1 \qquad \text{(A21a)}$$

$$\mp\frac{K_1\tilde{P}_1(\pm k_o)}{k_o^2 ab} + \frac{\tilde{P}_2(\pm k_o)\left(1\mp\frac{k_o}{\beta_{11}}\right)\left(1\mp\frac{k_o}{\beta_{31}}\right)(R_1 \pm R_2 k_o)}{\beta_{21} \pm k_o} = 0 \qquad \text{(A21b,c)}$$

The scattering matrix parameters S_{i2} are given by:

$$S_{12} = \frac{\hat{f}_{n=1}}{k_{11}^2}\,\frac{\tilde{P}_2(-\beta_{11})\left(1+\frac{\beta_{11}}{\beta_{31}}\right)(R_1 - R_2\beta_{11})}{\beta_{11} - \beta_{21}} \qquad \text{(A22a)}$$

$$S_{22} = -\frac{1}{k_{21}^2 \hat{f}_{m=1}}\left(1-\frac{\beta_{21}}{\beta_{11}}\right)\left(1-\frac{\beta_{21}}{\beta_{31}}\right)\frac{R_1+R_2\beta_{21}}{2\beta_{21}}$$

$$\times \text{ Residue } \tilde{P}_2 \text{ at } \beta_{21} \qquad \text{(A22b)}$$

$$S_{32} = \frac{\hat{g}_{n=1}\, \tilde{P}_2(-\beta_{31})\left(1 + \frac{\beta_{31}}{\beta_{11}}\right)(R_1 - R_2\beta_{31})}{k_{31}^2\,(\beta_{31} - \beta_{21})} \qquad \text{(A22c)}$$

$$S_{42} = \frac{\gamma_{21}\, K_1}{\ell_{21}^2\, k_o^2\, ab\, \hat{\alpha}_{m=1}} \qquad \text{Residue } \tilde{P}_1 \text{ at } \gamma_{21} \qquad \text{(A22d)}$$

Case III

From $a_1^+ = b_1^+ = 0$ we find that Q_2 has a zero at $w = \beta_{11}$ and no pole at $w = -\beta_{21}$. From $B_1^+ = 0$ we get that Q_1 has no pole at $-\gamma_{21}$. Thus

$$Q_1 = K_1\tilde{P}_1 \,, \qquad Q_2 = \tilde{P}_2\left(1 - \frac{w}{\beta_{11}}\right)(R_1 + R_2 w)$$

The equations that determine K_1, R_1, and R_2 are:

$$\frac{\hat{g}_{n=1}}{2\,k_{31}^2}\,\tilde{P}_2(\beta_{31})\left(1 - \frac{\beta_{31}}{\beta_{11}}\right)(R_1 + R_2\beta_{31}) = 1 \qquad \text{(A23a)}$$

$$\mp \frac{K_1\tilde{P}_1(\pm k_o)}{k_o^2\, ab} + \tilde{P}_2(\pm k_o)\left(1 \mp \frac{k_o}{\beta_{11}}\right)(R_1 \pm R_2 k_o) = 0 \,, \qquad \text{(A23b,c)}$$

The scattering matrix parameters S_{i3} are given by:

$$S_{13} = \frac{\hat{f}_{n=1}\,\tilde{P}_2(-\beta_{11})(R_2\beta_{11} - R_1)}{k_{11}^2} \qquad \text{(A24a)}$$

$$S_{23} = - \frac{(1 - \frac{\beta_{21}}{\beta_{11}})\ (R_1 + R_2\beta_{21})}{k_{21}^2\ \hat{f}_{m=1}} \quad \text{Residue } \tilde{P}_2 \text{ at } \beta_{21} \tag{A24b}$$

$$S_{33} = - \frac{\hat{g}_{n=1}}{2k_{31}^2}\ \tilde{P}_2(-\beta_{31})\ (1 + \frac{\beta_{31}}{\beta_{11}})\ (R_1 - R_2\beta_{31}) \tag{A24c}$$

$$S_{43} = \frac{\gamma_{21}}{\ell_{21}^2\ k_o^2\ ab\ \hat{a}_{m=1}}\ K_1 \quad \text{Residue } \tilde{P}_1 \text{ at } \gamma_{21} \tag{A24d}$$

Case IV

From $a_1^+ = b_1^+ = c_1^+ = 0$ we get that Q_2 has zeroes at $w = \beta_{11}$ and β_{31} and no pole at $w = -\beta_{21}$. Thus

$$Q_1 = \frac{\tilde{P}_1\ (K_1 + K_2 w)}{w + \gamma_{21}} \quad , \quad Q_2 = \tilde{P}_2\ (1 - \frac{w}{\beta_{11}})\ (1 - \frac{w}{\beta_{31}})\ R_1$$

The constants K_1, K_2, and R_1 are determined by:

$$\frac{-\gamma_{21}}{\ell_{21}^2\ k_o^2\ ab\ \hat{a}_{m=1}}\ \tilde{P}_1(-\gamma_{21})\ (K_1 - K_2\gamma_{21}) = 1 \tag{A25a}$$

$$\mp \frac{\tilde{P}_1\ (\pm k_o)(K_1 \pm K_2 k_o)}{(\gamma_{21} \pm k_o)k_o^2\ ab} + \tilde{P}_2(\pm k_o)(1 \mp \frac{k_o}{\beta_{11}})\ (1 \mp \frac{k_o}{\beta_{31}})\ R_1 = 0 \tag{A25b,c}$$

The scattering matrix parameters S_{i4} are given by:

$$S_{14} = - \frac{\hat{f}_{n=1}\, \tilde{P}_2(-\beta_{11})(1 + \frac{\beta_{11}}{\beta_{31}})R_1}{k_{11}^2} \qquad \text{(A26a)}$$

$$S_{24} = - \frac{R_1}{k_{21}^2\, \hat{f}_{m=1}} (1 - \frac{\beta_{21}}{\beta_{11}})(1 - \frac{\beta_{21}}{\beta_{31}}) \text{ Residue } \tilde{P}_2 \text{ at } \beta_{21} \qquad \text{(A26b)}$$

$$S_{34} = - \frac{\hat{g}_{n=1}\, \tilde{P}_2(-\beta_{31})(1 + \frac{\beta_{31}}{\beta_{11}})R_1}{k_{31}^2} \qquad \text{(A26c)}$$

$$S_{44} = \frac{\gamma_{21}(K_1 + K_2\gamma_{21})}{2\ell_{21}^2\, k_o^2\, ab\, \hat{\alpha}_{m=1}\, \gamma_{21}} \text{ Residue } \tilde{P}_1 \text{ at } \gamma_{21} \qquad \text{(A26d)}$$

The scattering matrix parameters have been evaluated for λ_o = 2.5 cm (12 ghz.) as a function of the inner guide radius "a" and outer guide radius "b" over a range of values corresponding to TE_{11} mode propagation only in regions 1 and 3 and to TE_{11} and TM_{11} mode propagation in the large guide (region 2). The accuracy and correctness of the computational program was verified by checking that the scattering matrix is unitary for a lossless junction (power conservation) i.e.

$$\sum_{i=1}^{4} S_{ij}\, S_{ji}^{*} = \delta_{jk}$$

Since the junction is reciprocal $S_{ij} = S_{ji}$ so only 10 S_{ij} parameters need to be evaluated.

APPENDIX B

APERTURE SCATTERING PARAMETERS

This Appendix summarizes the formulas used to compute the aperture scattering coefficients Γ_{ij} and the radiated field. The formulas are based on the solution given by Weinstein (Weinstein, 1969). After suitable coordinate transformation, change in notation, and complex conjugation (see Schilling, 1982, for detailed derivations).

The TE_{11} mode reflection coefficient is given by

$$\Gamma_{11} = \frac{k_o}{\beta} \frac{(k_o+\beta)^2 b^2}{k_c^2 b^2 - 1} M_-^2(\beta b) \left[\frac{\chi^2}{1-\chi^2} - \frac{(k_o-\beta)^2}{4 k_o \beta} \right] \quad \text{(B1)}$$

where β is the propagation constant and k_c is the cutoff wave number. The TM_{11} mode reflection coefficient is given by

$$\Gamma_{22} = \frac{k_o}{\gamma} L_-^2(\gamma b) \left[\frac{\chi^2}{1-\chi^2} + \frac{(k_o+\gamma)^2}{4 k_o \gamma} \right] \quad \text{(B2)}$$

where γ is the propagation constant. The TE_{11} to TM_{11} mode coupling coefficient is given by

$$\Gamma_{12} = \frac{k_o}{(\beta\gamma)^{1/2}} \frac{(k_o+\beta)b}{(k_c^2 b^2 - 1)^{1/2}} M_-(\beta b) L_-(\beta b) \frac{\chi}{1-\chi^2} \quad \text{(B3)}$$

The function χ is given by

$$\chi = \frac{L_-(k_o b)}{2 k_o b \, M_-(k_o b)} \quad \text{(B4)}$$

The functions L_- and M_- are given in terms of integrals which were evaluated numerically (see Schilling, 1982, for details).

$$L_{-}(\beta b) = \exp \frac{1}{2\pi j} \int_{-\infty+j\eta}^{\infty+j\eta} \frac{\ell n[-\pi j\, J_1(b\sqrt{k_o^2 - \xi^2})\, H_1^2(b\sqrt{k_o^2 - \xi^2})]}{\xi + \beta} d\xi \quad \text{(B5)}$$

$$M_{-}(\beta b) = \exp \frac{1}{2\pi j} \int_{-\infty+j\eta}^{\infty+j\eta} \frac{\ell n[-\pi j\, J_1'(b\sqrt{k_o^2-\xi^2})\, H_1^{2'}(b\sqrt{k_o^2-\xi^2})]}{\xi + \beta} d\xi \quad \text{(B6)}$$

Let the incident TE_{11} mode transverse field be $d_1^+ \vec{e}_{21} e^{-j\beta z}$ while the incident TM_{11} mode transverse field is $D_1^+ \vec{E}_{21} e^{-j\gamma z}$ with the modal functions as defined in Appendix A. The radiated electric field is then given by

$$\begin{bmatrix} E_\theta \\ E_\phi \end{bmatrix} = \begin{bmatrix} \sin\phi & 0 \\ 0 & \cos\phi \end{bmatrix} \begin{bmatrix} E_{\theta,TE} & E_{\theta,TM} \\ E_{\phi,TE} & E_{\phi,TM} \end{bmatrix} \begin{bmatrix} d_1^+ \\ D_1^+ \end{bmatrix} \frac{e^{-jk_o r}}{r} \quad \text{(B7)}$$

where

$$E_{\theta,TE} = j \left(\frac{2k_o Z_o}{\pi\beta}\right)^{1/2} \frac{k_c k_o b}{k_o - \beta} \frac{k_c b}{(k_c^2 b^2 - 1)^{1/2}} \frac{\chi}{1-\chi^2}$$

$$\times \frac{M_{-}(\beta b)}{L_{-}(k_o b \cos\theta)} \frac{J_1(k_o b \sin\theta)}{k_o b \sin\theta} \quad \text{(B8a)}$$

$$E_{\phi,TE} = j \left(\frac{2k_o Z_o}{\pi\beta}\right)^{1/2} \frac{k_c b}{(k_c^2 b^2 - 1)^{1/2}} \frac{k_c}{k_o - \beta} \frac{M_{-}(\beta b)}{M_{-}(k_o b \cos\theta)}$$

$$\times \left[\frac{\chi^2}{1-\chi^2} - \frac{(k_o - \beta)(1+\cos\theta)}{2(\beta - k_o \cos\theta)}\right] \frac{J_1'(k_o b \sin\theta)}{1 + \cos\theta} \quad \text{(B8b)}$$

$$E_{\theta,TM} = j \left(\frac{2k_o Z_o}{\pi \gamma} \right)^{1/2} \frac{L_-(\gamma b)}{L_-(k_o b \cos\theta)} \left[\frac{\chi^2}{1-\chi^2} + \frac{(k_o+\gamma)(1-\cos\theta)}{2(\gamma - k_o \cos\theta)} \right]$$

$$\times \quad k_o b \, \frac{J_1(k_o b \sin\theta)}{k_o b \sin\theta} \tag{B8c}$$

$$E_{\phi,TM} = j \left(\frac{2k_o Z_o}{\pi \gamma} \right)^{1/2} \frac{\chi}{1-\chi^2} \frac{L_-(\gamma b)}{M_-(k_o b \cos\theta)} \frac{J_1'(k_o b \sin\theta)}{1 + \cos\theta} \tag{B8d}$$

APPENDIX C

RADIATION FROM A CIRCULAR WAVEGUIDE (APPROXIMATE THEORY)

Radiation from a circular waveguide aperture may be computed from a knowledge of the tangential electric field or tangential magnetic field on the z = 0 aperture plane. In practice the aperture field is assumed to be that of the incident mode (or modes) in the circular guide opening and zero outside this region. One then finds that the resultant radiation pattern is somewhat dependent on whether only the aperture electric field, or aperture magnetic field, or both are used in the formulation.

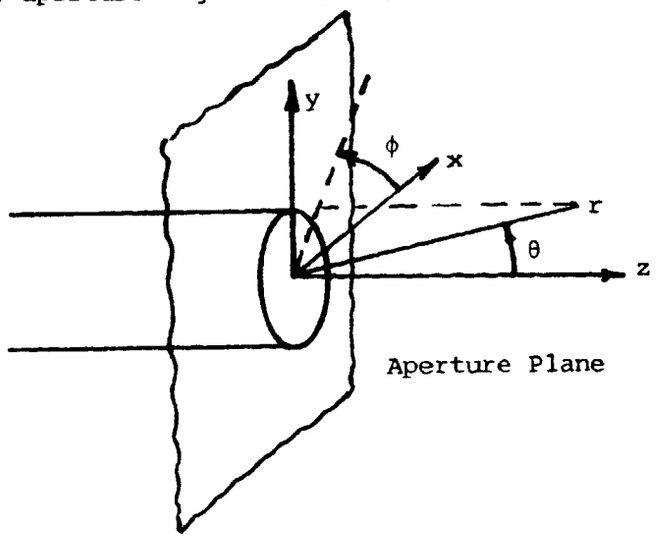

Figure C1 - Radiation from a Circular Waveguide

In terms of the aperture tangential electric field the radiated field is given by

$$\vec{E} = \frac{jk_o}{2\pi r} e^{-jk_o r} [\vec{a}_\theta (f_x \cos\phi + f_y \sin\phi) + \vec{a}_\phi \cos\theta (f_y \cos\phi - f_x \sin\phi)] \quad \text{(C1a)}$$

where $\vec{f}_t$ is the Fourier transform of the aperture electric field. In terms of the aperture tangential magnetic field the radiated field is given by

$$\vec{E} = \frac{jk_o}{2\pi r} e^{-jk_o r} Z_o [\vec{a}_\theta \cos\theta (g_y \cos\phi - g_x \sin\phi) - \vec{a}_\phi (g_y \sin\phi + g_x \cos\phi)] \quad \text{(C1b)}$$

where $\vec{g}_t$ is the Fourier transform of the aperture magnetic field. If both the aperture electric and magnetic fields are used the radiated field is the average of that given by (C1a) and (C1b).

Let $\vec{e}$ be the tangential electric field of an incident waveguide mode. Then the corresponding tangential magnetic field is given by

$$\vec{h} = Y_w \vec{a}_z \times \vec{e}$$

where Y_w is the mode admittance. If we assume negligible reflection at the guide-free space junction and negligible higher mode excitation and no fringing fields then

$$\vec{f}_t = \int_{S_a} \vec{e}(x,y) e^{jk_x x + jk_y y} \, dxdy$$

$$\vec{g}_t = \int_{S_a} \vec{h}(x,y) e^{jk_x x + jk_y y} \, dxdy$$

$$= Y_w \vec{a}_z \times f_t \quad \text{(C2)}$$

Thus $g_x = -Y_w f_y$ and $g_y = Y_w f_x$ and the average of (C1a) and (C1b) becomes

$$\vec{E} = \frac{jk_o}{4\pi r} e^{-jk_o r} [\vec{a}_\theta (1 + Z_o Y_w \cos\theta)(f_x \cos\phi + f_y \sin\phi)$$

$$+ \vec{a}_\phi (\cos\theta + Z_o Y_w)(f_y \cos\phi - f_x \sin\phi)] \quad \text{(C3)}$$

In the radiation zone $k_x = k_o \sin\theta\cos\phi$ and $k_y = k_o \sin\theta\sin\phi$.

Radiation from TE_{11} Mode

In a guide of radius b the normalized tangential electric field of the TE_{11} mode is

$$\vec{e} = \left(\frac{k_o Z_o}{\beta}\right)^{1/2} \frac{\vec{a}_z \times \nabla_t J_1(k_c r)\cos\phi}{\left[\frac{\pi}{2}(k_c^2 b^2 - 1)\right]^{1/2} J_1(k_c b)} \qquad (C4)$$

By using only the electric field in the aperture it is found that the radiated field is given by

$$\vec{E} = \frac{jk_o e^{-jk_o r}}{2\pi r}\left(\frac{k_o Z_o}{\beta}\right)^{1/2} \left[\frac{\pi}{2}(k_c^2 b^2 - 1)\right]^{-1/2} (2\pi k_c^2 b)$$

$$\times \left[\vec{a}_\theta \frac{J_1(k_o b\sin\theta)}{k_c^2 k_o b\sin\theta)} \sin\phi + \vec{a}_\phi \cos\theta \frac{J_1'(k_o b\sin\theta)}{k_c^2 - k_o^2\sin^2\theta} \cos\phi\right] \qquad (C5)$$

The relations (C1), (C2), and (C3) may be used to find the radiated field in terms of the aperture tangential magnetic field or in terms of both $\vec{e}$ and $\vec{h}$. In this case $Z_o Y_w = \beta/k_o$.

Radiation From TM_{11} Mode

The normalized electric field of a TM_{11} mode is

$$\vec{e} = \left(\frac{2\gamma}{\pi k_o} Z_o\right)^{1/2} \frac{\nabla_t J_1(\ell_c r)\sin\phi}{\ell_c b\, J_1'(\ell_c b)} \qquad (C6)$$

In terms of this field alone the radiated electric field is given by

$$\vec{E} = \frac{jk_o e^{-jk_o r}}{2\pi r} \left(\frac{2\gamma Z_o}{\pi k_o} \right)^{1/2} \vec{a}_\theta \frac{2\pi k_o \sin\theta \, J_1(k_o b \sin\theta)}{k_o^2 \sin^2\theta - \ell_c^2} \qquad \text{(C7)}$$

Note that $E_\phi = 0$ and that $\vec{E} = 0$ on the z axis. For the TM_{11} mode $Z_o Y_w = {}_o/\gamma$ where γ is the propagation constant.

Co-polarized and Cross-polarized Radiation Patterns

If both the aperture electric and magnetic fields are used to compute the radiation field then from the TE_{11} mode (apart from irrelevant constants) the radiated field is given by

$$E_\theta = q_1(\theta) \sin\phi \qquad \text{(C8a)}$$

$$E_\phi = q_2(\theta) \cos\phi \qquad \text{(C8b)}$$

where

$$q_1 = \left(\frac{k_o}{\beta} \right)^{1/2} \frac{b}{(k_c^2 b^2 - 1)^{1/2}} \left(1 + \frac{\beta}{k_o} \cos\theta\right) \frac{J_1(k_o b \sin\theta)}{k_o b \sin\theta}$$

$$q_2 = \left(\frac{k_o}{\beta} \right)^{1/2} \frac{b}{(k_c^2 b^2 - 1)^{1/2}} \left(\frac{\beta}{k_o} + \cos\theta \right) \frac{J_1'(k_o b \sin\theta)}{1 - \frac{k_o^2}{k_c^2} \sin^2\theta}$$

$$J_1'(k_c b) = 0 , \quad k_c b = 1.841, \quad \beta^2 = k_o^2 - k_c^2$$

Let $\vec{n}_1 = \vec{a}_\theta \sin\phi + \vec{a}_\phi \cos\phi$ be a unit co-polarized vector and $\vec{n}_2 = \vec{a}_\theta \cos\phi - \vec{a}_\phi \sin\phi$ is then a unit cross-polarized vector. The co-polarized radiation is given by

$$\vec{E}\cdot\vec{n}_1 = \frac{q_1+q_2}{2} - \frac{q_1-q_2}{2}\cos 2\phi \qquad \text{(C9a)}$$

while the cross-polarized field is given by

$$\vec{E}\cdot\vec{n}_2 = \frac{q_1-q_2}{2}\sin 2\phi \qquad \text{(C9b)}$$

and is a maximum in the $\phi = \pi/4$ or $\frac{3\pi}{4}$ plane. The principal E-plane pattern is given by $q_1(\theta)$ and the principal H-plane pattern is given by $q_2(\theta)$. The principal plane patterns and cross-polarized patterns are shown in Fig's. C2-C7 for λ_o = 2.5 cm. (12 ghz.) and different values of b.†

The radiation pattern for the TM_{11} mode, as computed using both the aperture tangential electric and magnetic fields, is given by

$$E_\theta = -q_3(\theta)\sin\phi \qquad \text{(C10)}$$

where

$$q_3 = \left(\frac{\gamma}{k_o}\right)^{1/2}\left(1+\frac{k_o}{\gamma}\cos\theta\right)\frac{k_o\sin\theta\, J_1(k_o b\sin\theta)}{\ell_c^2 - k_o^2\sin^2\theta}$$

and $J_1(\ell_c b) = 0$, $\ell_c b = 3.832$, and $\gamma^2 = k_o^2 - \ell_c^2$. The radiation pattern is shown in Fig. C8.

If the patterns are computed using only the electric field in the aperture then the radiation fields for the TE_{11} mode are:

$$E_\theta = p_1(\theta)\sin\phi \qquad \text{(C11a)}$$

$$E_\phi = p_2(\theta)\cos\phi\cos\theta \qquad \text{(C11b)}$$

where

---

†The patterns shown in this Appendix were computed by Georg Karawas.

$$(1 + \frac{\beta}{k_o} \cos\theta) p_1 = 2q_1$$

$$(\frac{\beta}{k_o} + \cos\theta) p_2 = 2q_2$$

The E- and H-plane principal patterns are given by p_1 and $p_2\cos\theta$ respectively and the cross-polarized pattern in the $\phi = \pi/4$ plane is given by $(p_1 - p_2\cos\theta)/2$. These patterns are shown in Figs. C2-C7 also.

The combined pattern from a TE_{11} mode and a TM_{11} mode of relative amplitude α is given by (both tangential electric and magnetic aperture fields are used in the computation)

Co-polarized pattern

$$\vec{E}\cdot\vec{n}_1 = \frac{q_1+q_2-\alpha q_3}{2} - \frac{q_1-q_2-\alpha q_3}{2} \cos 2\phi \qquad \text{(C12)}$$

Cross-polarized pattern

$$\vec{E}\cdot\vec{n}_2 = \frac{q_1-q_2-\alpha q_3}{2} \sin 2\phi \qquad \text{(C13)}$$

Representative patterns are shown in Figs. C9-C14.

If only the aperture electric field is used then the cross-polarized pattern is given by

$$\vec{E}\cdot\vec{n}_2 = \frac{p_1-p_2\cos\theta-\alpha p_3}{2} \qquad \text{(C14)}$$

This pattern is shown in Figs. C15-C17 for various values of α and b .

In (C14) $(\gamma + k_o\cos\theta)p_3 = 2\gamma q_3$.

Discussion of Results

The patterns for single mode radiation shown in Fig's. C2-C7 show considerable differences between the two methods of evaluation (using aperture electric field only or using both the aperture electric and magnetic fields) for small values of b. This is due to the strong influence of the $\cos\theta$ factor as θ approaches 90°. For the larger values of b (Fig's. C6 and C7) both methods give nearly the same results. For single mode radiation the cross-polarized radiation is high, typically between -20dB to -30dB. An exception is the case for b = 0.9 cm. where the cross-polarized pattern $(q_1-q_2)/2$ is at or below -40dB for most values of θ when the fields are computed using both the electric and magnetic fields in the aperture. However, in this case the waveguide is near cut-off and the principal plane patterns are very broad so this is not normally a useful feed for paraboloids with angular apertures of half-angular openings of 75° or less.

The TM_{11} mode radiation pattern in Fig. C8 shows little variation with the guide radius for b in the range 1.6 cm. to 2 cm. The on-axis field is zero.

The co-polarized and cross-polarized radiation patterns for combined TE_{11} and TM_{11} mode radiation are shown in Figs. C9-C14. These patterns are computed using both the electric and magnetic aperture fields. The TM_{11} mode amplitude is α while that of the TE_{11} mode is unity. A value of α around -0.4 gives very low cross-polarized radiation (-40dB for b = 1.6 cm. and below -50dB for b = 2 cm.).

Figures C15-17 show the cross-polarized patterns computed by using only the aperture electric field. Based on this theory the cross-polarized radiation level is generally higher and $\alpha = -.4$ is not the best α value to use for all values of the guide radius b.

When the results of this approximate evaluation of the radiation patterns and the cross-polarization is compared with the exact results given in Chapter 2 it is seen that there is considerable error in the cross-polarization patterns. The reflection of the TE_{11} and TM_{11} modes at the aperture could be taken into account and the formulas to use in this case are given by Silver (Silver, 1949). However, the reflection coefficients are known only after solving the problem exactly, in which case the exact radiation patterns are then also known.

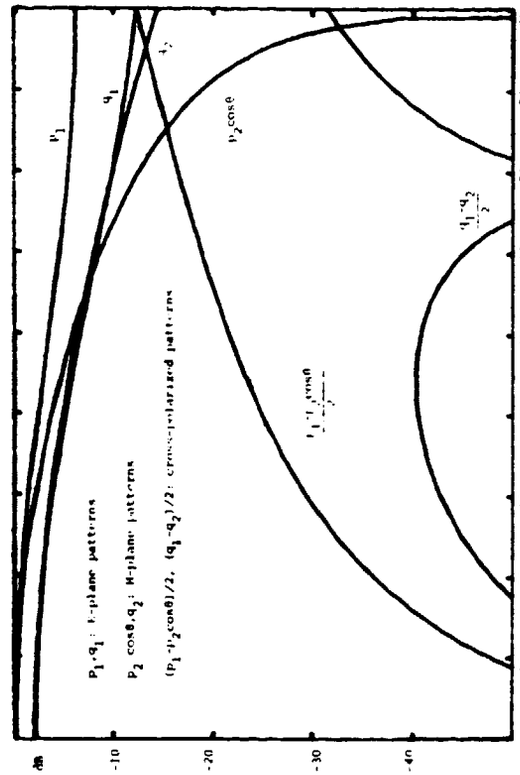

Figure C3. E- and H-plane principal patterns and cross polarized patterns for $b = 0.9$ cm. $\lambda_o = 2.5$ cm. The P_i functions are computed from aperture electric field only. The q_i are computed using the aperture electric and magnetic fields.

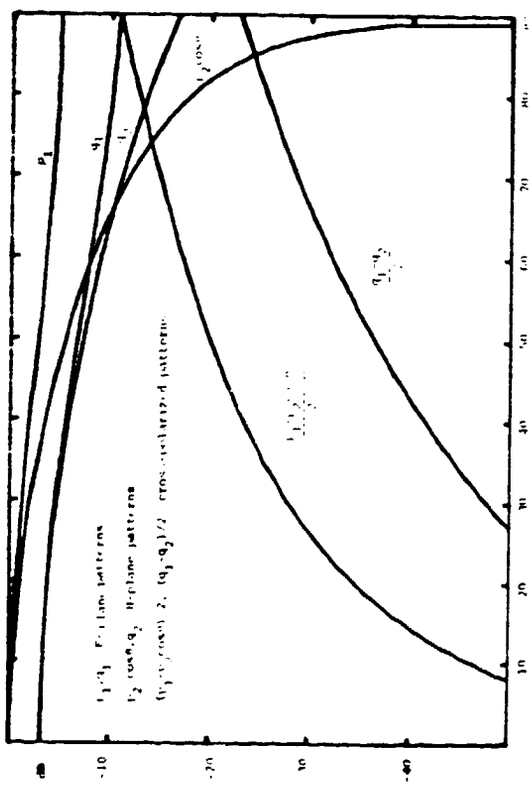

Figure C2. E- and H-plane principal patterns and cross polarized patterns for $b = 0.9$ cm. $\lambda_o = 2.5$ cm. The P_i functions are computed from aperture electric field only. The q_i are computed using the aperture electric and magnetic fields.

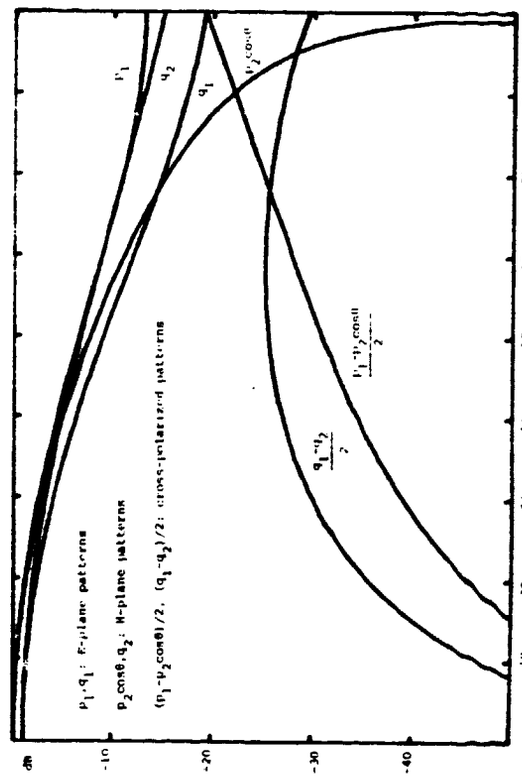

Figure C5 E- and H-plane principal patterns and cross polarized patterns for $b = 1.2$ cm. $\lambda_o = 2.5$ cm. The P_i functions are computed from aperture electric field only. The q_i are computed using the aperture electric and magnetic fields.

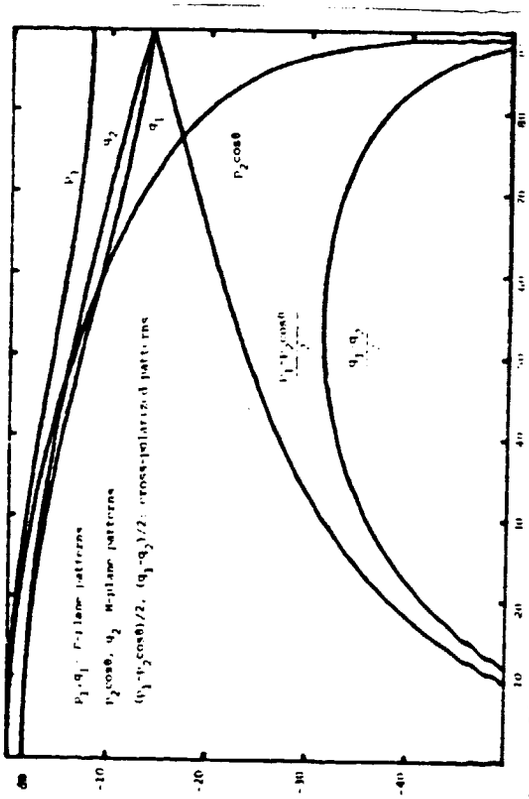

Figure C4 E- and H-plane principal patterns and cross polarized patterns for $b = 1.0$ cm. $\lambda_o = 2.5$ cm. The P_i functions are computed from aperture electric field only. The q_i are computed using the aperture electric and magnetic fields.

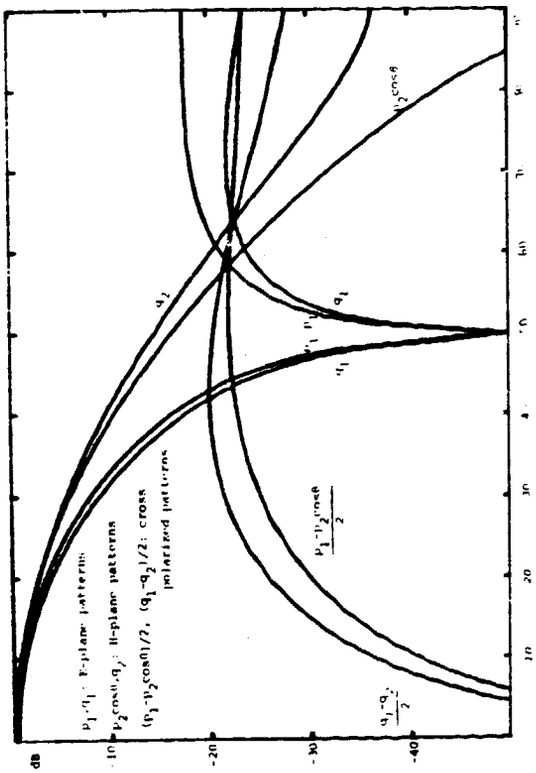

Figure C7 E- and H-plane principal patterns and cross polarized patterns for $b = 1.6$ cm, $\lambda_0 = 2.5$ cm. The I_1 functions are computed from aperture electric field only. The q_1 are computed using the aperture electric and magnetic field.

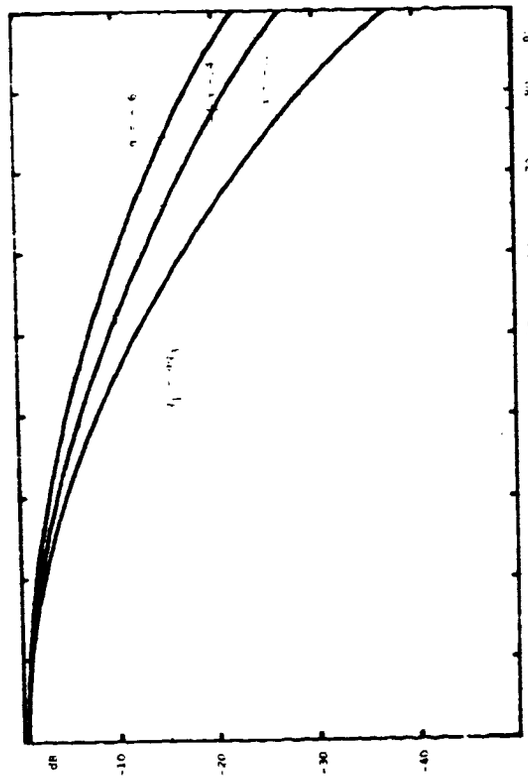

Figure C9 Co-polarized pattern for combined TE_{11} and TM_{11} mode radiation for $b = 1.6$ cm, $\lambda_0 = 2.5$ cm.

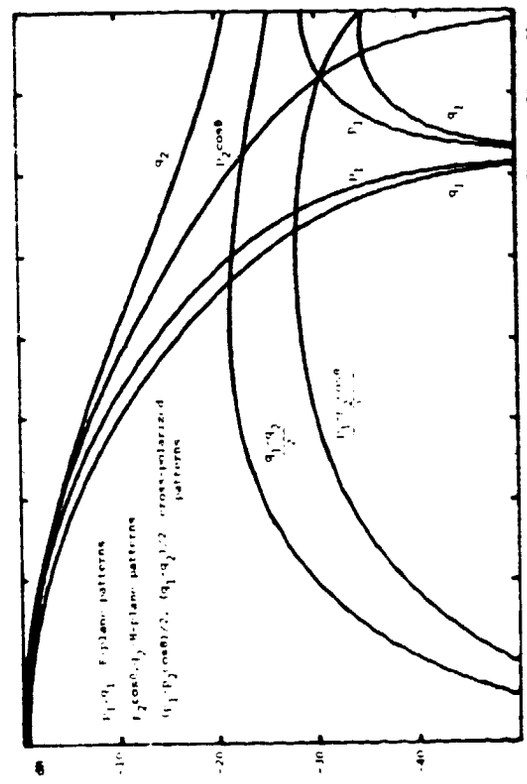

Figure C6 E- and H-plane principal patterns and cross polarized patterns for $b = 1.6$ cm, $\lambda_0 = 2.5$ cm. The I_1 functions are computed from aperture electric field only. The q_1 are computed using the aperture electric and magnetic fields.

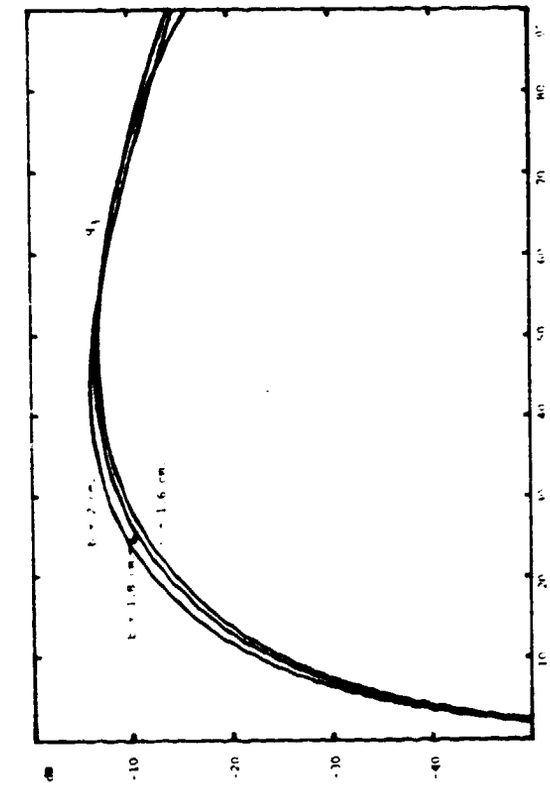

Figure C8 TM_{11} mode E-plane patterns for various values of b, $\lambda_0 = 2.5$ cm.

ORIGINAL PAGE IS
OF POOR QUALITY

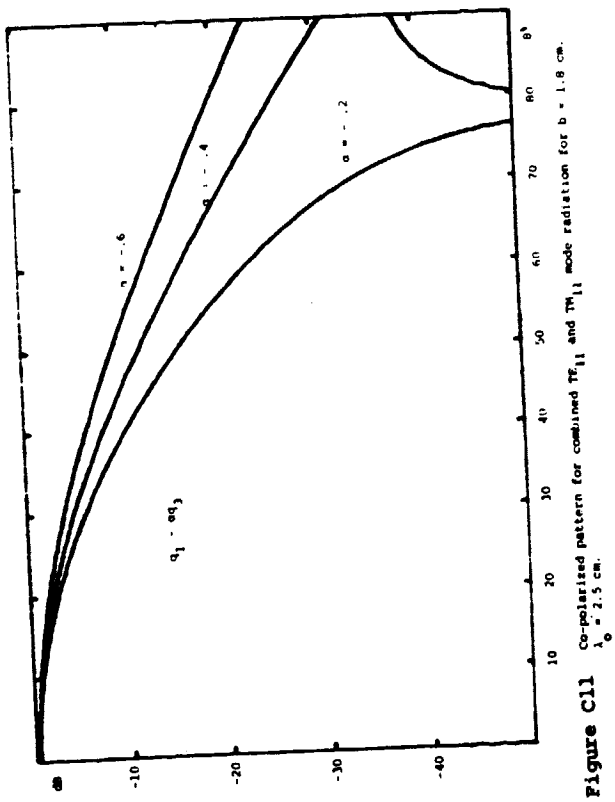

Figure C11 Co-polarized pattern for combined TE_{11} and TM_{11} mode radiation for b = 1.8 cm. λ_o = 2.5 cm.

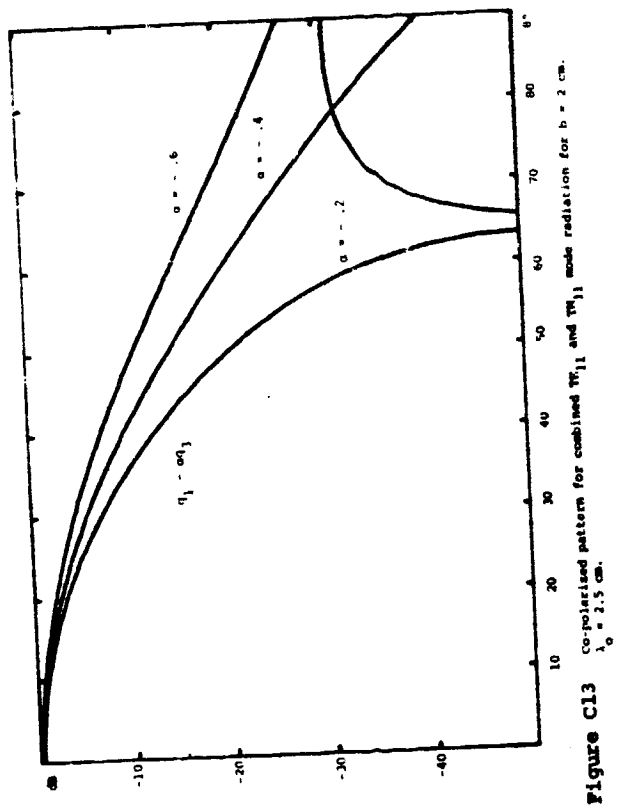

Figure C13 Co-polarized pattern for combined TE_{11} and TM_{11} mode radiation for b = 2 cm. λ_o = 2.5 cm.

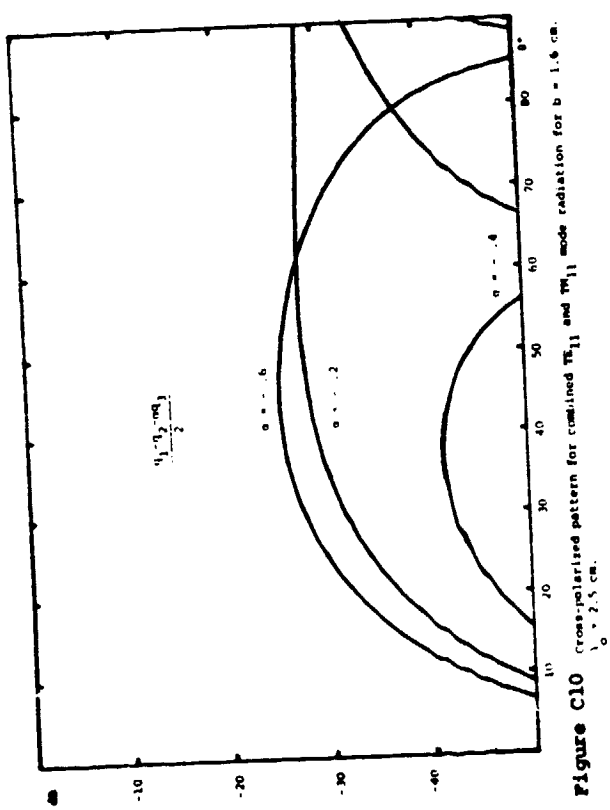

Figure C10 Cross-polarized pattern for combined TE_{11} and TM_{11} mode radiation for b = 1.8 cm. λ_o = 2.5 cm.

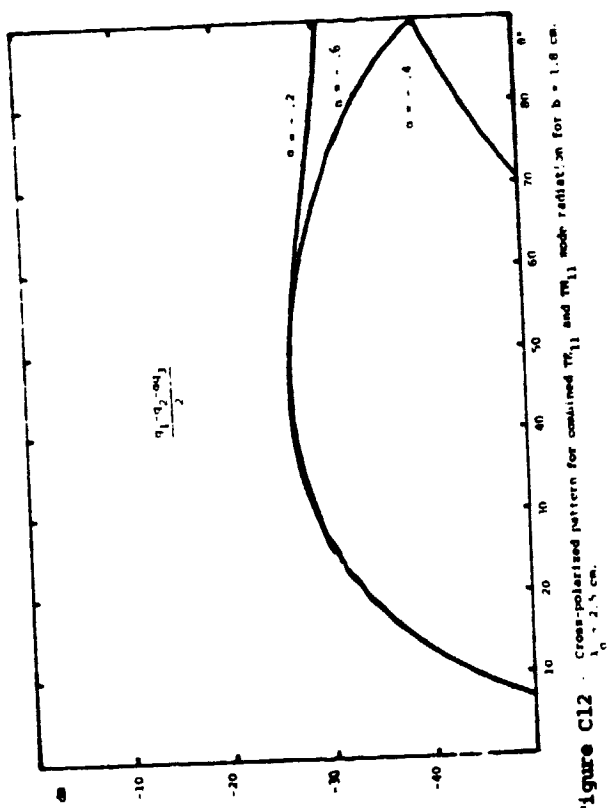

Figure C12 Cross-polarized pattern for combined TE_{11} and TM_{11} mode radiation for b = 2 cm. λ_o = 2.5 cm.

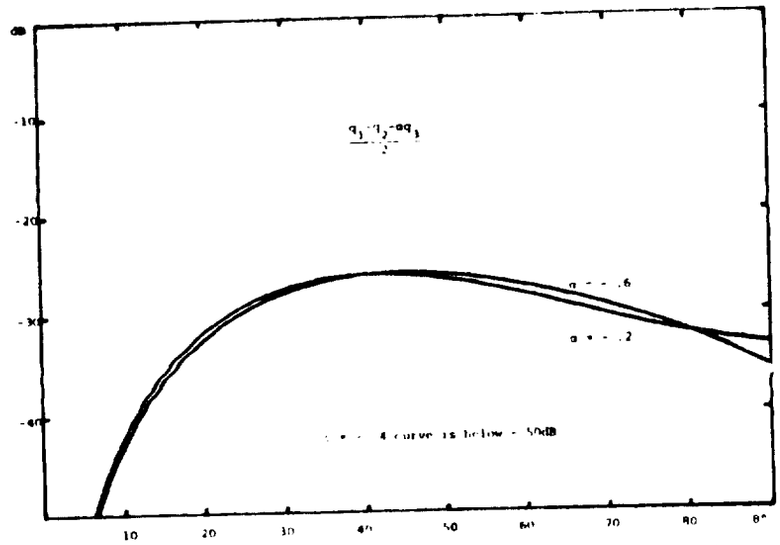

Figure C14 Cross-polarized pattern for combined TE_{11} and TM_{11} mode radiation for b = 2 cm. λ_o = 2.5 cm.

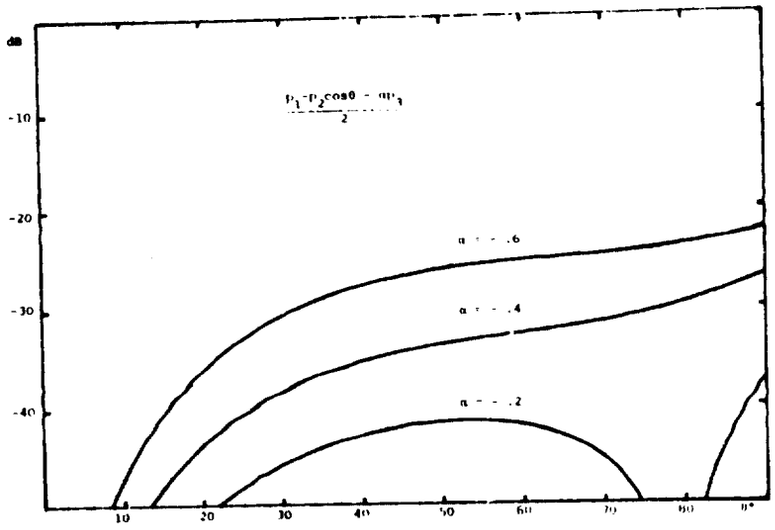

Figure C15 Cross-polarized pattern for combined TE_{11} and TM_{11} mode radiation for b = 1.6 cm. Pattern computed using aperture electric field only.

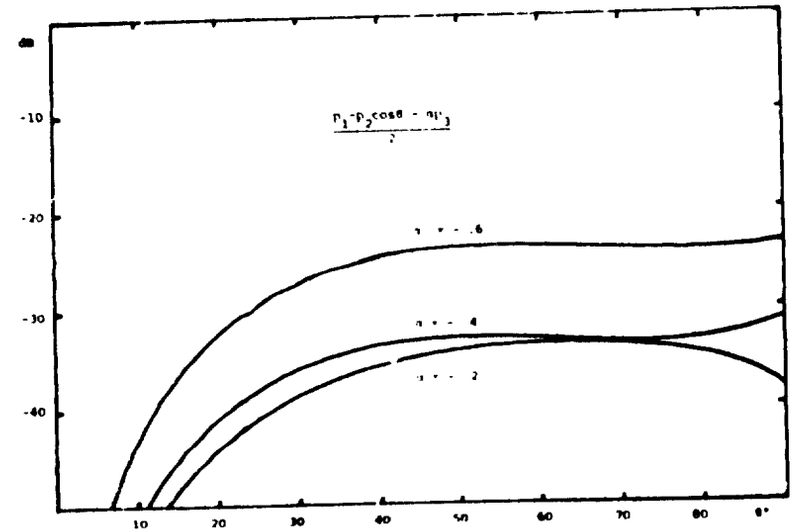

Figure C16 Cross-polarized pattern for combined TE_{11} and TM_{11} mode radiation for b = 1.8 cm. Pattern computed using aperture electric field only.

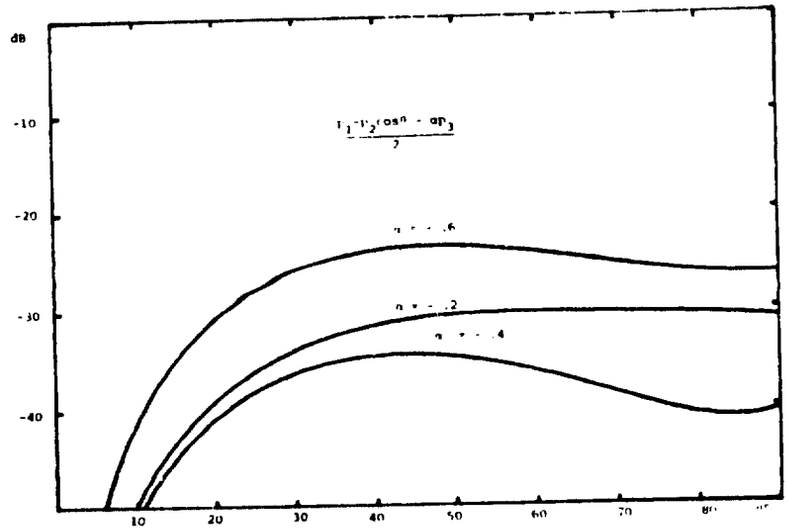

Figure C17 Cross-polarized pattern for combined TE_{11} and TM_{11} mode radiation for b = 2 cm. Pattern computed using aperture electric field only.